Exploring the role of CHRFAM7A in the early stages of Alzheimer's disease : in vitro studies and development of a novel humanized mouse model

Maria Llach Pou

Sorbonne Université

Ecole doctorale ED3C « Cerveau, cognition, comportement »

Neurobiologie Intégrative des systèmes cholinergiques, Institut Pasteur

Exploring the role of *CHRFAM7A* in the early stages of Alzheimer's disease: in-vitro studies and development of a novel humanized mouse model

Maria Llach Pou

THÈSE DE DOCTORAT DE NEUROSCIENCES

Dirigée par Dr. Isabelle Cloëz-Tayarani

Présentée et soutenue publiquement le 13 Juillet 2023

Devant un jury composé de :

Président : Pr. Jean-Louis Bessereau, PU, Université Claude Bernard Lyon 1
Rapportrice : Dr. Hélène Hirbec, CR-HDR, Université de Montpellier
Rapporteur : Pr. Peter Penzes, PU, Northwestern University, Chicago, USA
Examinateur : Dr. Régis Grailhe, DR, UST - Institut Pasteur Korea
Examinatrice : Dr. Laurence Goutebroze, DR-HDR, Institut du Fer à Moulin
Directrice de thèse : Dr. Isabelle Cloëz-Tayarani, CR Expert-HDR, Institut Pasteur
Membre invité : Dr. Uwe Maskos, DR, Institut Pasteur

To Damien, for being my rock…

Abstract

CHRFAM7A is a human-specific gene that encodes the nicotinic acetylcholine receptor (nAChR) subunit dupα7. This gene originated after a fusion between a partial duplication of the *CHRNA7* α7-nAChR gene and *ULK4* 200.000 years ago. The ancestral *CHRNA7* gene has been linked to several neurological disorders such as Alzheimer's disease (AD). In particular, α7-nAChR can directly bind to the Amyloid ß peptide (Aβ), one of the primary molecular hallmarks of the disease, and facilitate its intracellular toxic accumulation. Although extensive research has been carried out to dissect the role of α7-nAChR in AD, no clinical trials have been successful. This translational gap could be attributed to the lack of dupα7 subunit in classical pre-clinical models. Importantly, dupα7 can incorporate into pentamers of α7-nAChRs and negatively regulate its function by reducing its number of ligand binding domains and retaining the receptor in the endoplasmic reticulum (ER). In the context of AD, dupα7 reduces Aß uptake when expressed in neuronal cultures and is associated to the activation of Aβ-induced pro-inflammatory responses.

In the first part of the thesis, the role of the human subunit in mediating Aβ-induced toxicity in human induced pluripotent stem cells (hiPSC)-derived interneurons was studied in-vitro.

In-vivo, interneurons can be xenografted and studied at longer time-periods when compared to in-vitro cultures. In this direction, a technique to transplant human neurons into the mouse brain at embryonic stages was developed. Human neuronal progenitors transplanted in-utero were shown to populate and integrate different brain areas. In this model, local environment had a significant effect on neuronal maturation and spinogenesis, after transplantation.

The implications of the findings described in this dissertation highlight the importance of considering the human-specific *CHRFAM7A* in the complex interplay between Aβ and α7-nAChR and paves the way for future development of α7-nAChR-targeted therapies for AD.

Key words: CHRFAM7A, α7-nAChR, Alzheimer’s disease, amyloid beta

Long résumé

La maladie d'Alzheimer (MA) est la principale cause de démence et touchera plus de 139 millions de personnes dans le monde à l'horizon 2050. Depuis plus d'un siècle, d'intenses recherches ont été entreprises pour élucider la cause de cette maladie et trouver des médicaments efficaces. Bien que des études précliniques aient permis d'identifier certains des mécanismes importants impliqués dans la MA, aucune d'entre elles n'a pu conduire au développement de traitements cliniques efficaces, ce qui constitue une lacune sur le plan translationnel. L'une des explications possibles pourrait être l'absence du gène CHRFAM7A dans les modèles de recherche utilisés jusqu'à présent. CHRFAM7A est un gène spécifique à l'homme codant pour la sous-unité dupα7 du récepteur nicotinique à l'acétylcholine (nAChR). Ce gène résulte de la fusion ancestrale apparue il y a 200 000 ans entre d'une part la duplication partielle du gène CHRNA7 et d'autre part le gène ULK4 codant pour une protéine kinase. Situé dans une région du génome très instable, CHRFAM7A peut se présenter sous forme d'un nombre de copies différent au sein de la population générale. Un variant caractérisé par une délétion de 2 pb a également été identifié (variant 2pb).

Dupα7 peut s'assembler avec les sous-unités α7, codées par le gène ancestral CHRNA7, pour former des récepteurs qui demeurent fonctionnels. L'incorporation de dupα7 dans les pentamères α7-nAChRs peut réguler cependant négativement la fonction des α7-nAChRs en réduisant le nombre de sites de liaison aux ligands et en retenant le récepteur dans le réticulum endoplasmique (RE). Le gène ancestral CHRNA7 a été associé à plusieurs troubles neurodégénératifs tels que la MA. En particulier, le récepteur α7-nAChR peut lier directement le peptide β amyloïde (Aβ). L'accumulation intracellulaire de Aβ conduit à terme à la formation des plaques amyloïdes représentant l'une des principales caractéristiques de cette maladie. Des recherches approfondies ont été menées pour disséquer le rôle du α7-nAChR dans la MA, et de nombreuses molécules modulatrices de l'activité de ce récepteur ont été développées avec l'objectif de restaurer la fonction du α7-nAChR chez les patients atteints de la MA. Cependant, aucune étude préclinique réalisée à partir de modèles cellulaires humains n'a permis la découverte de médicaments actifs en clinique. Selon les travaux d'autres équipes, nous émettons l'hypothèse selon laquelle la sous-unité nicotinique dupα7 pourrait jouer un rôle important dans la MA, expliquant alors le déficit translationnel observé entre les modèles précliniques classiques non porteurs de la sous-unité et la population générale. Il est intéressant de noter que les études GWAS ont pu établir un lien entre le nombre de copies du gène CHRFAM7A et la pathologie de la MA. Les données cliniques indiquent que seulement 25 % de la population composée de personnes non porteuses de CHRFAM7A -simulant ainsi la situation des divers modèles précliniques- ou porteuses de la variante 2bp, pourraient bénéficier de médicaments ciblant le système cholinergique. Sur des modèles de neurones en culture, il a été montré que la présence de dupα7 réduit la capture de Aβ et est associée à l'activation de réponses pro-inflammatoires induites par ce peptide Aβ. Bien que ces données pionnières suggèrent un rôle protecteur de dupα7 contre la toxicité induite par Aß, les mécanismes par lesquels la sous-unité dupα7 interfère sur l'interaction de Aβ avec la sous-unité α7-nAChR sont encore inconnus.

L'objectif de cette thèse a été de développer un modèle in-vivo pour étudier le gène CHRFAM7A et son interaction avec les α7-nAChR et Aβ, sous forme d'oligomères. Deux axes principaux ont été définis pour atteindre cet objectif. Le premier axe a consisté en une étude comparative in-vitro de l'interaction Aβ à partir d'interneurones (hINs) dérivés de cellules souches pluripotentes induites humaines (hiPSCs), exprimant ou non la sous-unité dupα7 humaine. Les hINs sont un modèle pertinent pour l'étude des nAChRs, puisque ces récepteurs sont significativement exprimés dans les neurones inhibiteurs. Le deuxième axe de la thèse a été orienté vers la xénotransplantation des progéniteurs neuraux humains dans le cerveau de la souris pour une étude in-vivo à plus long terme.

[redacted]

[redacted]

[redacted]

[redacted]

Bien qu'elle réponde à plusieurs questions proposées, notre étude in-vitro présente certaines limites. En particulier, l'absence d'un environnement physiologique, le contact avec d'autres types cellulaires retrouvés dans le cerveau et aussi l'absence d'une modélisation plus intégrée de la MA, permettant de mieux appréhender les effets néfastes de Aβ, lorsque sa concentration n'est plus contrôlée localement dans le cerveau. En outre, les expériences in-vitro sont limitées dans le temps car les cellules ne peuvent être maintenues pendant des périodes prolongées. Pour surmonter ces limites et approfondir l'étude dans un contexte se rapprochant des conditions physiologiques, les neurones humains peuvent être transplantés dans le cerveau chez la souris. Les deux approches les plus courantes sont d'une part la xénogreffe chez l'animal adulte, ce qui implique des injections stéréotaxiques pour cibler une région particulière du cerveau. D'autre part, diverses études de xénogreffe ont été réalisées chez l'animal nouveau-né, avec une injection manuelle des cellules dès la naissance selon des repères visuels sur le crâne. Cette dernière approche permet de suivre au cours du temps la migration des cellules greffées dans le cerveau hôte et d'établir une cartographie précise des projections neuronales. Cependant, les deux techniques nécessitent l'utilisation de souris immunodéprimées afin d'éviter le rejet du greffon, ce qui pourrait être considéré comme un inconvénient car les souris immunodéprimées sont délicates et plus fragiles pour les expériences à long terme. En outre, les modèles classiques de souris atteintes de la maladie d'Alzheimer ne sont pas immunodéprimés.

Pour relever ce défi, un protocole a été mis au point visant à transplanter des cellules souches humaines dans un environnement immunocompétent. Des études antérieures ont montré la possibilité de greffer des cellules embryonnaires d'origine humaine ou non, à des stades embryonnaires précoces du développement de l'hôte. Du fait de l'état immature du système immunitaire au stade embryonnaire, les cellules humaines ont pu être tolérées et se sont intégrées dans le cerveau hôte jusqu'à un mois après la transplantation (1MPT).

Dans nos expériences, des progéniteurs neuronaux humains (hNPCs) ont été transplantés in-utero dans deux zones cérébrales différentes, les ventricules latéraux (LV) et le cortex préfrontal (PFC), ce qui a permis leur bonne intégration dans différentes régions cérébrales. Dans un premier temps, la migration, la distribution et les projections des cellules humaines dans le cerveau de la souris après la transplantation dans le VL ont été étudiées. Des distributions similaires des cellules et de leurs prolongements ont été observées entre plusieurs expériences indépendantes. Les cellules ont montré une migration accrue vers des structures plus éloignées du site d'injection jusqu'à 3 MPT. Les hNPCs ont été détectées dans des structures telles que le cortex ou l'hippocampe à 1 et 3 MPT, la majorité des projections se trouvant dans des fibres neuronales telles que le corps calleux et la fimbria.

Nous avons émis l'hypothèse selon laquelle la maturation des cellules humaines greffées pouvait être sous l'influence de l'environnement local de la greffe au sein du cerveau hôte. Aussi, nous avons entrepris une analyse comparative de la maturation neuronale après transplantation des NPC dans le LV vs. le PFC. Il est intéressant de noter que les cellules transplantées dans le PFC présentent un état global de

maturation plus élevé, comme en atteste leur réactivité aux marqueurs post-mitotiques NeuN et vGlut. Nous avons étudié la morphologie des épines dendritiques et celle des dendrites comme index de maturation. Les épines dendritiques présentent une grande diversité, et peuvent être schématiquement classées en 4 catégories principales. Les filopodes se distinguent par l'absence de tête et représentent le stade le plus labile et le moins mature tandis que les « champignons » sont un stade de maturation permettant une zone de contact synaptique la plus élaborée par rapport aux autres catégories d'épines. Nos résultats montrent une forte proportion de filopodes au stade 1 MPT, proportion encore plus élevée dans les greffons dans le LV par rapport à ceux du PFC. A 3 MPT, les proportions d'épines plus matures de forme « champignon » et de forme « trapue (stubby) » sont augmentées, ceci de façon différentielle selon la région greffée. Ainsi, les densités d'épines dendritiques augmentent au cours du temps après greffe, avec en particulier une augmentation significative dans le cas des NPCs transplantées dans le PFC, qui présentent une maturation plus élevée en particulier au stade 3MPT. La morphologie des dendrites et leur ramification ont été également analysées. Nous observons des modifications morphologiques significatives illustrant une maturation dendritique plus élaborée à 3 MPT par rapport à 1 MPT, à la fois dans les greffes LV et PFC, et ceci de façon plus accentuée dans les greffes PFC par rapport au LV pour un stade donné.

En résumé, ces résultats ont démontré l'intégration et la survie des hNPCs dans un environnement immunocompétent, soulignant également la capacité de ces cellules à migrer et à se projeter dans différentes structures cérébrales du cerveau hôte murin, jusqu'à 3 MPT. Nous montrons également que les cellules transplantées dans le PFC présentent un phénotype plus mature que les cellules transplantées dans le LV. Ces données suggèrent fortement que l'environnement local de l'hôte joue un rôle crucial dans le développement et la maturation des neurones. La mise en place de ce modèle représente une avancée prometteuse pour l'étude des interneurones humains, dont les capacités de migration sont importantes.

En conclusion et sur la base des résultats acquis, nous apportons quelques nouveaux éclairages sur sur le gène CHRFAM7A et son rôle possible dans la MA. Bien que la transplantation des hINs à l'aide de l'approche de xénotransplantation in-utero n'a pu être menée à son terme dans le cadre de la préparation de ma thèse de doctorat, les données initiales obtenues s'avèrent très encourageantes. A ce stade, il apparait important de poursuivre les analyses afin de confirmer les hypothèses proposées à la fois in-vitro et in-vivo à plus long terme. Les résultats décrits dans cette thèse peuvent permettent d'ores et déjà de montrer la nécessité de prendre en compte le gène CHRFAM7A spécifique à l'homme pour mieux comprendre cette interaction complexe existante entre le peptide Aβ et le récepteur α7-nAChR. La poursuite de ces études ouvrira la voie à de futurs développements thérapeutiques ciblant le α7-nAChR pour la MA.

Mots clés : *CHRFAM7A*, α7-nAChR, Alzheimer's disease, peptide β amyloïde

Acknowledgments

I would like to express my deepest gratitude to the members of my jury for their valuable time and effort in evaluating my thesis manuscript. I am sincerely grateful to each of you for carefully reading my work, providing insightful comments, and enhancing it with your feedback.

I extend a special thank you to Isabelle Cloëz-Tayarani for her support and constant presence throughout my PhD journey. I am grateful to her for initially selecting me and for maintaining unwavering belief in my abilities until the very end. Thank you for your kindness, patience, and guidance throughout these past four years.

I would also like to express my gratitude to Uwe Maskos for providing me with the opportunity to work in his laboratory. I am deeply appreciative of his trust in me and for granting me the space and time to develop my skills and abilities, even in difficult times. Thank you for being proud of our “lady power”.

Foremost, I would like to thank Stéphanie Pons. For your knowledge, advice, for always having my best interest at heart. For challenging me to do better and believe in myself. For your support, unwavering dedication and patience in my “bad-french-days”. Thank you for mentoring and inspiring me, I look up to you and I am grateful to have had the opportunity to share a part of our journeys.

I would like to extend my thanks to the entire team at the NISC laboratory. You have created an environment that fosters growth, support, collaboration and positivity. I am grateful for the opportunities I have received and for the knowledge and experiences I have gained through each one of you. Morgane, Gabi, Chloé and Jimena, thank you for all the lessons (scientific and not) that you’ve given me throughout this journey, sometimes without probably even knowing. Thank you, Francisco, for all the “hola guapa” and “dulce Maria”. Thank you for being you, for our deep talks and for brightening up my days with your made-up songs. I would also like to thank the ones that left the unit before. Thank you, Celia, Laurène, Hudson and Jérémy. A special thank you to Marie, for all the moments shared, for being the perfect mix between calm and fun. To the Erasmus students Marta, Giulia, Michelle, Fatima and Paula that have brought to the lab joy, energy and international richness. Thanks for being the sometimes-invisible engine of the lab. I would like to thank Sylvie for helping with administrative issues.

Thank you Annousha and Astrid, my two internship students that I have loved supervising. Thank you for your positivity, energy and dedication.

I would also like to thank my PhD fellows and friends Michiel, Enzo, Estelle, Stefano, Daniela, Iago, Miruna and Camille. Thank you for understanding every up and down, for your unconditional help, love and support. Thank you, Estelle, for your humor that help me through tough days and thank you Daniela for always being there for everyone at any time. Miruna, this PhD would have been very different if we wouldn't have taken that animal course together on our first year, thank you for your friendship. Thank you, Iago, for making me feel like home wherever we are in the world, Barcelona, Finland, Paris, where next?

Camille, this PhD would have not been possible without you. Thank you for making me feel included since the very first day. Thank you for all the mornings "on my way" and all the long evening discussions at the entrance of the Pasteur metro station. Thank you for every day, only you can truthy understand what we have been through during this journey. Thank you for your friendship, I couldn't have hope for a better person to share my PhD experience with.

I would like to thank the department of neuroscience, specially to Marie, Ben, Fred, Alex, Aline, Tara, and Rhizlane. For all the morning "bonjour ça va?", all the silent smiles crossing in the corridor and all the little talks in the coffee corner.

I would also like to thank the Paris-Pasteur University programme (PPU). For both your financial and personal support. A special thank you to Susanna and Nathalie for your work and effort to ensure the well-being of PhD students and for your special help in the origins of Piplettes.

I extend my gratitude to the members of my thesis advisor committee Miria and Richard, thank you four valuable feedback and scientific discussions that have helped shape this thesis.

I would like to thank my family, especially my parents Pere and Mariàngela that have given me the tools to overcome any challenge. Thank you for always taking care of me and teaching me how to balance ambition and professional aspirations with living and enjoying the moment. To my sister Alba, for helping me see things with perspective, being my role model and best friend. To Eva, because you are family to me, thank you for being my center. I would also like to thank my french family, Eric and Agnès. Thank you for welcoming me with open arms. Thank you for your love and support during this journey.

Finally, I would like to thank you, Damien. Thank you for your unconditional love and support during these years. Thank you for being my safe-space, my energy boost, my motivation and inspiration. Thank you for taking care of me, never stop believing and always reminding me that I can do anything I put my head at. I can’t wait to start our next exciting adventure together.

Abbreviations table

A

α-BGT: Alpha-bungarotoxin

Ach: Acetylcholine

AChE: Acetylcholinesterase

AD: Alzheimer's disease

ADAM: A desintegrin and metalloprotease

Akt: Ak strain transforming

APH-1: Anterior pharynx defective 1

ApoE: Apolipoprotein E

APP: Amyloid precursor protein

ASD: Autism spectrum disorder

ATP: Adenosine triphosphate

Aβ: Amyloid beta peptide

Aβo: Amyloid beta oligomer

B

BACE: Beta-site amyloid precursor protein cleaving enzyme-1

BBB: Blood-brain barrier

BMP: Bone morphogenetic proteins

C

c-Myc: Cellular myelocytomatosis oncogene

Cas1/8: Caspase 1/8

CCL1: Chemokine C-C motif ligand 1

CCL5: Chemokine C-C motif ligand 5

CDK5: Cyclin-dependent kinase 5

CGE: Caudal ganglionic eminence

ChAT: Choline acetyltransferase

ChT: Choline transporter

CNS: Central nervous system

CNV: Copy number variation

CSF: Cerebral spinal fluid

CTIP2: Coup-TF-interacting protein 2

Cux1: Cut like homeobox 1

CXCL1: Chemokine C-X-C motif ligand 1

D

DCX: Doublecortin

DLX1: Distal-less homeobox 1

DNA: Deoxyribonucleic acid

DTM: Disease-modifying treatments

E

E: Embryonic day

EB: embryoid body

ECD: Extracellular domain

EOAD: Early-onset Alzheimer's disease

ER: Endoplasmic reticulum

ESC: Embryonic stem cells

F

fAD: Familiar Alzheimer's disease

FDA: Food and Drug Administration

FDG-PET: Fluorodeoxyglucose positron emission tomography

FGF: Fibroblast growth factors

Fyn: Formerly tyrosine protein kinase 5

G

GABA: Gamma-aminobutyric acid

GAD1: Glutamic acid decarboxylase

GFAP: Glial fibrillary acidic protein

GSK3β: Glycogen synthase kinase-3 beta

GWAS: Genome-wide association studies

H

H_2O_2: Hydrogen peroxide

HFIP: 1,1,1,3,3,3-hexafluoro-2-propanol

I

IBA1: Ionized calcium binding adaptor molecule 1

IL: Interleukin

iPSC: Induced pluripotent stem cell

J

JAK2: Janus kinase 2

K

Kd: Dissociation constant

KLF4: Krüppel-like factor 4

L

LBD: Ligand binding domain

LBP: Ligand binding pocket

LOAD: Late-onset Alzheimer's disease

LV: Lateral ventricle

M

mAChR: Muscarinic acetylcholine receptors

MAPT: Microtubule-associated protein tau

MCI: Mild cognitive impairment

MGE: Medial ganglionic eminence

MLA: Methyllycaconitine

MPT: Month post-transplant

MRI: Magnetic resonance imaging

N

NACHO: nAChR chaperone TMEM35a

nAChR: Nicotinic acetylcholine receptor

NADPH: Nicotinamide adenine dinucleotide phosphate

NAM: Negative allosteric modulators

NBM: Nucleus basalis of Meynert

NF-kB: Nuclear factor kappa light chain enhancer of activated B cells

NFT: Neurofibrillary tangles

NK: Natural killer

Nkx2.1: Thyroid transcription factor 1

NO: Nitric oxide

NOD-SCID: Nonobese diabetic/severe combined immunodeficient

Nrf2: Nuclear factor erythroid 2-related factor 2

NSC: Neural progenitor cells

NSC: Neural stem cells

O

$O_2^{\cdot-}$: Superoxide radical

OCT4: Octamer-binding transcription factor

·OH: Hydroxyl radicals

P

p-tau: Phosphorylated tau

PAM: Positive allosteric modulators

PAX6: Paired box protein

PET: Positron emission tomography

PFC: Prefrontal cortex

PHFs: Paired helical filaments

PI3K: Phosphatidylinositol 3-kinase

PNS: Peripheral nervous system

PP1: Protein phosphatase 1

PP2: Protein phosphatase 2

PSC: Pluripotent stem cell

PSEN1: Presenilin 1

PSEN2: Presenilin 2

PV: Parvalbumin

R

RA: Retinoic acid

RIC3: Resistance to inhibitors of cholinesterase 3

RMS: Rostral migratory stream

ROS: Reactive oxygen species

S

sAD: Sporadic Alzheimer's disease

SAM: Silent allosteric modulators

Shh: Sonic hedgehog

SMAD: Suppressor of mothers against decapentaplegic

SOM: Somatostatin

SOX2: Sex determining region Y-box 2

SOX6: Sry-box transcription factor 6

STAT3: Signal transducer and activator of transcription 3

SVZ: Subventricular zone

SYK: Spleen tyrosine kinase

T

TGFβ: Transforming growth factor beta

TM: Transmembrane domain

TNF: Tumor necrosis factor

TREM2: Triggering receptor expressed on myeloid cells 2

TUJ1: Class 3 beta-tubulin

V

VAChT: Vesicular acetylcholine transporter

vGAT: Vesicular GABA transporter

VGLUT: Vesicular glutamate transporter

VIP: Vasointestinal peptide

W

WHO: World Health Organization

Wnt: Wingless/integrated

Table of figures

Table of contents

INTRODUCTION

Alzheimer's disease

1.1. Definition

Alzheimer's disease (AD) is a progressive neurodegenerative disorder characterized by distinctive brain histopathological features that lead to a gradual decline in cognitive functions. Alois Alzheimer first described AD in 1906 as a type of dementia characterized by brain atrophy and the presence of two hallmark features: the neurofibrillary tangles (NFT) and plaques [1].

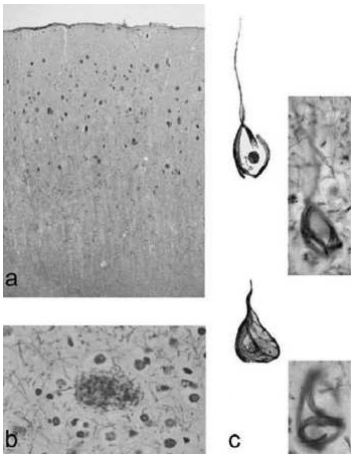

Figure 1. Original drawings from tissue sections from the first patient diagnosed with AD.
A and b. extracellular insoluble accumulations of amyloid beta (Aβ) in the cerebral cortex, also known as plaques. c. intracellular NFTs formed by aggregated hyperphosphorylated tau [2].

Through intensive research in the field, we have come to understand that AD is a far more complex disorder than originally described. Along with the hallmark features of NFT and extracellular plaques, other pathological mechanisms such as neuroinflammation, neuronal hyperexcitability, cholinergic signaling dysfunction, and oxidative stress also play a significant role in the disease. However, despite this increased knowledge, the initial histopathological hallmarks described by Alois Alzheimer remain crucial to AD diagnosis and continue to guide research aimed at developing better diagnostic tools and more effective treatments for the disease.

AD can be classified into two forms based on the age at which symptoms appear and the underlying cause. Familiar AD (fAD), also known as early-onset AD (EOAD), is a less common form accounting for only 5% of AD cases, and typically affects individuals under 65 years of age with a family history of dementia. It is an inherited form of the disease caused by mutations in genes that encode the amyloid precursor protein (APP) and its cleavage enzymes [3]. Although fAD is rare, studying the specific genetic mutations that cause this form of the disease has provided valuable insights into the underlying mechanisms

of AD. Sporadic AD (sAD) or late-onset AD (LOAD), on the other hand, is the more common form and affects individuals over 65 years of age. It is caused by a complex interplay between normal aging, genetic and environmental factors. Research has revealed that about 60-80% of the causative factors in LOAD are heritable, with the most important genetic risk factor being the Apolipoprotein E (ApoE) 4 allele. However, despite a long list of reported risk factors, the exact cause of sAD remains unknown.

1.2. Epidemiology and economic burden

Alzheimer's Disease is one of the top 10 causes of death worldwide [4]. In 2019, about 1,62 million people died from AD and other types of dementia, which included 0,56 million men and 1,06 million women [5]. Despite being one of the main causes of mortality in the world, AD has the lowest mortality rate and longer life expectancy among the different types of dementia after diagnosis. The average life expectancy in the US is reported to be 4-8 years, and up to 20 years for some individuals, following diagnosis [6].

As the baby boomer generation reaches the age group with the greatest risk for AD (older than 65 years), the number of people suffering from this disease increases exponentially every year. In 2019, about 55.2 million people were living with dementia worldwide, and projections that account for population growth estimate that this number will increase to 139 million by 2050 [5]. In Europe, the number of people living with dementia is projected to increase from 14.1 million in 2019 to 25 million by the same time period [7].

The most relevant factor in AD and other dementia's prevalence is age. Therefore, prevalence ranges from 4.6-5% in the 65-74 age group to 10-13% in people aged 75 to 84 years old, and 31-33% in people older than 85 years old. However, other factors such as gender, ethnicity and socioeconomic level, play a role. Firstly, AD is more prevalent in women (Figure 2). This could be attributed to the fact that women have a higher life span when compared to men. However, when comparing the age-standardized prevalence rate of dementia, women have higher scores than men, indicating a higher prevalence independent from the absolute total number of women [8]. Lower access to education and occupational work in women, who were born before the year 1950, may play an essential role with respect to such differences. In the future, additional data from women, who have access to the same levels of education and occupy similar social and occupational activities, should provide more insights into the prevalence differences.

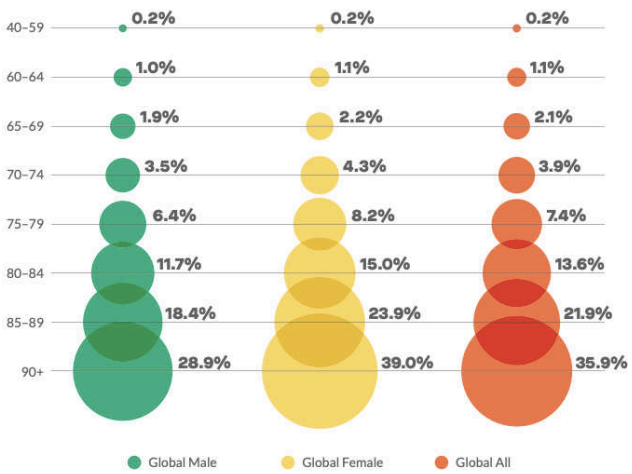

Figure 2: Global prevalence rate of dementia by age and gender.

Populational prevalence increases as a function of age, and it is significantly higher in women in AD-risk age groups [5].

Ethnicity has a high impact on the prevalence of the disease as well. According to data from the US, the African American population would be the most affected group followed by Hispanic American and the least affected group would be represented by White Americans. Similar to gender, prevalence differences could be explained by historically-restricted access to education but also by the quality of health care due to racism and marginalization of Black and Hispanic communities [6].

When considering the country's educational and economic situation together with the fertility rate, a positive correlation is observed between a high level of social development and a high prevalence of dementia [8]. The latest report from the WHO estimated 1.4 million, 8.8 million, 23.6 million and 21.4 million people with dementia in low-income, lower-middle-income, upper-middle-income, and high-income countries, respectively. Specifically middle-income countries are expected to become the fastest-growing population affected by AD (Figure 3).

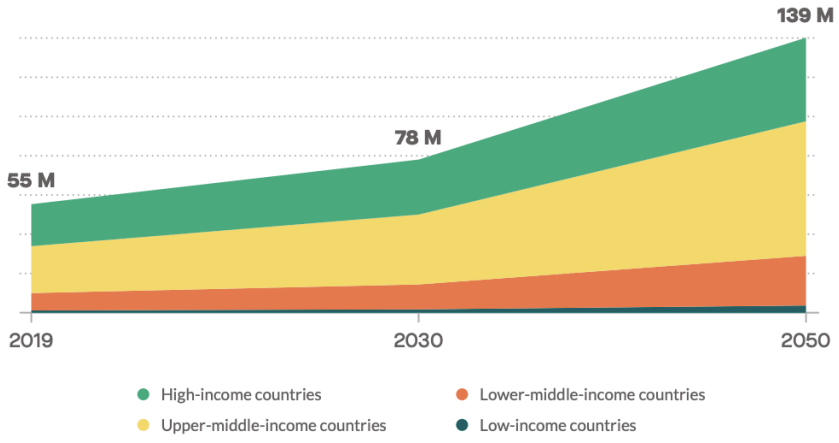

Figure 3. Prevalence predictions according to income.

Middle-income countries are experiencing exponential growth in the aging population. Although some improvements have been made in education, environmental factors such as air pollution and nutrition may exacerbate the prevalence of AD in this group [5].

AD is and will thus represent one of the most challenging diseases in terms of economic burden. The estimation of annual costs for a patient with dementia varies according to each country. The highest cost per person is in North-America (32,276 EUR), closely followed by Europe (28,315 EUR), Western Pacific (19,901 EUR) and Eastern Mediterranean (12,208 EUR) countries. African and South-East Asian countries have the lowest costs per person (7,457 and 3,319, respectively)[5]. In Europe, informal health care represents about 50% of the global dementia care cost. However, striking differences are observed between Southern and Northern European countries. While in South Europe, the predominant care for dementia patients is informal, representing about 71% of all care costs, in Northern European countries informal care represents only about 27% of the cost. These differences might be attributed to different cultures and family structures together with accessibility to direct or formal medical care [7]. An urgent need for increasing health care infrastructures will be essential to ensure the well-being of the aging population in the years to come. By 2050, the global cost of AD is projected to reach about 13 trillion euros [9], implying an economic impact that could reach as high as 10.5% of the G20-GDP[1].

1.3. Continuum and biomarkers

AD is a long progressive disorder that starts years before the symptoms appear [10]. As early as 20 years before the onset of symptoms, the accumulation of pathological proteins like Aβ or hyperphosphorylated tau occur together with other changes in the brain. Biomarkers are currently accessible to monitor the advancement of the disease and assist in making a diagnosis. In 2016, the National Institute of Aging released the A/T/N framework aimed to guide the diagnosis of AD in clinical research purely based on biomarkers [11]. According to this framework, biomarkers can be categorized into three groups: A (Aβ), T (phosphorylated-Tau), and N (Neurodegeneration or neuronal injury). Category (A) refers to the detection of Aβ in the cerebral spinal fluid (CSF) and in the brain using positron emission tomography (PET). Similarly, category (T) includes CSF detection of phosphorylated tau (p-tau) and tau-PET brain detection. Lastly, (N) refers to biomarkers of neurodegeneration including CSF total tau and cerebral hypometabolism, which can be observed using fluorodeoxyglucose positron emission tomography (FDG-PET) (Examples of scan images in Figure 4).

1.3.1. Pre-clinical Alzheimer's Disease

Pre-clinical or asymptomatic AD is the stage of the disease when brain changes detectable with AD biomarkers are present, but individuals have no clinical symptoms. At this stage of the disease, PET imaging can detect increased levels of both (A) and (T) in the brain. However, the levels of Aβ in the CSF are

[1] G20-GDP: gross domestic product of the member countries of the G20

decreased, while the levels of phosphorylated-Tau are increased. This may indicate a problem in the brain's ability to clear Aβ, leading to its accumulation and subsequent formation of amyloid plaques. Another important biomarker of AD preclinical stages is cerebral hypometabolism detected with FDG-PET. This impairment of energy metabolism is believed to cause synaptic dysfunction [12].

1.3.2. Mild cognitive impairment

The first symptoms of AD appear as a mild cognitive impairment (MCI), a phase also called pre-dementia or prodromal AD. MCI is defined by a cognitive decline with no significant impact on daily life activities. The symptoms can be caused by AD but also by normal aging or several other pathologies including dementia with Lewy bodies and vascular cognitive impairment of frontotemporal lobe degeneration. If caused by AD, MCI eventually develops into dementia.

At this disease stage, besides the (A) and (B) biomarkers described above, effects of neuronal degeneration and neuronal injury can be observed with volumetric magnetic resonance imaging (MRI). By detecting changes in texture, volume, and thickness in critical brain structures responsible for cognition, such as the hippocampus, amygdala, and parietal lobe, this technique can identify individuals with MCI who have an underlying cause of AD[13,14].

1.3.3. Dementia

Dementia is a spectrum of diseases affecting memory, other cognitive abilities and behavior, that are severe enough to interfere with daily living[15]. In AD, dementia marks the final stage of pathohistological progression. At this stage of the disease, a gradual decline in cognitive functions is observed, which is caused by an evident atrophy of the brain due to extensive neurodegeneration. AD dementia can be further classified into three stages: mild, moderate, and severe AD, based on the severity of cognitive decline and functional impairment.

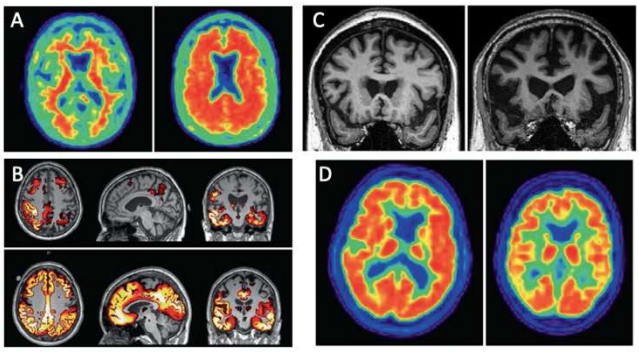

Figure 4. Normal and abnormal PET and MRI images.

a. Normal (left) and abnormal (right) amyloid PET. b. Low (above) and high (below) tau PET superimposed with MRI. c. Early (left) and late (right) AD in MRI. d. Normal (left) and abnormal (right) FDG-PET[16].

1.4. Diagnostic

In 1984, a workgroup composed by the National Institute of Neurological and Communicative Disorders and Stroke (NINCDS) and the Related Disorders Association (ADRADA), put together a clinical criterion for AD diagnosis. The NINCDS-ADRADA guidelines were primarily focused on cognitive evaluation, while the available biomarker at that time such as cerebral atrophy on computerized tomography or increased slow-wave activity as measured by electroencephalography, were considered supplementary and recommended only for improving diagnostics accuracy. [17]. Due to the absence of specific biomarkers, a confirmed diagnosis of AD was only possible postmortem.

The diagnosis of probable AD as described by the NINCDS-ADRADA criteria had a successful sensitivity of 81% and specificity of 70% [18], for almost 27 years. However, because of the intense research and accumulated new knowledge, a need emerged to redefine and update the 1984 criterium. In 2007, the International Working Group (IWG) published a new classification of AD stages considering new biomarkers, that were not available in 1984 [19], which was later revised in 2014 as the IWG-2 criteria [20]. In parallel, the National Institute on Aging and the Alzheimer's Association (NIA-AA) created a workgroup to meet the need for updated diagnoses criteria and published three series of guidelines addressing each stage of AD progression: preclinical AD [21], MCI [22] and dementia due to AD [23]. In 2018, an update was published by NIA-AA including guidelines addressed to clinical research. Even though the current AD diagnoses are based on the NIA-AA and IGW-2 criteria, alternative guidelines such as the A/T/N framework are used for research proposes [11].

If we look at the different possible combinations of A/T/N biomarkers, the two currently used diagnostic classification systems result in similar but not always comparable diagnoses (Table 1). Contrarily to the older guidelines, both criteria acknowledge a pre-clinical stage of AD and include the use of biomarkers in the diagnosis pipeline. Nevertheless, routine screening of early biomarkers of AD is not yet implemented in primary healthcare practices. Improving early diagnosis of AD and standardization of biomarkers is of essential importance, as the effect of some therapeutic interventions could be optimal only when given before symptomatology starts.

		Cognitive stage					
		Asymptomatic or pre-clinical		MCI or prodromal AD		Dementia	
		NIA-AA (2011 & 2018)	IWG (2007 & 2014)	NIA-AA (2011 & 2018)	IWG (2007 & 2014)	NIA-AA (2011 & 2018)	IWG (2007 & 2014)
Biomarker	**A-T-N-**	Not defined	Not defined	MCI, unlikely due to AD	Not defined	Dementia, unlikely due to AD	Not defined
	A+T-N-	Stage 1 preclinical AD	Asymptomatic at risk of AD (if A+ established by amyloid PET)	MCI, core clinical criteria*	Typical prodromal AD (If A+ established by amyloid PET)	Intermediate likelihood probable AD dementia, based on clinical criteria.	Typical AD (If A+ established by amyloid PET)
	A+T+N-	Stage 2/3 preclinical AD	Asymptomatic at risk of AD	MCI, core clinical criteria* (2011), Prodromal AD (2018)	Typical prodromal AD	High likelihood probable AD dementia, based on clinical criteria (2011). AD dementia (2018)	Typical AD
	A+T+N+	Not addressed (2011), preclinical AD (2018)	Asymptomatic at risk of AD (if A+ established by amyloid PET)	MCI, core clinical criteria* (2011), Prodromal AD (2018)	Typical prodromal AD (If A+ established by amyloid PET)	High likelihood probable AD dementia, based on clinical criteria (2011). AD dementia (2018)	Typical AD (if A+ established by amyloid PET)
	A+T-N+	Stage 2/3 pre-clinical AD (2011), and concomitant non-AD's pathological changes (2018)	Asymptomatic at risk of AD	MCI due to AD, high likelihood (2011), MCI due to AD and concomitant suspected non-AD's pathological changes (2018)	Typical prodromal AD	High likelihood probable AD pathophysiology (2011). AD dementia and concomitant suspected non-AD's pathological changes (2018)	Typical AD
	A-T+N-	Not defined (2011), non-AD's pathologic changes (2018)	Not defined*	Not defined (2011), MCI with non-AD's pathological changes (2018)	Not defined*	Probable AD dementia, based on clinical criteria (2011). Dementia with non-AD's pathological changes (2018)	Not defined*
	A-T-N+	Not defined (2011), non-AD's pathologic changes (2018)	Not defined*	Not defined (2011), MCI with non-AD's pathological changes (2018)	Not defined*	Intermediate likelihood probable AD dementia, based on clinical criteria. Dementia with non-AD's pathological changes (2018)	Not defined*
	A-T+N+	Not defined (2011), non-AD's pathologic changes (2018)	Not defined*	Not defined (2011), MCI with non-AD's pathological changes (2018)	Not defined*	Intermediate likelihood probable AD dementia, based on clinical criteria. Dementia with non-AD's pathological changes (2018)	Not defined*

Table 1. Table of AD continuum classification according to the NIA-AA and IWG guidelines and in function of the A/T/N framework.

11

1.5. Pathophysiology

1.5.1. Plaques and amyloid beta

In 1906, Alois Alzheimer identified amyloid plaques as one of the histopathological hallmarks of AD. Several lines of evidence discussed in this chapter led scientists to propose Aβ as the origin of AD pathogenesis. The amyloid beta hypothesis supports the idea that Aβ is the trigger of a pathological cascade that ends up in synaptic dysfunction, inflammation, and neuronal death, ultimately resulting in cognitive decline and dementia. Even though this linear explanation was supported by initial data, growing controversial evidence has emerged in recent years, questioning the proposed causative mechanism [24]. Interestingly, while the characteristic amyloid plaques do not correlate with disease progression and do not necessarily co-localize with dystrophic neurites and dying neurons in the brain, Aβ oligomers, an intermediate structure formed during the amyloid aggregation process, do so [25–28]. These soluble aggregates have multiple targets in neuronal and glial cells and have been proposed to be the origin of Aβ-induced neuronal toxicity [29].

1.5.1.1. Amyloid precursor protein and its processing

Amyloid beta is a peptide produced by sequential cleavages of the amyloid precursor protein (APP) and the major component of the amyloid beta plaques. APP is an integral membrane glycoprotein present in the brain at a high level. It is composed of a large extracellular N-terminal domain, a single transmembrane region, and a shorter cytoplasmic C-terminal. The physiological function of this protein, and the peptides resulting from its processing, are still poorly understood. However, some evidence indicates roles such as cell-to-cell adhesion, synaptic support, synaptic plasticity and cell survival (reviewed in [30]).

The amyloid precursor protein is processed by three enzymes named α-secretase, β-secretase and γ-secretase that differ in their cleaving site. While α- and β-secretases can cut APP at its extracellular domain, γ-secretase's cleaving site resides in the transmembrane region. These proteolytic enzymes are formed by different proteins; α-secretases are composed of the ADAM protein family, the most common β-secretase in the brain is BACE, and γ-secretase is a multiprotein complex with four core components including the presenilins, nicastrin, and APH-1. It is important to notice that the cleavage of APP occurs not only in the plasma membrane but also in 1) trans-Golgi network-derived secretory vesicles that transport newly formed APP and enzymes to the plasma membrane, 2) early endosomes before APP is recycled back to the cell

surface, 3) lysosomes before APP degradation. While APP in the plasma membrane is mostly cleaved through a "non-amyloidogenic pathway", acidic compartments like lysosomes favor the "amyloidogenic processing" that leads to Aβ synthesis [31] (Figure 5).

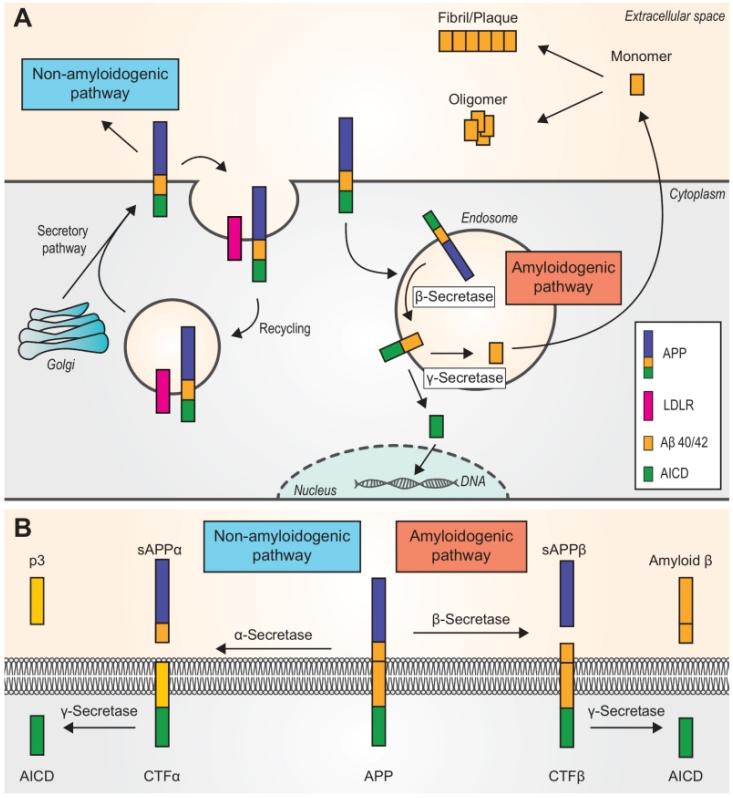

Figure 5. APP processing in different cell compartments.

The cleaving of APP can occur in two different directions according to which secretase participates in the process. The named non-amyloidogenic pathway starts with a cleavage of α-secretase that splits the APP protein into a transmembrane portion (CTFα) and a soluble product (APPsα) that gets released extracellularly. The process is followed by a γ-secretase-mediated cleavage at the transmembrane domain of CTFα that cuts loose an extracellular peptide (p3, also known as $Aβ_{17-40/42}$) and a cytoplasmic product (AICD). The alternative APP cleaving sequence, and the most well-studied due to its high therapeutical potential, is the amyloidogenic pathway. In this molecular cascade, β-secretase is the first to intervene, cleaving the extracellular side of the full-size APP. β-secretase-mediated cleavage forms similar products as those obtained with α-secretase; a slightly smaller extracellular product (APPsβ) and a bigger transmembrane fragment (CTFβ or C99). The subsequent cleavage by γ-secretase at its transmembrane site originates the notable Aβ peptide, released at the extracellular domain, and the AICD cytoplasmic product [32].

Under physiological conditions, the dominant pathway of APP cleavage is the non-amyloidogenic pathway. However, several factors including genetic mutations, aging or others (see in risks factors chapter) can shift this balance towards the amyloidogenic way. In AD patients, a higher activity of β-secretases and a reduction in α-secretases activity is detected when compared to aged-matched controls, resulting in an increase in Aβ production [33,34]. It is important to note that in normal aging, β-secretase increases as well and correlates with insoluble levels of Aβ40 and 42 [35].

1.5.1.2. Amyloid beta oligomerization: from monomers to oligomers to plaques

After the cleavage of APP by β-secretase, the resulting CTFβ or C99 fragment is further cleaved by γ-secretase. The cleavage can be done in various sites and lead to different Aβ lengths including 1-37, -38, -39, -40, -42 and -43. In addition, a further fragmentation by α-secretases can result in shorter peptides like $A\beta_{1-14}$, $A\beta_{1-15}$, $A\beta_{1-16}$. Nevertheless, the most common products in the brain are $A\beta_{1-40}$ and $A\beta_{1-42}$. $A\beta_{1-40}$ is the most abundant isoform produced at about 10-fold higher levels than $A\beta_{1-42}$. The longer isoform is, however, the most prone to self-assembly and the main responsible for the formation of toxic Aβ aggregates and plaques. Under both normal aging and AD pathological conditions, $A\beta_{1-42}/A\beta_{1-40}$ ratio is increased and, consequently, progressive deposition of amyloid can be observed in the brain [36].

Aβ peptides possess very low secondary or tertiary structure stability, and they go through complex conformational changes leading to oligomerization and fibrillation. Consequently, the characterization of the Aβ aggregation process has been experimentally challenging to resolve. In addition, this process is highly dependent on environmental factors such as pH, metal ions or temperature [29]. Nevertheless, scientists now agree on an overall process of aggregation involving a lag phase, followed by an elongation exponential phase, and reaching a steady or plateau of fibril formation.

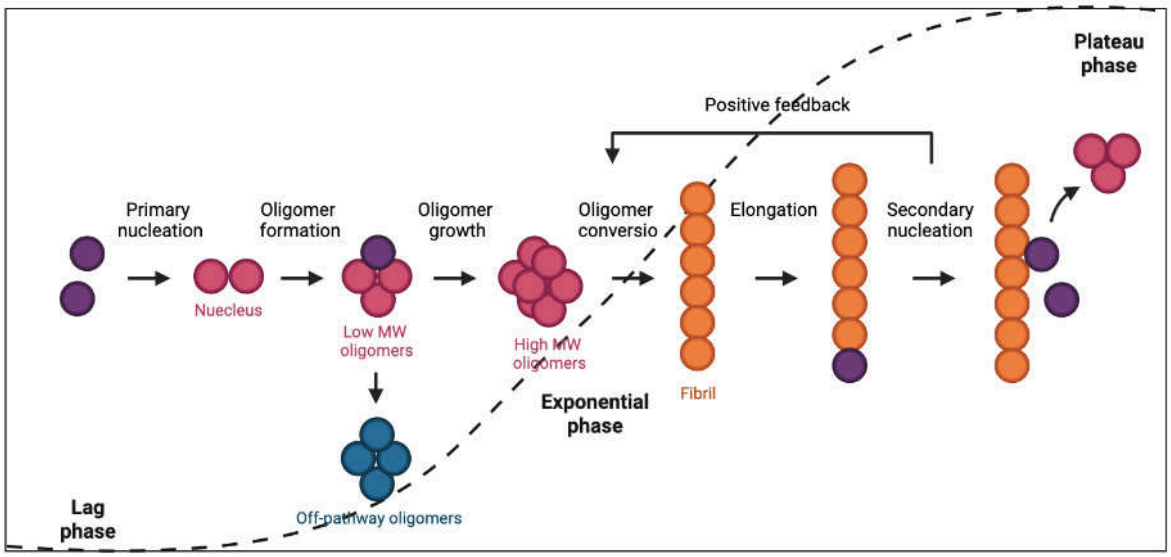

Figure 6. Aβ oligomerization.

The lag phase of Aβ oligomerization starts with monomers interacting with one another and forming small aggregates, a process called primary nucleation. These small aggregates or low-mass oligomers continue to develop with the addition of new monomers. Aβ oligomers (Aβo) are soluble aggregates of different sizes, with structural conformation ranging from α-helix to coiled-coil or β-sheet [37]. Some oligomers are stable

(off-pathway intermediates) and others continue to form larger and higher-ordered fibrillar structures during the exponential phase [38]. Fibrils are insoluble aggregates composed of a characteristic cross-β structure that can be detected with Thioflavin T [39]. Another aggregation pathway can occur when fibrils directly interact with monomer budling nuclei by recruiting them at the fibril end, a process known as secondary nucleation [40], done with biorender.

Fibrils that can auto-catalyze their own growth and pass these "growth instructions" to daughter fibrils after breakage, will prevail and outnumber all other types of aggregates. This capacity of Aβ fibrils to induce a change in conformation with self-perpetuating and self-propagating capacities is also known as prion-like property, and it is at the base of the Aβ prion hypothesis of AD [41]. Aβ fibrils can then further assemble in extracellular deposits called amyloid beta plaques. Plaques are one of the first AD hallmarks to be discovered, as they display birefringence characteristics, which are easily detected with Congo Red staining [42]. Diffused and small plaques are believed to develop into bigger aggregates with a core-space-corona organization, which contains neurites and reactive glial cells.

1.5.1.3. Aβ oligomer toxicity at early pathological stages

Aβo are capable of triggering AD pathological consequences, as evidenced both through in vivo behavioral experiments and in vitro studies. Prior to the formation of plaques in the brain, Aβo can initiate several AD-related cascades including Tau phosphorylation, disrupted axonal transport, synaptic loss, oxidative stress, neuroinflammation, impairment of the cholinergic system and neuronal death (reviewed in [43]). In addition, Aβo have been shown to be sufficient to initiate AD-like behavioral phenotypes. In animals models, cognitive impairments can be detected prior to plaque formation, or even in its absence [44,45]. An injection of Aβo in the cerebral ventricular system alone, induces memory deficits in wild-type mice [46]. Complementary, administration of Aβo targeted antibodies, that reduce Aβ load in the brain, can diminish memory impairment in AD transgenic mouse models [47].

At the cellular level, the high toxicity of Aβo can be explained, at least in part, by its ability to interact with neuronal membranes. Aβ oligomers can exist freely in the extracellular space or remain attached to the cell membrane and lipid rafts that favor their pathological aggregation. Aβo can also integrate the plasma membrane and form pores that disrupt neuronal ionic homeostasis. In addition, Aβo can directly bind to a wide variety of surface receptors, leading to receptor-mediated endocytosis and activation of harmful signaling pathways. For instance, the direct binding of Aβ to NMDA receptors and α7 nicotine acetylcholine receptor (α7-nAChR) can disrupt calcium homeostasis and induce neuronal hyperactivity at

early-stages of the disease - the interaction of Aβ and α7-nAChR and the resulting toxicity is further discussed in Chapter 2.6 -. Abnormal levels of intracellular calcium can lead to mitochondrial dysfunction and induce the production of free radicals (see Chapter 1.4.1.4). In addition, changes in neuronal activity can promote the formation of long-term depression at the synaptic level, an essential mechanism for memory formation. Aβo can also bind prion protein receptors with high affinity and signal the activation of intracellular Fyn kinase through mGluR5 receptors. Fyn kinase can in turn induce disruption of synapses through hyperphosphorylation of tau. Importantly, through its interaction with α7-nAChR, Aβo can block physiologic anti-inflammatory signaling and promote neuroinflammation (see Chapter 2.6.1).

1.5.2. Neurofibrillary tangles (NFT) and Tau

The second-best-known hallmark of AD is the intracellular neurofibrillary tangles formed by an accumulation of hyperphosphorylated tau. These brain lesions are not only observed in AD but also in other pathologies known as tauopathies. Tau is a microtubule-associated protein present in different isoforms product of the alternative splicing from the gene MAPT. There are 6 possible isoforms of tau combining the presence of 0, 1 or 2 N-terminal repeats (0N, 1N or 2N) and 3 or 4 microtubule binding sites at C-terminus (3R or 4R). In physiological conditions, 3R and 4R tau isoforms are in a 1:1 ratio balance. However, in AD, 4R expression is increased, specifically in neurons suffering from Tau-induced toxicity.

Similarly to other microtubule-associated proteins, tau participates in microtubule formation, microtubule stabilization and axonal transport. Post-translational modifications, such as phosphorylation, can alter its capacity to bind the microtubules (Figure 7). In AD, the kinase/phosphatase activity balance is disrupted and an increase in kinases and/or decrease in phosphatase activity is observed [48]. The consequent hyperphosphorylation of tau results in cytoskeleton instability, which in turn leads to impaired axonal transport, neuronal dysfunction, synapse loss and ultimately, degeneration. In addition, tau hyperphosphorylation induces conformational changes in the protein towards a β-sheet conformation. Like Aβ, tau does not have a stable secondary or tertiary structure. Rich β-sheet conformation, which is induced by post-translational modifications, makes tau more prone to aggregate into oligomers, fibers, and finally neurofibrillary tangles (NFTs). NFTs are abnormal intracellular insoluble aggregates formed by hyperphosphorylated tau organized mainly in paired helical filaments (PHFs) (reviewed in [49]).

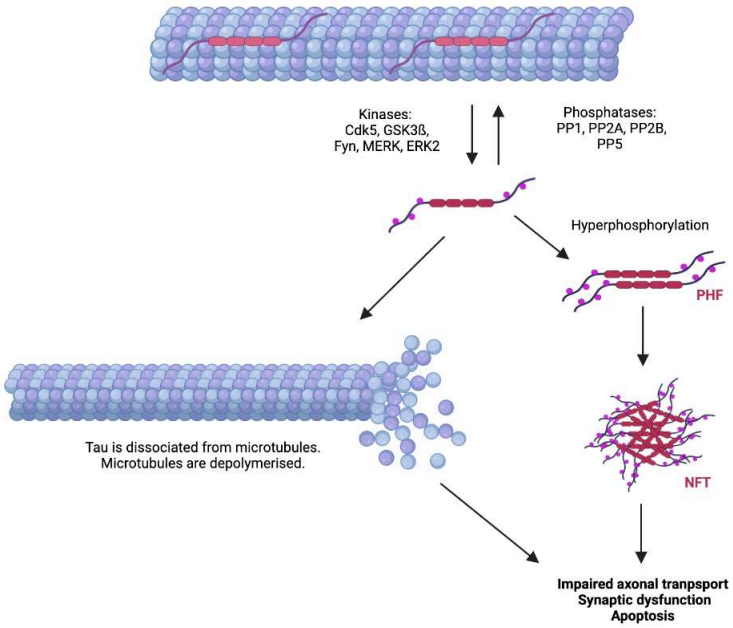

Figure 7. Consequences of tau hyperphosphorylation.

Dysregulated activity balance between kinases (GSK3β, CDK5 and Fyn) and phosphatases (PP1, PP2A, PP2B and PP5), leads to tau hyperphosphorylation. Consequently, tau is dissociated from microtubules, which collapse. This, together with the oligomerization of hyperphosphorylated tau, leads to axonal transport impairment, synaptic dysfunction and consequently, apoptosis. Adapted from [50] done with Biorender.

Neurofibrillary tangles have been shown to propagate in very distant areas of the brain. In AD, they first appear in the entorhinal cortex followed by other connected regions like the hippocampus and the cortex. It is believed that hyperphosphorylated tau aggregates can be transferred from one cell to another, and induce the formation of NFTs in apparently healthy cells. The prion-like Tau propagation hypothesis postulates that the toxic protein can be released from donor cells through exosomes or directly from the plasma membrane. Thereafter, both neurons and microglia can internalize tau through endocytosis and once inside the cell, induce endogenous tau to aggregate through mechanisms, which are still poorly understood (reviewed in [49]). In mouse models, injection of synthetic tau aggregates or brain extracts from human patients induces pathological tau and its spreading to distant brain areas [51]. In-vitro, NFTs have been shown to be transferred from one cell to another [52]. In-vivo, there is a sequential progression of NFTs throughout the brain. This begins with the formation of NFTs in the entorhinal cortex, followed by the CA1 region of the hippocampus, limbic structures, amygdala, thalamus, and claustrum. Subsequently, cortical areas are affected, and lastly, NFTs appear in the primary sensory, motor, and visual cortical regions of the brain [53].

1.5.3. Neuroinflammation

Neuroinflammation is a complex inflammatory response that protects the brain from aggressions and is also observed in neurodegenerative diseases. In the brain, astrocytes and microglia are the principal cell types responsible for the inflammatory response. They do so by producing inflammatory signals, such as

cytokines (IL-1β, IL-1, IL-18, and TNF), chemokines (CCL1, CCL5, and CXCL1), nitric oxide (NO) and activating the complement response. Other cell types like capillary endothelial cells and peripheric cells, that can infiltrate after damage to the blood-brain barrier (BBB), are also of great importance [54].

In AD, pathogenic Aβ and Tau misfolded species can activate glial cells and start an inflammatory cascade. It is believed that at the initial stages of the disease, the inflammatory response can be beneficial and help neuronal repair. However, when the inflammation persists, chronic exposure to pro-inflammatory cytokines and increased oxidative stress can damage the neurons by exacerbating the Aβ and Tau-induced toxic effects.

1.5.3.1. Microglia in AD

Microglia are the central nervous system (CNS) innate immune cells, equivalent to resident macrophages in non-CNS tissues [55]. During development, they are derived from myeloid progenitors in the bone marrow and have important roles such as synaptic pruning, synaptic plasticity and immune surveillance [56]. In contrast to macrophages, microglia are self-renewed and, in physiological conditions, do not depend on circulating monocytes in adulthood. These glial cells have phagocytic capacity that can be activated in pathogenic conditions. Activated microglia change drastically their morphology from a highly ramified distribution to an ameboid form. In normal conditions, once the inflammation is resolved, the cells return to their physiological phenotype and carry beneficial functions.

In AD, abnormal Aβ aggregates activate microglial cells, which can internalize the toxic peptide and degrade it through endocytic pathways. This phagocytosis-mediated Aβ clearance mechanism is also accompanied by an upregulation of inflammatory gene cascades. Several surface receptors have been identified to recognize Aβ and facilitate its internalization. For instance, the membrane receptor TREM2 binds Aβo and internalizes it for further degradation. In addition, TREM2 activates intracellular cascades through SYK and GSK3β pathways that subsequently lead to an anti-inflammatory response. In mouse models, TREM2 deficiency leads to increased amyloid load, and an increased TREM2 expression reduces plaques and cognitive impairment [57,58]. Interestingly, genome-wide association studies (GWAS) have identified some variants of the receptor to significantly increase AD risk by 2-4-fold, through the reduction of the binding affinity of the receptor to Aβ [59].

1.5.3.2. Astrocytes in AD

Astrocytes are the most abundant glial cells in the brain. They contribute to neuronal synapse formation, support, and transmission. In addition, they closely regulate cerebral blood by maintaining the BBB. Like microglia, astrocytes are reactive to pathological insults and can change their morphology and gene expression to prevent and resolve inflammation. This phenotype, also known as A1, is accompanied by an increased expression of inflammatory molecules that can lead to neuronal death.

In AD, both Aβ aggregates and pro-inflammatory cytokines released by microglia can lead to astrocyte activation. Activated astrocytes play an important role in the clearance of Aβ through phagocytosis and synthesis of ApoE. This apolipoprotein mediates the delivery of lipids and cholesterol to neurons and glia and participates in Aβ clearance mechanisms. Controversially, astrocytes can also induce inflammation by releasing pro-inflammatory cytokines and activating reactive nitrogen species and reactive oxygen species (ROS), which then aggravated the disease. In post-mortem samples of AD patients, recruitment of A1-activated astrocytes is often detected close to amyloid plaques [60,61]. At the synaptic level, pathologically activated astrocytes release excessive levels of GABA, glutamate and ATP, leading to neuronal hyperexcitability and synaptic lost [62,63]. In addition, their close regulation of BBB can be compromised**,** and an increased permeability of the barrier can lead to infiltration of peripheral cells into the brain.

1.5.4. Oxidative stress and mitochondrial dysfunction

Oxidative stress refers to an imbalance between the production of ROS and the cellular antioxidant capacity [64]. Because of a natural low antioxidant capacity and high oxygen consumption rate, neurons are very sensitive to changes in oxidative stress and mitochondrial damage [65]. ROS are chemical species formed after incomplete reduction of molecular oxygen including superoxide radical ($O_2^{\cdot-}$), hydrogen peroxide (H_2O_2) and hydroxyl radicals (·OH). These highly reactive species can be produced by endogenous processes or obtained through extrinsic sources. In the cytosol, the transmembrane NADPH oxidase enzyme can transfer electrons from NADPH to oxygen molecules creating $O_2^{\cdot-}$. In the mitochondria, ROS can be obtained through the electron-transport chain reaction, which is the cell's essential mechanism of ATP generation. Oxygen molecules are the ultimate acceptors of electrons in this process, resulting in superoxide radicals as well. Superoxide is quickly processed by the mitochondrial superoxide dismutase obtaining H_2O_2, the majoritarian ROS species in our system. In addition, metal ions like iron can catalyze the conversion of $O_2^{\cdot-}$ or H_2O_2 to the highly reactive ·OH. Exogenous insults such as ultraviolet light, pollutants or radiation can also rapidly generate ROS. Highly reactive species like ·OH have very short lifetimes as they oxidate a wide variety of molecules. Lower reactivity species including H_2O_2 or $O_2^{\cdot-}$ have more

selective targets. Proteins like phosphatases containing a Cysteine residue can be oxidated by ROS inducing a conformational and consequent activity change. Interestingly, oxidation of PP2A facilitates activation GSK3β, one of the kinases responsible for Tau phosphorylation. ROS can further oxidate lipids and directly interact with DNA, changing cell membrane fluidity and inducing toxic damage, respectively (reviewed in [66]).

In physiological conditions, mitochondria can modulate intracellular calcium levels by quickly absorbing the ion when rising levels are detected in the cytoplasm. This is an essential buffering mechanism to keep in-range levels of cytoplasmic calcium and avoid toxic overload [67]. However, when excessive calcium is absorbed in the mitochondria, an increase in ROS production and inhibition of ATP synthesis is induced. An important player in the electron-transport chain reaction, the cytochrome C is released to the cytosol, a signal to induce caspase activity and cell apoptosis. In AD, a deficiency in cytochrome c oxidase accompanied by an increase in ROS production and a deficiency in ATP is observed [68]. Throughout the pathology progression, mitochondria are simultaneously the producer of ROS and a major target of its toxic effect [69]. Reduced mitochondrial function leads to oxidation of the previously mentioned molecular targets, reduced energy sources, calcium signaling deregulation and ultimately cell death.

1.5.5. Cholinergic loss

In 1976 Peter Davies and A.J.F. Maloney introduced the cholinergic hypothesis of AD based on the observations of a deficit in choline acetyltransferase (ChAT), the enzyme responsible for the synthesis of Acetylcholine (ACh), specifically in the amygdala, hippocampus and cortex of AD patients [70–72]. In addition, a specific loss of cholinergic cells in the nucleus basalis of Meynert (NBM) of the basal forebrain, the source of cortical cholinergic innervation, was identified [73,74]. NBM cholinergic neurons have a pivotal role in cognitive function and attention, therefore their loss could partially explain the clinical manifestations of AD. In addition, loss of ACh-mediated control of the BBB could lead to impaired drainage and Aβ clearance from the brain. These series of events inspired a growing number of clinical trials. Three of the successful trails resulted in the development of Donepezil, Rivastigmine and Galantamine, three drugs that target the cholinergic system by inhibiting the enzyme responsible for metabolizing ACh in the synaptic cleft; acetylcholinesterase (AChE), which then increases the neurotransmitter levels in the synapse [75].

Currently, we know that the cholinergic system is extensively impaired in AD. Of interest, nAChR, are significantly reduced in the cerebral cortex of patients with AD [76–79], and have been proposed to be the key

players of the disease pathophysiology [80]. The homopentameric α7 receptor was the first nAChR to be linked to AD due to its capacity to bind Aβ and facilitate the peptide internalization through endocytosis [80–82]. Aβ binding to αnAChR can lead to both the activation and inhibition of intracellular pathways related to plasticity, neuroprotection, learning, and memory. The effects of Aβ-nAChR interactions highly depend on the exposure time and Aβ concentration; when Aβ is present in low concentrations and for a short period of time, it is believed to have an α7-nAchR-driven physiologic and homeostatic effect. However, when its concentrations and incubation time increase, like in AD, it can lead to the opposite effects. Another type of nAChR containing the β2 subunits were also shown to be involved in the disease. β2 subunit usually forms heterotetrametric receptors with α4, but it can also assemble to α7 composing the α7β2 nAChR. This receptor shows the highest sensitivity to Aβ toxicity and it is only expressed in basal forebrain cholinergic neurons and hippocampal interneurons [83–85] .

Recently, GWAS have reported a link between nAChR expression doses and AD. Interestingly, the low number of copy number variance (CNV) of the newly discovered human-specific *CHRFAM7A* receptor correlate with a higher risk of developing the disease [86–88]. *CHRFAM7A* is a recent partial duplication of the α7-nAChR which is present only in humans. This species specificity could explain, at least in part, the reported higher vulnerability of human cells to neurodegeneration when compared to mouse counterparts [89]. A deeper evaluation of the roles of α7-nAChR and *CHRFAM7A* in AD is presented in Chapter 2.6.

1.6. Risk and protective factors

EOAD or fAD is mostly caused by familiar mutations with autosomal dominant heritability. The most common genetic variants affect either APP or the gamma-secretase complex, which is responsible for APP processing. Mutations in the APP gene were the first events that were discovered due to pioneering research on Down syndrome pathology. Patients with trisomy 21 commonly suffer from AD-like symptomatology and histopathological hallmarks. Therefore, genes in this chromosome were evaluated and several mutations in the APP gene were detected in LOAD families [90]. To date, about a hundred mutations have been described in the APP gene, clustering near the secretases cleaving sites and promoting the amyloidogenic pathway by favoring the action of β and gamma-secretase (Figure 8). While mutations near the β-secretase cleaving site increase both the production of $A\beta_{1-40}$ and $A\beta_{1-42}$ [91], mutations around the gamma-secretase cleavage site specifically increase $A\beta_{1-42}$ [92]. Other mutations in the APP gene include single nucleotide polymorphisms at the Aβ sequence region that increase the self-aggregation capacity of the peptide after cleavage. Interestingly, a rare Icelandic APP mutation (Ala673Thr) can be protective against the disease [63]. Even though mutations in the APP gene are frequent in fAD patients, the most

common mutations are found in the PSEN1 and PSEN2 genes, components of the gamma-secretase complex [94]. Like APP mutations, these modifications can change the enzyme cleavage activity and result in an increase in $A\beta_{1-42}$ production.

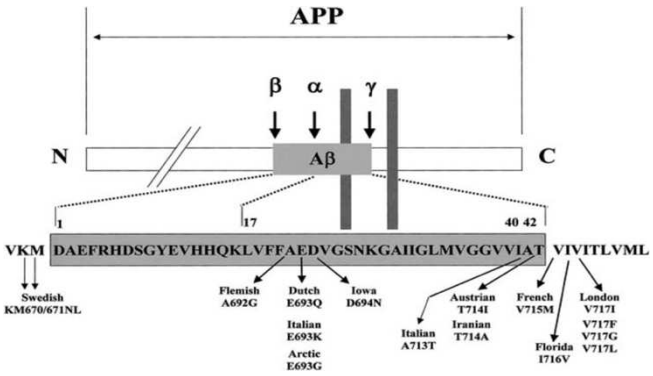

Figure 8. APP mutations found in fAD patients.

Most mutations are in the Aβ coding sequence and around the gamma-secretase cleaving site [95].

LOAD has a complex multifactorial etiology that results from a combination of genetic and environmental factors. Twin studies have shown that the risk of AD is 60-80% hereditable [96] (Figure 9). The most well-known genetic risk factor of AD is the ApoE genotype. Three possible ApoE alleles exist in the population: ApoE2, ApoE3 and ApoE4. The last one, ApoE4, shows the highest affinity to Aβ peptide**,** and it is associated with a poorer clearance capacity and increased aggregation of amyloid plaques. Populational studies indicate that while carrying one allele of ApoE4 increases the risk of AD 3 to 4 times, carrying the E2 isoform decreases risk by 2-fold [97]. Most recently, many polymorphisms in genes involved in microglia function and inflammatory response have been identified through GWAS studies. For instance, TREM2 mutations increase AD risk to similar ratios to those carrying one copy of ApoE4.

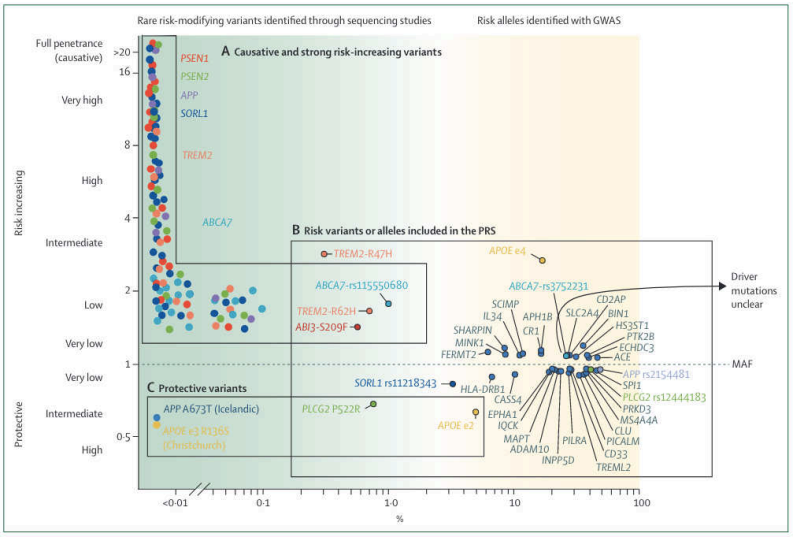

Figure 9. Genetic risk factors of AD.

The top left side of the plot represents the highest penetrance genomic factors with the lowest populational frequency, often detected in fAD patients. LOAD risk factors including mutations in TREM2 or carrying the ApoE4 allele have lower penetrance but are more frequent in the population. Some protective mutations like the Icelandic APP variant or the ApoE2 isoform are also shown [98].

Non-genetic factors like aging, metal exposure, traumatic brain injury, malnutrition, diabetes, or viral infections have also been proposed to be risk factors for the disease. By contrast, a healthy lifestyle involving physical exercise, cognitive activity and a well-balanced diet could be beneficial [99].

1.7. Available treatments and clinical trials

Extensive efforts to develop drug treatments for AD have been carried out over the past decades with little to no success. The constant failure to translate basic research into successful clinical outcomes could be explained by the lack of human complexity in the classic research models used such as animals or cells. Firstly, AD is a pathology directly linked with aging, a difficult factor to reproduce in these models. Secondly, observations obtained from surely simplified research models can be difficult to interpret when considering the etiological and pathophysiological complexity of the disease.

Until recently, the only drugs available for AD were the 3 cholinesterase inhibitors; Donepezil, Rivastigmine and Galantamine, and the NMDA receptor antagonist; Memantine. However, none of these drugs are disease-modifying treatments (DMT) as their effects are palliative. In 2021, the US Food and Drug Administration (FDA) approved the use of Aducanumab, the first DMT AD drug to be accepted. Aducanumab is an anti-Aβ antibody that selectively binds to aggregated firms of Aβ (oligomers and fibrils). In 2019, two Aducanumab phase 3 clinical trials were stopped early due to insufficient treatment efficiency. The drug administration convincingly reduced Aβ plaques in the brain but clinical improvement was only reported in one of the studies [100]. In 2021, the FDA controversially changed their decision and approved the drug through an accelerated program based on a re-evaluation of the clinical trial's data and endpoints. FDA argued that, even though the clinical benefit was not clearly demonstrated, clinical improvement was expected as Aβ levels in the brain were robustly decreased [101]. More recently, a second anti-Aβ antibody-based drug, Lecanemab was approved. In a phase 3 clinical study, 18 months of treatment showed a reduction of cognitive decline and a significant decrease of amyloid plaques in the brain [102].
Despite new drugs are encouraging and bringing hope to the field, no curative treatment is available. A combination of reliable biomarker-based diagnosis and DMT administration at the early stages of the disease will be essential for future therapy development.

The cholinergic system and its role in Alzheimer's disease

2.1. Introduction to the cholinergic system

The cholinergic system is composed of a group of neurons in the brain that use acetylcholine (ACh) as a neurotransmitter. Although cholinergic neurons are relatively few in number, they participate in a wide variety of cognitive functions including learning, memory, attention, sleep-wakefulness, sensory processing, and motor coordination [103]. ACh serves as a neuromodulator in the brain by its action through both muscarinic acetylcholine receptors (mAChR) and nicotinic acetylcholine receptors (nAChR) [104]. Due to the significant involvement of nAChR in AD, this chapter will primarily focus on these receptors.

2.2. Cholinergic system anatomical distribution and physiological roles

Cholinergic neurons are found in two brain structures: the basal ganglia and the basal forebrain [105–108]. Cells in these two structures share similar morphologies but have distinct projection patterns. On the one hand, basal ganglia cholinergic neurons project locally [107,109] and participate in the transitions from sleep to awake states and the regulation of voluntary movement (reviewed in [110]. On the other hand, neurons located in the basal forebrain project to distant brain areas [107] and are implicated in multiple cognitive functions, including synaptic plasticity, learning, memory, arousal and attention and in sleep-wakefulness regulation [111–113] (Figure 10).

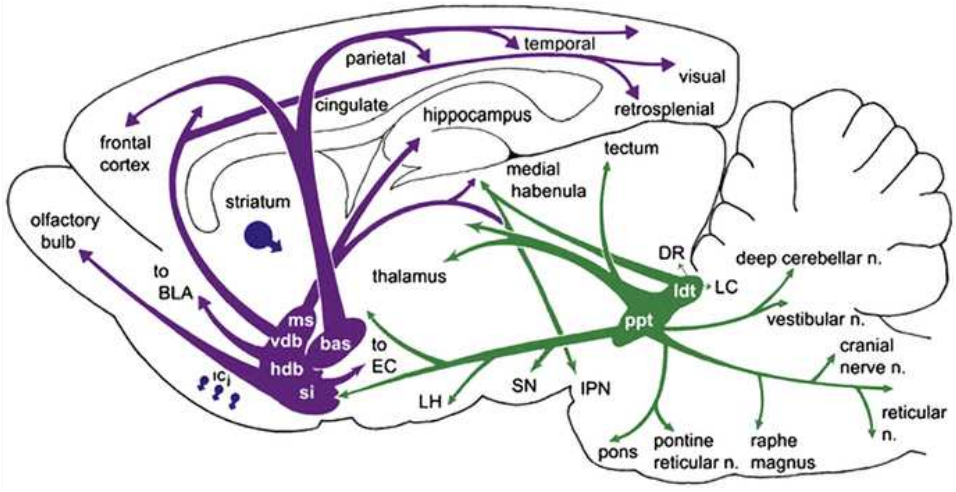

Figure 10. Cholinergic system in the rodent brain.

Representation of the two nuclei of cholinergic cells and their innervation patterns. According to the section classification proposed by Mesulam and colleagues (Mesulam, Mufson, Wainer, et al., 1983), the basal

forebrain system (purple) is composed of regions Ch1 to Ch4. The Ch1 region is localized in the medial septal nucleus (ms) and the Ch2 section is in the vertical diagonal band nucleus (vdb). Both nuclei project mostly to the hippocampus area. The Ch3 region refers to the horizontal diagonal band nucleus (hbd) which projects to the olfactory bulb. Cholinergic neurons in the nucleus basalis of Meynert (bas) compose the Ch4 region which projects to the neocortex and amygdala. The basal ganglia system (green) is divided into Ch5 and Ch6 regions, contained in the pedunculopontine tegmental nucleus (ppt) and the laterodorsal tegmental nucleus (ltd), respectively. Both sections project to the thalamus, basal ganglia structures, and basal forebrain [114].

2.3. Acetylcholine

ACh, the neurotransmitter used by the cholinergic neurons, is an essential neurotransmitter of the brain and of the peripheral nervous system (PNS) where it regulates both the somatic and autonomic systems [115]. ACh is synthetized, and recycled through a well-established mechanism in pre-synaptic neurons as detailed in Figure 11.

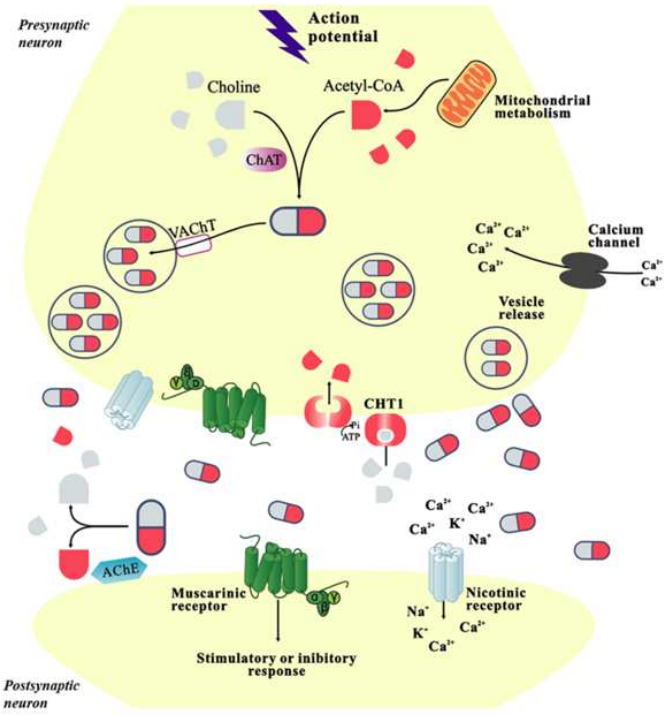

Figure 11. Acetylcholine synthesis and recycling.

In pre-synaptic neurons, ChAT uses choline and acetyl-CoA to produce ACh in the cytosol. Following its synthesis, the vesicular acetylcholine transporter (VAChT) transfers the neurotransmitter to synaptic vesicles. After neuronal depolarization, ACh is released into the synaptic cleft, where it is rapidly hydrolyzed by the extracellular enzyme AChE. This last reaction results in the production of acetate and choline that are re-uptaken by the pre-synaptic neurons by the choline transporter (ChT) and recycled to produce new ACh. In the synaptic cleft, ACh can bind to both mAChR and nACh receptors, leading to G protein-mediated intracellular signaling and the opening of channels, respectively [116].

To carry its actions, ACh binds to both pre- and post-synaptic receptors, including mAChR and nAChR [117], reviewed in [118]. The mAChR are transmembrane proteins coupled with G proteins that trigger intracellular signaling cascades after receptor activation [117]. Through ACh activation, mAChR participate in the regulation of the parasympathetic nervous system needed for maintenance of homeostasis of physiologic processes including heart rate, blood pressure, breather or digestion (Reviewed in [119]). The nAChR are non-selective ion channels that, when activated, enable the movement of ions across the cell membrane. In the PNS, nAChR participate both in somatic and autonomous responses [120].

2.4. The nicotinic acetylcholine receptors

Nicotine acetylcholine receptors (nAChR) are ligand-gated ion channels which consist of five subunits arranged together to form a central hydrophilic pore [121]. nAChR can be found in both the PNS and in the brain. In the PNS, nAChR reside, in the skeletal neuromuscular junction where they mediate voluntary muscle contraction (muscle nAChR)[122]. While neuronal nAChR withing the PNS are typically located in autonomic ganglia where they modulate both the parasympathetic and sympathetic nervous system [123]. In the brain, nAChR are expressed both presynaptically and postsynaptically in various structures (Figure 12).

In mammals, a total of seventeen different subunits for nAChR have been identified and shown to exhibit varying expression patterns in the body [124]. These subunits include α (α1-10), β (β1-4), γ, δ and ε. Muscle nAChR are heteropentameric receptors composed of two α1 subunits, a β1 subunit, a γ subunit and a δ (fetal AChR) or ε subunit (adult AChR) [122]. In the brain, nine α-subunits (α2-10) and three β-subunits (β2-4) have been identified. While α7, α9 and α10 subunits can form homopentameric receptors, α2-6 β2-4 and can form heteropentamers (reviewed in [125]). The different subunit combinations result in distinct pharmacological and kinetic properties, and brain distribution (Figure 12).

Figure 12. Distribution of nAChR in the brain.
Brain regions contain distinct combinations of α and β subunits forming both homo- and heteropentameric receptors. Adapted from [124].

2.4.1. Structure of neuronal nAChR

The detailed structure of nAChR has now been solved by different techniques including high resolution electron microscopy [126,127], X-ray crystallography [128] and computational modeling [129]

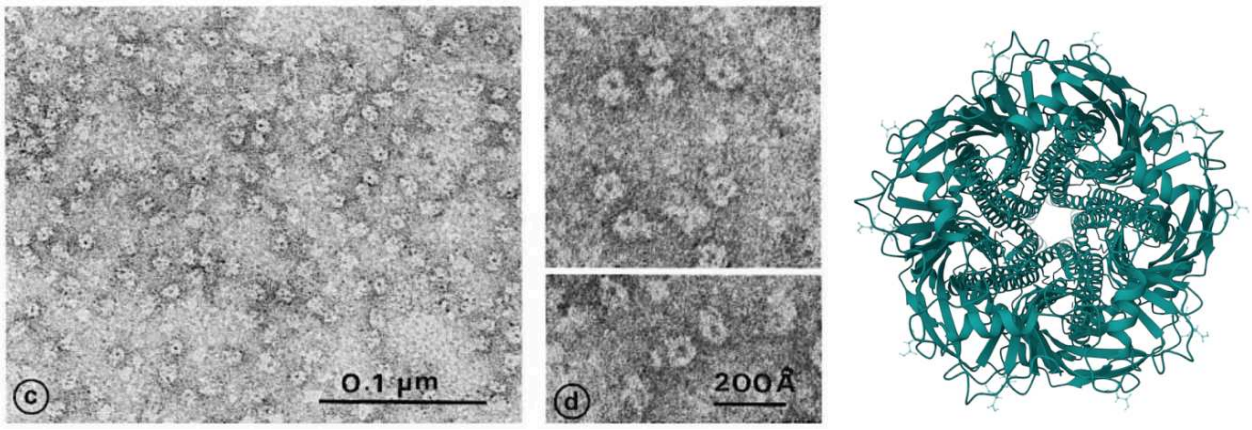

Figure 13. The ring-like structure of nAChR.
First images of nAChR in the electric organ of Torpedo fish using electron microscopy from [127]. Cryo-electron microscopy structure of α7-nAChR in its activated state by epibatidine binding [130].

As previously mentioned, nAChR are composed of 5 subunits forming a ring-like structure. Each subunit consists of an N-terminal extracellular domain (ECD) that contains the distinct Cys-loop[2], 4 transmembrane domains (TM1-4), and a large intercellular loop that connects TM3 and TM4 (Figure 14). The ECD is folded in an immunoglobulin-like β sandwich and contains the ligand binding pocket (LBP), where ACh and nicotine can bind to induce receptor activation and subsequent channel opening.

LBP is located at the interface between two adjacent subunits and consists of a principal and a complementary component. The principal component is formed by three loops (A, B and C) in the α-subunit that directly interact with the agonist through specific amino acid residues. Additional D, E and F loops form the complementary component in the neighboring subunit, which facilitates ligand binding by helping to maintain a proper LBP conformation [124]. In the brain, ligand binding sites occur at the interface between α-subunits and β-subunits, except for the homomeric α7-nAChR where two adjacent α-subunits form the LBP. According to the pentamer composition, the number of binding sites can range from 2 to 5.

The transmembrane domains are folded in α-helix conformation and arranged into a bundle, with the TM2 segment of each subunit forming the pore wall. Within this domain, there are allosteric sites that can be targeted by receptor modulators. Allosteric modulators are components that can bind to the receptors in positions other than the ligand binding site, also known as orthosteric site. Some allosteric sites can also be found in the cytoplasmic and extracellular domains of the channel.

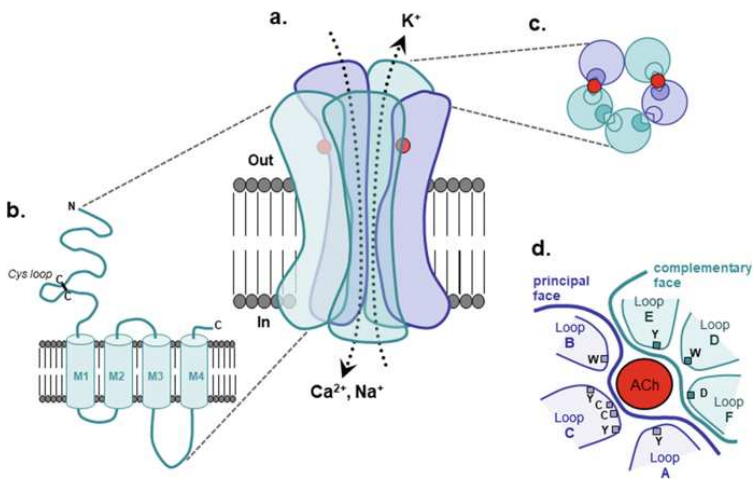

Figure 14. Structure of nAChR.
a. Nicotinic receptors are pentameric transmembrane proteins. When open, these ion channels allow the diffusion of Ca^{+2}, Na^{+} and K^{+} through the membrane. b. Each subunit of the pentamer is formed by an extracellular, transmembrane, and cytosolic domain. c. Agonists like ACh or nicotine can bind at the interface between two adjacent subunits. d. The complementary and principal faces of adjacent subunits form the LBP for ACh binding [131].

[2] Cys-loop: structural motif formed by a pair of conserved cysteine residues that form a disulfide bond. Ligand-gated ion channels that contain this motif are known as cys-loop receptors. This superfamily of receptors includes nAChR, GABA-A receptors, glycine receptors, and serotonin 5-HT3 receptors.

2.4.2. Neuronal nAChR function

nAChR present three configuration states; resting, active or desensitized. The resting state consists of the closed ion channel and can be stabilized by nAChR antagonists like α-bungarotoxin (α-BGT). When the agonist binds to the receptor binding domain, a fast conformational change occurs and results in the opening of the pore. This process can also be initiated by non-endogenous agonists like nicotine and epibatidine. At this stage, the channel facilitates Na^+ and Ca^{+2} inward currents while allowing the efflux of K^+. After the initial activation of the receptor, subsequent conformational changes cause the channel to close, resulting in the desensitized state. In this state, nAChR channels remain closed even in the presence of an agonist, rendering them unresponsive to further stimulation (Reviewed [130]). Counterintuitively, the fast active state of nAChR exhibits low affinity to agonists with a dissociation constant (Kd) for ACh ranging from 50-100 mM, while the desensitized state shows higher affinity to both agonist and antagonist, with Kd values for ACh of approximately 1 mM for fast desensitized state and 3-5 nM for slow desensitized state. It is thought that the low affinity of agonist for the receptor in its open state enables repetitive and fast signal transmission [132–135].

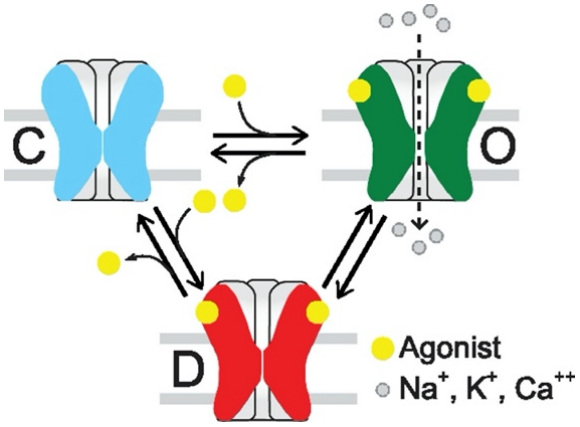

Figure 15. nAChR configuration states.
Closed (C), open (O) and desensitized (D) [136].

The transition between the different receptor configuration states can be altered by allosteric modulators. Allosteric modulators have two potential modes of action: they can inhibit receptor activation by agonists (known as negative allosteric modulators or NAM), or they can amplify the effects of agonist activation (known as positive allosteric modulators or PAM). This can be achieved by altering the agonist's efficacy or by modifying the energy barrier between different conformational states of the receptor [137]. In addition to classical PAMs and NAMs, there are also silent allosteric modulators (SAMs) which do not directly potentiate or inhibit the receptor, but instead can block the effects of other allosteric modulators by competing for the binding site [138].

2.5. The alpha7 nicotinic receptor and its human specific duplication: *CHRFAM7A*

2.5.1. The α7-nAChR

The α7-nAChR represents one of the most prevalent nAChR in the CNS expressed in brain regions that are important for cognitive functions such as the hippocampus, cortex, amygdala and basal forebrain [136]. The homopentamer is present in both pre-synaptic and post-synaptic neuronal compartments, primarily functioning as an ion channel. The α7-nAChR has distinctive traits like fast activation and desensitization upon agonist stimulation, as well as a notably elevated calcium permeability, low affinity for nicotine and selective inhibition by α-BGT and methyllycaconitine (MLA). In neurons, an increase in intracellular calcium levels mediated by the α7-nAChR can trigger various physiological responses, such as cell depolarization, neurotransmitter release, and the liberation of additional calcium from intracellular stores. These responses are crucial mechanisms of synaptic plasticity, and their precise regulation by α7-nAChR is essential for maintaining proper synaptic function. For example, in the CA1 hippocampal region, activating α7-nAChR through cholinergic input during 100 ms before the glutamatergic input via the Schaffer collateral pathway induces long-term potentiation [139]. However, if α7-nAChR is activated only 10 ms prior to the glutamatergic input, short-term depression occurs, which is mediated by pre-synaptic inhibition of glutamate release [139].

α7-nAChR is also highly expressed in immune cells including resident macrophages and lymphocytes in the periphery and by microglia and astrocytes in the brain [140]. In these non-neuronal cells, the receptor primarily facilitates metabotropic signaling to modulate inflammatory responses through the cholinergic anti-inflammatory pathway. When the vagus nerve releases acetylcholine as part of its functions within the parasympathetic nervous system, it activates α7-nAChR. This, in turn, triggers two major intracellular pathways: Jak2/STAT3 and PI3K/Akt. The Jak2/STAT3 pathway involves the phosphorylation of Jak2, which then phosphorylates STAT3. This inhibits the translocation of NF-kB to the nucleus and prevents it from acting as a transcription factor for inflammatory gene expression, such as pro-inflammatory cytokines. Furthermore, phosphorylated STAT3 can form dimers and translocate into the nucleus, where it regulates the transcription of suppressor of cytokine signaling 3, a cytokine-inducible negative regulator of cytokine signaling. The second pathway involves PIK3 and Akt, where PIK3 activation leads to the phosphorylation of Akt, which induces the translocation of Nrf2 into the nucleus. In the nucleus, Nrf2 coordinates cellular antioxidant response by activating genes such as heme-oxygenase 1 (reviewed in [141]). Therefore, the proper functioning of α7-nAChR is vital for regulating inflammatory responses in immune cells.

2.5.1.1. Genomic and protein structure

α7-nAChR subunits are encoded by the *CHRNA7* gene. This 75000 bp gene consists of 10 exons and 9 introns that transcribe a 1509 bp cDNA sequence. *CHRNA7* is located in the chromosome 15q13 region, which is particularly susceptible to genome instability due to the presence of low copy repeats within the sequence. Genomic variation in this region involving deletions and duplications have been implicated in a variety of neuropsychological disorders including schizophrenia, bipolar disorder, autism spectrum disorder and AD [142–144].

CHRNA7 encodes a 57 KDa protein structured in a similar fashion to other nAChR with an ECD, four transmembrane domains and an intracellular loop (Figure 16).

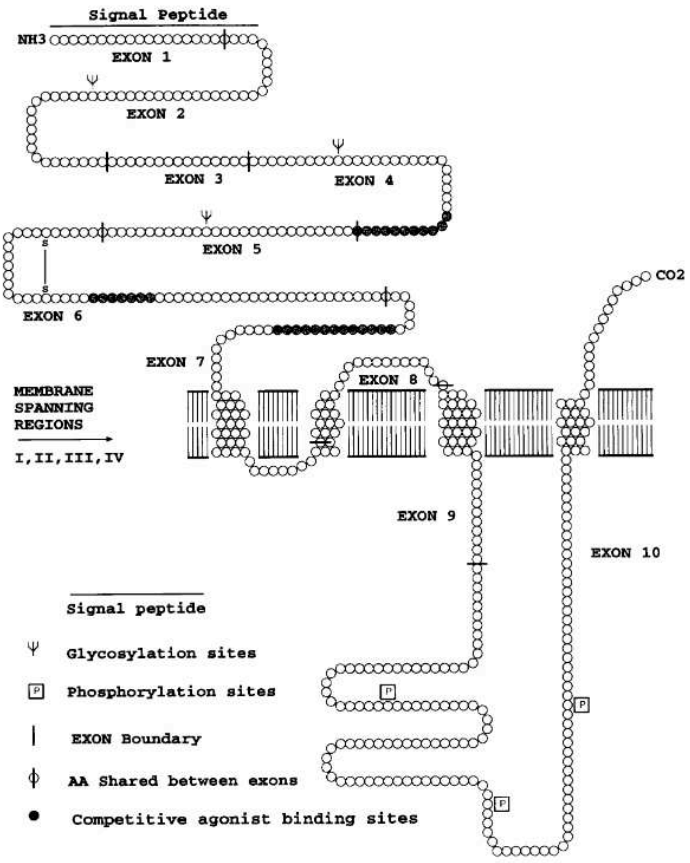

Figure 16. Structure of an α7-nAChR subunit.

The extracellular domain is composed of exons 1 to 7. In this region, important sites for receptor trafficking and ligand binding are found, namely the signal peptide[3] (exon 1-2), glycosylation sites (exon 2, 4 and 5) and the well-known Cys-loop (exon 6). Exon 7, exon 8 and exon 9 encode the transmembrane domains 1, 2 and 3, respectively. The cytoplasmic loop is encoded by exon 10 and contains several sites for post-translational modification like phosphorylation by protein kinases [145].

[3] Signal peptide: N-terminal sequence used for directing the entry of a protein into the endoplasmic reticulum for assembly and transport.

2.5.1.2. Synthesis and trafficking

nAChR are glycoproteins synthetized through the classical protein biosynthesis pathway. Ribosomes within the endoplasmic reticulum (ER) translate mRNA to produce the protein's amino acid sequence. In the ER, preassembled oligosaccharides that are rich in mannose sugars are added to the newly synthesized protein. With the assistance of ER-residing chaperones, folding and oligomerization of proteins is possible at this stage. To prevent the accumulation of incorrectly folded proteins, the quality control mechanism known as ER-associated degradation can identify any folding abnormalities and, by a ubiquitin-dependent mechanism, relocate the protein to the cytosol where it is then degraded. Correctly folded proteins are transported to the Golgi apparatus for further processing. The Golgi apparatus contains enzymes that can trim and modify the oligosaccharides into more complex structures before reaching the final destination. Mature proteins are then packed into vesicles and transported to the cell surface [146].

The α7-nAChR subunits, like all glycoproteins, undergo synthesis in the ER. After the amino acids sequence is generated, the peptide undergoes a series of post-translational modifications, including cleavage of the signal sequence, oxidation of disulfide bonds, and glycosylation at three specific sites (N46DS, N90MS, and N13AS) (reviewed in [147]). In the case of nAChR receptors, correct folding and pentamer assembly are believed to be necessary before the protein can be exported to the Golgi apparatus and ultimately to the membrane [148,149]. The receptor maturation process is complex and inefficient, taking around 2-3 hours, with only a fraction of the nAChR synthesized reaching their final destination. Two chaperones, the nAChR chaperone TMEM35a (NACHO) and resistance to inhibitors of cholinesterase 3 (RIC3), are believed to play key roles in the assembly and transportation of the receptor to the plasma membrane.

2.5.1.2.1. α7-nAChR chaperones NACHO and RIC3

NACHO and RIC3 are both resident ER chaperones involved in α7-nAChR folding and oligomeric assembly of pentamers. The role of RIC3 in the maturation process of receptors was initially discovered in *C elegans* [150,151]. In this system, the expression of the chaperone is essential for nAChR assembly and function. However, the impact of RIC3 on α7-nAChR processing in mammalian systems appears to be moderate and highly dependent on cell line and experimental conditions [152–154]. NACHO, on the other hand, is essential for α7-nAChR assembling and maturation in mammalian cells. In culture systems, α7-nAChR transfections typically do not result in robust surface expression of the receptor. However, co-expression with NACHO enhances its surface expression [155]. Recent data have demonstrated that RIC3 and NACHO work synergically to induce the receptor expression in the membrane.

Studies from Bredt's laboratory have found that expression of α7-nAChR alone or co-expression with RIC3 expression did not result in receptor surface expression nor intracellular folded α7-nAChR pentamers. However, co-expression of α7-nAChR with NACHO led to a robust increase in both membrane and intracellular receptors. Furthermore, co-expression of α7-nAChR with NACHO and RIC3 induces an increase in receptor expression on the cell surface, without any additional effect on the intracellular pool of receptors [155].

Recent studies from the same laboratory provided insights into the specific molecular interactions between chaperones and receptors. Through the creation of receptor domain chimeras, Bredt and collegues identified that residues L264 and G265 in the transmembrane domain 2 were critical for NACHO-mediated effects. In contrast, and in accordance with previous studies, RIC3 did not interact with the transmembrane domain but instead interacted with the intracellular loop [156]. In addition to the TM2 region, the glycosylation of α7-nACHR was found to be essential for NACHO-mediated chaperone function. Single mutations in any of the three α7-nAChR glycosylation sites lead to reduced NACHO-mediated surface receptor labeling of at least 90%. Lastly, NACHO was found to interact with ribophorin 1 and 2 and calnexin, all of which are key players in the initial glycosylation at the ER. Mutations in the ligand binding pocket region did not influence the effects of either chaperone [157].

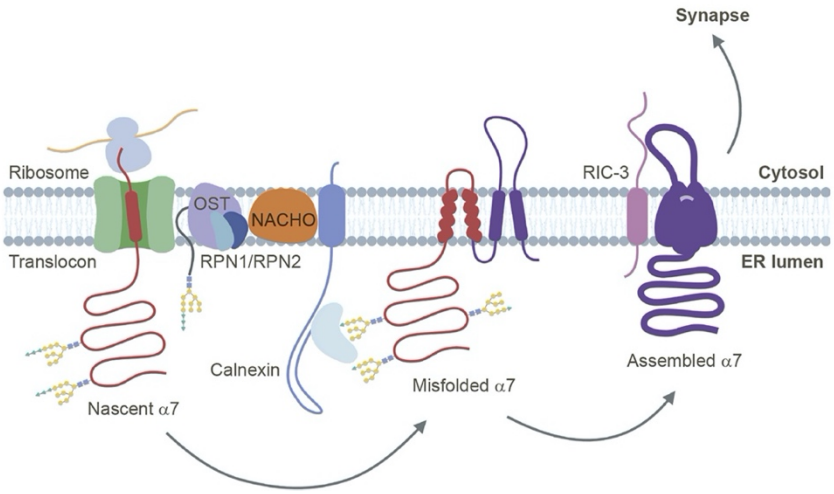

Figure 17. The model proposed for α7-nACHR biosynthesis and trafficking.
NACHO mediates the folding of nascent nAChR by assembling with RPN1 and 2 and with calnexin which may mediate α7-nAChR assembly by regulating glycosylation and folding. After proper folding, pentameric nAChR go to the Golgi and plasma membrane a step facilitated by RIC3 [157].

2.5.1.2.2. Nicotine – chemical chaperone

Nicotine has been shown to upregulate its own receptors, with evident effects in the high-affinity α4β2 nAChR but also α7-nAChR [158,159]. The up-regulation occurs via a post-transcriptional mechanism, as there are no changes in nAChR mRNA levels [158]. Additionally, the up-regulation is present even when protein

synthesis is blocked, indicating a post-translational regulation. Furthermore, nicotine appears to specifically increase high-mannose species of nAChR without altering the receptor's trafficking towards the Golgi and cell surface. This suggests a mechanism in which nicotine acts as a chemical chaperone or maturation enhancer, enabling nAChR species to escape from the ER-associated degradation and reach the cell surface [160].

2.5.2. *CHRFAM7A*

CHRFAM7A is a human-specific gene that encodes the nicotinic acetylcholine receptor (nAChR) subunit dupα7. This gene originated about 200,000 years ago, after a fusion between the *CHRNA7* gene, encoding the α7-nAChR, and the *ULK4* gene [161]. *CHRFAM7A* is located in the genomic unstable 15q13.3 region. The human nicotinic subunit can assemble with α7 subunits, and form functional receptors [162]. Importantly, various pieces of evidence suggest that the expression of the dupα7 subunit results in the dominant negative regulation of the α7-nAChR [163,164].

2.5.2.1. Genetic origin and population variation

CHRFAM7A is a hybrid gene resulting from the fusion of exons 5 to 10 from the original *CHRNA7* gene and exons A-D from the *FAM7A* genetic element. *FAM7A*, in turn, was created by a duplication of the *ULK4* gene found on chromosome 3 and the incorporation of exons from the *GOLGA8B* gene on chromosome 15. The newly formed *CHRFAM7A* gene, located approximately 1.6 Mb upstream of *CHRNA7*, consists of 9 exons arranged in the order 5'-D-C-B-A-5-6-7-8-9-10-3' (direct allele)[145]. In some individuals, a 2-base pair deletion polymorphism in exon 6 has been detected (Δ2bp variant) and associated with the inversion of the gene orientation (inverted allele) [165]. Due to 99.9% homology between exons 5 to 10 of *CHRFAM7A* and *CHRNA7* [145], distinguishing between the two genes in GWAS can be difficult as reads are often mistakenly aligned to the ancestral genes.

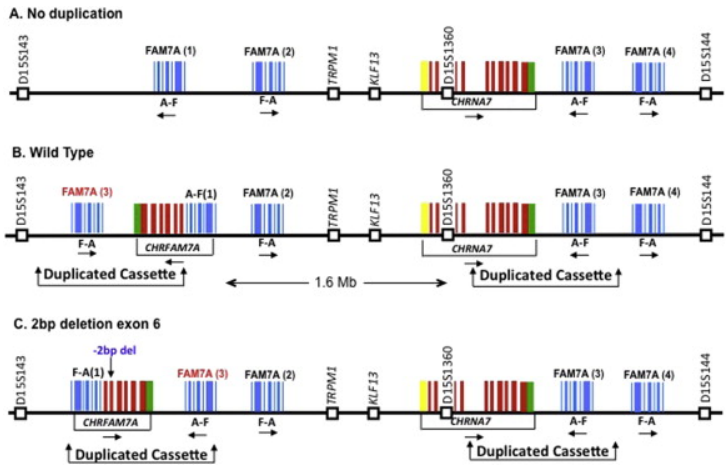

Figure 18. Origin of the *CHRFAM7A* fusion gene.

a. ancestral genotype not carrying the human-specific duplication. b. Wild type genotype in the human population, one copy of *CHRFAM7A* in head to tail orientation with *CHRNA7* parental gene. c. Δ2bp variant carrying the deletion in exon 6 and in an inverted orientation compared to the wild type *CHRFAM7A* allele [161].

CHRFAM7A exhibits CNV in the human population, with some people having between zero and three copies (Table 2). This genomic diversity has been associated with several cognitive disorders including bipolar disorder, endophenotypes of schizophrenia such as P50 sensory processing deficit [165–169], tobacco addition [170] and AD [86,143,171]. The specific role of *CHRFAM7A* in AD is further discussed in chapter 2.6.

	Flomen 2006 [166]	**Sinkus 2009** [169]			**Petrovskyet** [167]
Genotype	**-**	***A-A***	***C***	***H***	**-**
11	2%	5%	0%	0%	-
12	10%	3%	16%	32%	12%
13	6%	2%	6%	11%	16%
22	26%	58%	23%	11%	17%
23	39%	20%	46%	43%	41%
33	17%	12%	10%	3%	15%
***n* =**	*187*	*60*	*192*	*37*	*103*

***** 1 = Ancestral allele, 2 = Direct allele, 3 = Inverted allele (2bp)

		Sinkus 2015 [161]	**Szigeti 2014** [171]	**Cameli 2018** [170]	**Szigeti 2020** [172]
Genotype	**Copies**				
11	**0**	1%	2%	1%	1%
12, 13	**1**	20%	16%	18%	18%
22, 23, 33	**2**	78%	82%	77%	80%
-	**3**	3%	2%	5%	2%
Genotype	**Allele**				
11, 12, 13	**A**		-	9%	9%
12, 22, 23	**D**		-	46%	49%
12, 23, 33	**I**		-	44%	42%
	***n* =**		*499*	*194*	*657*

***** 1 / A = Ancestral allele, 2 / D = Direct allele, 3 / I = Inverted allele (2bp)

Table 2. *CHRFAM7A* CNVs in the population.

Three possibilities including not having the *CHRFAM7A* gene (ancestral allele, genotype 1 or A), having the direct allele (genotype 2 or D) or the inverted form (genotype 3 or I) exist. The combination of these three possibilities can give 6 possible genotypes including 11 (two ancestral alleles, 0 copies of *CHRFAM7A*), 12 (one ancestral allele and one copy of the direct form of *CHRFAM7A*), 13 (one ancestral allele and one copy of the inverted form of *CHRFAM7A*), 22 (two copies of the direct form of *CHRFAM7A*), 23 (one copy of the direct form of *CHRFAM7A* and one copy of the indirect form of *CHRFAM7A*) and 33 (two copies of the indirect form of *CHRFAM7A*).

2.5.2.2. Sequence and structure

As previously mentioned, *CHRFAM7A* shares a homologous sequence with *CHRNA7* from exon 5 to exon 10, implying that the receptor's transmembrane and intracellular domains are conserved. Therefore, the human-specific subunit dupα7 is capable of forming an ion channel when incorporated in the pentamer. However, the ECD is different due to the incorporation of exons A to D from which only B and A are translated. The substitution of exons 1 to 4 from *CHRNA7* for exons B and A of *FAM7A* leads to the loss of essential sequences including the signal peptide, two of the three glycosylation sites, and the ligand binding domain. Consequently, the subunit cannot form an ligand binding domain (LBD) and is likely to encounter difficulties in synthesis, folding and trafficking [173].

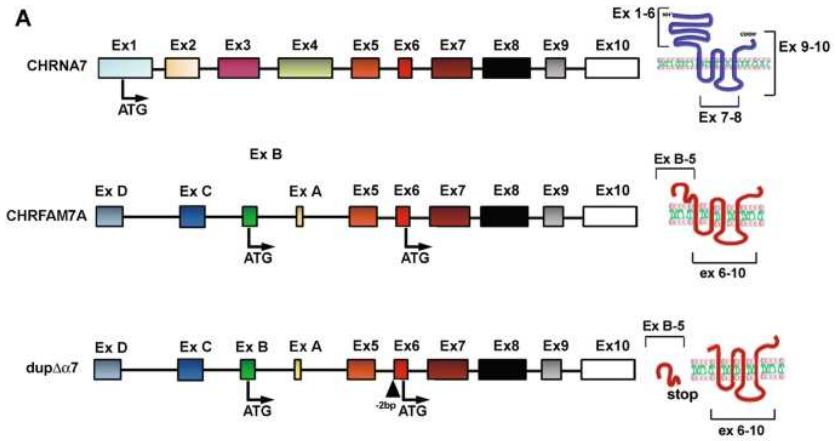

Figure 19. Exons and protein structures of human genotypes. In the ancestral *CHRNA7* gene, the start codon sequence is in exon 1. In the *CHRFAM7A* gene, two possible starting sequences can potentially be used, one in exon B and one in exon 6. In the Δ2bp variant, a premature stop codon appears in exon 6 caused by a shift in the reading frame. This potentially leads to the generation of a small soluble product and a transmembrane protein translated from the second start codon in exon 6. Nonetheless, the translation of Δ2bp variant is still to be proven and some argue that it is highly improbable to occur [172].

2.5.2.3. *CHRFAM7A* is a *CHRNA7* dominant negative regulator

CHRFAM7A acts as a dominant negative regulator of *CHRNA7* through two possible and non-exclusive mechanisms. Firstly, the dupα7 protein can incorporate the α7-nAChR pentamer and reduce the number of ligand binding sites. Specifically, the pentamer can accommodate up to 3 dupα7 subunits, and for the receptor to be functional, it needs to possess at least two adjacent α7 subunits [163,174]. Supporting this hypothesis, when dupα7 is expressed alone in oocytes, no nicotine- or acetylcholine-induced currents are detected. In addition, when the human duplication and α7 subunits are co-expressed, the agonists-induced currents are decreased as a function of dupα7 dosage [163,164,175] while the receptor sensitivity to ACh is not changed. Conflicting reports exist regarding the impact of dupα7 on the enhancement of the agonist response by the positive allosteric modulator PNU-12596, whose binding site remains unchanged in the human subunit. While one study reported an increase in agonist response [163], others have failed to replicate these findings [162,176] and some have shown a decrease in the receptor's open channel probability when dupα7 is present in the pentamers [177].

Another hypothesis suggests that dupα7 may function as a negative regulator by trapping α7 subunits within the ER compartment. This idea was initially supported by observations of reduced membrane binding sites for ligands in oocytes containing dupα7, as detected by α-BGT labeling [163,164]. Further evidence showed that dupα7 did indeed sequester α7 subunits in the ER, resulting in lower levels of mature α7 receptors at the plasma membrane [178].

CHRFAM7A is highly expressed in immune cells such as macrophages and lymphocytes [179–181]. Here, its expression could significantly change the cholinergic anti-inflammatory response. Studies have shown that during pro-inflammatory stimuli, *CHRFAM7A* expression is downregulated while *CHRNA7* is increased [179,181]. This up-regulation of *CHRNA7* during inflammation may lead to an increase of functional α7-nAChR in the membrane and the activation of the anti-inflammatory pathway. Indeed, in acute sepsis, there is an increase in *CHRNA7* levels that returns to normal when inflammation subsides [182] and patients with a high *CHRNA7/CHRFAM7A* ratio show better prognosis [178]. However, when a chronic inflammatory stimulus is present, an abnormal expression ratio of the genes could lead to a dysregulation of the cholinergic anti-inflammatory response. Indeed, in chronic inflammatory disorders like inflammatory bowel disorder, there is an increase in *CHRFAM7A* expression at the expense of *CHRNA7*, suggesting a potential imbalance in the cholinergic anti-inflammatory response [183].

2.6. Roles of α7nAChR and dupα7 subunit in AD

The α7-nAChR have attracted considerable interest in the context of AD pathology due to their involvement in multiple mechanisms. As previously discussed, these receptors are crucial for synaptic plasticity, which is essential for learning and memory, both of which are commonly impaired in AD. Moreover, the regulation of neuroinflammation through α7-nAChR mechanisms is critical in the pathogenesis of the disease. Additionally, α7-nAChR can mediate Aβ-induced toxic effects, a process that will be explored in greater detail in this chapter.

2.6.1. Aβ-α7nAChR complex: binding and consequences

α7nAChR can directly bind to Aβ peptides with high affinity and mediate its internalization through endocytic mechanisms [184,185]. The internalization of soluble Aβ, shown to precede the formation of amyloid plaques, is highly toxic for the cell as previously discussed in Chapter 1.5.1.3.

The implications of Aβ binding on receptor activity are controversial, as some studies have demonstrated an activation of the receptor while others have proved an inhibition. This disagreement in the literature is probably due to differences in Aβ concentration, conformation, incubation time and experimental system, which could highly alter the effect of the toxic peptide towards the receptor. The general agreement is that short incubation of low picomolar doses of Aβ induces activation of the receptor [186–189], similar to those naturally occurring after agonist activation, where the receptor is in an active or desensitized state. However, at high picomolar concentrations, Aβ inhibits the receptor that is found in a resting-state-like structure [186,188,190,191]. This could explain the discrepancies observed in α7-KO AD mice models, where both exacerbation [192] and improvement [193] of cognitive deficits have been reported.

In addition to its effects on the ionotropic capacities of the α7-nAChR, Aβ also impacts the metabotropic signaling pathway. Briefly, toxic levels of Aβ can trigger neurotoxic signaling pathways, including apoptotic signaling (activation of caspase 3 and inhibition of Bcl2 anti-apoptotic protein) and activation of GSK-3β, which in turn causes tau phosphorylation. By blocking α7-nAChR, Aβ reduces the cholinergic anti-inflammatory response by decreasing the retention of NF-kB in the cytoplasm, which allows it to translocate to the nucleus and trigger the transduction of pro-inflammatory cytokines. These findings suggest that targeting both the α7-nAChR and metabotropic signaling pathways could be a promising therapeutic approach for treating AD by potentially mitigating the toxic effects of Aβ and reducing neuroinflammation.

2.7. *CHRFAM7A* implications in Aβ-α7nAChR interaction

One of the major challenges in the development of cholinergic therapies for AD is the translational gap observed between pre-clinical models and clinical trials. A possible explanation for this gap is the modulation that *CHRFAM7A* exerts on α7-nAChR function. Animal models of AD that respond positively to α7-nAChR targeted drugs only represent a scarce percentage (1%) of the population carrying the ancestral allele. Therefore, preclinical models accounting for *CHRFAM7A* are crucial to understand drug responses and AD vulnerability in the human population.

2.7.1. Human genomic association studies

Some studies have aimed to investigate the possible association between *CHRFAM7A* CNVs and AD. It is important to note that genomic association studies rely on single nucleotide polymorphisms and CNV microarrays from Illumina sequencing data, where each read is typically around 10 to 100 kb. However, exons 5 to 10 of *CHRFAM7A* are identical to *CHRNA7* and exons 1 to 4 are identical to the *FAM* sequence, found multiple times in the genome. Therefore, short reads can lead to misalignment to the ancestral genes.

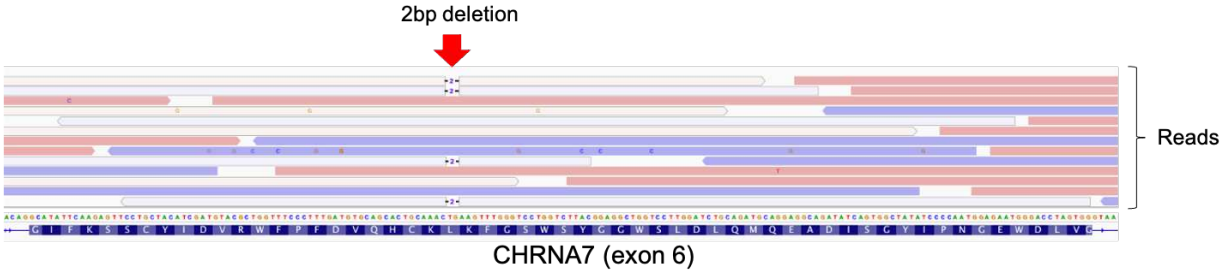

Figure 20. Example of misaligned reads in the *CHRNA7* gene region.
Cell line carrying the 2bp deletion variant (WTSli071-A, Wellcome Trust). Eventhough the 2bp deletion variant is specific to *CHRFAM7A*, some reads containing the deletion (-2-) are mapped in the exon 6 of *CHRNA7*.

Despite the difficulties of proper *CHRFAM7A* genotyping, several GWAS have suggested that CNVs in this gene may be associated with an increased risk of AD (Table 3), with one study reporting an over-representation of individuals who do not carry the Δ2bp *CHRFAM7A* variant in the AD population compared to controls [194].

	Heinzen 2010 [195]	Swaminathan 2012 [87]	Chapman 2013 [196]	Szigeti 2014 [171]
Phenotype	Case/Control	Case/Control	Case/Control	AAO
Sample Size	331/368	794/196	3260/1290	781
Assay	Illumina	Illumina	Illumina	SNP array
Design	SNP association	Enrichment	Enrichment	GWAS
P-value	0,053	0,059	0,22	0,0000137

Table 3. *CHRFAM7A* CNVs associated to AD risk.
The first two Case/Control studies describe a weak association of *CHRFAM7A* CNVs to the risk of AD and the third reported no association. In the latest article by Szigeti et all, they used ordered subset analysis by age at onset (AAO) of AD and found a significant association between the disease and *CHRFAM7A* CNVs [86].

In contrast, a recent study that carefully genotyped patients and controls using PCR and capillary sequencing found no significant link between AD and *CHRFAM7A* CNVs or the Δ2bp variant. Interestingly, this study found that individuals who did not carry a direct *CHRFAM7A* allele showed a significantly greater cognitive improvement in response to donepezil, an AChEI commonly used to treat the moderate forms of AD. The authors suggested that the *CHRFAM7A* genotype could play a critical role in cholinergic-targeted drug responses, which may explain the disparity observed between preclinical research and clinical studies. Under the assumption that the Δ2bp *CHRFAM7A* variant does not produce a protein, individuals lacking the direct form of *CHRFAM7A* may exhibit a predicted successful outcome based on preclinical data, given that animal models also lack this gene. In contrast, individuals with the direct form of *CHRFAM7A* may respond differently to AChEI, suggesting that the *CHRFAM7A* genotype could influence treatment outcomes. This could be of extreme importance as people who positively respond to AChEI treatment represent up to 25% of the population [172].

2.7.2. *CHRFAM7A* interaction with α7-nAChR: in vitro studies

Using induced pluripotent stem cell (iPSC)-derived neuronal progenitors and microglia, Szigeti and colleagues demonstrated a protective role of *CHRFAM7A* in Aβ-induced toxicity. In their studies, they evaluated the impacts of *CHRFAM7A* in the α7-nAChR function, Aβ uptake and inflammatory responses and observed differing yet coherent responses in neuronal progenitors and microglia [172,177,197].

In neuronal progenitors, *CHRFAM7A* carriers displayed lower α7-nAChR channel open probability and currents that desensitized faster after the combined application of ACh and PNU (PAM). After exposure to Aβ, neurons with *CHRFAM7A* showed lower levels of Aβ uptake and increased levels of pro-inflammatory cytokines (IL1β and TNFα) production through a non-NF-kB dependent mechanism. In contrast, cells lacking the human subunit exhibited higher levels of Aβ uptake and increased activation of apoptotic markers (Cas1, Cas8). The Aβ toxic effects could be ameliorated by blocking α-nAChR with MLA. Szigeti and colleagues concluded the extended desensitization in cells with *CHRFAM7A* could result in a shift from ionotropic to metabotropic signaling, which would facilitate intracellular communication. In the presence of Aβ accumulation, neurons may utilize this mechanism to limit Aβ uptake and activate pro-inflammatory cytokines as a "cry for help". [177]. In a later study, the researchers showed that the variant known as Δ2bp-*CHRFAM7A* acted as a null allele. This was demonstrated by the fact that cells expressing this variant displayed similar levels of channel open probability (after agonist and PNU administration) than non-carrier cells, and a high uptake of Aβ [172].

The observations in microglia revealed slightly divergent responses. While Aβ uptake remained lower in *CHRFAM7A*-carrying cells compared to non-carriers, MLA had no effect on the former but increased uptake in the latter. Szigeti et al proposed that in non-carrier cells, blocking α-nAChR signaling hinders the α-nAChR-mediated anti-inflammatory signaling, leading to inflammation and activation of microglia. However, in *CHRFAM7A*-carrying cells, the effect of MLA was insignificant because the normal α-nAChR-mediated anti-inflammatory signaling may have been disrupted. The *CHRFAM7A*-carrying cells did in fact exhibit higher baseline levels of NF-kB-dependent pro-inflammatory cytokines and a stronger immune response to Aβ exposure than non-carriers, where the response only occurred at high Aβ concentrations. In light of these results, the researchers postulated that dupα7 in these cells interacts with the α7-nAChR anti-inflammatory pathway, augmenting immune responsiveness, which could potentially be an advantageous mechanism in AD pathology. [197].

It is noteworthy that cholinergic targeting treatment with AChEI (donepezil, rivastigmine) and encenicline (a selective α7 agonist) showed beneficial effects on Aβ-induced toxicity in cells without a direct allele of *CHRFAM7A*, including cells lacking the human subunit and cells with the Δ2bp variant. In such cells, the AChEI and encenicline treatment reduces Aβ uptake, cytotoxicity, protease activity, and apoptosis, while there is no significant difference observed in cells carrying the direct *CHRFAM7A* allele. This, in conjunction with previously cited clinical data, ~~s~~uggest that individuals who do not carry the direct form of *CHRFAM7A* (accounting for approximately 25% of the population) could derive significant benefits from AChEI drugs for AD [172].

The study model

3.1. Induced pluripotent stem cells (iPSCs) and iPSCs-derived neurons

The discovery of induced pluripotent stem cells (iPSCs) has been a remarkable breakthrough that has revolutionized the possibilities of modeling human diseases. By reprogramming somatic cells from human individuals and patients into iPSCs, and subsequently guiding their differentiation into specific cell types, we now have the means to construct accurate models of human disorders. Moreover, thanks to our deep understanding of the development of the nervous system, it is now possible to differentiate in-vitro iPSCs into neurons in culture. This new approach offers exciting possibilities for better modeling human neuronal disorders and paves the way for personalized medicine.

3.1.1. Stem cells

3.1.1.1. Definition and classification

Stem cells are characterized by two fundamental features: their ability to self-renew and their capacity to differentiate into any type of cell within the organism, under appropriate conditions. Stem cells exhibit the highest degree of "potency," as they can differentiate into both embryonic and extraembryonic tissues. During development, as cells become more specialized, their potency capacity is gradually reduced, a process referred to as differentiation (Reviewed in [198]). Conrad Waddington introduced the "epigenetic landscape model" as a metaphor to explain cell differentiation during early development [199]. According to this model, a ball rolling down an inclined plane illustrates the natural progression of cell development. The top of the hill represents the cell with the highest potency capacity (stem cell), while the bottom of the hill shows several possible alternative mature cell states (Figure 21). However, recent advancements in the field have demonstrated that cell differentiation is not always unidirectional, and development from the bottom to the top (reprogramming) is also possible. In fact, Shinya Yamanaka's discovery of iPSCs in 2006 revolutionized the field of stem cells by demonstrating that cell differentiation is not an irreversible mechanism and that mature cells can be reprogrammed into a high-potency state [200]. Additionally, some cell lineages can undergo a direct transition from one mature fate to another, known as trans-differentiation.

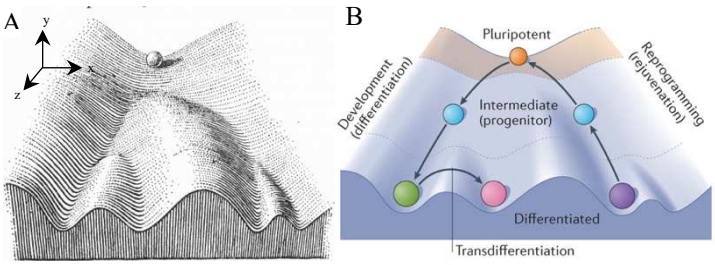

Figure 21. The Waddington epigenetic landscape model.

a. Original drawing by Conrad Waddington. The model is based on an inclined surface with several ridges and valleys, with each ridge representing fate choices that cells undergo during development. The x-axis refers to cell phenotype, the y-axis represents the order of development, and the z-axis represents time. Waddington proposed that the presence or absence of particular genes is what determines a cell's path at a branching point. The model also shows that development potential is gradually restricted over time, leading towards stable, terminal cell fates. b. The current adaptation of Waddington's model includes new discoveries including cell reprogramming and trans-differentiation. Illustrations from [199,201].

As described in Waddington's metaphor, during development, cells undergo a reduction in potency as they differentiate into specific cell types. Stem cells can be classified in several levels of potency, including totipotency, pluripotency, multipotency, oligopotency, and unipotency, each characterized by the range of cell types they can produce. Totipotent cells can differentiate into all cell types, including those in embryonic and extra-embryonic tissues. Pluripotent stem cells (PSC) can differentiate into all three embryonic germ layers, but not extra-embryonic tissues (further described in the following section). Multipotent cells give rise to multiple cell types within a specific lineage, while oligopotent cells have a more limited differentiation potential, producing only a few cell types within a lineage. Lastly, unipotent cells can only differentiate into a single cell type but can divide repeatedly. Dermatocytes, for example, are unipotent cells that produce only one type of cell while keeping its dividing capacity (reviewed in [198]).

3.1.1.2. Origin

3.1.1.2.1. Early embryogenesis and embryonic stem cells

Embryonic development starts with fertilization, a process in which a spermatozoid fuses with an egg in the fallopian tubes to form the zygote. In humans, early embryogenesis occurs during the first week of pregnancy. During that time, the zygote goes through several steps of maturation while traveling through the fallopian tubes until it reaches the uterus, where it implants around the 5th day of pregnancy (Figure 22).

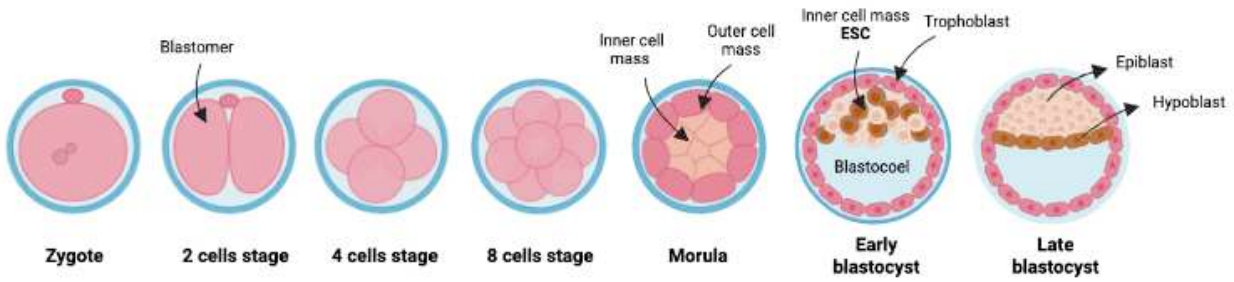

Figure 22. Early embryonic development.

During early embryogenesis, the zygote undergoes multiple cell divisions to form a spherical structure called a morula. This further divides into a blastocyst consisting of an outer layer of cells called the trophoblast and an inner cell mass. The inner cell mass, also called embryoblast contains embryonic stem cells and gives rise to all the embryonic structures and organs. The blastocyst makes contact with the uterus, triggering polarization pushing the inner cell mass towards one pole, letting space to form a cavity. The embryoblast continues to develop and forms two organized layers, the epiblast and hypoblast, that further develops into a flattened structure known as the bilaminar plate. While the hypoblast contributes to the formation of extra-embryonic structures, the epiblast eventually give rise to all the embryonic structures and organs. Done with Biorender.

Embryonic stem cells (ESCs) are pluripotent cells obtained from the inner mass of a blastocyst. In 1981, Evans and Kaufman successfully derived ESCs and established a stable cell line from mouse blastocysts [202]. The first successful derivation of human ESCs and production of a stable line was achieved in 1998 [203]. Since then, researchers have generated over a hundred different lines of human ESCs. However, the generation of these cell lines involves the use and destruction of embryos, which raises ethical concerns and has sparked political debates. To address this issue, one approach is to isolate single cells at earlier stages of development, such as the 8-cell or morula stage, which does not destruct the embryo [204]. Nonetheless, the groundbreaking discovery by Takahashi and colleagues has significantly reduced the need for using human ESCs.

3.1.1.3. Adult stem cells

Adult stem cells, also known as somatic or tissue stem cells, are a crucial but minority population of cells responsible for maintaining tissue homeostasis and repair after injury. Adult stem cells are typically found in specialized niches that provide a supportive microenvironment essential to maintain their dividing capacity. Examples of well-studied adult stem cells include those found in blood, skin, intestine, and muscle

tissue. Although stem cells can be found to a lesser extent in the brain, two neurogenic niches have been identified in rodents: the subgranular zone of the dentate gyrus in the hippocampus and the subventricular zone (SVZ) of the lateral ventricles [205–207]. The existence of adult neurogenesis in humans has been a subject of controversy in the past decade, but recent evidence supports its occurrence (reviewed in [208]).

The regenerative capabilities of stem cells have generated considerable interest in the field of regenerative medicine. For instance, a good illustration of the potential of stem cells in regenerative medicine is skin stem cell therapy, which has demonstrated success in treating burn injuries using multipotent mesenchymal cells derived from the debrided burned tissue to improve wound healing [209]. However, one significant limitation of stem cells' use in clinical therapies is their inherent tendency to form tumors. Nonetheless, the study of the cellular mechanisms that stem cells use to fine control their proliferation in physiological conditions has been a valuable source of knowledge in cancer research [210].

3.1.1.4. Induced pluripotent stem cells

In the early 1960s, the linear view of cell development proposed in the Waddington's model was challenged. Pioneering experiments demonstrated that transferring the nucleus of a somatic cell into an enucleated egg could generate a genetically identical embryo, or clone. Although initial experiments were done in frogs [211,212], they quickly escalated to mammals, leading to the cloning of the world-famous sheep, "Dolly" [213]. These experiments proved that a tissue cell at the bottom of the Waddington's stope could be converted back to the top under the right conditions.

Inspired by these discoveries, Yamanaka and colleagues hypothesized that modulators of gene expression, such as transcription factors, could hold the key to inducing pluripotency in differentiated cells. This was based on the knowledge that, while all cells in our body share the same genomic information, it is the expression or silencing of this information through epigenetic modifications that give them their specific phenotypes. With this in mind, they set out to identify the specific factors that would be necessary for inducing pluripotency in somatic cells. In 2006, the team proved that inducing PSCs from tissue cells was possible, revolutionizing the field of stem cells. The administration with retroviruses of the four transcription factors, Oct4, Sox2, Klf4, and c-Myc, was enough to induce cells like fibroblasts into what they named iPSCs [200]. This discovery drastically impacted the field, eliminating the ethically challenging need for ESC.

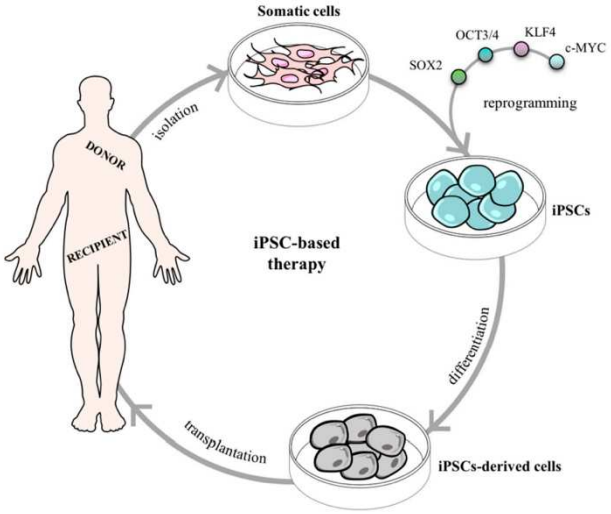

Figure 23. Promising clinical applications of human iPSCs (hiPSCs).

iPSCs pave the way towards personalized medicine. For instance, drugs can be tested in the individual's cells prior to administration or transplantation can be done with no risk for immune rejection [214]. In addition, iPSCs can be used to model diseases directly from patients, avoiding the use of genetically modified systems. However, due to the **potential risk of** tumorigenicity associated with the use of iPSCs, their application in clinics is still in its early stages and approached with caution [215].

3.1.2. Neuronal differentiation

The intricate mechanisms and signaling pathways involved in embryonic neurodevelopment can be imitated in vitro to promote neuronal differentiation. This chapter will explore the process of neurodevelopment and explain the methods used to induce neuronal differentiation in vitro.

3.1.2.1. Early neurodevelopment

Neurodevelopment is a complex process that begins during the third week of human gestation. Before this, two critical steps take place: the formation of the blastocyst and gastrulation. The blastocyst is formed during the first week of development, and it consists of two layers: the outer layer called the trophoblast, and the inner cell mass, which will give rise to the embryo. By the end of the first week of development, the inner cell mass is organized into two layers: the epiblast and hypoblast. During the second week of gestation in humans and by embryonic day (E) 6.5 in mouse, gastrulation occurs. This process involves the invagination of the epiblast along the primary streak, giving rise to the three germ layers: the endoderm, mesoderm, and ectoderm [216].

During the third week of human gestation, the process of neurodevelopment begins with the induction of the ectoderm to form the neuroectoderm. This is followed by neurulation, which leads to the formation of the neural tube. Neural induction and neural tube formation in mouse embryos occurs between embryonic day E6.5 and E8.5 [217] (Figure 24).

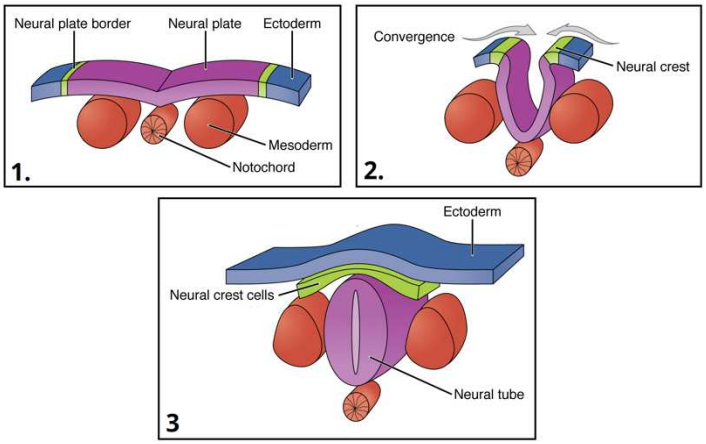

Figure 24. Early neural development. During gastrulation, mesodermal cells (shown in red) invaginate from the epiblast to form a structure called the notochord. The notochord secretes signaling molecules, which induce the overlying ectoderm to differentiate into the neural plate or neuroectoderm (shown in purple). Subsequently, the neural plate undergoes a process called neurulation where it progressively folds in on itself, forming the neural tube. The neural tube is the primitive structure that subsequently develops into both the spinal cord and the brain [218].

During the fourth week of gestation in humans, the neuronal tube undergoes regionalization. This process is regulated by neighboring structures such as the notochord and the ectoderm, which secrete signaling molecules including Sonic hedgehog (Shh), Bone morphogenetic proteins (BMP), Fibroblast growth factors (FGF), Wingless/integrated (Wnt) and retinoic acid (RA). These molecules create concentration gradients along the embryonic axis, which guide the differentiation of the neural tube (Figure 25).

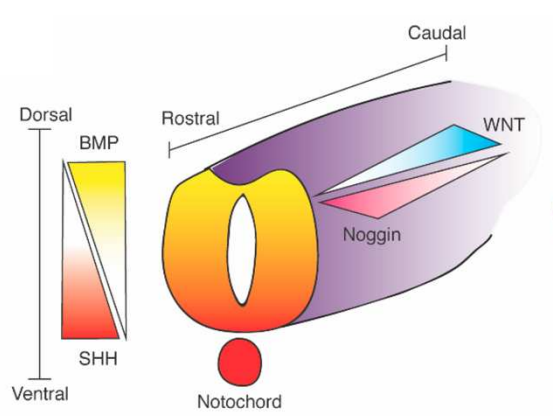

Figure 25. Signaling gradients establish the dorsoventral and rostrocaudal axis. The dorsoventral axis is defined by the antagonist signaling between ventralizing factors like Shh, which is produced in the notochord and ventral part of the neural tube, and dorsalizing factors like BMP, which is secreted from the overlaying non-neuronal ectoderm. The rostrocaudal axis is defined by gradients of Wnt signaling (caudal) and the BMP antagonist Noggin (rostral). In addition, Shh not only has antagonist interactions with BMP but also with Wnt. The combination of gradients obtained from the interplay between these signaling molecules will define the regionalization of the different structures of the CNS [219].

Several steps of regionalization conclude with the formation of the different structures of the CNS. While the anterior portion of the neural tube eventually forms the cerebral hemispheres, the posterior portion forms the spinal cord (Figure 26).

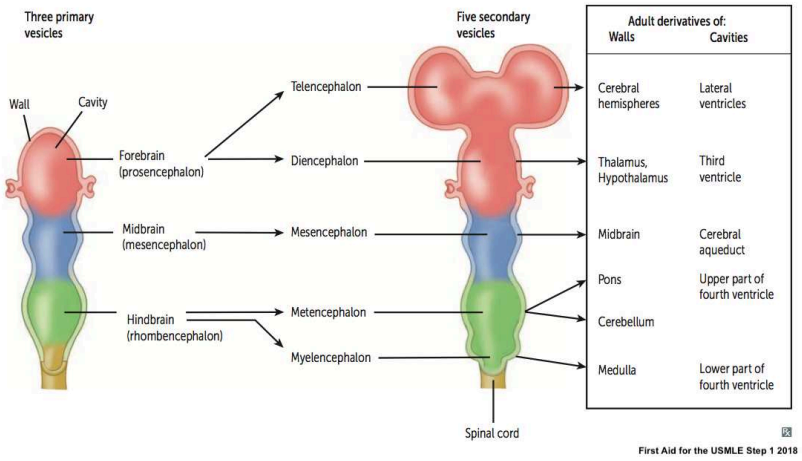

Figure 26. Regionalization of the neuronal tube.

Initially, three primary vesicles are formed: the prosencephalon (forebrain), the mesencephalon (midbrain), and the rhombencephalon (hindbrain). These primary vesicles further divide into five secondary vesicles, with the forebrain dividing into the telencephalon and the diencephalon, the hindbrain dividing into the metencephalon and myelencephalon, while the mesencephalon remains unchanged. These five vesicles are responsible for the formation of all the brain areas of an adult brain.

During this growing phase of development, the neural tube consists of a single layer of neuroepithelial cells, which are bordered by the meninges on the outer side and contain the ventricle cavity on the inner side. In the telencephalon, the ventricle is referred to as the lateral ventricle. Neural stem cells (NSCs), also known as neuroepithelial cells, actively proliferate during this phase [220]. As development progresses, NSCs gradually develop long processes on both sides of the cell body, which give them a radial shape and are known as radial glial cells. These cells are multipotent and can undergo symmetric division to expand the NSC pool or asymmetric division to generate neuronal progenitors [221]. The wall of the ventricle, where this process happens, is called the SVZ [222]. These newly formed neurons subsequently migrate from the SVZ towards the outer part of the neural tube, forming the different cerebral layers.

Notably, excitatory and inhibitory cells originate from distinct regions of the SVZ. Excitatory cells are formed in the dorsal wall, whereas interneurons are generated in the ventral part of the SVZ, specifically in an area referred to as the ganglionic eminences (Figure 27).

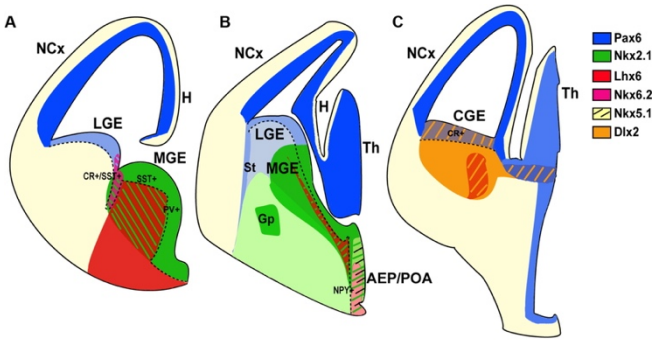

D

	LGE	MGE	CGE	POA
Dlx2	++	++	++	++
Gsh2	++	++	++	-
Couptf1	++	++	++	++
Lhx6	-	++	+	-
Lhx7	-	++	-	-
Nkx2.1	-	++	-	++
Nkx5.1	-	-	-	+
Nkx6.2	-	+	-	+
Olig2	+	++	+	+
Pax6	+	-	+	-

Figure 27. Expression of neurodevelopmental markers in progenitor zones of the telencephalon.

The dorsal SVZ (in dark blue) generates excitatory neurons that express characteristic markers like Pax6. Interneurons originating at the most ventral part of the SVZ (light blue, green, and orange) are characterized by other markers like Nkx2.1. At this region defined by ganglionic eminence, further subclassification of interneurons occurs according to their location at birth. While interneurons located in the medial ganglionic eminence (MGE) will predominantly generate parvalbumin (PV) and somatostatin (SOM) interneurons, the caudal ganglionic eminence (CGE) generates vasointestinal peptide (VIP) inhibitory cells. Image from [223].

Due to their distinct locations, excitatory and inhibitory cells have different migration routes to reach their final destination in the cortex. Excitatory cells migrate from the SVZ directly towards the outer part of the neural tube following radial glial cells, as previously reviewed [224]. On the other hand, inhibitory cells undergo tangential migration over longer distances before reaching the cortex, where they refine their local position and integrate into neural circuits (reviewed in [225]).

3.1.2.1.1. Neuronal differentiation in-vitro

In-vitro neuronal differentiation aims to mimic neurodevelopment during embryonic days by exposing iPSCs to small molecules similar to those secreted during the neurogenic process.

The first step in this process is neuronal induction, which interestingly occurs by default in iPSCs, without the need for additional signaling molecules [226]. Nevertheless, inhibiting the SMAD signaling pathway downstream of BMP and TGFβ has been shown to increase the efficiency of neuronal differentiation [227] (Figure 28).

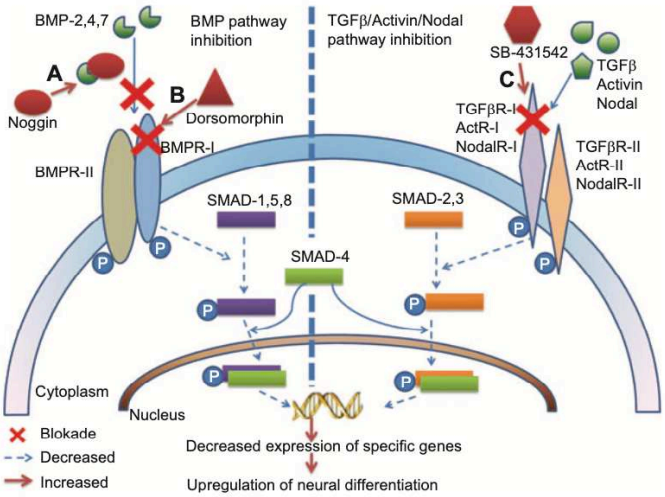

Figure 28. The dual SMAD inhibition and synthetic molecules.

During neurodevelopment, signaling molecules such as noggin or nodal are secreted by the notochord to induce the overlying ectoderm to form the neural plate. In vitro, small molecules such as SB-431542 or dorsomorphin can be used to inhibit the SMAD signaling pathway. Dorsomorphin and similar inhibitors block the receptors of BMP, impairing its signaling pathway, while SB-431542 blocks the phosphorylation of Nodal/activin/TGFβ receptors. The inhibition of both pathways ultimately leads to a decrease in the nuclear translocation of SMAD, enhancing neuronal differentiation at the expense of epidermal fate. Illustration from [228].

In the case of inhibitory neurons, a second step of differentiation is needed. As previously explained, excitatory cells are originated in the dorsal part of the telencephalon, the differentiation of which, happens also by default [229]. However, interneurons have their origin in the ventral telencephalon. Therefore, differentiation of these cells in vitro requires ventralisation of the neuroectoderm achieved by Shh stimulation, either alone or in combination with Wnt signaling inhibition [213, 214]. Further subclassification of interneuron types can be accomplished by exposing the cells to varying concentrations and durations of Shh, corresponding to the levels present in the ganglionic eminences, where the interneurons originate [230].

3.1.3. The use of hiPSC-derived neurons in AD in-vitro modeling

The use of stem cells to model an adult neurodegenerative disease may seem counter-intuitive, since age is a key factor in the disease, and these cells represent embryonic stages of development. Nevertheless, experiments have demonstrated that iPSCs-derived neurons from AD patients can reproduce most of the disease phenotypes [232–234]. Since the establishment of efficient protocols of neuronal differentiation, a significant amount of research has been conducted using iPSC derived from both EOAD and LOAD patients. One advantage of using these young cells is the possibility to access early stages of the disease not accessible in patients.

The first studies using this technology focused on replicating previous research conducted on animal models by using familiar AD (or EOAD) mutations. iPSC-derived neurons carrying AD causative mutations in APP or PSEN, successfully reproduce AD phenotype in-vitro. Hallmarks like Aβ production, Tau phosphorylation and oxidative stress were reported in these models (reviewed in [235]). With the use of iPSC-derived neurons, researchers have been able to model not only EOAD but also LOAD. In-vitro cultures of neurons derived from patients with LOAD exhibit AD-associated traits, although the effects reported were more variable compared to those observed in EOAD-derived cells [236,237]. Additionally, the use of iPSC-derived neurons has enabled the study of the contribution of genetic risk factors in the disease, one of the most well-characterized being ApoE4. As anticipated, ApoE4-carrying neurons produce heightened levels of Aβ and tau phosphorylation[238–240]. Intriguingly, a study revealed selective degeneration of ApoE4-GABAergic interneurons in comparison to glutamatergic or dopaminergic cells [239].

Although the use of iPSC-derived neuronal models holds great promise for studying AD, it is important to note that the interpretation of results can be challenging due to the multifactorial nature of sporadic AD and the inter-individual variability of hiPSCs. For example, when studying the effect of a particular risk factor gene, other genes may interact and confound the effect of the gene of interest. To overcome this issue, isogenic controls using technologies like CRISPR-Cas9 or viral-mediated overexpression are frequently used. This strategy eliminates the influence of confounding factors, making it possible to obtain more accurate comparisons between experimental groups. Another limitation of hiPSC-derived neuronal cultures is their lack of interaction with other brain cell types such as microglia and astrocytes, which play significant roles in the development of the disease. To address this limitation, co-cultures with multiple cell types and 3D organoid cultures are being developed, which have shown promising results in reproducing AD phenotypes that 2D cultures could not retrieve, such as Aβ aggregation [241]. Nevertheless, these in-vitro models lack the complete connectivity of in-vivo circuitries and are limited in time. To overcome these limitations, chimeric models offer an alternative approach. In this method, hiPSC-derived neuronal progenitors can be transplanted into the brains of animal models, enabling the study of cell's behavior in-vivo, within a more physiological environment (discussed in the following chapter) (reviewed in [242]).

3.1.4. Xenografting of hiPSC derived neurons

The field of in vivo modeling of human neurodegenerative diseases is experiencing a rapid growth. Transplanting human cells into animal brains provides a unique opportunity to study these diseases over extended periods of time, as cells benefit from a more physiological environment. In addition, parameters such as neuronal activity, network connectivity and integration within the host can be studied. Studies using

xenotransplantation of human-derived neurons are presented in Results: Book chapter. Despite the success of grafting experiments, a significant limitation of this model is the occurrence of immune rejection. As a result, immunocompromised hosts are often required to prevent rejection of the transplanted cells.

3.1.4.1. Introduction

Human neuronal progenitors have been successfully transplanted into mouse brains, resulting in well-integrated and functional grafts [243,244]. Neuronal progenitors can be transplanted both in the neonatal as well as adult brains. While the first one allows the cells to integrate into a less complex and more plastic host circuitry, the second allows the transplantation in a more specific and localized region of the brain.

3.1.4.1.1. Xenotransplantation in neonates

Transplants in the neonatal brain directly in the cortex have been shown to remain relatively confined within the injection site but to project to various cortical regions such as the hippocampus, striatum, hypothalamus and thalamus [243–245]. Espuny-Camacho and colleagues demonstrated that cells project to different cortical structures according to their cortical identity. Under their experimental conditions, human cells projecting to the thalamus were mainly of layer VI identity, as shown by TBR1 labeling, while human neurons projecting to the midbrain were mostly CTIP2 positive, a typical layer V marker [245].

An alternative method of transplanting cells in the neonatal brain involves injecting cells in the lateral ventricles, which allows them to contact with the ventricle walls, where the generation of neurons occurs during development, and then migrate towards the cortical layers. Studies have shown that cells transplanted using this method can follow radial migration along radial glial processes still present in the neonatal brain. However, these cells are only partially localized in cortical layers according to their identity, with CTIP2 cells primarily located in L5/L6 and some in layer 2/3, while Cux1 cells, a marker of superficial layers, exclusively migrate to layer 2/3 [246]. Other similar experiments have demonstrated that after transplanting neuronal projections in the lateral ventricles, cells can be observed initially in the walls of the lateral ventricles, with subsequent migration from the ventricular zone and through the rostral migratory system, eventually reaching the olfactory bulbs [243,244].

Both transplantation methods showed an increase in the maturation of human neurons over time. This is evidenced by more mature electrophysiological properties characteristics and increased dendritic complexity, spine formation and spine maturation [243,245,246]. Linaro and collegues et all. demonstrated that these cells also functionally integrate into the host tissue. In vivo experiments showed that the transplanted

cells responded to visual stimulation by firing in response to sensory inputs from host neurons that process visual stimuli. This indicates that the transplanted cells can not only survive but also contribute to the functional activity of the host brain [246].

3.1.4.1.2. Xenotransplantation in adults

The human brain is a complex and organized structure. While one might assume that it would be difficult for new cells to integrate into this structure and form functional connections, adult neurogenesis is a natural process that occurs in the brain. This process demonstrates that the brain has the plasticity to integrate new cells even after development has been completed. In that direction, studies have successfully demonstrated the efficient integration of transplanted human cells into the adult brain's circuitry [247–249].

This technique has shown great promise in studying a variety of neurological disorders such as Parkinson's disease, Epilepsy, Down syndrome, and Autistic spectrum disorder [248–252]. Transplantation of GABAergic cells has become particularly popular for this type of procedure because the loss of inhibition is a major contributor to neurological disorders. Moreover, GABAergic cells show excellent integration and migration capacities [253]. For example, in a mouse model of temporal lobe epilepsy, transplantation of hiPSC-derived MGE-like interneuron precursor cells into the hippocampus was found to decrease seizures and improve cognitive functions, memory, and mood [248].

3.1.4.2. Graft rejection and tolerance induction

Traditionally, the brain was believed to be immune-privileged, but recent research has shown that the CNS is not isolated from the immune system. First, activated T lymphocytes have been shown to be able to penetrate the BBB and infiltrate the brain, and second, brain glial cells have similar capacities to immune cells of the periphery. In addition, when neuronal progenitors are transplanted into the brain of immunocompetent mice, the graft is rejected [254].

Alternative methods to maintain the cells in the brain and avoid rejection have been explored. One such method is the use of immunosuppressants like Cyclosporine A. Although grafts in these mice survive, the administration of this drug significantly damages the host's health [255]. Another approach is to use immunosuppressed mice, such as the NOD-SCID transgenic line, lacking lymphocytes B and T, NK, and having immature macrophages [89,243,245,247,249]. However, these mice are highly sensitive to infections, and like animals treated with immunosuppressants, their lifespan is short.

A third alternative is the induction of immune tolerance, which involves exposing the donor cells to the host before the host's immune system is fully developed. Unfortunately, when hiPSC-derived NPCs were transplanted in the neonatal brain, they did not achieve tolerance and it resulted in graft rejection [256]. Although the immune system is not fully developed in the neonatal stages, it might be too late for the body to achieve immunotolerance. Our new model of xenotransplantation in immune-competent mice by targeting embryonic stages of brain development is exposed in Results: Article 2.

3.1.4.3. Stem cell transplantation to model AD

In the context of AD, the transplantation of hiPSC-derived neurons has only been used in a few pioneering studies. In 2017, Espuny-Camacho and colleagues described the first model of AD using this technique. After transplanting the human-derived neurons in a mouse model of AD, the authors found that human cells were more susceptible to the disease than their mouse counterparts. Specifically, the human cells showed more diffused Aβ plaques, higher levels of neurite dystrophy, and Tau hyperphosphorylation. Furthermore, this model successfully replicated neurodegeneration of these human cells, one of the AD hallmarks that has been missing in previous in vivo models of AD [89].

In a more recent study, hiPSC-derived astrocytes were transplanted into a mouse model of AD, and the results showed that these astrocytes could change their morphology to an activated state in response to the presence of amyloid plaques in the host tissue. [257] Additionally, another group of researchers have demonstrated that intranasally transplanted hiPSC-derived NPCs can ameliorate both AD pathological hallmarks and rescue cognitive deficits in a mouse model of AD. The administration and integration of these cells in the brain reduced Aβ-amyloid accumulation, neuroinflammation, and synaptic loss, while simultaneously improving BBB integrity and cholinergic dysfunction [258].

THESIS OBJECTIVES

AD is recognized as one of the greatest medical care challenges of our century. Although encouraging new therapies have been discovered in recent years, a curative treatment for AD is yet to be found. One of the major systems affected in AD is the cholinergic system, characterized by a reduction of acetylcholine in the brain. However, drugs aimed at increasing ACh levels have shown only partial and non-lasting effects. Furthermore, the interaction between Aβ and nicotinic acetylcholine receptors, such as the α7-nAChR, plays a crucial role in AD pathology. Aβ can directly bind to a7-nAChR, inhibiting its function. Researchers have attempted to target this interaction using agonists and PAMs. However, a translational gap has emerged, potentially due to the absence of the human-specific gene *CHRFAM7A* in animal models. *CHRFAM7A*, present in copy number variations in the population, has been associated with AD. Additionally, the presence or absence of this gene affects individual responses to AChE inhibitors.

The objective of this thesis was to develop an in-vivo model to study the *CHRFAM7A* gene and its interaction with α7-nAChR and Aβ. Due to the ambitious nature of this project, it was divided into two axes. The first axis involves conducting an in-vitro study of Aβ interaction in hiPSC-derived interneurons, expressing or not the human *CHRFAM7A* gene product (dupα7 subunit). Interneurons are a relevant cell type to study this interaction as they express high levels of nAChRs. In addition, Aβ exposure induces hyperactivity of these cells in-vivo (submitted manuscript, in revision). By studying the responses of hiPSC-derived interneurons to Aβ in-vitro, valuable insights into the role of *CHRFAM7A* in AD pathology can be obtained.

To achieve the in-vitro study, an initial plan was to use a control hiPSC line with two copies of *CHRFAM7A*, and to establish a knockout strategy to eliminate the gene and create an isogenic control. However, upon characterizing the genetic dosage of *CHRFAM7A* in the available hiPSC line, we unexpectedly found that the gene was naturally missing in this individual. Consequently, new hiPSC lines were ordered, but their delayed delivery resulted in a one-year setback. To overcome this challenge, an alternative strategy involving the induction of *CHRFAM7A* expression using a lentiviral vector was developed. The infected hiPSCs were cloned, and a protocol for interneuron differentiation was established. Another challenge arose from the unavailability of specific antibodies for labeling the human receptor. As a result, the analysis based on protein expression were limited to the α7 subunit. Due to these challenges, the experiments conducted in the in-vitro phase of this project require further complementary studies to strengthen our current data.

To address the limitations of the in-vitro study, which lacked a physiological environment with natural ligands of nicotinic receptors, endogenous processing of Aß species and interneuron communication with other cell types, a complementary model was developed. The second axis of this thesis focuses on the

development of an in-vivo model to study the *CHRFAM7A* gene. For this purpose, a xenotransplantation model was developed using hiPSC-derived NPCs transplanted into the brains of immune-competent mice at earlier stages of development (in utero). Previous laboratory studies have relied on the xenotransplantation of human neurons into the brains of immunocompromised mice, and at the neonatal stage. However, the use of immunocompromised mice may not be well suited for the study of aging disorders. In one hand, these mice models are fragile and have shorter life spans, limiting the experimental timeline. In the other hand, the study of the xenotransplant cells in an AD context, would require crossing of immunocompromised strains and AD mouse models. Therefore, exploring the transplantation of NPC~~s~~ at earlier developmental stages in immune-competent mice became a promising alternative.

In this study, two sites of injection were tested: local transplantation in the prefrontal cortex (PFC), enabling direct exposure to the cortical environment, and transplantation in the lateral ventricles, which allowed exposure to the SVZ germinal layer. By examining these different environments, the aim was to investigate whether variations in the microenvironment could slightly alter the maturity stage of the transplanted human cells, thereby exploring the interplay between intrinsic and extrinsic determinants of cell development. To expedite the initiation of this project, NPCs labeled with GFP, which were developed by a former PhD student in the lab, were directly used. This allowed for a head start in the experimental process and facilitated the smooth progression of the project and its publication.

Due to the challenges posed by the COVID-19 crisis and the technical obstacles encountered, the project advanced at a slower pace, and regrettably, the in-vivo study of CHRFAM7A could not be accomplished within the designated timeframe of this thesis. Nonetheless, the research described in the following chapter has yielded significant insights. The in-vitro experiments have provided valuable data on the interaction between Aβ and nAChRs, shedding light on the role of CHRFAM7A in AD pathology. Additionally, the establishment of the xenotransplantation model using human iPSC-derived NPCs represents a notable achievement. Encouragingly, the initial preliminary transplantations of interneurons in-utero have shown promising results.

RESULTS

Summary of the objectives, techniques and results

Article 1 (in preparation)

Article 2: *Developmental Changes of Human Neural Progenitor Cells Grafted into the Ventricular System and Prefrontal Cortex of Mouse Brain in Utero.*

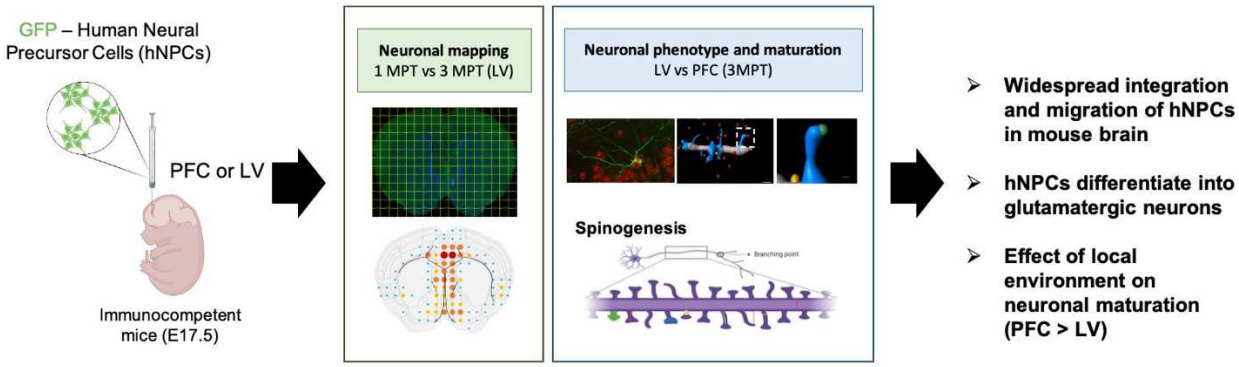

Objective: Investigate the development, migration, maturation, and integration of human NPCs (hNPCs) after transplantation into the embryonic brains of immunocompetent mice

Methodology: was examined both in vitro and in vivo by assessing the expression of development markers through RT-qPCR and immunolabeling. The migration and integration of hNPCs were investigated by mapping their cell somas and neuronal projections at 1- and 3-month post transplantation (MPT). Additionally, spinogenesis was analyzed in the LV and PFC transplantation models at 1 and 3 MPT to evaluate the maturity of the grafts and their integration within the neural network. The potential for graft rejection and the viability of human NPCs were assessed using immunolabeling techniques targeting iba1+ cells and caspase 3.

Main results: Under our experimental conditions, hNPCs differentiated into young glutamatergic neurons both in-vitro and in-vivo. Following transplantation, LV-injected cells migrated and populated cortical structures, expanding their reach to more distant regions after 3 MPT. The maturation and integration of hNPCs varied depending on the transplantation method. Both PFC and LV transplants exhibited increased maturity and spine numbers from 1 MPT to 3 MPT. At 3 MPT, PFC transplants displayed a higher density of spines, although the morphology appeared slightly less mature compared to LV transplants. Notably, microglia recruitment was detected at the grafting site, particularly in PFC transplants, but no signs of graft rejection or cell death were observed.

Book chapter: *Humanized Chimeric Mouse Models to Study Human Neural Development and Pathogenesis of Brain Diseases*

This chapter provides an insightful review of various transplantation techniques employed in the laboratory to model neurodevelopment and neurological disorders in the mouse brain. Specifically, the focus is on the transplantation of human neural progenitor cells (NPCs) at different stages of host development, including embryonic, neonatal, and adult stages. Detailed protocols and methodologies for each transplantation technique are described, offering a comprehensive resource for researchers interested in utilizing similar transplantation methods.

Article 1

Article 2

Developmental Changes of Human Neural Progenitor Cells Grafted into the Ventricular System and Prefrontal Cortex of Mouse Brain in Utero.

Maria Llach Pou[1,2,†], Camille Thiberge[1,2,†], Michiel Van der Zwan[1,2], Annousha Devi Govindan[1], Stéphanie Pons[1,2], Uwe Maskos[1,2] and Isabelle Cloëz-Tayarani[1,2*]

[1]Institut Pasteur, Université Paris Cité, Unité de Neurobiologie Intégrative des Systèmes Cholinergiques, CNRS UMR 3571 "Gènes, Synapses et Cognition", Institut Pasteur, 25 rue du Docteur Roux, 75015 Paris, France.

[2]Sorbonne Université, Collège doctoral, 75005 Paris, France.

*Correspondence: Isabelle Cloëz-Tayarani. Tel +33 (0)1 45 68 88 04

† These authors contributed equally to this work.

cells

MDPI

Article

Developmental Changes of Human Neural Progenitor Cells Grafted into the Ventricular System and Prefrontal Cortex of Mouse Brain in Utero

Maria Llach Pou [1,2,†], Camille Thiberge [1,2,†], Michiel Van der Zwan [1,2], Annousha Devi Govindan [1], Stéphanie Pons [1], Uwe Maskos [1,2] and Isabelle Cloëz-Tayarani [1,2,*]

[1] Institut Pasteur, Université Paris Cité, Unité de Neurobiologie Intégrative des Systèmes Cholinergiques, CNRS UMR 3571 "Gènes, Synapses et Cognition", 25 Rue du Docteur Roux, 75015 Paris, France
[2] Collège Doctoral, Sorbonne Université, 75005 Paris, France
* Correspondence: isabelle.cloez-tayarani@pasteur.fr; Tel.: +33-(0)1-45-68-88-04
† These authors contributed equally to this work.

Abstract: The transplantation of neural progenitors into a host brain represents a useful tool to evaluate the involvement of cell-autonomous processes and host local cues in the regulation of neuronal differentiation during the development of the mammalian brain. Human brain development starts at the embryonic stages, in utero, with unique properties at its neotenic stages. We analyzed the engraftment and differentiation of human neuronal progenitor cells (hNPCs) transplanted in utero into the mouse brain. The influence of the environment was studied by transplanting human NPCs within the lateral ventricles (LV), compared with the prefrontal cortex (PFC) of immunocompetent mice. We developed a semi-automated method to accurately quantify the number of cell bodies and the distribution of neuronal projections among the different mouse brain structures, at 1 and 3 months post-transplantation (MPT). Our data show that human NPCs can differentiate between immature "juvenile" neurons and more mature pyramidal cells in a reproducible manner. Depending on the injection site, LV vs. PFC, specific fetal local environments could modify the synaptogenesis processes while maintaining human neoteny. The use of immunocompetent mice as host species allows us to investigate further neuropathological conditions making use of all of the engineered mouse models already available.

Keywords: xenografting; in utero transplant; human stem cells; human-induced pluripotent stem cells; chimeric mouse models; brain development; brain disorders

Citation: Llach Pou, M.; Thiberge, C.; Van der Zwan, M.; Devi Govindan, A.; Pons, S.; Maskos, U.; Cloëz-Tayarani, I. Developmental Changes of Human Neural Progenitor Cells Grafted into the Ventricular System and Prefrontal Cortex of Mouse Brain in Utero. *Cells* **2023**, *12*, 1067. https://doi.org/10.3390/cells12071067

Academic Editor: Nina Graffmann

Received: 26 January 2023
Revised: 6 March 2023
Accepted: 29 March 2023
Published: 31 March 2023

1. Introduction

Experimental models of the human brain are needed for a better understanding of its development and the cellular and molecular dysfunctions that can occur during different stages of neuronal development, leading to autistic disorder, Asperger's disorder, childhood disintegrative disorder, Rett's disorder, and pervasive developmental disorder, and also other brain disorders such as schizophrenia, dementia, and Parkinson's disease. There has been a significant progress in the field of human stem cells in recent years, with the main objective of reproducing the landmarks of neuronal disorders in vivo and decipher the altered underlying mechanisms in a context that resembles pathophysiological conditions. The development of stem cell transplantation models using human-induced pluripotent stem cells (hiPSCs) is also expected to offer new advances for regenerative medicine purposes, with the possibility of using specifically the allogeneic sources of these cells to produce autografts without the need for immunosuppression [1,2]. However, such clinical translations are still premature and more difficult to explore and adapt for therapeutic purposes. A large number of pre-clinical studies have already demonstrated the capacity for neuronal transplants to integrate within rodent brains and respond to guiding molecules

and signals, under in vivo conditions [3,4]. In addition, it has been shown that transplanted pyramidal neurons derived from human embryonic stem cells can be specifically directed toward their appropriate sites of differentiation and maturation [5,6]. So far, the neuronal xenotransplants which have been obtained from hiPSCs include human neurospheres [7], human neuronal progenitor cells (hNPCs) [8,9], purified hiPSC-derived neurons with defined phenotypes [5,10], and, more recently, human brain organoids [11–13]. In parallel, experimental conditions have been set up which allow the integration of xenotransplants as single neurons within the mouse cortex where they can develop morphologically and functionally with a prolonged maturation period similar to that of the human developing brain [14]. Under such conditions, the transplanted neurons reach a more advanced stage of dendritic spine maturation as compared to those reported previously [15,16]. Therefore, the host brain seems to provide a permissive environment and the adapted cues for spinogenesis and synaptogenesis. In light of earlier reports, the transplantation paradigm used in conditions which allow the transplanted neurons to integrate as single cells represents a key determining factor during the final stages of the maturation and connectivity of these neurons within the host brain.

A major obstacle facing the transplantation of hiPSC-derived cells is the observed rejection of the grafts by the immune system of the host. Consequently, most transplantation models consist of grafting human cells into the brain of immunodeficient animals. The short-term immunosuppressive method allows for immunological tolerance with a significant improvement in the integration of transplanted iPSCs [17]. However, to increase the survival of transplanted cells, current methods are predominantly based on the use of transgenic immunodeficient rodent models. The brain is thought to possess an "immunological privilege" with a relatively large degree of permissible mismatching between the donor and the host [18–20]. In general, the main immune processes that occur during graft rejection involve the natural immunity of the host, which corresponds to the immune responses that naturally exist prior to transplantation. Some of these responses include the production of antibodies by B1 and B lymphocytes, mainly during the first weeks of life [21–23]. However, only the natural antibody of the IgG class can cross the barrier of placenta to assure fetal immunity [22,24]. Since innate responses are necessary to trigger the adaptative immune responses, some of the host immune responses cannot be fully active at the late embryonic stage or even at the early neonatal stages [24].

In the present study, we described a human neuronal-chimeric mouse by transplanting hNPCs into the brain of immunocompetent mice at the embryonic stage in utero. Our aim was to develop a new approach which prevents graft rejection and avoids bias due to the usage of immunodeficient mouse models. We specifically grafted NPCs within the mouse lateral ventricles at an embryonic stage at which only a small number of lymphocytes can infiltrate during brain development [25]. We used our previously characterized and established hiPSC-derived NPCs [9–26] to study some of the key morphological parameters at cellular levels at early stages of neuronal development. We showed that grafted neuronal precursors in the ventricles move towards their target regions during the first months following transplantation. When grafted into the embryonic neocortex at the same stage, we observed that these precursors integrated directly in the cortical areas with a more advanced maturation profile.

2. Materials and Methods

2.1. Study Design and Ethics Statement

All methods were carried out in accordance with relevant guidelines and regulations. This protocol was approved by the Institut Pasteur Ethics Committee and the French "Ministère de l'Education Nationale, de la Recherche et de l'Innovation" under reference APAFiS #25221. Pregnant Swiss OF1 mice (Charles River Laboratories) were habituated at the animal facility for at least 3 days and surgeries were performed at the embryonic stage of E17.5.

2.2. Production of hiPSC and Their Derivation into hNPCs

The production of hiPSCs, their characterization, commitment to the neural lineage, and derivation of stable NPCs were performed according to Boissart et al. [27]. For this study, we used a control cell line from Coriell Biorepository (Coriell Institute for Medical Research, Camden, NJ, USA), the GM04603 (https://www.coriell.org/Search?q=GM04603, accessed on 25 January 2023) provided by Dr Alexandra Benchoua (I-Stem Institute, Evry) together with the derived NPCs [27]. For the initial experiments, we used the WTSIi002-A line (https://cells.ebisc.org/WTSIi002-A/, accessed on 25 January 2023, Wellcome Trust, UK), as described in a previous study [28]. For the data presented here, we selected those obtained with the GM04603 iPSC line which has been fully characterized in vitro and in vivo in our previous studies [9,26,27].

The T25 flasks were coated under the flow hood with poly-ornithine (15 µg/mL in sterile H_2O). After an overnight exposure at 37 °C, the flasks were washed three times with H_2O. Then, the flasks were coated with laminin (1 mg/mL), diluted to 1/1000 in Advanced DMEM F12 medium, and incubated for at least 4 h at 37 °C. The NPCs were then plated at the density of 50,000 cells/cm^2 in 5 mL of culture medium. The composition of the culture medium is described in Table S1 and prepared as previously described [9]. After the removal of the culture medium, fresh N2B27 medium containing 5 µL/mL of fresh laminin solution was added to keep the neurons attached and to avoid clumping. The medium was changed every 3 days. For the in vivo transplantation into the mouse embryos, we used hNPCs derived from the GM04603.

2.3. Culture and Amplification of NPCs before Transplantation

The culture and amplification of NPCs were performed in sterile conditions. For their labeling, NPCs were transduced with a CMV-GFP-lentiviral vector to obtain green fluorescence, as described previously [9,29]. Lentiviral vectors were prepared according to a published protocol [30]. The map of the CMV vector is detailed in Figure 1A. Briefly, NPCs were thawed in T75 flasks at a density of 50,000 cells/cm^2 in 25 mL of NPCs medium supplemented with Rock Inhibitor Y27632 (10 µM). The NPCs were transduced with 99.5 ng of lentivirus (p24) in a 6-well culture plate filled with 500 µL of fresh culture medium for 3 h. The volume was completed to 2 mL, incubated for the next 48 h, and then rinsed with the culture medium. All media and products are described in Thiberge, Llach Pou et al. [31] and are summarized in Table S1.

2.4. In Utero Transplantation of Mouse Embryos

Before their transplantation, the cells were kept in a water bath at 37 °C. The injection solution also contained 20 mM EGTA to avoid cell aggregation upon transplantation [14,31,32]. The transplantation protocol has been previously detailed [31]. Briefly, 2 µL containing 2×10^5 cells were injected within 1 lateral ventricle or within 1 side of the PFC of E17.5 embryos. The injection within LV is depicted in Figure 2A and the injection within PFC was described previously using mouse neonates (P0-P1) [8,9]. Thirty minutes before surgery, buprenorphine (0.05 to 0.1 mg/kg) was injected subcutaneously at the back of the neck of the pregnant mouse for initial analgesia. The pregnant mouse was then anesthetized with isoflurane and oxygen and placed on a heating pad connected to the anesthesia unit. A drop of ocryl gel was applied on each eye. The abdomen was shaved locally for ventral laparotomy and lidocaine gel was applied locally before and after the laparotomy. A sterile towel drape was positioned on the mouse abdomen. An incision of 1 to 1.5 cm was made in the lower abdomen in a manner to cut both the skin and the thin fascia layer. The whole uterus was carefully extracted from the abdomen. During surgery, drops of sterile PBS kept at 37 °C were consistently applied on the exposed fetuses. The sharp glass pipette was carefully inserted through the fetal skull, and cells were injected into each fetus, except the first one to be delivered on each uterine horn (Video S1). After the injection, the pipette was carefully withdrawn. Then, the uterus was reentered into the abdominal cavity. The peritoneal cavity was rehydrated with 0.5 to 1 mL of sterile PBS to replace any fluid loss

during the surgery. Then, the incision was closed with two types of sutures: for fascia and skin, we used sterile resorbable sutures (ProleneTM, EH7471, Ethicon, LLC, Issy les Moulineaux, France) and non-resorbable sutures (Coated Vicryl, V302, Ethicon, LLC), respectively. After the surgery, the pregnant mouse was positioned on a warming pad until the mouse was fully awake. Analgesia treatment (acetaminophen 4 mg/20 mL) was administered in the drinking water for 3 to 5 days after the surgery. Hydrogel was also given to the mice for one day after the surgery. We could observe that the presence of EGTA significantly reduced the cell aggregation and increased the possibility of identifying single cells within the mouse brain, as described previously [14].

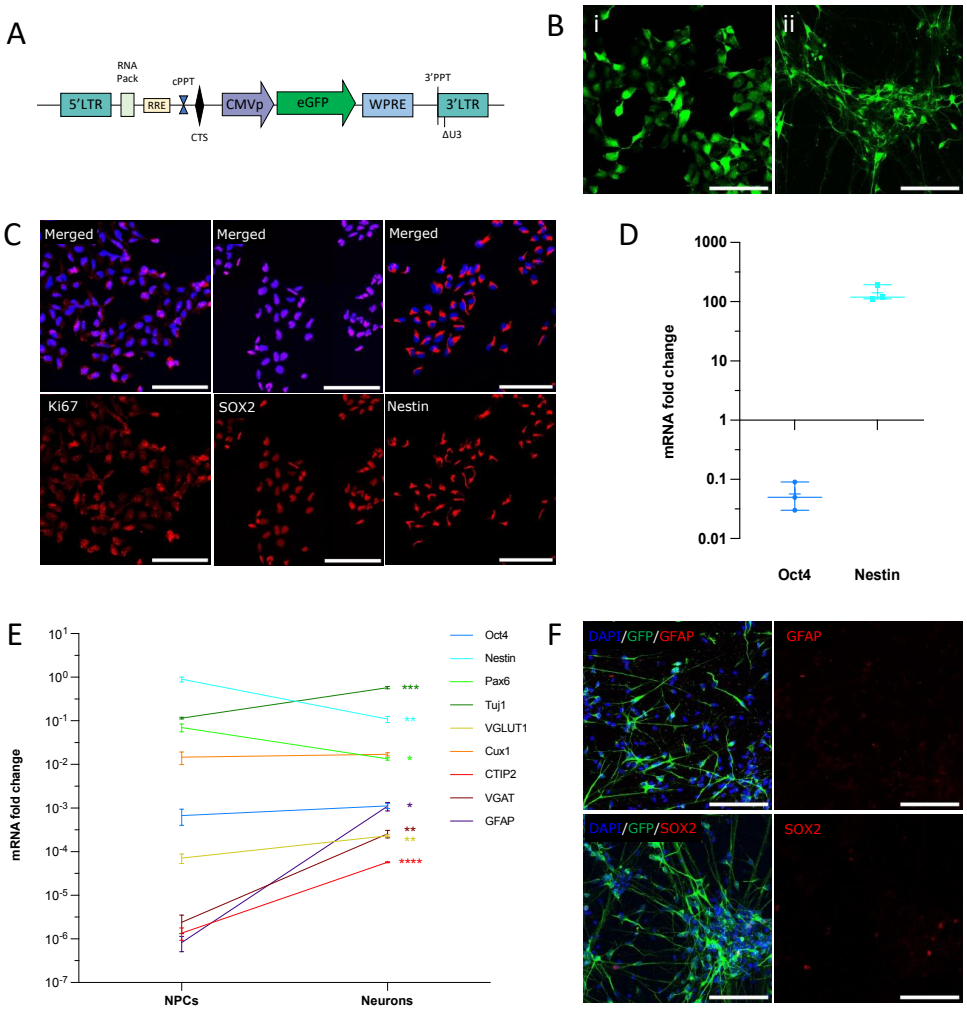

Figure 1. NPCs differentiate into immature cortical neurons in vitro. (**A**) Lentiviral construct expressing GFP used for NPCs labeling, adapted from [9]. (**B**) GFP is expressed in NPCs (left panel) and 30-day-old neurons (right panel). Scale bar = 100 µm. (**C**,**D**) NPCs express the neuronal progenitor markers Ki67, SOX2, and Nestin at passage 28 (**C**). The plot (**D**) shows mRNA expression fold-change as compared to human fetal brain. qPCR results were normalized to GAPDH and calculated with the ΔCT method (data are from three independent cultures). (**E**) mRNA relative expression of differentiation markers at NPCs and neuronal stage. Data are expressed as fold change to GAPDH calculated with the ΔCT method (* $p < 0.05$; ** $p < 0.002$; *** $p < 0.0002$; **** $p < 0.0001$, unpaired *t*-test). (**F**) Neurons do not express the astrocyte marker GFAP. Only a small proportion of cells remained SOX2 positive after 30 days of differentiation. Scale bars = 100 µm.

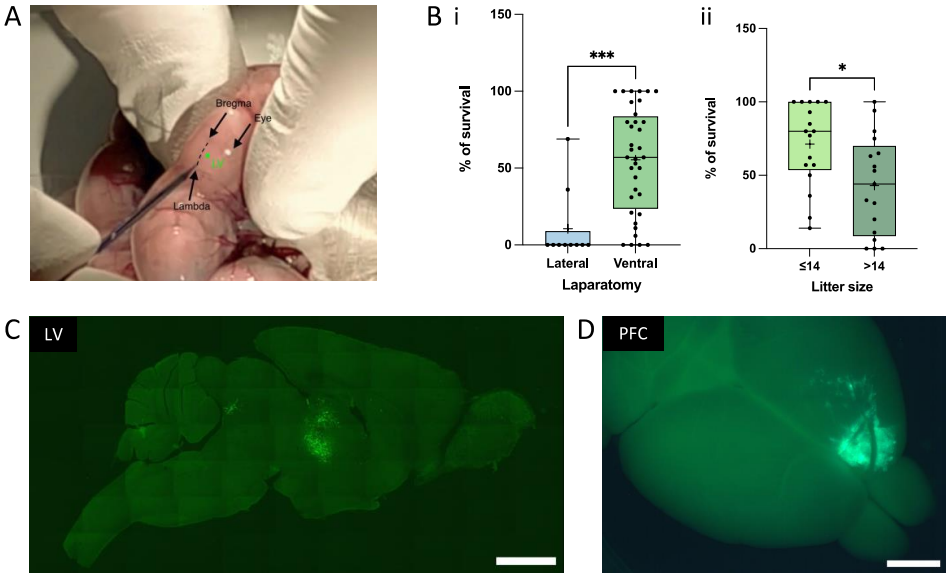

Figure 2. The in utero technique. (**A**) Illustration of the site of injection for Lateral Ventricle (LV) surgery. (**B**) Pup survival as a function of the laparotomy technique (Bi) and litter size (Bii). Pup survival is higher when the ventral laparotomy is performed on mice that have less than 14 embryos. Each point of the boxplot corresponds to the survival percentage in one litter. (* = $p < 0.05$; *** = $p < 0.001$, unpaired *t*-test). (**C**) Sagittal picture of a brain section at 1 MPT into LV taken with an epifluorescence microscope. Cells are labeled with GFP. (**D**) Illustration of a graft within the PFC at 1 MPT taken with an epifluorescence macroscope. Scale bars = 2 mm.

2.5. Quantitative Real-Time PCR (qRT-PCR)

The total mRNA from NPCs and neuronal cultures was extracted with the RNeasy Plus Mini Kit (ref. 74034, Qiagen). cDNA was generated using the High Capacity cDNA Retro-Transcription Kit, according to the manufacturer's instructions (Ref. 4368814, ThermoFisher). For mRNA expression level quantification, real-time PCR was performed on the Applied Biosystems 7500 Real-Time PCR System. UDG activation (1 cycle, 2 min, 50 °C) and polymerase activation (1 cycle, 10 min, 94 °C) were followed by 40 cycles of denaturation (15 s, 95 °C) and anneal/extend (1 min, 60 °C). The PCR reactions contained 500 nM of each primer, 0.5 × PowerUP SYBR Green Master Mix (2×) (A25742, Applied Biosystems), and 20 ng of cDNA in a final volume of 10 µL. The primers were manually designed to amplify mRNA only (at least one of the primer pairs spans the exon-to-exon junction). The list of primers is presented in Table S2. The specificity of the primers was verified with a melting curve and agarose gel electrophoresis of the PCR confirmed amplicon size. The mRNA expression level was expressed as the fold change to the housekeeping gene GAPDH (Figure 1E) using the $2^{-\Delta CT}$ method or normalized to GAPDH and compared to a control condition using the $2^{-\Delta\Delta CT}$ method (Figure 1D) [33].

2.6. Immunofluorescence (IF)

Immunofluorescence analysis on brain sections was performed at 1 and 3 MPT, according to our previously described protocol with slight modifications [9,31]. Animals received a lethal dose of a mixture of Ketamine (Imalgen®, 100 mg/kg, Merial) and Xylazine (Rompun®, 10 mg/kg, Bayer), and were transcardially perfused with 15 mL of DPBS, followed by 40 mL of ice-cold paraformaldehyde (PFA) (4%) in 0.1 M phosphate buffer (pH 7.4). The brains were dissected and post-fixed overnight at 4 °C in 4% PFA. In total, 40 µm coronal sections were obtained using a microtome (Leica SM2010 R), collected in 12-well culture plates, and stored in DPBS + Azide (0.02%) at 4 °C until use. The free-floating sections were rinsed twice in PBS (pH 7.4) and then incubated in a DPBS solution

containing 0.2% Triton X-100 and 10% goat or horse serum at room temperature (RT) for 30 min to block nonspecific binding. An extra step of blocking using MOM (Ready Probes ™ Mouse on Mouse IgG Blocking Solution (30×), R37621, Invitrogen) was added if a mouse primary antibody was used. The primary antibodies, diluted in blocking solution, were added overnight at 4 °C. The list of all antibodies and their dilutions is presented in Table S3. An additional incubation with DAPI diluted in PBS was performed for 10 min at room temperature [29].

2.7. Mapping and Semi-Quantification of Cell Bodies and Projections

Fluorescence images of whole brain slices were captured using a laser-scanning confocal microscope (Axio Scan.Z1, Inverted LSM 700 from the Histology Platform at Institut Pasteur). Three different tile images at 20× magnification from three independent transplanted animals were taken per condition and analyzed by two distinct experimenters. To overcome the limits of conventional manual counting of labeled cells, we implemented a novel analysis pipeline allowing for the reconstruction of the expected shape of each brain slice (Figure S1). This method reduces any bias in brain mapping that may result from slight variations of slicing conditions along the anterior-posterior axis of the brain. This pipeline allows the precise mapping of single neuron positions and projections by automatically setting a grid of squares of ~500 μm^2. The Allen Brain Atlas was used as a reference for the precise matching of experimental brain slices with the expected brain cartography. A grid of squares was applied to each section and the cells were manually counted. Semi-quantification of the cell bodies and projections was performed, and color codes were applied. To avoid bias due to possible graft heterogeneity, we selected brains with similar grafting for all quantifications.

2.8. Quantification of Dendritic Spines

We reported a protocol for the imaging of dendritic spines after immunofluorescence in a video journal [29]. Briefly, confocal images were acquired with a confocal laser-scanning microscope (LSM 700, Zeiss) using a 40× oil NA = 1.3 objective, and a 488 nm laser for GFP excitation. A Z spacing of 200 nm was used for Z-stack acquisitions. A semi-automatic tracing of dendrites and automated segmentation of spines was performed using the Filament Tracer module of Imaris 9.5 software (Bitplane AG, Zürich). The spine categories were defined by their morphology as follows: Stubby: length < 1 µm; Mushroom: max-width-head > min-width-neck*2; Thin: length (spine) < 2 and mean-width-head ≥ mean-width-neck; Filopodia-like: length ≤ 4 µm and >1 µm, by the MATLAB, version 2022a. Spines were quantified at a 20 µm distance from the soma [34]. The 3D images and videos (.mp4 files) of spines were obtained from Z-stacks of confocal images and processed using the animation functions in Imaris software to zoom and navigate around the dendrites and spines. For LV transplantation, we did not include hNPC-derived neurons that were present in matter tracts or present in non-neuronal environments, but quantified only those present in cortical areas.

2.9. Statistical Analysis

Statistical analyses were performed using GraphPad Prism Version 9 software (GraphPad, San Diego, CA, USA) and are reported in each figure legend. Confidence levels of 95% were used.

3. Results and Discussion

3.1. hNPCs Differentiate into a Homogeneous Population of Immature Neurons In Vitro

For this study, we used a well-characterized human iPSC line for which derived hNPCs were GFP-labeled, as we described previously [9,26,29]. We did not exceed the number of cell passages that could have altered the NPCs' amplification and proliferation [10]. We first checked that these cells could differentiate into a homogeneous population of cortical neurons in vitro, as we have shown previously. Our data indicate that human

NPCs and hNPC-derived neurons express similar levels of green fluorescence (GFP), with a more mature shape after 30 days of in vitro differentiation (Figure 1A,B). The hNPCs displayed positive immunoreactivity for the cortical radial glial markers SOX2 and Nestin, and for the proliferation marker Ki67 (Figure 1C). The mRNA level of OCT4, a marker for undifferentiated cells, was decreased when compared to the fetal brain, while Nestin mRNA was increased (Figure 1D). Only a few cells expressed SOX2 in the cultures of 30-day-old neurons (Figure 1F), indicating successful neuronal differentiation. Figure 1E presents the comparative expression of differentiation (CTIP2, Oct 4, Pax 6, and Nestin), neuronal (VGLUT1, VGAT, Tuj1, Cux1), and astrocytic (GFAP) markers in NPCs and neuron stages. mRNA was measured by RT-qPCR and the levels were normalized to GADPH. The Nestin mRNA levels decreased in the 30-day-old neurons, as compared to the NPCs, while those for Oct 4 remained very low. The expression of CTIP2, the vesicular GABA transporter (VGAT), TUJ1, GFAP, and, to a lesser extent, Cux1 were increased in neurons as compared to NPCs (Figure 1E). CTIP2 is a transcription factor expressed in the cortical layers V-VI neurons, which has also been linked to axonal growth and the establishment of the cellular architecture of the striatum, in vivo [35,36]. VGAT, the vesicular GABA transporter, has been shown to play a role in the embryonic development [37]. Although our protocol provides a large majority of excitatory cells [27], we cannot exclude some VGAT expression during the earlier stages of neuronal differentiation. In parallel, we did observe higher levels of VGLUT1 mRNA as compared to VGAT, in NPCs and similar levels in neurons. A slight increase in VGLUT1 mRNA was also found in neurons as compared to NPCs. Tuj1 is a marker of neuronal lineage, expressed at early stages of maturation as well as in mature neurons. This is in accordance with a slight increase in its expression in neurons, as compared to NPCs. The GFAP mRNA levels were increased in neurons, but this increase was not correlated to the increase in protein levels since no GFAP could be detected at the same stage of neuronal maturation (Figure 1F). In accordance with Boissart et al. [27], Cux1 mRNA was higher than CTIP2 mRNA in both conditions. As expected for more mature neuronal cells, Pax6 and Nestin expressions were slightly decreased in the neurons as compared to the NPCs.

3.2. In Utero Grafting of Human iPSC-Derived NPC into Embryonic Mouse Brain

The xenotransplantation of neural progenitors represents a very useful method to study the contribution of the intrinsic mechanisms and their dynamic crosstalk with the host factors that control and regulate cell migration and differentiation within the developing brain [38]. The regional determination of neural progenitors is an early event, which is still ongoing at the stage of E17.5 [39]. During the course of this study, we first aimed at demonstrating that human NPCs could integrate, differentiate, and migrate after their transplantation into the E17.5 mouse brain, in utero. For that purpose, we used experimental conditions which allow the human precursors to integrate as single cells, which will, in turn, result in a coordinated morphological and physiological development of their dendritic spines similarly to our previously reported observations in neonatal xenotransplantations [14]. In order to target the earlier stages of development, we set up a technique which allows for the in utero transplantation of NPCs into the LV and PFC embryonic regions. We first compared the percentage of pups' survival between lateral and ventral laparotomy and observed that ventral laparotomy was the most adapted method, at least in the case of large litters, such as those expected with Swiss OF1 mice (Figure 2Bi). The percentage of pups' survival was also significantly increased when the litter did not exceed 14 pups (Figure 2Bii). Figure 2C illustrates that a large number of cells can survive and integrate into the periventricular areas, as well as the whole ventricular system, including the third ventricle, when grafted into the LV, as shown at 1 MPT (left panel). Figure 2D also shows a direct view of an in utero transplant within the PFC, as shown at 1 MPT (right panel). The scanned cortical transplant can be observed directly within the transplanted hemisphere. This would allow the exclusion or rejection of any abnormal transplant before further analysis. Regardless of the mechanisms that may be involved locally, these initial

observations indicate that progenitor cells are able to survive and integrate within distinct brain regions.

3.3. Achievement of a Stable Cell Engraftment Using Immunocompetent Mice and Maturation Pattern of Axonal Projections up to 3 MPT

According to our differentiation protocol, we expect hNPCs to differentiate mainly into glutamatergic pyramidal excitatory neurons, morphologically characterized in vivo by a conical "tear-shaped" soma, an apical dendrite, and basal spiny dendrites. Pyramidal neurons can extend their axon at long distances from the cell body. It has recently been shown that axons can also originate from dendrites in mammals and in humans to a lesser extent [39]. Under our experimental conditions, we could not detect any axon arising from dendrites. Detailed mapping of somas and axonal projections originating from ventricular transplants are depicted in Figures 3 and 4. hNPCs were transplanted in utero within the mouse LVs. The distributions of cells and their projections were quantified independently by two (somas) and three (projections) observers, as described in the experimental procedures section. The integration of GFP-labeled cells, their survival, maturation, and phenotypic fate over time was followed up to 3 MPT. The transplants did not increase the brain surface, nor did they remain confined within the LV. We could easily identify GFP+ neurons within different mouse brain regions with a typical pyramidal morphology (Video S2; Figure 4). The semi-quantitative analysis at 1 MPT and 3 MPT indicates the presence of variable densities of GFP+ projections within distinct brain areas. Many GFP+ projections were detected within the brain structures close to the external walls of the lateral and third ventricles. As we were able to observe at different levels of the host brain, the GFP+ projections reached their highest densities in the corpus callosum, septum, caudate putamen, hippocampus, and thalamic nuclei. The projections were distributed both ipsi- and contralaterally to the same extent at 3 MPT (Figure 3). These findings are in accordance with those reported previously after in utero grafting of mouse neurons into the embryonic rat brain [40]. The two hemispheres are connected by commissural fiber systems, including the corpus callosum and hippocampal commissures, which were enriched in axonal projections (Figure 3). The two LVs are separated from each other by a thin vertical sheet [41] but they communicate with the third LV in which projections were also found (Figure 3). Perpendicular projections could also be detected between the ventricular wall dorsal to the CA1 hippocampal brain region of the host. GFP+ projections were also detected to a lesser extent in the cortex and the subcortical areas, including the hippocampus and thalamus (Figure 3). The pattern of projections was slightly different from that we previously observed under ventricular transplantation in neonates [9]. More precisely, we did not observe any visible axonal projections along the rostral migratory stream, nor the presence of cells within the olfactory structures. This indicates that under in utero grafting conditions, the NPCs endogenously predisposed to become excitatory cells did not significantly follow the same pathways promoting the migration of interneurons to olfactory structures. Espuny-Camacho et al. reported a widespread distribution of cell projections [5]. However, the distribution of GFP-labeled cell bodies has not been fully investigated in xenotransplantation studies with human iPSC-derived neurons. This may be due to the fact that a precise quantification of GFP-labeled cell bodies within a specific brain structure requires volumetric analysis among several transplanted brains. It should also be noted that small variations in the cell location and integration at the embryonic stage could lead to larger variations in the adult brain. It should be noted that assessing the number of grafting cells would require the use of the same grafted brain for analysis at different time points, which is not technically possible by standard methods. Such quantifications have not been reported so far. One of our objectives for this study was to determine the capacity of cells to survive upon their in utero transplantation, while keeping their migratory properties over time. Despite some variabilities among the three independent brains which were analyzed, we observed similar patterns of cell distributions in the regions close to the ventricular system at 1 MPT (Figure 4). At 3 MPT, the transplanted

cells displayed the properties needed to migrate into more distant regions, which include lateral and medial septum, caudate putamen, retrosplenial, motor and anterior cingulate cortex, hippocampus, some thalamic nuclei, and preoptic areas (Figure 4). Similar patterns were observed among the 3 brain samples which were evaluated independently at 1 MPT and 3 MPT. During neuronal migration, NPCs are expected to adapt their migration and final location by following well-known migratory pathways [42]. Our results indicate that at least some of the intrinsic migratory properties of human cells remain unchanged while they develop in the murine host in a similar manner among independent transplanted mice. Our data also indicate that the number of GFP+ cells remained similar between 1 MPT and 3 MPT in 3 independent experiments and according to the quantification of 3 brain sections per region and brain (Figure 4).

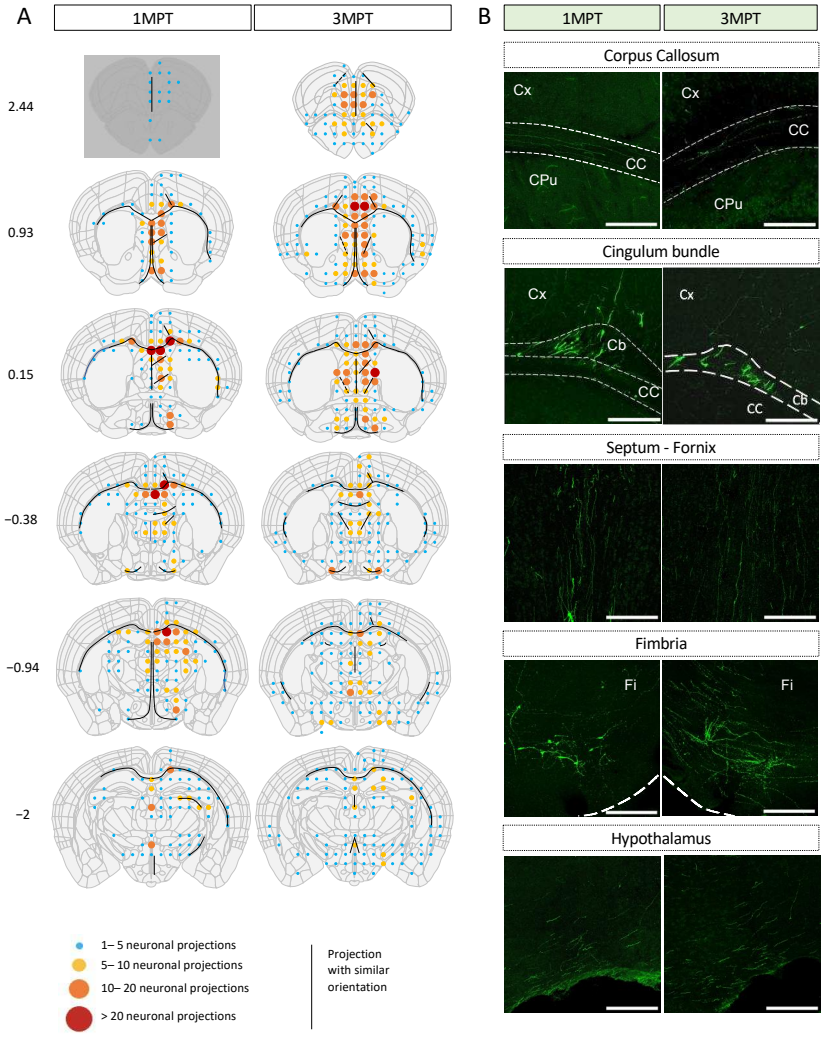

Figure 3. Mapping of neuronal projections from transplanted human cells within the LV of the embryonic mouse brain at 1 MPT and 3 MPT. (**A**) Camera lucida drawings are according to Allen Brain Atlas (https://mouse.brain-map.org/, accessed on 25 January 2023). Image credit: Allen Institute. The densities of neuronal projections are depicted using a code-color schematic representation. Results are calculated as the mean value from three independent mice. Two to three brain sections were analyzed for each coordinate (Bregma, indicated in mm) and per mouse. (**B**) Representative images of GFP+ projections at 1 MPT and 3 MPT in fiber tracks and brain regions such as the cortex (Cx), corpus callosum (CC), cingulum bundle (Cb), septum/fornix, fimbria (Fi), and hypothalamic region. The illustrated data are from the three representative brains. Scale bars = 200 µm.

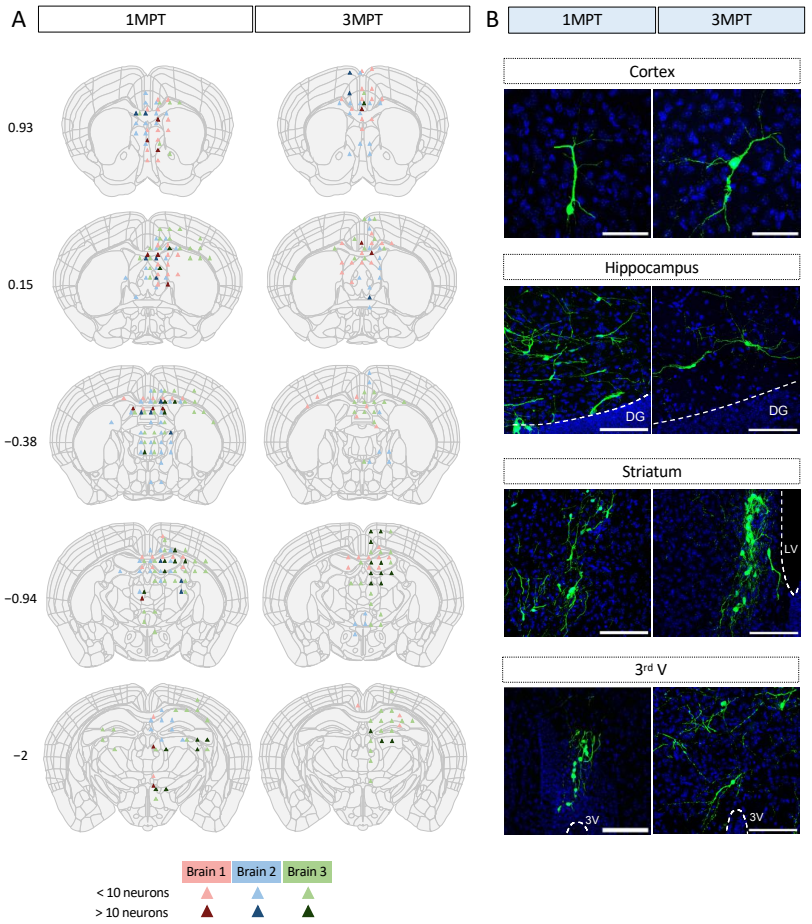

Figure 4. Mapping of neuronal somas from transplanted human cells within the LV of the embryonic mouse brain at 1 MPT and 3 MPT. (**A**) Camera lucida drawings are according to Allen Brain Atlas (https://mouse.brain-map.org/, accessed on 25 January 2023). Image credit: Allen Institute. Two brain sections were analyzed for each coordinate (Bregma, indicated in mm) and per mouse. Each brain analyzed is represented in a different color and the number of neuronal somas is represented in a color-code manner. For each brain and coordinate, 40-µm thick images were used and the counted values summed. (**B**) Representative images of brain regions where the grafted human cells tended to migrate.

In contrast to previous studies, we did not observe any significant graft rejection at 1 MPT despite the use of an immunocompetent host, as previously observed by other authors [43]. We, therefore, believe that under our experimental conditions, human-transplanted cells might express some specific antigens at least prior to the maturation of the mouse immune system, thereby preventing the rejection of a transplant by the host immune system. Additionally, it has been reported that iPSC-derived NPCs display low immunogenicity [44]. More recently, immature neural precursors have also been reported to partially suppress the proliferation of murine CD4 and CD8 T cells involved in the adaptative immune responses [43]. Such adaptative immune responses are under the control of the host natural immunity which is not fully active at late embryonic or even at early neonatal stages [24]. Since the brain has been considered immunologically to be a privileged organ [44,45], these findings could provide further explanations and help understand the reasons for the absence of graft rejection in our experiments.

3.4. Analysis of Human Cell Neuronal Phenotypes after in Utero Transplantation at 3 MPT

During brain development, specific neuronal subtypes are produced in a specific temporal manner. The protocol we used for the derivation of human NPCs into cortical pyramidal neurons was adapted from Boissart et al. [27]. It allows the NPCs to differentiate into large proportions of excitatory neurons (≅80%), mainly from the cortical layers II-IV, and, to a lesser extent, into GABAergic cells (≅20%) in vitro. Using the immunostaining approach, there was an absence of SOX2 and GFAP labeling of human cells after in utero transplantation at 3 MPT, and in LV and PFC conditions. We did not observe any SOX2 or GFAP expression in the differentiated cells in these conditions (Figure 5A–C, Video S3). Our data are consistent with those obtained in vitro (Figure 1) and indicate that human cells have lost their capacity to proliferate without differentiating into astrocytes at 3 MPT after LV and PFC transplantation. It has been previously shown that sequential mechanisms may exist and confer young neurons to differentiate into astrocytes [46]. Therefore, one cannot exclude some derivation of human cells into astrocytes at later stages of neuronal differentiation as we could observe in vitro at 40–45 days of differentiation using the same iPSC line together with two other iPSC lines [26]. We analyzed the expression of the neuronal nuclear marker NeuN, a selective marker of postmitotic neurons. We could not clearly identify isolated mature neurons that co-expressed NeuN and GFP at 3 MPT after LV transplantation and in all of the neuronal migration brain subregions (Figure 5A). By contrast, NeuN was clearly expressed in the human NPC-derived pyramidal cells after PFC transplantation, as illustrated in Figure 5C. As a marker for glutamatergic neurons, we selected the vesicular glutamate transporter VGLUT1, which is expressed in all of the neuronal migration brain regions [47]. We could detect the expression VGLUT1 in NPC-derived neurons after LV and PFC transplantation at 3 MPT. The 3D reconstruction and zoomed-in visualization of dendrite segments and spines allowed us to demonstrate at a microscale the colocalization of VGLUT1 with GFP labeling (Figure 5B–D). We could observe that VGLUT1 was only expressed at the levels of dendritic shafts after LV transplantation but also at the spine levels after PFC transplantation (Figure 5D; Videos S4 and S5). We also analyzed the expression of the oligodendrocyte marker Olig2 and did not detect any colocalization of Olig2 with GFP labeling (Figure 5A,C). For analysis of progressive cell death over time, we tested the expression of apoptosis-related caspase-3 protein at 1 MPT and 3 MPT (Figure S2). Our results did not show any significant caspase-3 labeling at the two time points. To evaluate the maturation of the transplanted cells between LV and PFC transplants, we analyzed the differential expression of the NeuN marker for mature neurons with that of β3-tubulin, a marker of the early phases of neuronal differentiation (Figure S3). Our results strongly suggest higher levels of neuronal maturation with increased glutamate levels neurotransmission in human NPC-derived neurons transplanted in PFC, as compared to those transplanted in LV.

Microglia have been described as a regulator of the proliferation of neural precursors cells in the developing cerebral cortex [48]. They play a role in synaptic pruning and synaptic density and can rapidly detect changes in the brain environment [49,50]. Using single-cell and spatial transcriptomic profiling, it has been recently shown that the neuronal identity can influence microglia densities [51]. During the course of this study, we analyzed the potential enrichment of mouse microglia at transplantation sites at 1 MPT and 3 MPT after LV and PFC transplantations. For this purpose, we used Iba1 labeling to identify the presence of microglia cells at injected and non-injected hemispheres (Figure 6). Interestingly, we could observe differences in microglia labeling under all of the conditions tested. The number of Iba1+ cells remained within the same order between the injected and non-injected sites in LV transplantation at both 1 MPT and 3 MPT. A slight decrease in cell numbers was observed in the non-injected site, where the transplanted cells are expected to be less present, at least at 1 MPT (Figure 6). As compared to LV, the PFC transplantation induced higher levels of Iba1+ cells, initially surrounding the transplanted area at 1 MPT, and then integrating within the transplanted area at 3 MPT. In the PFC region, the level of resident microglial cells was twice higher as high as that of the LV region. These

observations are in agreement with previous reports on the regional heterogeneity of microglia within specific brain regions, among rodent brains [52]. We also analyzed the morphology of microglial cells as an index of their reactivity [53]. The small cell somas and large territories occupied correspond to a lower activity state, while cell body enlargement and more irregular cell shape correspond to a high activity [54]. After LV transplantation, we did not observe any significant variation between 1 MPT and 3 MPT, and between the ipsilateral and contralateral sites (Figure 6). After PFC transplantation, we observed a slight increase in the soma areas between 1 MPT and 3 MPT, and between the injected and non-injected sites. Microglia are expected to regulate the survival of neuronal cells without excluding a possible phagocytosis of dead cells and debris that may result during PFC transplantation, where the high densities of human cells may influence their glial environment. Further studies are needed to examine and confirm this hypothesis.

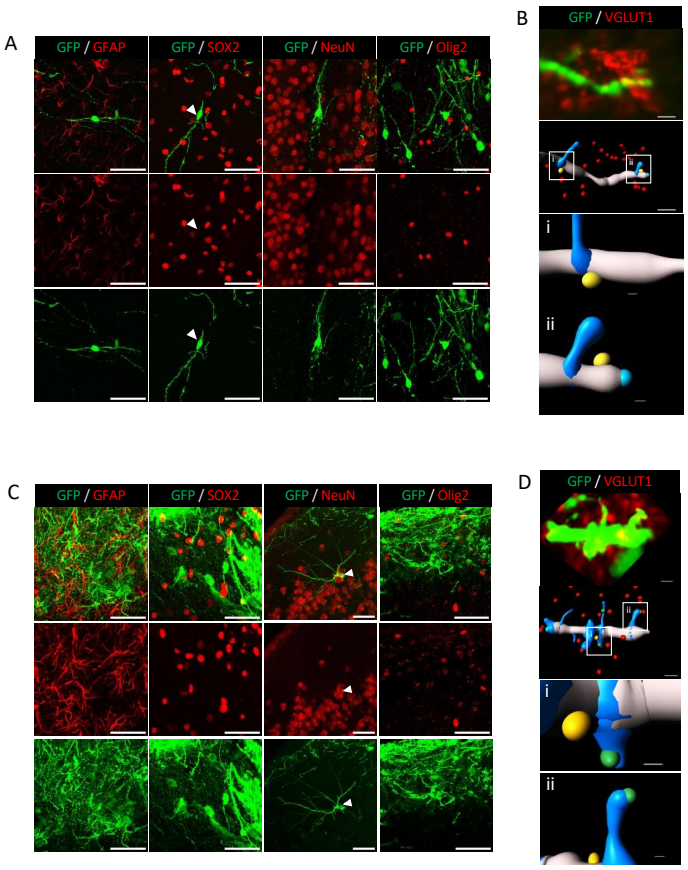

Figure 5. NPCs differentiate into glutamatergic neurons at 3 MPT. Immunofluorescence staining of NPC-derived neurons by GFAP, SOX2, NeuN, and VGLUT1 at 3 MPT after LV (**A**,**B**) and PFC (**C**,**D**) transplantation. Left to right panels, no positive human cells were found for GFAP, Sox2, NeuN, and Olig2 (no double-labeled cells). (**B**). Punctiform labeling of dendritic segment was observed for VGLUT1, clearly illustrated by a 3D zoomed-in image showing distinct VGLUT1 punctae represented in yellow (Bi, Bii). (**C**). Left to right panels, no positive human cells were found for GFAP, Sox2 and Olig2. Positive labeling for NeuN marker showing the nuclei of pyramidal neurons within the PFC (arrowhead). (**D**). Punctiform labeling of dendritic segment and associated spines was observed for VGLUT1, clearly illustrated by a 3D zoomed-in image showing distinct VGLUT1 punctae represented in yellow (dendrite) and green (spines) (Di, Dii). Scale bars = 50 µm (GFAP, SOX2, NeuN and Olig2 images), scale bars = 2 µm (reconstituted VGLUT1 images), and scale bars = 0.3 µm (zoomed images Bi, Bii, Di, Dii).

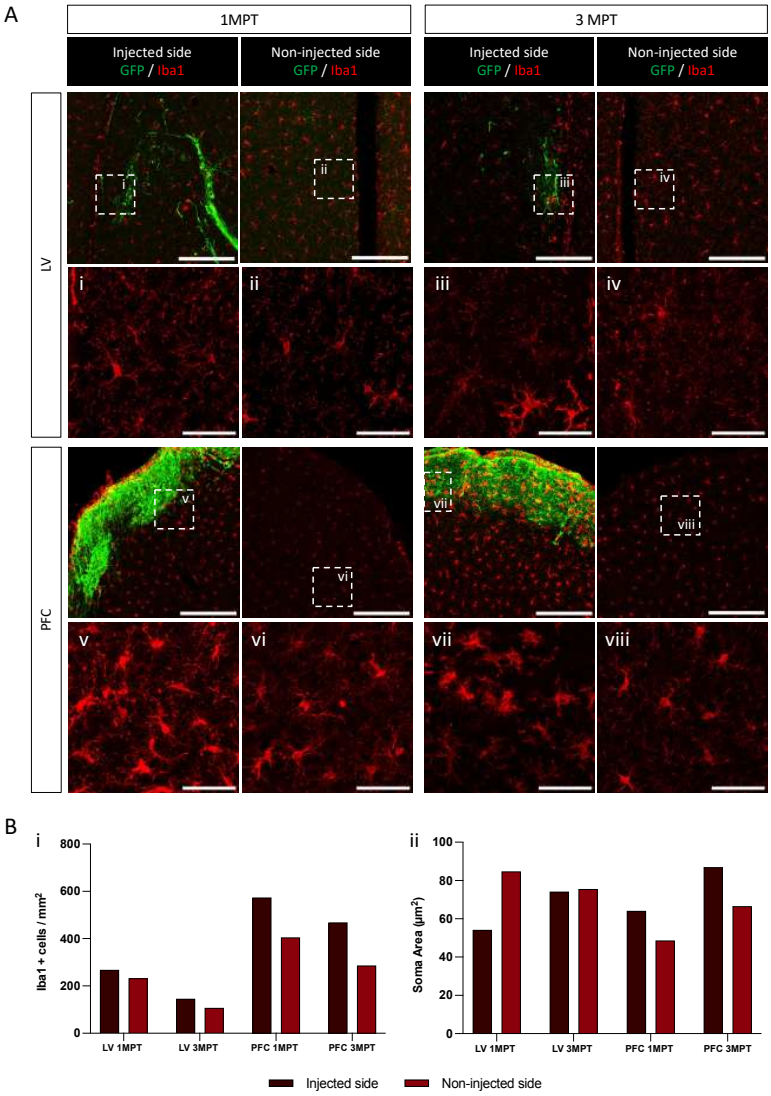

Figure 6. Microglia recruitment around the grafted area, related to Figure 5. (**A**) Confocal images at 1 MPT and 3 MPT of the injected and non-injected sides for LV- and PFC-transplanted mice. The transplanted cells are labelled with GFP, and microglia is shown in red. Pictures i–viii show the higher magnification of the area for the analysis of microglia morphology on one representative brain for each condition. Scale bar = 200 µm and 5 µm for i–viii. (**B**) Plot showing microglial density (Bi) and soma area (Bii) for each condition. Quantification was performed on the 20× images, using the MorphoLibJ plugin in Fiji.

3.5. Comparative Analysis of Dendritic Spines in LV- or PFC-Transplanted Human Cortical Pyramidal Neurons

Dendritic spines are important for the establishment of most excitatory synapses and the cortical circuits. Their density and structural plasticity are thought to directly reflect the glutamatergic synaptic transmission and synaptic plasticity in the brain cortex during development, as well as the developed adult brain. Each spine may allow the neuron to control its local activity. The aim of this study was to understand the contribution of the local host environment in spinogenesis processes. Our objectives were to compare the spine maturation in human cortical pyramidal neurons derived from transplanted NPCs at 1 and 3 MPT after their in utero engraftment into the LV of the mouse embryo (E17.5); and the spine maturation after transplanting the human NPC into two distinct embryonic regions,

namely the LV and the PFC, at 1 and 3 MPT. For these experiments, we used our previously reported method, which consists of the 3D reconstruction and quantitative analysis of diverse structural spine parameters on iPSC-derived pyramidal neurons [9,29] (Figure 7A; Video S6). The set of morphological parameters that have been measured in our study are depicted in Figure 7B. The diverse morphologies of dendritic spines have been reported previously with the classical distinction between filopodia, thin, stubby, and mushroom forms [54]. The spine diversity appears to be directly related to its stability and functional activity [54]. Figure 7C illustrates the proportion of the four spine categories, tested under each experimental condition. We could observe a large proportion (90%) of filopodia at 1 MPT after LV transplantation. The proportion of filopodia at 1 MPT was lower in PFC as compared to the LV transplants but remained in the major spine category (57.9%). This indicates that spines at this stage are still immature. The NPCs have moved forward to the cortical zones, and this may be the reason for the delay in the maturation process. In contrast to filopodia, the stubby and mushroom categories have been recently shown to possess a post-synaptic density with similar average protein copy numbers and topologies [55]. At 3 MPT we observed that the proportion of stubby and mushroom spines increased in the LV transplants, while only the proportion of stubby spines increased in the PFC transplants (Figure 7C). These data indicate an increase in the level of maturation until 3 MPT. We could also observe a significant increase in the total spine densities at 3 MPT compared to 1 MPT after transplantation of the NPCs into LV and PFC, with an even higher increase in the PFC-transplanted neurons compared to LV. Such increases were more pronounced for the filopodia and stubby than for the thin and mushroom categories (Figure 7D). The spine densities were very similar to those we reported previously in neonatal grafting [9], as well as those reported in a recent study using human-transplanted organoids [13]. By contrast, the total volume of spines remained unchanged over the four conditions tested. At 3 MPT, a slight but significant decrease in the relative spine head volume was observed in the PFC transplants compared to the LV transplants. This effect was predominantly observed for the filopodia spines (Figure 7D). Our results also indicate that the spine straightness and neck morphologies remained unchanged in all of the tested conditions, despite a slight decrease in the spine neck length between 1 MPT and 3 MPT in the LV transplants (Figure 7D). The total spine length was significantly lower in PFC as compared to LV at 1 MPT. We also observed a 38% increase in the total spine head volume together with a 37% decrease in the total spine neck length after transplantation within the LV. These data strongly suggest that a coordinated regulation of the neck morphology and synaptic maturation could occur and be linked to functional neuronal maturation [54]. Finally, we measured the morphological parameters of the dendrites from human cortical pyramidal neurons. While the dendrite length remained unchanged between all of the conditions tested, we could observe a significant increase in the dendrite diameter and dendrite volume, as well as the number of primary branching points at 3 MPT, when the NPCs were transplanted in the PFC compared to the LV (Figure 7E). In addition, the dendrite volume was significantly increased between 1 MPT and 3 MPT in the PFC transplants (Figure 7E). Altogether, our data show a higher complexity of dendritic arborization of the cortical pyramidal neurons when directly transplanted within the PFC compared to the LV. In parallel to higher dendritic complexity, higher spine densities were predominantly observed, while the spine intrinsic characteristics remained similar between the PFC and LV. Neuronal maturation represents a continuous process that is under the influence of local and extrinsic factors, which may affect cell migration and maturation. At the level of the LV transplants, the human-transplanted NPCs have migrated and adopted some specific trajectories toward the cortical zone before reaching a cortical destination. For the PFC-transplanted NPCs, the local and extrinsic factors were expected to increase the neuronal maturation while keeping the neotenic human phenotypes, which signifies that the xenografted cortical neurons are expected to retain some juvenile traits in adult mice [5,56].

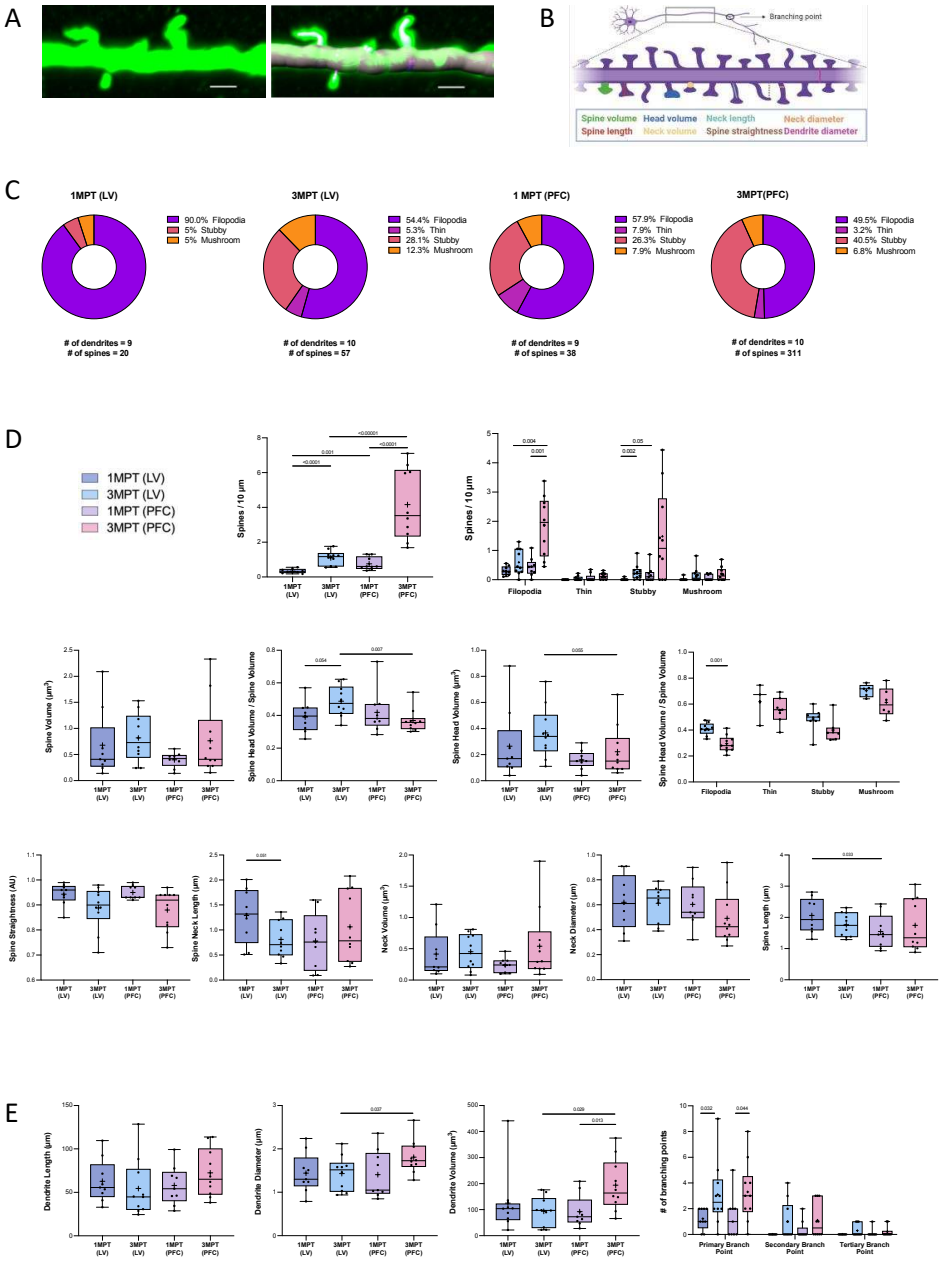

Figure 7. Quantitative analysis of spine and dendrite morphology in LV- and PFC-grafted NPCs at 1 MPT and 3 MPT. (**A**) Confocal image at 3 MPT of a pyramidal cell dendrite grafted in the PFC before (left) and after dendrite and spine reconstruction with the Imaris 9.5 software (right). (**B**) Schematic representation of the parameters evaluated. Created by BioRender. (**C**) Pie charts showing the distribution of the different spine categories at 1 MPT and 3 MPT in LV- and PFC-transplanted cells. Spines were classified into four different classes: filopodia, thin, stubby, and mushroom. Percentages were calculated over the total number of spines in all of the analyzed dendrites. In total 8, 8, 7, and 6 neurons, and 3, 3, 2, and 2 mice were used for 1 MPT-LV, 3 MPT-LV, 1 MPT-PFC, and 3 MPT-PFC, respectively. (**D**) Measurement of spine densities and spine morphology parameters. (**E**) Measurement of dendrite morphology parameters. Data are presented using a box and whiskers graph with plotted "min" and "max" and median values. Mean values are also indicated as "+". Each dot represents a dendrite and spine. Spine parameters were averaged per dendrite. Statistical analyses were performed using Mann-Whitney test.

4. Conclusions

Our data show that human neural precursors transplanted into the brain ventricles of embryonic immunocompetent mice can survive and differentiate into juvenile-like (not fully mature) and more mature neurons with specific patterns of migration and axonal projections over time with no abnormal proliferation, which we found reproducible and uniform among all the transplanted mice. We evaluated the functional neuronal differentiation using a detailed 3D analysis of spinogenesis. Depending on the injection site, LV vs. PFC, we discovered that the specific fetal local environments significantly modified the synaptogenesis processes while maintaining human neoteny. We are currently analyzing the molecular determinants of such processes at the level of transcriptome using single-nuclei RNA sequencing. Our in utero approach can be extended and applied in future studies using other embryonic brain regions in rodents to characterize the developmental patterns. In addition, our model enables the use of other host species for investigation and direct analyzes of the mechanisms that lead to neuropathological conditions and alterations in the development of brain circuits, with no further need for transgenic manipulations for immunosuppressive conditions at early stages of development. It also offers the possibility to investigate the possible sequelae of stem cell transplantation and provides the paths for future therapeutic approaches such as gene therapy through this technique.

Supplementary Materials: The following supporting information can be downloaded at: https://www.mdpi.com/article/10.3390/cells12071067/s1, Figure S1: Illustration of the pipeline to study neuronal projections, related to Figures 3 and 4; Figure S2: Absence of Caspase-3 expression at 1 MPT and 3 MPT, related to Figure 5; Figure S3: Maturation of grafted GFP cells in LV and PFC transplants, related to Figure 5; Tables S1–S3, related to Materials and Methods Section; Video S1: Illustration of the in utero surgery with a visible embryo's brain and injection process; related to Figure 2; Video S2: 3D representation of a GFP+ neuron in the PFC; related to Figure 3. Video S3: 3D representation of GFAP labeling, related to Figure 5; other videos available upon request; Video S4: 3D reconstruction of a dendrite segment (grey) and spines (blue) of a LV-transplanted cell for VGLUT1 labeling detection, related to Figure 5; Video S5: 3D reconstruction of a dendrite segment (grey) and spines (blue) of a PFC-transplanted cell for VGLUT1 labeling detection, related to Figure 5; Video S6: 3D reconstruction of a dendrite and the spines of a GFP+ pyramidal neuron in the PFC.

Author Contributions: Conceptualization, U.M. and I.C.-T.; collection and assembly of data, data analysis and interpretation: M.L.P., C.T., M.V.d.Z., I.C.-T., S.P. and A.D.G.; writing—original draft preparation, I.C.-T.; writing—review and editing, I.C.-T., U.M., M.L.P., C.T., S.P. and M.V.d.Z.; visualization, M.L.P., C.T. and M.V.d.Z.; supervision, I.C.-T. and U.M.; funding acquisition, U.M. and I.C.-T. All authors have read and agreed to the published version of the manuscript.

Funding: This research was funded by grants from the French National Research Agency ANR (ANR-17-NEU3-0004, IPS BRAIN), from ERA-NET NEURON (iPSC and Brain), from the "France Fondation Alzheimer", "Fondation Vaincre Alzheimer", from "Equipe 2019, Projet Explore 2021", and from ADPS-Allianz (to U.M., Head of Unit). This research was also funded by the Fondation pour la Recherche sur Alzheimer (to I.C-T.; C.T.'s PhD funding). The Pasteur-Paris University (PPU) international doctoral program provided the funding for M.L.P.'s PhD, and "Université de Paris" provided the funding for M.V.d.Z.'s PhD (I.C-T.'s grant applications).

Institutional Review Board Statement: Only commercial human cell lines were used. These have been recorded in the CEBOH inventory of the Institut Pasteur. Material transfer agreement for the reception of iPS cell lines has been established between the European Bank EbiSC and Institut Pasteur (reference MTA in 2021-109_Dr Maskos). This protocol was approved by the Institut Pasteur Ethics Committee and the French "Ministère de l'Education Nationale, de la Recherche et de l'Innovation" under reference APAFiS #20686.

Informed Consent Statement: Not applicable.

Data Availability Statement: Not applicable.

Acknowledgments: The authors are thankful to Alexandra Benchoua who performed the initial iPSC reprogramming at I-Stem Institute (Evry, France), to Aline Vitrac who performed the initial NPCs amplification and labeling, and to Astrid Castellanos for her participation in the experiments. The authors are also thankful to Myriam Mattei for advice in the surgery set up and to Florent Haiss for scientific support. We acknowledge the help of Image Analysis Hub of the Institut Pasteur for this work.

Conflicts of Interest: The authors declare no conflict of interest.

References

1. Zakrzewski, J.L.; van den Brink, M.R.M.; Hubbell, J.A. Overcoming Immunological Barriers in Regenerative Medicine. *Nat. Biotechnol.* **2014**, *32*, 786–794. [CrossRef] [PubMed]
2. Karantalis, V.; Schulman, I.H.; Balkan, W.; Hare, J.M. Allogeneic Cell Therapy: A New Paradigm in Therapeutics. *Circ. Res.* **2015**, *116*, 12–15. [CrossRef] [PubMed]
3. Ago, K.; Nagoshi, N.; Imaizumi, K.; Kitagawa, T.; Kawai, M.; Kajikawa, K.; Shibata, R.; Kamata, Y.; Kojima, K.; Shinozaki, M.; et al. A Non-Invasive System to Monitor in Vivo Neural Graft Activity after Spinal Cord Injury. *Commun. Biol.* **2022**, *5*, 803. [CrossRef] [PubMed]
4. Piao, J.; Zabierowski, S.; Dubose, B.N.; Hill, E.J.; Navare, M.; Claros, N.; Rosen, S.; Ramnarine, K.; Horn, C.; Fredrickson, C.; et al. Preclinical Efficacy and Safety of a Human Embryonic Stem Cell-Derived Midbrain Dopamine Progenitor Product, MSK-DA01. *Cell Stem Cell* **2021**, *28*, 217–229.e7. [CrossRef] [PubMed]
5. Espuny-Camacho, I.; Michelsen, K.A.; Gall, D.; Linaro, D.; Hasche, A.; Bonnefont, J.; Bali, C.; Orduz, D.; Bilheu, A.; Herpoel, A.; et al. Pyramidal Neurons Derived from Human Pluripotent Stem Cells Integrate Efficiently into Mouse Brain Circuits In Vivo. *Neuron* **2013**, *77*, 440–456. [CrossRef]
6. Martínez-Cerdeño, V.; Barrilleaux, B.L.; McDonough, A.; Ariza, J.; Yuen, B.T.K.; Somanath, P.; Le, C.T.; Steward, C.; Horton-Sparks, K.; Knoepfler, P.S. Behavior of Xeno-Transplanted Undifferentiated Human Induced Pluripotent Stem Cells Is Impacted by Microenvironment Without Evidence of Tumors. *Stem Cells Dev.* **2017**, *26*, 1409–1423. [CrossRef]
7. Nori, S.; Okada, Y.; Yasuda, A.; Tsuji, O.; Takahashi, Y.; Kobayashi, Y.; Fujiyoshi, K.; Koike, M.; Uchiyama, Y.; Ikeda, E.; et al. Grafted Human-Induced Pluripotent Stem-Cell–Derived Neurospheres Promote Motor Functional Recovery after Spinal Cord Injury in Mice. *Proc. Natl. Acad. Sci. USA* **2011**, *108*, 16825–16830. [CrossRef]
8. D'Alessio, R.; Koukouli, F.; Blanchard, S.; Catteau, J.; Raïs, C.; Lemonnier, T.; Féraud, O.; Bennaceur-Griscelli, A.; Groszer, M.; Maskos, U. Long-Term Development of Human IPSC-Derived Pyramidal Neurons Quantified after Transplantation into the Neonatal Mouse Cortex. *Dev. Biol.* **2020**, *461*, 86–95. [CrossRef]
9. Vitrac, A.; Pons, S.; Balkota, M.; Lemière, N.; Raïs, C.; Bourgeois, J.-P.; Maskos, U.; Bourgeron, T.; Cloëz-Tayarani, I. A Chimeric Mouse Model to Study Human IPSC-Derived Neurons: The Case of a Truncating SHANK3 Mutation. *Sci. Rep.* **2020**, *10*, 13315. [CrossRef]
10. Fortin, J.M.; Azari, H.; Zheng, T.; Darioosh, R.P.; Schmoll, M.E.; Vedam-Mai, V.; Deleyrolle, L.P.; Reynolds, B.A. Transplantation of Defined Populations of Differentiated Human Neural Stem Cell Progeny. *Sci. Rep.* **2016**, *6*, 23579. [CrossRef]
11. Daviaud, N.; Friedel, R.H.; Zou, H. Vascularization and Engraftment of Transplanted Human Cerebral Organoids in Mouse Cortex. *Eneuro* **2018**, *5*, ENEURO.0219-18.2018. [CrossRef] [PubMed]
12. Chen, C.; Kim, W.-Y.; Jiang, P. Humanized Neuronal Chimeric Mouse Brain Generated by Neonatally Engrafted Human IPSC-Derived Primitive Neural Progenitor Cells. *JCI Insight* **2016**, *1*, e88632. [CrossRef]
13. Revah, O.; Gore, F.; Kelley, K.W.; Andersen, J.; Sakai, N.; Chen, X.; Li, M.-Y.; Birey, F.; Yang, X.; Saw, N.L.; et al. Maturation and Circuit Integration of Transplanted Human Cortical Organoids. *Nature* **2022**, *610*, 319–326. [CrossRef] [PubMed]
14. Linaro, D.; Vermaercke, B.; Iwata, R.; Ramaswamy, A.; Libé-Philippot, B.; Boubakar, L.; Davis, B.A.; Wierda, K.; Davie, K.; Poovathingal, S.; et al. Xenotransplanted Human Cortical Neurons Reveal Species-Specific Development and Functional Integration into Mouse Visual Circuits. *Neuron* **2019**, *104*, 972–986.e6. [CrossRef] [PubMed]
15. Real, R.; Peter, M.; Trabalza, A.; Khan, S.; Smith, M.A.; Dopp, J.; Barnes, S.J.; Momoh, A.; Strano, A.; Volpi, E.; et al. In Vivo Modeling of Human Neuron Dynamics and Down Syndrome. *Science* **2018**, *362*, eaau1810. [CrossRef]
16. Raïs, C.; Gaspar Santos, D.; Sansone, G.; Blanchard, S.; Bourgeois, J.-P.; Jagla, B.; Saudemont, B.; Schlick, L.; Pons, S.; Maskos, U. A Systematic Approach for the Study of Functional Maturation of Human IPSC-Derived Neurons in Vivo (in preparation).
17. Pearl, J.I.; Lee, A.S.; Leveson-Gower, D.B.; Sun, N.; Ghosh, Z.; Lan, F.; Ransohoff, J.; Negrin, R.S.; Davis, M.M.; Wu, J.C. Short-Term Immunosuppression Promotes Engraftment of Embryonic and Induced Pluripotent Stem Cells. *Cell Stem Cell* **2011**, *8*, 309–317. [CrossRef]
18. Freed, W.J.; Dymecki, J.; Poltorak, M.; Rodgers, C.R. Chapter 30 Intraventricular Brain Allografts and Xenografts: Studies of Survival and Rejection with and without Systemic Sensitization. In *Progress in Brain Research*; Elsevier: Amsterdam, The Netherlands, 1988; Volume 78, pp. 233–241. ISBN 978-0-444-81012-0.
19. Engelhardt, B.; Coisne, C. Fluids and Barriers of the CNS Establish Immune Privilege by Confining Immune Surveillance to a Two-Walled Castle Moat Surrounding the CNS Castle. *Fluids Barriers CNS* **2011**, *8*, 4. [CrossRef]

20. Cascalho, M.; Platt, J.L. Challenges and Potentials of Xenotransplantation. In *Clinical Immunology*; Elsevier: Amsterdam, The Netherlands, 2008; pp. 1215–1222. ISBN 978-0-323-04404-2.
21. Muldoon, L.L.; Alvarez, J.I.; Begley, D.J.; Boado, R.J.; del Zoppo, G.J.; Doolittle, N.D.; Engelhardt, B.; Hallenbeck, J.M.; Lonser, R.R.; Ohlfest, J.R.; et al. Immunologic Privilege in the Central Nervous System and the Blood–Brain Barrier. *J. Cereb. Blood Flow Metab.* **2013**, *33*, 13–21. [CrossRef]
22. Baumgarth, N. B-1 Cell Heterogeneity and the Regulation of Natural and Antigen-Induced IgM Production. *Front. Immunol.* **2016**, *7*, 324. [CrossRef]
23. Palma, J.; Tokarz-Deptuła, B.; Deptuła, J.; Deptuła, W. Natural Antibodies—Facts Known and Unknown. *Cent. Eur. J. Immunol.* **2018**, *43*, 466–475. [CrossRef]
24. Panda, S.; Ding, J.L. Natural Antibodies Bridge Innate and Adaptive Immunity. *J. Immunol.* **2015**, *194*, 13–20. [CrossRef] [PubMed]
25. Morimoto, K.; Nakajima, K. Role of the Immune System in the Development of the Central Nervous System. *Front. Neurosci.* **2019**, *13*, 916. [CrossRef] [PubMed]
26. Gouder, L.; Vitrac, A.; Goubran-Botros, H.; Danckaert, A.; Tinevez, J.-Y.; André-Leroux, G.; Atanasova, E.; Lemière, N.; Biton, A.; Leblond, C.S.; et al. Altered Spinogenesis in IPSC-Derived Cortical Neurons from Patients with Autism Carrying de Novo SHANK3 Mutations. *Sci. Rep.* **2019**, *9*, 94. [CrossRef]
27. Boissart, C.; Poulet, A.; Georges, P.; Darville, H.; Julita, E.; Delorme, R.; Bourgeron, T.; Peschanski, M.; Benchoua, A. Differentiation from Human Pluripotent Stem Cells of Cortical Neurons of the Superficial Layers Amenable to Psychiatric Disease Modeling and High-Throughput Drug Screening. *Transl. Psychiatry* **2013**, *3*, e294. [CrossRef]
28. Mouilleau, V.; Vaslin, C.; Robert, R.; Gribaudo, S.; Nicolas, N.; Jarrige, M.; Terray, A.; Lesueur, L.; Mathis, M.W.; Croft, G.; et al. Dynamic Extrinsic Pacing of the HOX Clock in Human Axial Progenitors Controls Motor Neuron Subtype Specification. *Development* **2021**, *148*, dev194514. [CrossRef] [PubMed]
29. Gouder, L.; Tinevez, J.-Y.; Goubran-Botros, H.; Benchoua, A.; Bourgeron, T.; Cloëz-Tayarani, I. Three-Dimensional Quantification of Dendritic Spines from Pyramidal Neurons Derived from Human Induced Pluripotent Stem Cells. *J. Vis. Exp.* **2015**, *10*, 53197. [CrossRef]
30. Avale, M.E.; Faure, P.; Pons, S.; Robledo, P.; Deltheil, T.; David, D.J.; Gardier, A.M.; Maldonado, R.; Granon, S.; Changeux, J.-P.; et al. Interplay of B2* Nicotinic Receptors and Dopamine Pathways in the Control of Spontaneous Locomotion. *Proc. Natl. Acad. Sci. USA* **2008**, *105*, 15991–15996. [CrossRef]
31. Thiberge, C.; Pou, M.L.; Vitrac, A.; Maskos, U.; Cloëz-Tayarani, I. Humanized Chimeric Mouse Models to Study Human Neural Development and Pathogenesis of Brain Diseases. In *Translational Research Methods in Neurodevelopmental Disorders*; Martin, S., Laumonnier, F., Eds.; Neuromethods; Springer US: New York, NY, USA, 2022; Volume 185, pp. 135–158. ISBN 978-1-07-162568-2.
32. Nagashima, F.; Suzuki, I.K.; Shitamukai, A.; Sakaguchi, H.; Iwashita, M.; Kobayashi, T.; Tone, S.; Toida, K.; Vanderhaeghen, P.; Kosodo, Y. Novel and Robust Transplantation Reveals the Acquisition of Polarized Processes by Cortical Cells Derived from Mouse and Human Pluripotent Stem Cells. *Stem Cells Dev.* **2014**, *23*, 2129–2142. [CrossRef]
33. Livak, K.J.; Schmittgen, T.D. Analysis of Relative Gene Expression Data Using Real-Time Quantitative PCR and the $2-\Delta\Delta CT$ Method. *Methods* **2001**, *25*, 402–408. [CrossRef]
34. Elson, G.N.; DeFelipe, J. Chapter 10 Spine Distribution in Cortical Pyramidal Cells: A Common Organizational Principle across Species. In *Progress in Brain Research*; Elsevier: Amsterdam, The Netherlands, 2002; Volume 136, pp. 109–133. ISBN 978-0-444-50815-7.
35. Arlotta, P.; Molyneaux, B.J.; Chen, J.; Inoue, J.; Kominami, R.; Macklis, J.D. Neuronal Subtype-Specific Genes That Control Corticospinal Motor Neuron Development In Vivo. *Neuron* **2005**, *45*, 207–221. [CrossRef]
36. Arlotta, P.; Molyneaux, B.J.; Jabaudon, D.; Yoshida, Y.; Macklis, J.D. Ctip2 Controls the Differentiation of Medium Spiny Neurons and the Establishment of the Cellular Architecture of the Striatum. *J. Neurosci.* **2008**, *28*, 622–632. [CrossRef] [PubMed]
37. Saito, K.; Kakizaki, T.; Hayashi, R.; Nishimaru, H.; Furukawa, T.; Nakazato, Y.; Takamori, S.; Ebihara, S.; Uematsu, M.; Mishina, M.; et al. The Physiological Roles of Vesicular GABA Transporter during Embryonic Development: A Study Using Knockout Mice. *Mol. Brain* **2010**, *3*, 40. [CrossRef] [PubMed]
38. Silva, C.G.; Peyre, E.; Nguyen, L. Cell Migration Promotes Dynamic Cellular Interactions to Control Cerebral Cortex Morphogenesis. *Nat. Rev. Neurosci.* **2019**, *20*, 318–329. [CrossRef] [PubMed]
39. Wahle, P.; Sobierajski, E.; Gasterstädt, I.; Lehmann, N.; Weber, S.; Lübke, J.H.; Engelhardt, M.; Distler, C.; Meyer, G. Neocortical Pyramidal Neurons with Axons Emerging from Dendrites Are Frequent in Non-Primates, but Rare in Monkey and Human. *eLife* **2022**, *11*, e76101. [CrossRef] [PubMed]
40. Brüstle, O.; Maskos, U.; McKay, R.D.G. Host-Guided Migration Allows Targeted Introduction of Neurons into the Embryonic Brain. *Neuron* **1995**, *15*, 1275–1285. [CrossRef]
41. Fame, R.M.; Cortés-Campos, C.; Sive, H.L. Brain Ventricular System and Cerebrospinal Fluid Development and Function: Light at the End of the Tube: A Primer with Latest Insights. *BioEssays* **2020**, *42*, 1900186. [CrossRef]
42. Hatanaka, Y.; Zhu, Y.; Torigoe, M.; Kita, Y.; Murakami, F. From Migration to Settlement: The Pathways, Migration Modes and Dynamics of Neurons in the Developing Brain. *Proc. Jpn. Acad. Ser. B* **2016**, *92*, 1–19. [CrossRef]
43. Nato, G.; Corti, A.; Parmigiani, E.; Jachetti, E.; Lecis, D.; Colombo, M.P.; Delia, D.; Buffo, A.; Magrassi, L. Immune-Tolerance to Human IPS-Derived Neural Progenitors Xenografted into the Immature Cerebellum Is Overridden by Species-Specific Differences in Differentiation Timing. *Sci. Rep.* **2021**, *11*, 651. [CrossRef]

44. Itakura, G.; Ozaki, M.; Nagoshi, N.; Kawabata, S.; Nishiyama, Y.; Sugai, K.; Iida, T.; Kashiwagi, R.; Ookubo, T.; Yastake, K.; et al. Low Immunogenicity of Mouse Induced Pluripotent Stem Cell-Derived Neural Stem/Progenitor Cells. *Sci. Rep.* **2017**, *7*, 12996. [CrossRef]
45. Cascalho, M.; Platt, J.L. The Immunological Barrier to Xenotransplantation. *Immunity* **2001**, *14*, 437–446. [CrossRef]
46. Namihira, M.; Kohyama, J.; Semi, K.; Sanosaka, T.; Deneen, B.; Taga, T.; Nakashima, K. Committed Neuronal Precursors Confer Astrocytic Potential on Residual Neural Precursor Cells. *Dev. Cell* **2009**, *16*, 245–255. [CrossRef] [PubMed]
47. Vigneault, É.; Poirel, O.; Riad, M.; Prud'homme, J.; Dumas, S.; Turecki, G.; Fasano, C.; Mechawar, N.; El Mestikawy, S. Distribution of Vesicular Glutamate Transporters in the Human Brain. *Front. Neuroanat.* **2015**, *9*, 23. [CrossRef] [PubMed]
48. Cunningham, C.L.; Martinez-Cerdeno, V.; Noctor, S.C. Microglia Regulate the Number of Neural Precursor Cells in the Developing Cerebral Cortex. *J. Neurosci.* **2013**, *33*, 4216–4233. [CrossRef] [PubMed]
49. Matejuk, A.; Ransohoff, R.M. Crosstalk Between Astrocytes and Microglia: An Overview. *Front. Immunol.* **2020**, *11*, 1416. [CrossRef] [PubMed]
50. Popova, G.; Soliman, S.S.; Kim, C.N.; Keefe, M.G.; Hennick, K.M.; Jain, S.; Li, T.; Tejera, D.; Shin, D.; Chhun, B.B.; et al. Human Microglia States Are Conserved across Experimental Models and Regulate Neural Stem Cell Responses in Chimeric Organoids. *Cell Stem Cell* **2021**, *28*, 2153–2166.e6. [CrossRef]
51. Stogsdill, J.A.; Kim, K.; Binan, L.; Farhi, S.L.; Levin, J.Z.; Arlotta, P. Pyramidal Neuron Subtype Diversity Governs Microglia States in the Neocortex. *Nature* **2022**, *608*, 750–756. [CrossRef]
52. Tan, Y.-L.; Yuan, Y.; Tian, L. Microglial Regional Heterogeneity and Its Role in the Brain. *Mol. Psychiatry* **2020**, *25*, 351–367. [CrossRef]
53. Davis, B.M.; Salinas-Navarro, M.; Cordeiro, M.F.; Moons, L.; De Groef, L. Characterizing Microglia Activation: A Spatial Statistics Approach to Maximize Information Extraction. *Sci. Rep.* **2017**, *7*, 1576. [CrossRef]
54. Arellano, J.I. Ultrastructure of Dendritic Spines: Correlation between Synaptic and Spine Morphologies. *Front. Neurosci.* **2007**, *1*, 131–143. [CrossRef]
55. Helm, M.S.; Dankovich, T.M.; Mandad, S.; Rammner, B.; Jähne, S.; Salimi, V.; Koerbs, C.; Leibrandt, R.; Urlaub, H.; Schikorski, T.; et al. A Large-Scale Nanoscopy and Biochemistry Analysis of Postsynaptic Dendritic Spines. *Nat. Neurosci.* **2021**, *24*, 1151–1162. [CrossRef]
56. Linker, S.B.; Narvaiza, I.; Hsu, J.Y.; Wang, M.; Qiu, F.; Mendes, A.P.D.; Oefner, R.; Kottilil, K.; Sharma, A.; Randolph-Moore, L.; et al. Human-Specific Regulation of Neural Maturation Identified by Cross-Primate Transcriptomics. *Curr. Biol.* **2022**, *32*, 4797–4807.e5. [CrossRef] [PubMed]

Supplementary Materials

Developmental changes of human neural progenitor cells grafted into the ventricular system and prefrontal cortex of mouse brain in-utero

Figure S1

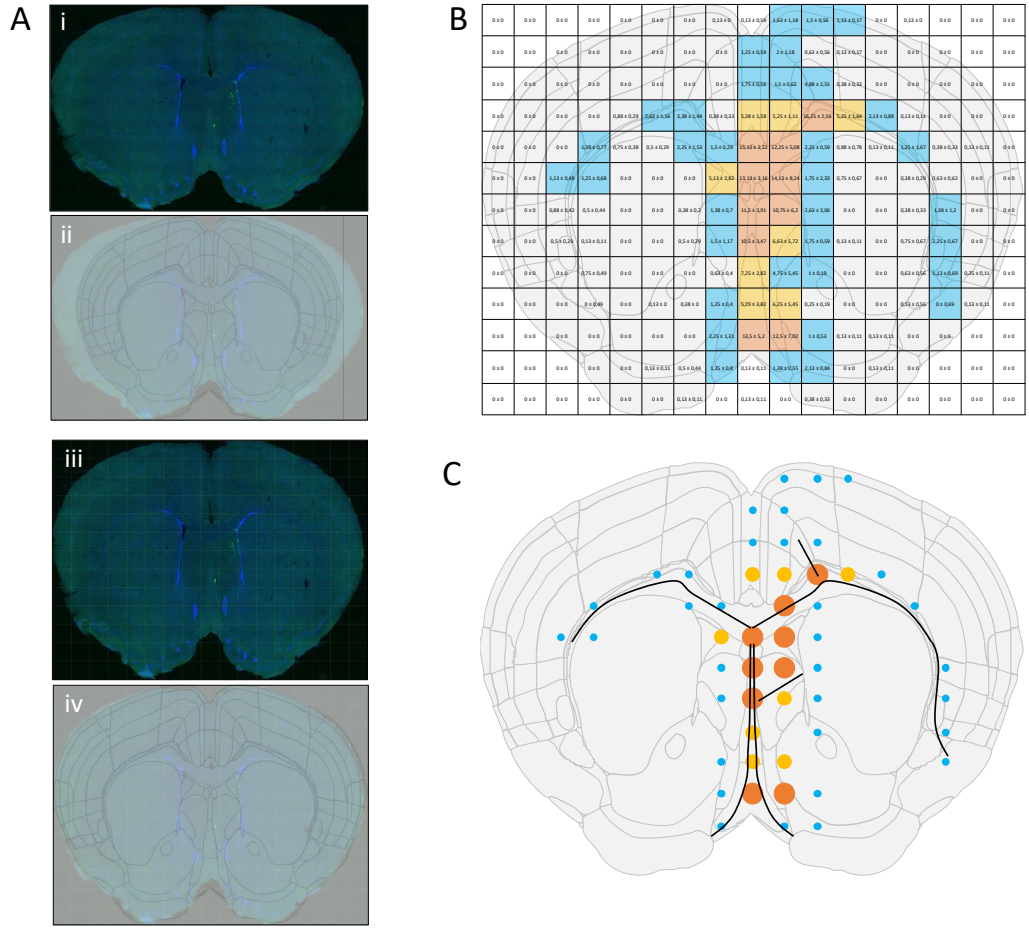

Figure S1 *Cont.*

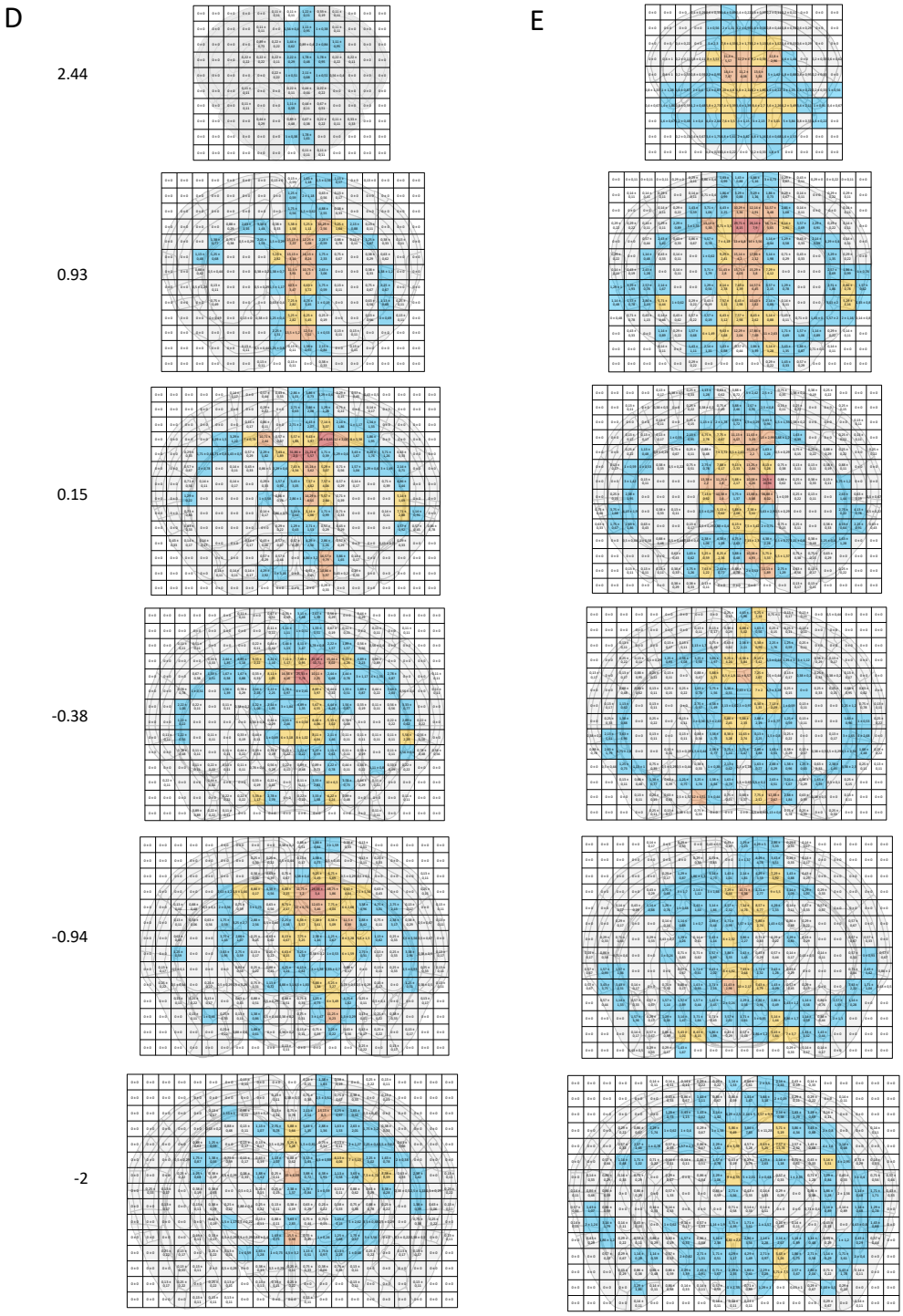

Figure S1. Illustration of the pipeline to study neuronal projections, related to Figure 3 and to Figure 4. (A) Pictures of the whole brain slice before (i, ii) and after (iii, iv) running a homemade macro (available upon request) to re-size the brain images to match the brain atlas drawings and create a grid. (B) The average and SEM of the counting of three brains are transferred into a numerical grid and merged to the coordinate illustration from the Allen Brain Atlas (Bregma, indicated in mm). A color code is used to better visualize the density and distribution of the projections. (C) Final visualization of the projection's distribution. (D-E) Extended data for the mapping of neuronal projections at 1 MPT (D) and 3 MPT (E).

Figure S2

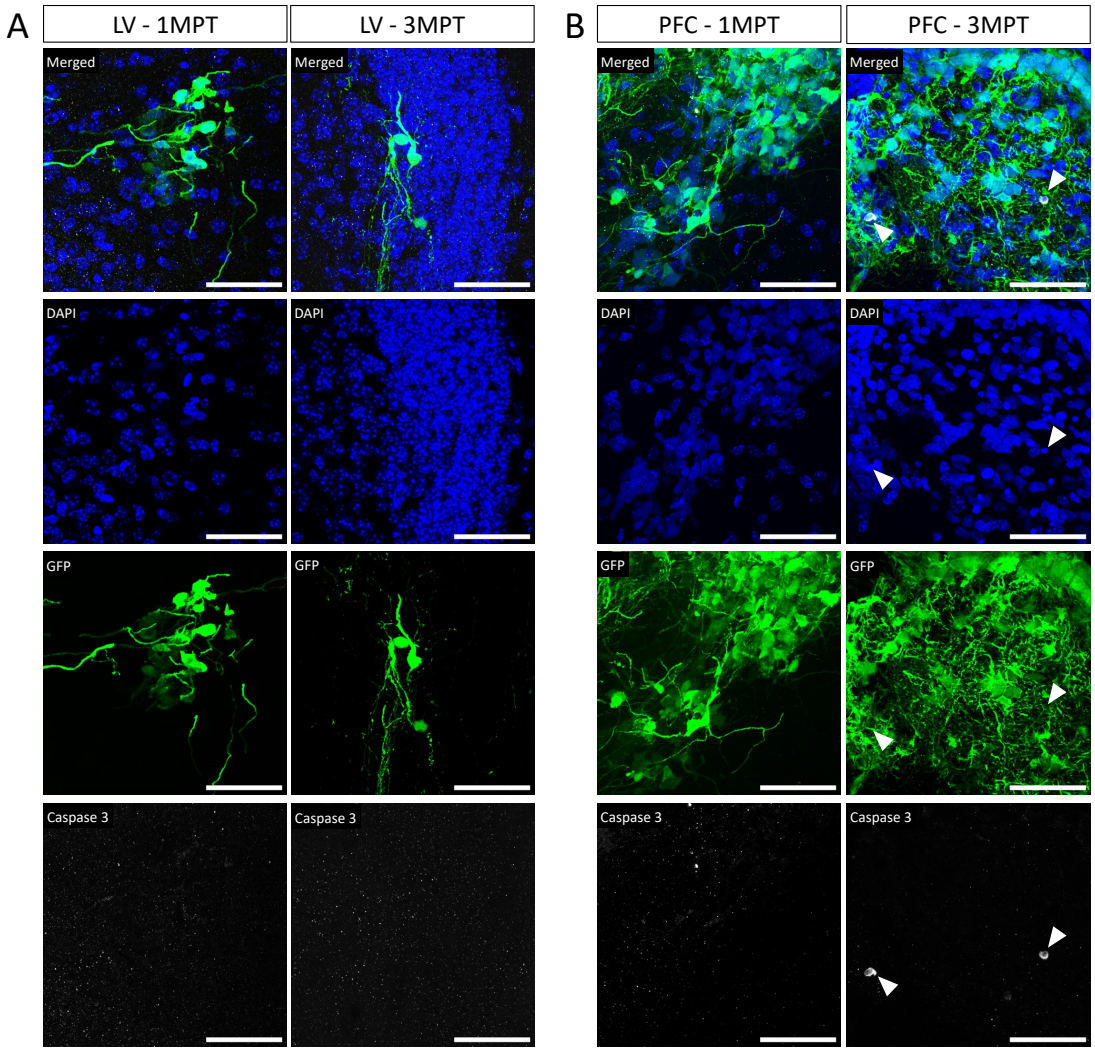

Figure S2. Absence of apoptotic GFP-cells at 1MPT and 3MPT in LV and PFC transplants, related to Figure 5. Confocal images at 1 MPT and 3 MPT for LV and PFC transplanted mice. The transplanted human cells are labeled with GFP. No GFP+ cells were labeled with the apoptotic marker Caspase3 in all conditions. Rare Caspase3+ cells (white arrows) were observed but no colocalization with the human cells is detected. Scale bar = 50µm. Results are from two independent experiments.

Figure S3

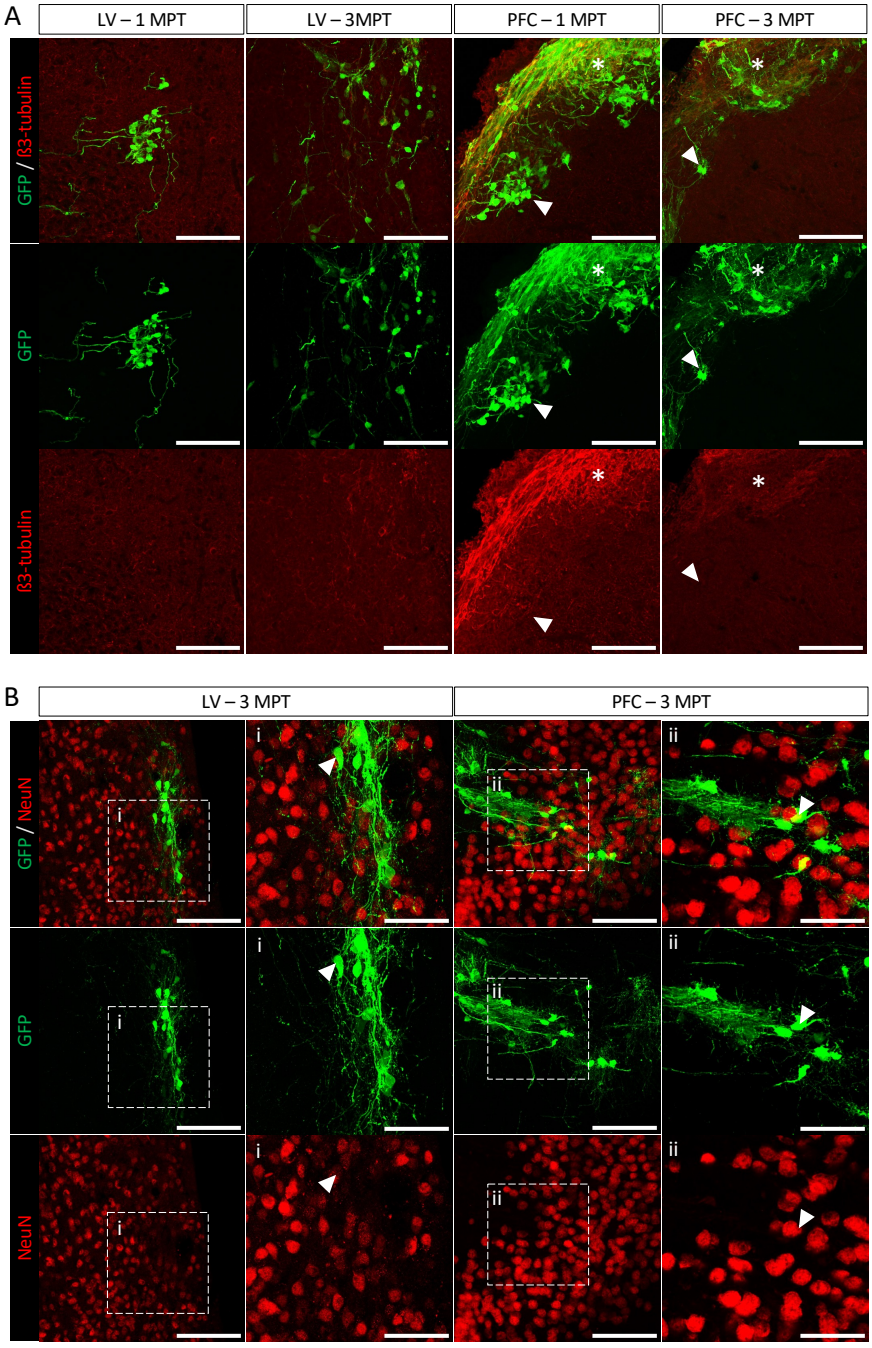

Figure S3. Maturation of grafted GFP-cells in LV (1 MPT and 3 MPT) and PFC (3 MPT) transplants, related to Figure 5. Confocal images at 3 MPT for LV and PFC transplanted mice. The transplanted human cells are labeled with GFP. (A) Immunofluorescence staining of β3-tubulin, a marker of the early phases of neuronal differentiation. (B) Immunofluorescence staining of NeuN, a post-mitotic neuronal marker. β3-tubulin-positive human cells is observed in the superficial parts of PFC transplants, where the host cells are scarce (indicated by asterisk). Only a few NeuN-positive human cells are detected within the same region. In LV transplants, only a few cells were positive for NeuN. Labeled cells are indicated by arrowheads. (A) Scale bar = 100μm. (B) Scale bar = 50μm.

Table S1. List of products with their reference and the used dilution of final concentration for NPCs medium, related to Materials and Methods Section.

NPC Medium	Ref	Company	Dilution factors
DMEM/F-12, GlutaMAXTM Supplement	31331028	ThermoFisher	1/2
Neurobasal medium	21103049	ThermoFisher	1/2
B27 supplement (50X)	11500446	ThermoFisher	1/50
N2 supplement (100X)	07152	StemCell	1/100
Penicillin Streptomycin (10 000 U/ml)	11548876	ThermoFisher	1/100
2-mercaptoethanol Stock solution (50mM)	11528926	ThermoFisher	1/1000
Factors	**Ref**	**Company**	**Final concentration**
Human EGF, premium grade	78006.1	StemCell	10ng/ml
Human FGF-2 IS, premium grade/BFGF	78003.1	StemCell	10ng/ml
Human Recombinant BDNF	78005	StemCell	20ng/ml
Coating	**Ref**	**Company**	**Final concentration**
Geltrex	A1413302	ThermoFisher	120-180µg/ml
Laminine (1mg/ml)	L2020	Sigma	10µg/ml
Poly-L-Ornithine (1mg/ml)	P3655	Sigma	15µg/ml

Table S2. List of primers used for Real-Time PCR, related to Materials and Methods Section.

Gene	Primers	Product size (bp)
Oct4	5'- CAGCAGATCAGCCACATCGC-3'	60
	3'- CCACACTCGGACCACATCCT-5'	
Nestin	5'-TTCCCTCAGCTTTCAGGACCC-3'	130
	3'-CTCAAGGGTAGCAGGCAAGG-5'	
Pax6	5'-GCAAGAATACAGGTATGGTTTTC-3'	155
	3'-GTGGGTTGTGGAATTGGTTG-5'	
Tuj1	5'-CTACAACGAGGCCTCTTCTCACAA-3'	60
	5'-GGTTCCAGGTCCACCAGAATG-3'	
VGLUT1	5'- CGACAGCCTTTTGTGGTTCC-3'	237
	3'-GGTTCATGAGTTTCGCGCTC-5'	
Cux1	5'- GCTCTCATCGGCCAATCACT-3'	75
	3'-TCTATGGCCTGCTCCACGT-5'	
CTIP2	5'-GAGTACTGCGGCAAGGTGTT-3'	98
	3'-TAGTTGCACAGCTCGCACTT-5'	
VGAT	5'-CCATCCAGGGCATGTTC-3'	103
	3'-GTGTAGCAGCACACAACG-5'	
GFAP	5'-TCCACGAGGAGGAGGTTCG-3'	200
	3'-GGCAGCAGCGTCTGTCAG-5'	
GAPDH	5'-TCTGCTCCTCCTGTTCGACA-3'	141
	3'-AAAAGCAGCCCTGGTGACC-5'	

Table S3. List of antibodies used for immunohistochemistry and immunocytochemistry, related to Materials and Methods Section.

PRIMARY ANTIBODIES				
Name	Ref	Company	Host	Dilution
GFAP	G-3893	Sigma	Mouse	1/200
GFP	A6455	Invitrogen	Rabbit	1/750
GFP	MAB3580	Millipore	Mouse	1/750
Iba1	019-19741	Wako Chemicals	Rabbit	1/500
Ki67	14-5698-80	Invitrogen	Rat	1/100
Nestin	MAB5326	Millipore	Mouse	1/200
NeuN	MAB377	Millipore	Mouse	1/200
SOX2	14-9811-80	Invitrogen	Rat	1/100
VGLUT1	135303	Synaptic System	Rabbit	1/1000
Olig2	Ab220796	Abcam	Rabbit	1/1000
ß3-Tubulin	Ab9354	Abcam	Chicken	1/200
Caspase-3	9661	Cell Signaling	Rabbit	1/300
SECONDARY ANTIBODIES				
Name	Ref	Company	Host	Dilution
Anti-mouse Alexa 488	715-545-150	Jackson Laboratory	Donkey	1/500
Anti-rabbit Alexa 488	711-545-152	Jackson Laboratory	Donkey	1/500
Anti-mouse Alexa 594	715-585-150	Jackson Laboratory	Donkey	1/500
Anti-rabbit Alexa 594	711-585-152	Jackson Laboratory	Donkey	1/500
Anti-rat Alexa 594	712-585-153	Jackson Laboratory	Donkey	1/500
Anti-chicken Alexa 594	703-585-155	Jackson Laboratory	Donkey	1/500
Anti-mouse Alexa 647	715-605-151	Jackson Laboratory	Donkey	1/500
Anti-rabbit Alexa 647	711-605-152	Jackson Laboratory	Donkey	1/500
Anti-rat Alexa 647	712-605-153	Jackson Laboratory	Donkey	1/500

Video S1. Illustration of the in -utero surgery with a visible embryo 's brain and injection process, related to Figure 2.

Video S2. 3D representation of a GFP+ neuron in the PFC, using Imaris 9.5 software, related to Figure 3.

Video S3: 3D representation of GFAP labeling using Imaris 9.5 software, related to Figure 5. GFAP labeling is in red fluorescence. The results show the absence of GFAP colabeling with human GFP+ cells. Other videos are available upon request.

Video S4. 3D reconstruction of a dendrite segment (grey) and spines (blue) of a LV transplanted cell, related to Figure 5. Yellow dots represent colocalization of VGLUT1 with the dendrite and the red dots represent a negative colocalization between VGLUT1 and the neuron.

Video S5. 3D reconstruction of a dendrite segment (grey) and spines (blue) of a PFC transplanted cell using the Imaris 9.5 software, related to Figure 5. Green dots represent colocalization between VGLUT1 and the spine and yellow dots represent colocalization of VGLUT1 with the dendrite. The red dots represent a negative colocalization between VGLUT1 and the neuron.

Video S6. 3D reconstruction of a dendrite and the spines of a GFP+ neuron in the PFC using the Imaris 9.5 software, related to Figure 6. Color classification of the spines is as follows: purple = filopodia, red = stubby, green = mushroom, blue = thin.

Book Chapter

Humanized Chimeric Mouse Models to Study Human Neural Development and Pathogenesis of Brain Diseases.

Camille Thiberge[1,2,†], Maria Llach Pou[1,2,†], Aline Vitrac[3], Uwe Maskos[1,2] and Isabelle Cloëz-Tayarani[1,2*]

[1]Institut Pasteur, Université Paris Cité, Unité de Neurobiologie Intégrative des Systèmes Cholinergiques, CNRS UMR 3571 "Gènes, Synapses et Cognition", Institut Pasteur, 25 rue du Docteur Roux, 75015 Paris, France.

[2]Sorbonne Université, Collège doctoral, 75005 Paris, France.

[3]Human Genetics and Cognitive Functions, CNRS UMR 3571 « Genes, Synapses and Cognition », Université de Paris, Institut Pasteur, Paris, France

*Correspondence: Isabelle Cloëz-Tayarani. Tel +33 (0)1 45 68 88 04

† These authors contributed equally to this work.

Chapter 8

Humanized Chimeric Mouse Models to Study Human Neural Development and Pathogenesis of Brain Diseases

Camille Thiberge, Maria Llach Pou, Aline Vitrac, Uwe Maskos, and Isabelle Cloëz-Tayarani

Abstract

The development of humanized neural chimeric mouse models consists in grafting human neuronal progenitor cells (NPC) or differentiated neurons derived from induced pluripotent stem cells (iPSC) into the mouse brain at different time points. As the main features of cortical networks and their alterations during brain development cannot be reproduced in vitro, these in vivo models have been used to investigate the mechanisms by which reprogrammed human neurons and non-neuronal cells integrate and migrate into the mouse brain at early stages of brain development and display functional activities several months after their grafting. Here, we describe the neonatal grafting technique of human NPC which we use in our laboratory. We also present a new method based on the grafting of human NPC into the brain of mouse embryos, in utero. A third method consists in the stereotaxic grafting of human NPC into selected brain regions of adult mice. The iPSC technology combined with the use of chimeric mouse models offers numerous possibilities to study human neural development within well-controlled and defined temporal windows and to model neuropathological disorders.

Key words Xenografting, In utero transplant, Human stem cells, Induced pluripotent stem cells, Chimeric mouse models, Neurodevelopment, Neurodevelopmental Disorders

1 Introduction

The reprogramming of human embryonic stem cells (ESC) or induced pluripotent stem cells (iPSC) into neuronal progenitor cells (NPC) and mature neurons is of major interest to study brain development during the critical periods of establishing diversity, connectivity, and functional maturation of neurons within the central nervous system (CNS). These properties are particularly important within the cortical regions and the targeted areas of their innervation. A specificity of the cerebral cortex resides in the

Authors Camille Thiberge and Maria Llach Pou have equally contributed to this chapter.

Stéphane Martin and Frédéric Laumonnier (eds.), *Translational Research Methods in Neurodevelopmental Disorders*, Neuromethods, vol. 185, https://doi.org/10.1007/978-1-0716-2569-9_8,

existence of multiple cortical sections that are structurally and functionally organized into connected units to exert different functions through a large variety of neuronal subtypes [1]. At later stages of development, postmitotic neocortical neurons conserve a high degree of plasticity which allows the postnatal reorganization of specific neural microcircuits in vivo [2] .

To date, different ESC and iPSC reprogramming protocols have been developed which can be used to produce various neuronal subtypes [3] . In particular, the reprogramming of stem cells into human cortical neurons has made it possible to study various developmental features after their grafting within the prefrontal cortex [4] . Interestingly enough, it has been shown that grafted ESC-derived human cortical neurons can integrate functionally into the lesioned mouse brain, when their cellular identity corresponds to that of the brain area under grafting [5]. In humans, the cortex is organized into six layers [6] which contain neurons with selective spatial organization and distinct biochemical, morphological, and electrophysiological characteristics [7–10] . The axonal projections of these cells are also specific not only to their cortical location but also to the neuronal phenotype. Thus, the excitatory pyramidal cortical neurons project into various but specific regions of the brain, while the interneurons' projections remain local within the cortical layers.

Xenografting of human neuronal progenitor cells into a rodent host allows their study in vivo on an extended time scale (up to 10–12 months) [11, 12] as compared to in vitro studies (70–80 days in culture) [13]. In addition to such an important temporal aspect, the growth of human xenografted neurons takes place in a vascularized environment, which is essential for the survival of the transplanted cells. It has also been shown that the oligodendrocytes of host mice have the ability to myelinate the axons of grafted human neurons [4], which is an essential process to their long-term functional activity. The cortical identity of the grafted neurons, which depends on the layer in which they are positioned, as well as the temporal characteristics of their development is also maintained after transplantation [4, 11, 14]. Thus, the maturation of human neurons can take place over several months despite their development in a more mature murine environment [11]. A recent study has shown that when NPC are transplanted together with deep-layer cortical neurons into the brain of adult mice, the first synapses are visible after only 20 days of development and their number increases gradually overtime [14].

A summary of the xenografting studies carried out to date with human cells is presented in Table 1. It should be noted that most of these studies have been performed in newborn or adult rodents with ES- or iPS-derived human neurons. The main phenotypes studied are also indicated, whether they are morphological and/or functional.

Table 1
Reported studies using xenotransplantation of human stem cell-derived neurons

Human cell origin	Host	Brain region	Graft integration	Functionality	References
Fetal brain cells	Rat embryo	Brain ventricles	Widespread incorporation of neurons	n.d.	[22]
Embryonic NSC	Adult rat	SVZ and Hp	Migration along the routes taken by endogenous precursors. Substantial migration within the striatum	n.d.	[23]
Fetal brain cells	Mouse neonate	Brain ventricles	Proliferation, migration, and neural differentiation (7 MPT)	n.d.	[24]
NSC	Monkey fetus at 12–13-week gestation	Brain ventricles	At 16–17 weeks of gestation: Two subpopulations: Differentiated neurons and glia Undifferentiated cells (SVZ)	n.d.	[25]
ESC-derived NPC	Mouse neonate	Brain ventricles	At 1–4 WPT: Incorporation of cells in cortex, Hp, OB, septum, thalamus, hypothalamus, striatum midbrain, and some white matter regions Differentiation into neurons and astrocytes	n.d.	[26]
ESC	Chick embryo	In ovo grafting into somites; 1.5–2 days of development	6–7 days post-surgery Differentiation and migration into DRG, neural tube	n.d.	[27]
Immortalized NS-like cells	Rat with focal cerebral ischemia	i.v. injection	Differentiation into neurons and astrocytes in lesioned areas; survival up to 56 days after grafting (cortex and striatum)	Generation of AP and synaptic integration- Miniature EPSC	[28]
Differentiated ESC	Mouse embryo (E14)	Brain ventricles	2 MPT: Widespread incorporation including within cortex and hippocampus	8 MPT: Action potentials	[29]

(continued)

Table 1
(continued)

Human cell origin	Host	Brain region	Graft integration	Functionality	References
ESC-derived NPC	Young/adult rat brain	Brain ventricles	Integration into SVZ; migration along the rostral migratory stream to olfactory bulb; contribution to neurogenesis	n.d.	[30]
ESC-derived DA neurons (+ astrocytes)	6-OHDA-lesioned adult rat	Striatum	Substantial neuronal recovery	Behavioral testing	[31]
ESC-derived striatal progenitors	Adult rat	Striatum	Xenograft overgrowth and persistent proliferation of NPC	n.d.	[32]
ESC-derived DA neurons	Parkinsonian models in mouse, rat, and monkey	Striatum	4–5 MPT. No neural overgrowth. In vivo survival. Restoration of behavioral symptoms	Membrane potential oscillations	[33]
ESC-derived retinal progenitors	Mouse neonate	Subretinal space and intravitreal space	Migration in mouse retina. Differentiation into functional photoreceptors	Restoration of visual functions in *Crx*-deficient mice	[34]
ESC-derived neural rosettes	Adult rat	Striatum	Survival and integration 4 weeks after transplantation	n.d.	[35]
iPSC-derived DA neurons from patients with Parkinson	Adult rat	Striatum	4–16 WPT: High level of cell survival, arborization with few projections into host striatum	Reduced motor asymmetry of 6-OHDA-lesioned rats	[36]
ESC-derived cortical neurons	Mouse neonate	Cortex	Integration, establishment of specific axonal projections and dendritic patterns of cortical neurons	9 MPT: Firing patterns, synaptic potentials	[4]

ESC-derived MGE-like cells	Mouse	Hippocampus	Synaptic connections with endogenous neurons	Improvements in learning and memory deficits	[37]
PSC-derived MGE progenitors	Mouse neonate (P2)	Cortex	3–7 MPT: Cell migration in the cortex; maturation into GABAergic interneuron subtypes	7 MPT: Firing patterns, synaptic potentials	[38]
Fetal NSC	Monkey	Midbrain	Generation of neurons that project long fibers in adult brain (+GDNF)	n.d.	[39]
ESC- and iPSC-derived interneurons	Mice	Hippocampus	Differentiation method to MGE or CGE cells and subclasses of GABAergic interneurons	n.d.	[40]
ESC-derived cortical neurons	Adult mouse	Lesioned visual cortex	Restoration of damaged cortical pathways	Mature electrical neuronal profile	[5]
iPSC-derived NPC	Mouse neonate (P0)	Brain ventricles	Migration and wide dispersion of transplanted cells into the mouse brain (detection in the cerebellum at 6 MPT) Differentiation into excitatory neurons, astrocytes, and oligodendrocytes	Functional mature neurons at 13 MPT	[41]
MGE-derived progenitors	Mouse neonate (P1-4)	Dorsal hippocampus	Differentiation of transplanted cells in PV and SOM interneurons	Functional inhibitory synapses with the host	[42]
ESC-derived interneurons	Adult rat	Prefrontal cortex	In situ differentiation of PV interneurons after grafting	Firing analysis of the host pyramidal cells	[43]
iPSC-derived progenitors and cortical excitatory neurons	Adult mouse	Somatosensory cortex	Graft vascularization 5 MPT: long-range selective projections	Inhibitory and excitatory inputs, firing patterns	[14]
PSC-derived cortical interneurons	Mouse	Cortex	Protocol optimization for cell banking before grafting. Graft integration and cell migration	n.d.	[44]

(continued)

for

Table 1
(continued)

Human cell origin	Host	Brain region	Graft integration	Functionality	References
iPSC-derived interneuron precursors	Rat model of epilepsy	Hippocampus	Synapse formation between graft-derived axons and host hippocampal excitatory neurons in DG and CA1 field	Involvement of graft-derived interneurons in seizure control	[45]
Embryonic PSC-derived cortical neurons	Mouse neonate (P0-1)	Brain ventricles	Integration in the mouse cortex as single cells	10 MPT: mature firing patterns	[11]
H9 stem cell-derived NPC	Adult mouse and rat	Frontal cortex	Transduction with human channel rhodopsin. At 3MPT: differentiation into GABAergic neurons. Dense terminal fields and innervation of dendrites in host cortical neurons	Light stimulation of hChR2-hNP transplants: variability in grafted neuron response	[46]
MGE-derived interneurons	ASD model and WT mouse neonate (P1-3)	Prefrontal cortex	At 8 WPT: Integration into PFC, anterior cingulate, dorsal insular, primary motor, and somatosensory areas In WT mouse: higher differentiation into SOM interneurons In ASD mouse model: higher differentiation into PV interneurons	Rescue of social interaction of ASD model mouse	[47]
iPSC-derived NPC	Mouse neonate	Frontal cortex/brain ventricles	At 2 MPT: Axonal projections in the mouse cortex Differentiation into pyramidal neurons, SOM neurons, astrocytes, and oligodendrocytes 4 MPT: Graft vascularization	n.d.	[12]

iPSC-derived NPC	Mouse neonate	Frontal cortex or brain ventricles	At 50 DPT into: Brain ventricles: migration to olfactory bulbs following the rostral migratory stream Cortex: axonal projections into different brain areas following white mater fibers (fimbria and stria terminalis)	n.d.	[15]
ESC-derived midbrain DA or cortical glutamate neurons	Adult Parkinson mouse model	Substantia nigra or striatum	Projection of axons in different brain areas depending on neuron subtypes	Functional (/anatomical) synaptic inputs dependent of neuronal subtypes (/graft site) Rescue of motor deficits by dopaminergic grafted neurons	[48]

Abbreviations: *AP* action potentials, *ASD* autism spectrum disorders, *CGE* caudal ganglionic eminence, *DA* Dopaminergic, *DPT* days post-transplantation, *DRG* dorsal root ganglion, *EPSC* excitatory postsynaptic current, *Hp* hippocampus, *MGE* medial ganglionic eminence, *MPT* month post-transplantation, *OB* olfactory bulb, *PSC* pluripotent stem cells, *PFC* prefrontal cortex, *PSC* pluripotent stem cells, *PV* parvalbumin, *SOM* somatostatin, *SVZ* subventricular zone

neonatal transplants. This protocol has provided the means to analyze some of the processes which take place during the early stages of neuronal maturation, and on the role of SHANK3, a postsynaptic protein which is altered in autism spectrum disorders (ASD) as we reported previously [15]. In the course of this study, we also found that the maturation of the same reprogrammed neurons was slower in vivo as compared to in vitro conditions, using the same cells in both studies [15, 16] .

We will then describe a step-by-step protocol which consists in grafting human-derived NPC in mice in utero. This new method, which has not been used in mice to date, provides the means to study the early stages of human development and neural precursor events before they start differentiating. Another important aspect resides in the fact that in utero grafting allows the use of immunocompetent mice. Finally, we describe a transplantation method in adult mice which can be particularly adapted to the grafting of inhibitory neurons which have limited projections to cortical areas. We will highlight the diverse applications of each of these methods for studying different pathologies at their earliest stages during brain development.

2 Materials

2.1 Media

NPC Culture Medium The culture medium consisted of 500 mL of DMEM/F-12 mixed with 500 mL of Neurobasal medium and supplemented with two vials (5 mL each) of N2 supplement (Gibco^{TM}, ref. 17502048), two vials (10 mL each) of B27 supplement (Gibco^{TM}, ref. 17504044), 10 mL of penicillin-streptomycin (penicillin = 10,000 units/ml and streptomycin = 10,000 units/mL), and 0.1 mM of 2-ßmercaptoethanol. Growth factors were selectively added as described in Fig. 1.

Flask Coating Culture flasks were initially coated with Geltrex (Gibco^{TM} ref. A1413302) diluted to 1/100 in DMEM/F-12 and incubated for at least one hour at 37 °C.

The following is the list of primary antibodies and their corresponding secondary antibodies as well as DAPI reference

Primary antibody			Secondary antibody		
Name	**Ref**	**Dilution**	**Name**	**Ref**	**Dilution**
Anti-GFP rabbit serum	A6455, Invitrogen	1/750	Donkey anti-rabbit Alexa 488	DZP030, Jackson Interchim	1/200

(continued)

Primary antibody			Secondary antibody		
Name	**Ref**	**Dilution**	**Name**	**Ref**	**Dilution**
Anti-GFP rabbit serum	A6455, Invitrogen	1/750	Donkey anti-rabbit Alexa 594	Jackson Interchim	1/200
Rabbit anti-VGluT1	135303, Synaptic Systems	1/1000	Donkey anti-Rabbit Alexa 488	DZP030, Jackson Interchim	1/200
DAPI	D9542, Merck	1/200			

Equipment Stretcher apparatus (Narishige PB-7 needle puller), glass pipettes: dimensions: 1.0 OD × 0.78 ID × 100 L mm, Sterile Towel Drape 18″ × 26″ – 46 × 66 cm (4410-IMC) Imcoinc; Harvard Syringe Pump (Harvard apparatus PHD 2000); vibratome (Leica Biosystems, V1000S); microtome (Leica SM 2010R); confocal laser scanning microscope with a 488 nm laser for GFP excitation, and a 555 nm laser for mCherry excitation.

3 Methods

3.1 Neuronal Progenitor Cells (NPC) from Human iPSC Lines

The purpose of this section is to specifically describe the protocols which allow amplification and labeling of neuronal progenitor cells (NPC) before their grafting into the mouse brain.

For this study, we used two control cell lines from Coriell Biorepository (Coriell Institute for Medical Research), the GM04603 (https://www.coriell.org/Search?q=GM04603) and GM01869 (https://www.coriell.org/Search?q=GM01869). Their derivation into NPC and their characterization have been described elsewhere [17]. For protocol optimization, we used the WTSIi002-A line (https://cells.ebisc.org/WTSIi002-A/ Wellcome Trust, UK) as in a previous study [18]. Protocol modifications result from the constant development of new commercial products to simplify and optimize iPSC-derivation protocols, without altering the cell differentiation. For the illustrations presented here, we only selected the original data obtained with the GM04603 iPSC line. Figure 1a shows the experimental conditions used, according to Boissart et al. (2013) [17], to derive human iPSC with slight modifications. Figure 1b shows NPC amplification and labeling, with the selected growth and transcription factors used in this study. Figure 1c describes the map of a lentiviral vector for GFP labeling [15].

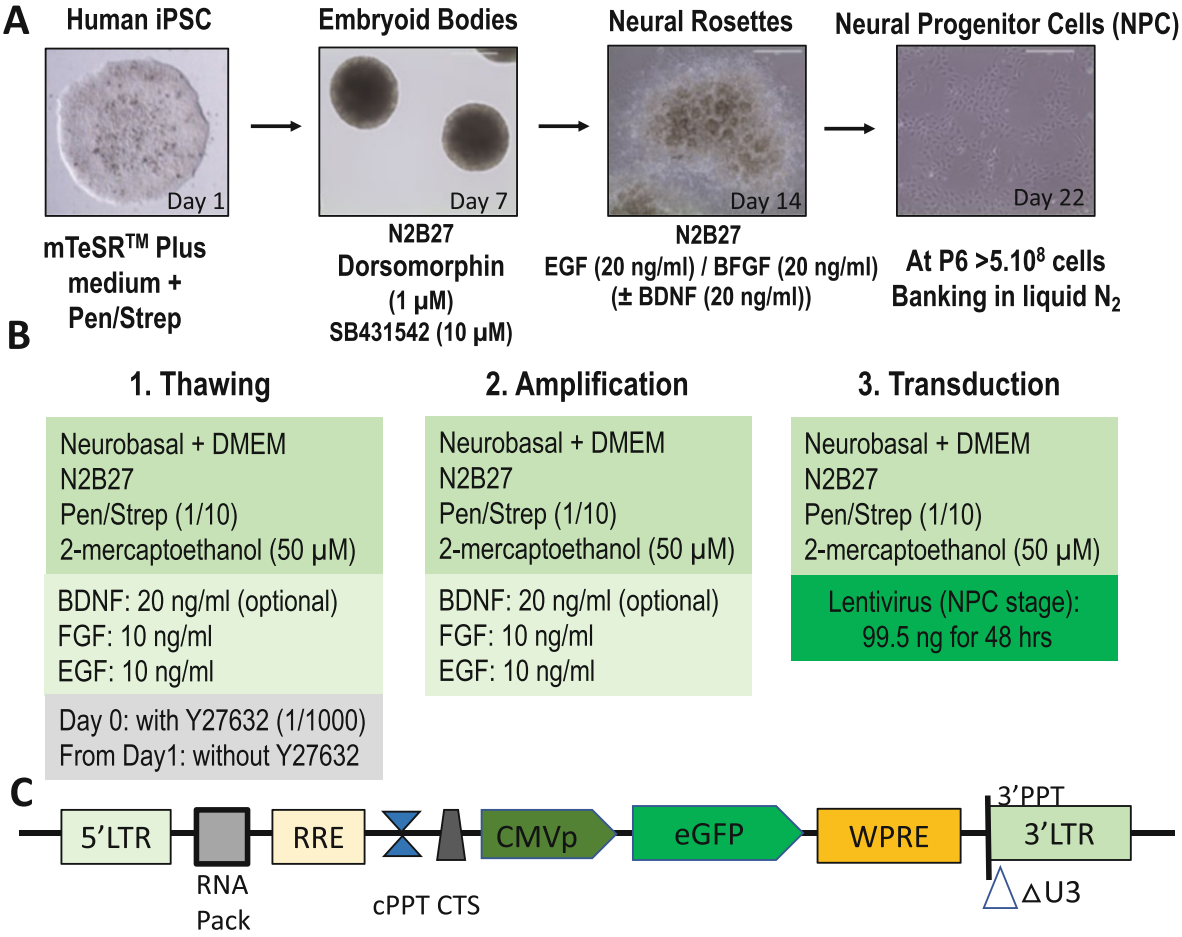

Fig. 1 In vitro cell differentiation, amplification, and labeling before engraftment. (**a**) Human iPSC are first amplified and then differentiated in early cortical progenitors, and then to NPC with further amplification before banking. (**b**) Description of NPC amplification and labeling before grafting into mouse brain. GFP labeling (green fluorescence) can be started directly from the stock of frozen NPC. (**c**) Schematic representation of the lentiviral construct for transduction of NPC with GFP using a human cytomegalovirus promoter (CMVp)

3.2 NPC Labeling and Amplification

All the following steps were performed in sterile conditions under the flow hood. For their labeling, NPC were transduced with a CMV-GFP-lentivirus (green fluorescence) or with a CMV-mCherry-lentivirus (red fluorescence) as described previously [13]. Lentiviral vectors were prepared according to a published protocol [19]. The map of the CMV vector is detailed in Figure 1c. NPC were transduced with 99.5 ng of lentivirus in a 6-well culture plate filled with 500 µL of fresh culture medium for 3 h. The volume was completed to 2 mL and incubated for the next 48 hours, and then rinsed with culture medium. For co-transplantation with two distinct populations [15], transduced NPC should be initially purified by FACS to inject equivalent levels of green or red fluorescence intensities within cells. In the case of co-transplantation, the two populations of labeled NPC should be amplified using the same culture medium.

For amplification, NPC were thawed in T75 flasks at a density of 50,000 cells/cm^2 in 25 mL of NPC medium supplemented with Rock inhibitor Y27632 (10 μM). The next day, medium was changed in order to remove the Rock inhibitor. Once confluency was reached, cells were passaged into a T175 flask. Medium was changed every 2–4 days during NPC amplification.

3.3 Grafting into Mouse Neonates

Cultured NPC were dissociated and resuspended in DPBS (10^5 cells/μL) before their transplantation into the neonatal brain. GFP-labeled cells were transplanted into the motor cortex of immunodeficient NOD/SCID mice (Charles River Laboratories), at postnatal days 1–2. Pups were first locally anesthetized using a lidocaine gel. The head of newborn pups was gently held horizontally between the operator's fingers. Bregma was used as a visible landmark to localize the injection site. We used the published coordinates dorsolateral = +1 mm, anteroposterior = −1 mm, depth = −1 mm to target the cortex, or depth = −2 mm to target the ventricles. Two μL of resuspended cells were slowly injected unilaterally using a Hamilton syringe (Hamilton, ref. 65460). The syringe needle was set for injecting at 1- or 2-mm depth and kept in the pups' brain for 30 s following the injection before its removal. The injection lasted over 1 min. This protocol was approved by the Institut Pasteur Ethics Committee and the French *Ministère de l'Education Nationale, de la Recherche et de l'Innovation* under reference APAFiS #20686. The accuracy of injection was monitored by immunofluorescence labeling of GFP-labeled transplants, after brain slicing at different periods post-injection. All pups per litter were injected and their survival was evaluated at ~60%. For analysis, we recommend keeping only the mice that present well-defined GFP-labeled transplants within the same cortical areas. We excluded the brains with small number of labeled transplanted cells from analysis even though they presented similar phenotypes.

3.4 In Utero Grafting of Mouse Embryos

This protocol was approved by the Institut Pasteur Ethics Committee and the French "Ministère de l'Education Nationale, de la Recherche et de l'Innovation" under reference APAFiS #25221. Swiss OF1 mice (Charles River Laboratories) were habituated to the animal facility at least 3 days, and surgeries were performed at the embryonic stage of E17.5. We observed that this developmental stage allows high rate of pup's survival (~65%).

3.4.1 Material and Equipment Settings

A Hamilton syringe was connected to the pump by a plastic capillary, at the end of which a sterile glass micropipette was fixed (~ 50 μm diameter). Parafilm can be used to tightly connect plastic and glass micropipette. Before each surgery, the Hamilton syringe was filled with sterile distilled water and placed in a Harvard pump. A set of glass injection micropipettes were prepared by hand, using

the needle puller, without any further autoclaving. These are the only type of needles that can be used for in utero injection. Once embryos were ready to be injected, the glass micropipette was carefully filled with cell suspension (~10^5 cells/μL), to avoid the formation of air bubbles. Injection settings were as follows: infusion rate, 30,000 μL/min; target volume, 2 μL; and diameter, 0.4600 mm. Depending on experimenter, the injection can be performed using a magnification loupe or under a dissection microscope, or directly without any magnification device. At the stage E17.5, the ventricles can be easily distinguished in the Swiss OF1 mouse strain. Cold light and sterile surgical instruments are necessary and should be ready to use.

3.4.2 In Utero Surgery Procedures

Before their grafting, cell suspensions were prepared according to the protocol described in Subheading 3.2 and kept in a water bath at 37 °C. For the in utero approach, the injection solution also contains 20 mM EGTA [11, 20] in sterile DPBS to dissociate apical junctions in the neuroepithelium and avoid cell aggregation upon transplantation. For transplantation, we injected 2 μL containing 2. 10^5 cells within one lateral ventricle of E17.5 embryos. Thirty minutes before surgery, buprenorphine (0.05–0.1 mg/kg) was injected subcutaneously at the back of the neck of pregnant mouse, for initial analgesia. The pregnant mouse was then anesthetized in a box with isoflurane and oxygen delivered via a continuous flow anesthesia unit and then placed on a heating pad which was also connected to the anesthesia unit. A drop of Ocryl gel was applied on each eye to avoid eye dryness. The abdomen was shaved locally for ventral laparotomy at the white midline level. A betadine solution was applied on the skin, and then rinsed with 70% ethanol using cotton swabs. A lidocaine gel was applied locally, before and after the laparotomy. Before starting the surgery, the sterile towel drape was positioned on the mouse abdomen. An incision of 1–1.5 cm was made in the lower abdomen in a manner to cut both the skin and the thin fascia layer. Abdominal organs should not be injured during this critical step. The whole uterus was carefully extracted from the abdomen, right and left ovaries were identified, and the total number of fetuses was counted. During surgery, drops of sterile PBS kept at 37 °C were consistently applied on the exposed fetuses. Then, each fetus was held to clearly identify the lateral ventricle. The fetus was stabilized between the thumb and forefinger within or close to the amniotic cavity. Any fetus rotation or damage should be avoided as it can affect embryo survival. The sharp glass pipette was carefully inserted through the fetal skull, and cells were injected into each fetus, except the first one to be delivered, on each uterine horn. After the injection, the pipette was carefully withdrawn with well-controlled movements. Note that leakage of amniotic fluid should not be observed.

Injections should not take more that 15–20 min per mouse. If the duration of injection is longer, some of the injected fetuses can be put back into the abdomen to keep them at the body temperature. Then, the uterus was carefully reentered into the abdominal cavity in a way to avoid any twist between the embryos and with a controlled holding pressure. The peritoneal cavity was rehydrated with 0.5–1 mL of sterile PBS to replace any fluid loss during the surgery. Then, the incision was closed with two types of sutures: for fascia and skin, we used sterile resorbable suture (Prolene^{TM}, EH7471, Ethicon, LLC) and non-resorbable suture (Coated Vicryl, V302, Ethicon, LLC), respectively. After the surgery, the pregnant mouse was replaced in its own cage and positioned on a warming pad until the mouse was fully awake. Analgesia treatment (acetaminophen 4 mg/20 mL) was administered in drinking water for 3–5 days after the surgery, and stress (noise, excessive manipulation of cages, etc.) was minimized to avoid preterm delivery. Hydrogel was also given to mice for 1 day after surgery. We observed that grafted cells' distributions and density may slightly vary between each embryo, due to a possible aggregation of cells in the pipette and during injection. We could observe that the presence of EGTA significantly reduces cell aggregation, and increases the possibility of identifying single cells within the mouse brain, as described previously [11].

For a first in utero test or training, it is recommended to inject 1–2 μL of fast green or bromophenol blue solutions, without cells. If correctly injected into lateral ventricle, the solution will immediately fill the whole embryonic ventricular systems. In that case, the pregnant mouse and embryos should be sacrificed immediately by profound anesthesia followed by cervical dislocation.

3.5 Grafting into the Dentate Gyrus of Adult Mouse Brain

The protocol for cell preparation is identical to that for in utero grafting. Experiments were performed with adult NOD-SCID mice (Charles River Laboratories).

As for in utero grafting, the mice received an injection of buprenorphine (0.1 mg/kg) for initial analgesia 30 min before anesthesia by isoflurane. The mouse was placed on a stereotaxic frame connected to an isoflurane unit and to a heating pad. A drop of Ocryl gel was applied on each eye to avoid dryness. The skin was shaved and cleaned with betadine followed by 70% ethanol. For a local anesthesia, 150 μL of lidocaine (7 mg/kg) were injected subcutaneously at the skull level at least 10 min before the skin incision. Using a driller, two holes were done at the following coordinates A/P: −1.8; M/L: +/−1.25 for targeting the DG according to the Paxinos and Franklin Atlas [21]. Twenty nanoliters of cell suspensions were injected bilaterally at a rate of 3 nL/s in three steps along the D/V axis: 15 injections at −1.82 depth, 20 at −1.76, and 15 at −1.72 to achieve a final volume of

1 μL/hemisphere. To ensure reproducible injection volumes, we recommend to wait 10 s between each injection and 5 min before removing the glass capillary from the brain tissue.

For mouse recovery, Metacam (0.05 mg/kg) and 200 μL of sterile saline were injected separately subcutaneously before the end of anesthesia (~50 μL/mouse). As post-operatory care, Metacam (1 mg/kg/day) diluted in diet gel was given for at least 3 days. Mice were monitored for 5 days.

3.6 Immunofluorescence Labeling

For immunofluorescence labeling, mice received a lethal dose of a mixture of ketamine (Imalgen, 100 mg/kg, Merial) and Xylazine (Rompun, 10 mg/kg, Bayer), and were transcardially perfused with 15 mL of DPBS, followed by 50 mL of ice-cold 4% paraformaldehyde (PFA). Brains were removed and post-fixed overnight. Forty μm-coronal sections were obtained using a vibratome or a microtome, collected in 12-well or 24-well culture plates containing DPBS supplemented with 0.02% azide, and stored at 4 °C until use. Free-floating sections were rinsed twice in DPBS (pH 7.4) and then incubated in DPBS solution containing 0.5% Triton X-100 and 10% serum at room temperature for 30 min to block nonspecific binding. Primary antibodies were diluted in blocking solution and incubated overnight at 4 °C. In order to improve the labeling of neuron morphology, immunofluorescence was performed using an anti-GFP antibody in permeabilized conditions. An additional DAPI staining diluted in DPBS was performed for 10 min at room temperature.

3.7 Representative Data

In this chapter, we describe three different approaches for grafting the human NPC which result in the integration of human cells into the brain of adult mouse. Figure 1 illustrates the different steps of the protocol which we used for amplification, banking, and labeling of NPC before their grafting. We have previously shown that the neonatal engraftment of human NPC can lead to neurons that are able to differentiate into glutamatergic neurons [12, 15]. Figure 2 illustrates the precise site of injection and the cortical graft containing a large density of neuronal cell bodies together with numerous axonal projections within distinct brain regions. The full cartography of axonal projections in the brain has been published elsewhere [15]. Using the same human NPC, we set up the grafting into the lateral ventricle of mouse embryo (E17.5). Our results show that 2 weeks after their grafting, the cells are able to integrate within the brain parenchyma and start to migrate along known migratory pathways including cingulum bundle, corpus callosum, and fimbria (*see* Fig. 3a). At this early stage of post-grafting, a large number of cells remain close to the injection site. By contrast, the cells are found to be more dispersed after 1 month and in the process of integrating the distinct brain regions including the striatum (*see* Fig. 3a, b). Two months post-grafting, the cells start to

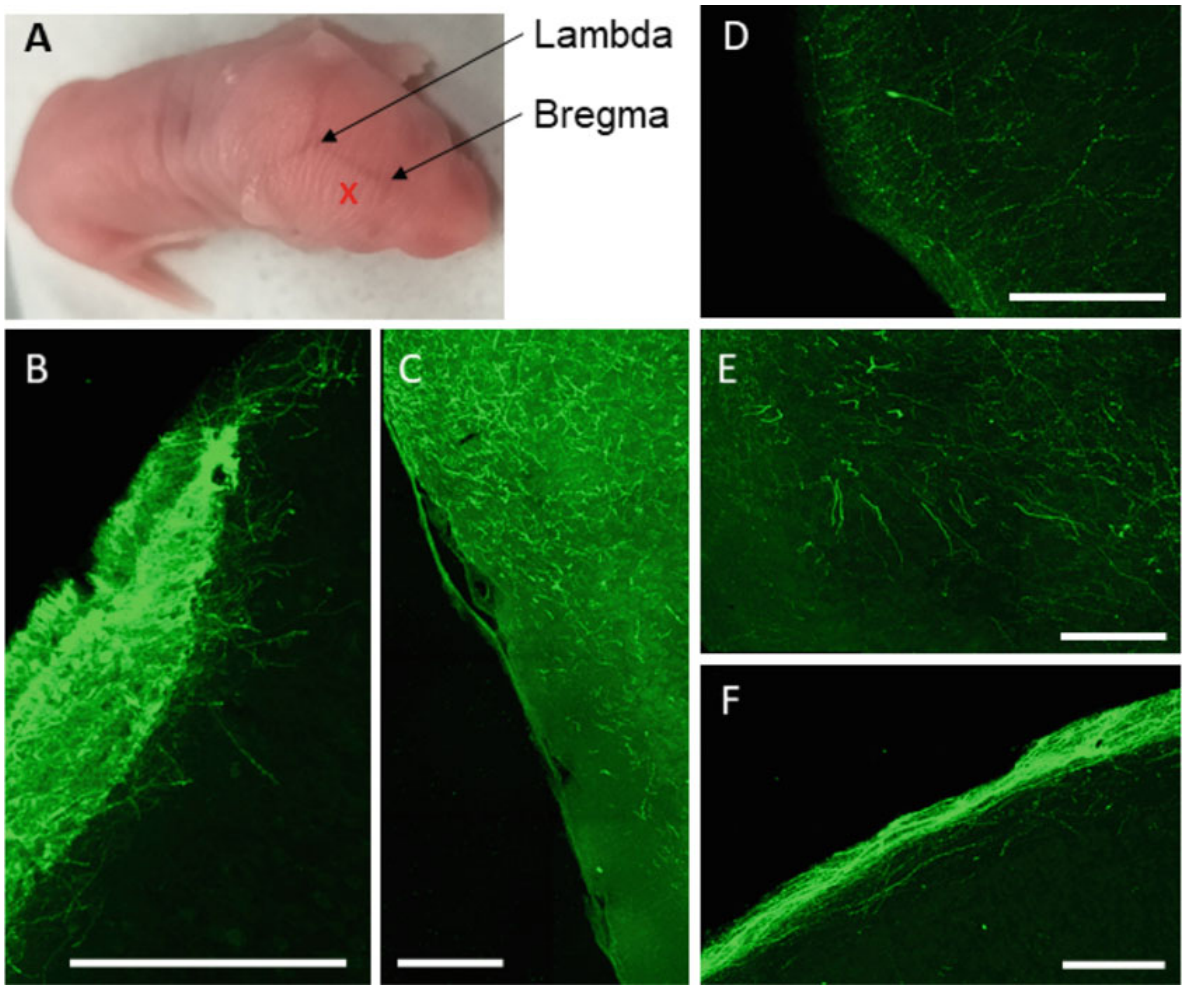

Fig. 2 Engrafting of human iPSC-derived NPC into the cortex of newborn mice. (**a**) Intracranial injection of human iPSC-derived NPC into the cortex of neonatal mice. The lambda and bregma landmarks are used to target the motor cortex as indicated in red. The injection site is located approximately 1 mm posterior to the bregma and 1 mm lateral to the sagittal suture, with 1 mm depth, as indicated by the red symbol. (**b**) Representative engraftments into the cortex of 50-day-old mice after neonatal injection of NPC. Graft location within the somatosensory cortex. Most of GFP-labeled neurons remain within the graft site, and extend their dendrites. (**c**) Axonal projections within the somatosensory cortex (bregma ≈ -0.955 mm). (**d**) Axonal projections in the somatosensory cortex (bregma ≈ 1.545 mm). (**e**) Long-range axonal projections in the retrohippocampal region (bregma ≈ -2.78 mm) (**f**) Long-range axonal projections in the somatosensory cortex (bregma ≈ -2.78 mm). Scale bars $= 200$ μm

differentiate into excitatory cells (*see* Fig. 3c). At this stage, the co-localization of VGlut labeling with the human cells is observed both in neuronal cell bodies and projections (*see* Fig. 3c). Figure 4 illustrates the grafting of the human NPC into the dentate gyrus (DG) of adult immunodeficient mice, 3 weeks post-grafting. Our data show that cells can survive and integrate within the hippocampal structures following a stereotaxic injection in adult mice.

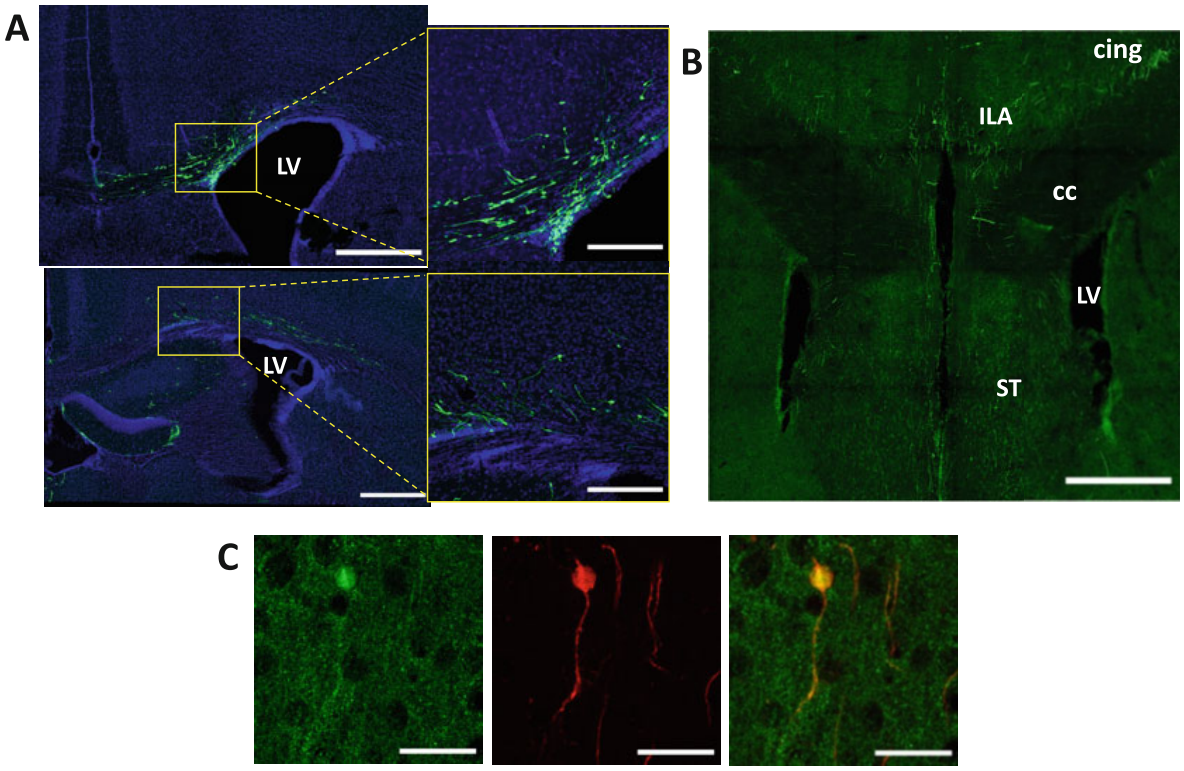

Fig. 3 Engrafting of human iPSC-derived NPC in utero, at different time points after transplantation. (**a**) Representative engraftments at 2 weeks post-transplantation (2 WPT) (bregma ≈ -0.1 mm) (upper panel) and at 1 month post-transplantation (1 MPT) (bregma ≈ -0.94 mm) (Lower panel). Graft core remains close to the lateral ventricle (LV) area. All pictures were taken using a 10× objective. Scale bar of mosaic (left panel) = 500 μm and scale bar of pictures (right panel) = 200 μm. (**b**) Projections of human NPC along different brain regions (*cing* cingulum bundle, *ILA* infralimbic area, *cc* corpus callosum, *ST* striatum area) at 3 MPT at 10× magnification (scale bar = 500 μm). In green, GFP-labeled human NPC and in blue cell nuclei stained with DAPI. (**c**) Excitatory phenotype of grafted human NPC shown by VGluT expression at 63× magnification (scale bar = 30 μm), and at 2 MPT

4 Notes

1. The use of humanized chimeric mouse models allows the study of neuronal development and associated pathogenesis and neurodegenerative diseases using human cells in an in vivo condition. Under the experimental approaches described here, the neonatal grafting allows the grafted progenitors to predominantly differentiate into excitatory neurons which can mature, migrate, and project their axons in different brain regions. The iPSC technology has offered the possibility to study some specific phenotypes, including cell differentiation and maturation, neuronal morphology, and functional activities by electrophysiological recordings of cultured cells under in vitro conditions [4]. However, in vitro models using human iPSC-derived neurons are limited as they do not offer the possibility

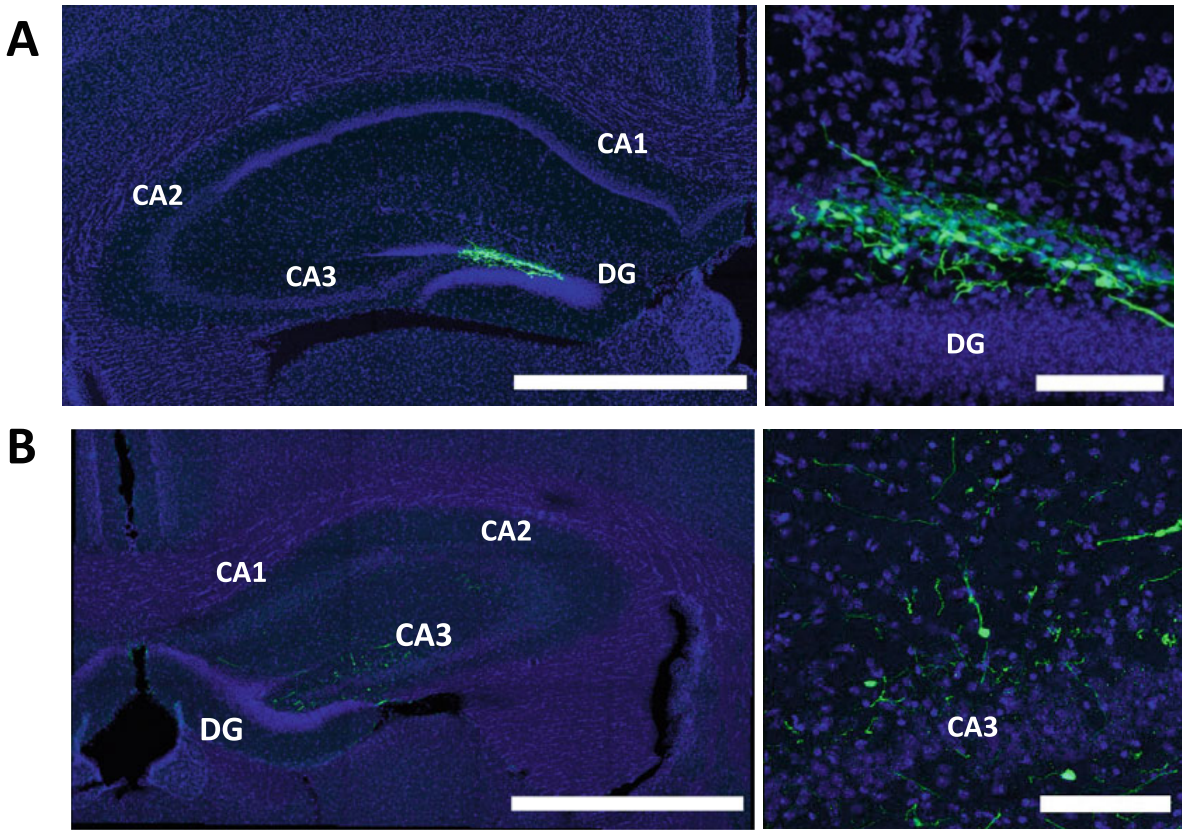

Fig. 4 Engrafting of human iPSC-derived NPC into the dentate gyrus (DG) of adult mice, at 3 weeks post-injection. Representative engraftments into the hippocampus area of NOD-SCID mice as shown by the graft core in the DG (bregma = −1.80 mm) (**a**) and projections (**b**) at low (left panel) and higher (right panel) magnifications. Low magnification mosaics are taken with a 10× objective (scale bar = 1000 μm) and higher magnification pictures with a 20× objective (scale bar = 100 μm). All pictures were acquired as a Z-stack with a confocal microscope to maximize the graft detection. In green, GFP-labeled human NPC and in blue cell nuclei stained with DAPI

to study disease pathogenesis at different stages of brain maturation within a such complex environment, and in the presence of external cues that are necessary for neuronal patterning. As shown in Table 1, the neonatal grafting of iPSC-derived neuronal progenitors has been successfully used by several authors. By comparing neonatal and in utero grafting, we observed that in both cases, the engrafted cells form initial clusters during the first month post-grafting which tend to remain over time, at least up to 7 months [12]. For neonatal grafting, it has been shown that grafted NPC appear to respond to region specific signals and are also responsive to neural patterning cues in vitro [4, 12, 41]. These human cells progressively expand and migrate in the murine forebrain. It has been difficult to understand to what extent the undifferentiated NPC or the immature neurons can integrate and recapitulate physiological neurogenesis in vivo. Moreover, most studies have been limited

due to the use of immunodeficient NOD-SCID mice, which have the tendency to form tumors at 7–8 months of age [49]. So far, these issues have not been considered for studying neurodevelopmental disorders. Interest has been focused on early stages of neuronal maturation, which has allowed the discovery of a panel of morphogenetic abnormalities that are linked to early development of neurons with ASD-associated mutations [15, 50]. It should also be noted that transplanted human PSC-derived NPC can be tumorigenic, if contaminated with residual pluripotent stem cells with sustained proliferation of residual stem cells [51]. As shown in Fig. 1, we used the SMAD inhibitor SB431542, based on previously reported studies [17], in order to avoid abnormal cell proliferation. For in utero grafting, we observed large densities of graft-derived fibers projecting into migratory pathways and in the host tissue as early as 15 days post-grafting (*see* Fig. 3). The in utero grafting method presents some advantages as it can be applied to immunocompetent mice with no graft rejection and no inflammation at injection sites (data not shown), while mouse neurogenesis continues which may favor further development of human cells.

Our results indicate that the cells can survive at least for 3 months after grafting and give rise to glutamatergic neurons (*see* Fig. 3). We also observed that they develop dendritic spines after neonatal grafting (data not shown), using the same GFP-labeled human iPSC line [15]. To our knowledge, there is no report on the in utero grafting of human iPSC-derived neuronal cells in rodent brain. The available data from using mouse embryonic cells grafted in the brain of rat embryos were analyzed within 7 weeks post-grafting [22]. However, human cells are expected to be found uniformly throughout the brain regions, including hippocampus, cerebral cortex, and striatum at later stages, up to 13 months, as observed in neonatally grafted mice [41]. Finally, we describe the grafting of NPC within hippocampus of the adult mice. This grafting method may help targeting a specific brain region, and to analyze more specifically how grafted cells can integrate within specific circuits. We illustrate this approach with NPC giving rise to excitatory neurons after grafting into the dentate gyrus of hippocampus. The same approach could be applied to interneurons that can be derived from human iPSC as well [40]. Interestingly, interneurons represent a large and diverse population of hippocampal neurons that are critical for information and memory processing. By grafting well-characterized mature interneurons, it is possible to identify more specifically how a specific human interneuron subtype may morphologically and functionally interact within the surrounding host cells.

2. Neurodevelopmental disorders are either due to various inherited mutations or acquired causal factors, and lead to dysfunction of brain development and cognitive deficits.

The pathogenesis of neurodevelopmental disorders has not been well elucidated, and no effective treatment has so far been found for these disorders. The establishment of accurate models which allow to investigate neurological disorders represents an important step toward better understanding and appropriate treatment of neurodevelopmental pathologies. To study the brain-associated diseases in vitro has been not possible, and to obtain the tissues from human brain represents a difficult alternative. The use of patient-derived iPSC, however, offers a unique opportunity to investigate pathological changes that may occur in the brain at early stages of neuronal development. In addition, human iPSC provide an auto-renewal source of cells which are identical to the donor [52]. Under the action of specific growth and transcription factors, they can differentiate into neurons of different phenotypes that are found within the six cortical layers, including excitatory and inhibitory neurons [53]. The grafting of iPSC-derived neurons into mouse brain offers the possibility to decipher cellular mechanisms in different temporal windows, from the neurogenic stages with undifferentiated cells to later stages of well-differentiated mature neurons, under control and pathological conditions. For genetic diseases, the iPSC from patients carry the genetic pattern of mutations from these donors and should display similar pathological and phenotypical changes. For autism spectrum disorders (ASD), recent studies have shown that the events underlying such disorders can occur during neonatal development, together with strong synaptic defects that are known to occur at later stages of development. In a previous in vitro study, we investigated the iPSC-derived pyramidal cortical neurons from patients with ASD carrying de novo heterozygous mutations in the postsynaptic SHANK3 protein. SHANK3 is a synaptic scaffolding protein located at the postsynaptic density of excitatory synapses [54]. The haploinsufficiency of *SHANK3* gene provokes a developmental disorder known as the 22q13.3 deletion syndrome (or Phelan-McDermid syndrome). *SHANK3* gene is also associated with pathogenesis and neuropathology of ASD, which involves synaptic dysfunctions and an imbalance in synaptic excitation/inhibition ratio. Using iPSC-derived neurons from ASD patients, we observed altered spinogenesis in all the patients who were included in the study [16]. In a subsequent study, we used the same cells from a control individual at precursor stages (NPC), and transplanted them into the cortex of newborn mouse brain [15]. We analyzed the integration of NPC, the maturation of the derived excitatory neurons, and their axonal projections

into the adult brain. We then co-transplanted the NPC from a control individual and from a patient carrying one de novo heterozygous mutation in *SHANK3*. In human neurons with the *SHANK3* mutation, we observed a reduction in cell soma size of selective neuronal populations and in axonal projections, as compared to control neurons, at 30 days post-transplantation. However, we did not observe any alteration in spinogenesis at this early stage, which are expected to occur at later stages of development. This indicates that in vivo models can recapitulate the early stages of the disease, which may help understand the initial mechanisms before the appearance of the well-described phenotypes observed in mouse models or in human cells kept in culture.

3. One of the strong aspects of our different grafting approaches is that humanized mouse models can be used for both neurodevelopmental and neurodegenerative diseases, depending on the stage at which the phenotypes of grafted cells are evaluated. At the early stages of development, regulation of cortical neurogenesis is very important as it is involved in neuronal fate [55]. For example, recent discoveries point out the permissive role of the amyloid precursor protein (APP) in the regulation of human cortical neurogenesis [56]. APP is also the precursor of β-amyloid peptide which can lead to progressive accumulation of β-amyloid oligomers, followed by their aggregation in amyloid plaques, one of the major hallmarks of the neurodegenerative Alzheimer's disease (AD). It would be possible to test whether the physiological functions of APP are related to the onset of AD, using in vivo approaches such as mouse chimeric models, xenografted in utero and appropriate genetic tools, to follow and control the production of endogenous APP within the whole brain or locally in specific brain regions. Humanized mouse models not only offer the possibilities to decipher the early events which underlie neuronal maturation and plasticity but also to investigate the pathological events that occur in the brain of patients with neurological disorders, including those with AD. Such models should also facilitate the preclinical evaluation of therapeutic measures and treatments as well as their consequences within the human neurons, in vivo. Finally, these models can help to set up appropriate transplantation therapies using neural stem cells. The xenografting strategies offer the possibility to compensate neural loss and neural tissue injury and should allow the discovery of therapeutic strategies for the future, in the context of both developmental disorders and degenerative diseases. One main challenge will be to face the complexity of human brain and consider its unique spatial and temporal development.

Acknowledgments

The authors are thankful to Dr. Alexandra Benchoua who performed the initial iPSC reprogramming. The "Fondation Recherche Alzheimer" provides the funding for CT's PhD. The Pasteur-Paris University (PPU) international doctoral program provides the funding for MLP's PhD. The French Ministry of Education and the LabEx BioPsy provided the funding for AV's PhD. Other funding for this study were provided by grants from the French National Research Agency ANR (ANR-17-NEU3-0004; IPS BRAIN), from ERA-NET NEURON (iPSC & Brain), and from the "France Alzheimer" foundation. We gratefully acknowledge the UtechS Photonic Bioimaging (Imagopole), C2RT, Institut Pasteur, supported by the French National Research Agency (France BioImaging; ANR-10-INSB-04; Investments for the future).

References

1. Barbas H (2015) General cortical and special prefrontal connections: principles from structure to function. Annu Rev Neurosci 38:269–289. https://doi.org/10.1146/annurev-neuro-071714-033936
2. De la Rossa A, Bellone C, Golding B et al (2013) *In vivo* reprogramming of circuit connectivity in postmitotic neocortical neurons. Nat Neurosci 16(2):193–201. https://doi.org/10.1038/nn.3299
3. Corti S, Faravelli I, Cardano M et al (2015) Human pluripotent stem cells as tools for neurodegenerative and neurodevelopmental disease modeling and drug discovery. Expert Opin Drug Discov 10(6):3–15. https://doi.org/10.1517/17460441.2015.1037737
4. Espuny-Camacho I, Michelsen KA, Linaro D et al (2013) Pyramidal neurons derived from human pluripotent stem cells integrate efficiently into mouse brain circuits in vivo. Neuron 77:440–456. https://doi.org/10.1016/j.neuron.2012.12.011
5. Espuny-Camacho I, Michelsen KA, Linaro D et al (2018) Human pluripotent stem-cell-derived cortical neurons integrate functionally into the lesioned adult murine visual cortex in an area-specific way. Cell Rep 23:2732–2743. https://doi.org/10.1016/j.celrep.2018.04.094
6. Amunts K, Zilles K (2015) Architectonic mapping of the human brain beyond Brodmann. Neuron 88:1086–1107. https://doi.org/10.1016/j.neuron.2015.12.001
7. Molyneaux B, Arlotta P, Menezes et al (2007) Neuronal subtype specification in the cerebral cortex. Nat Rev 8:428–437
8. Jiang X, Wang G, Lee AJ et al (2013) The organization of two new cortical interneuronal circuits. Nat Neurosci 16(2):210–218. https://doi.org/10.1038/nn.3305
9. Lake BB, Rizi A, Kaeser GE et al (2016) Neuronal subtypes and diversity revealed by single-nucleus RNA sequencing of the human brain. Science 352(6293):1586–1590. https://doi.org/10.1126/science.aaf1204
10. Martinez J, Rahsepar B, White JA et al (2017) Anatomical and electrophysiological clustering of superficial medial entorhinal cortex interneurons. ENeuro 4(5): ENEURO.0263-16.2017. https://doi.org/10.1523/ENEURO.0263-16.2017
11. Linaro D, Vermaercke B, Iwata R et al (2019) Xenotransplanted human cortical neurons reveal species-specific development and functional integration into mouse visual circuits. Neuron 104:972–986. https://doi.org/10.1016/j.neuron.2019.10.002
12. D'Alessio N, Koukouli F, Blanchard S et al (2020) Long-term development of human iPSC-derived pyramidal neurons quantified after transplantation into the neonatal mouse cortex. Dev Biol 461:86–95. https://doi.org/10.1016/j.ydbio.2020.01.009
13. Gouder L, Tinevez JY, Goubran-Botros H et al (2015) Three-dimensional quantification of dendritic spines from pyramidal neurons

derived from human induced pluripotent stem cells. J Vis Exp 104:e53197. https://doi.org/10.3791/53197

14. Real R, Peter M, Trabalza A et al (2018) In vivo modeling of human neuron dynamics and Down syndrome. Science 362:eaau1810. https://doi.org/10.1126/science.aau1810
15. Vitrac A, Pons S, Balkota M et al (2020) A chimeric mouse model to study human iPSC-derived neurons: the case of a truncating *SHANK3* mutation. Sci Rep 10:13315. https://doi.org/10.1038/s41598-020-70056-4
16. Gouder L, Vitrac A, Goubran-Botros H et al (2019) Altered spinogenesis in iPSC-derived cortical neurons from patients with autism carrying *de novo* SHANK3 mutations. Sci Rep 9: 94. https://doi.org/10.1038/s41598-018-36993-x
17. Boissart C, Poulet A, Georges P et al (2013) (2013) Differentiation from human pluripotent stem cells of cortical neurons of the superficial layers amenable to psychiatric disease modeling and high-throughput drug screening. Transl Psychiatry 3:e294. https://doi.org/10.1038/tp.2013.71
18. Mouilleau V, Vaslin C, Robert R et al (2021) Dynamic extrinsic pacing of the HOX clock in human axial progenitors controls motor neuron subtype specification. Development 148: dev194514. https://doi.org/10.1242/dev.194514
19. Avale ME, Faure P, Pons S et al (2008) Interplay of β2* nicotinic receptors and dopamine pathways in the control of spontaneous locomotion. Proc Natl Acad Sci 105(41): 15991–15996. https://doi.org/10.1073/pnas.0807635105
20. Nagashima F, Susuki IK, Shitamukai A et al (2014) Novel and robust transplantation reveals the acquisition of polarized processes by cortical cells derived from mouse and human pluripotent stem cells. Stem Cells Dev 23(18):2129–2142. https://doi.org/10.1186/s13287-018-0966-2
21. Paxinos G, Franklin KBJ (2004) The mouse brain in stereotaxic coordinates. Gulf Professional Publishing, pp 1–100. 012547640X, ISBN 9780125476409
22. Brüstle O, Choudhary K, Karram K (1998) Chimeric brains generated by intraventricular transplantation of fetal human brain cells into embryonic rats. Nat Biotechnology 16:1041–1044. https://doi.org/10.1038/3481
23. Fricker RA, Carpenter MK, Winkler C et al (1999) Site-specific migration and neuronal differentiation of human neural progenitor cells after transplantation in the adult rat brain. J Neurosci 19(14):5990–6005. https://doi.org/10.1523/JNEUROSCI.19-14-05990.1999
24. Uchida N, Buck DW, He D et al (2020) Direct isolation of human central nervous system stem cells. Proc Natl Acad Sci 97(26): 14720–14725. https://doi.org/10.1073/pnas.97.26.14720
25. Ourednik V, Ourdnik J, Flax JD et al (2001) Segregation of human neural stem cells in the developing primate forebrain. Science 293: 1820–1824. https://doi.org/10.1126/science.1060580
26. Zhang S-C, Wernig M, Duncan ID et al (2001) In vitro differentiation of transplantable neural precursors from human embryonic stem cells. Nature 19:1130–1133. https://doi.org/10.1038/nbt1201-1129
27. Goldstein RS, Drukker M, Reubinoff BE et al (2002) Integration and differentiation of human embryonic stem cells transplanted to the chick embryo. Dev Dyn 225:80–86. https://doi.org/10.1002/dvdy.10108
28. Chu K, Kim M, Chae SH et al (2004) Distribution and in situ proliferation patterns of intravenously injected immortalized human neural stem-like cells in rats with focal cerebral ischemia. Neurosci Res 50:459–465. https://doi.org/10.1016/j.neures.2004.08.015
29. Muotri A, Nakashima K, Toni N et al (2005) Development of functional human embryonic stem cell-derived neurons in mouse brain. Proc Natl Acad Sci 102(51):18644–18648. https://doi.org/10.1073/pnas.0509315102
30. Tabar V, Panagiotakos G, Greenberg ED et al (2005) Migration and differentiation of neural precursors derived from human embryonic stem cells in the rat brain. Nat Biotechnol 23(5):601–606. https://doi.org/10.1038/nbt1088
31. Roy NS, Cleren C, Singh SK et al (2006) Functional engraftment of human ES cell–derived dopaminergic neurons enriched by coculture with telomerase-immortalized midbrain astrocytes. Nat Med 12(11):1259–1268. https://doi.org/10.1038/nm1495
32. Aubry L, Bugi A, Lefort N et al (2008) Striatal progenitors derived from human ES cells mature into DARPP32 neurons in vitro and in quinolinic acid-lesioned rats. Proc Natl Acad Sci 105(43):16707–16712. https://doi.org/10.1073/pnas.0808488105
33. Kriks S, Shim J-W, Pia J et al (2011) Dopamine neurons derived from human ES cells efficiently engraft in animal models of Parkinson's

disease. Nature 480:547–551. https://doi.org/10.1038/nature10648

34. Lamba DA, Gust J, Reh TA (2009) Transplantation of human embryonic stem cell-derived photoreceptors restores some visual function in Crx-deficient mice? Cell Stem Cell 4:73–79. https://doi.org/10.1016/j.stem.2008.10.015
35. Kim D-S, Dongjin RL, Kim H-S et al (2012) Highly pure and expandable PSA-NCAM-positive neural precursors from human ESC and iPSC-derived neural rosettes. PLoS ONE 7(7): e39715. https://doi.org/10.1371/journal.pone.0039715
36. Hargus G, Cooper O, Deleidi M et al (2010) Differentiated Parkinson patient-derived induced pluripotent stem cells grow in the adult rodent brain and reduce motor asymmetry in Parkinsonian rats. Proc Natl Acad Sci. 107(36):15921–15926. https://doi.org/10.1073/pnas.1010209107
37. Liu Y, Weick JP, Liu H et al (2013) Medial ganglionic eminence–like cells derived from human embryonic stem cells correct learning and memory deficits. Nat Biotechnol 31(5): 440–447. https://doi.org/10.1038/nbt.2565
38. Nicholas CR, Chen J, Tang Y et al (2013) Functional maturation of hPSC-derived forebrain interneurons requires an extended timeline and mimics human neural development. Cell Stem Cell 12:573–586. https://doi.org/10.1016/j.stem.2013.04.005
39. Wakeman DR, Redmond DE, Dodiya HB et al (2014) Human neural stem cells survive long term in the midbrain of dopamine-depleted monkeys after GDNF overexpression and project neurites toward an appropriate target. Stem Cells Transl Med 3:692–701. https://doi.org/10.5966/sctm.2013-0208
40. Ahn S, Kim T-G, Kim KS et al (2016) Differentiation of human pluripotent stem cells into Medial Ganglionic Eminence vs. Caudal Ganglionic Eminence cells. Methods 101(2016): 103–112. https://doi.org/10.1016/j.ymeth.2015.09.009
41. Chen C, Kim W-Y, Jiang P (2016) Humanized neuronal chimeric mouse brain generated by neonatally engrafted human iPSC-derived primitive neural progenitor cells. JCI Insight 1(19):e88632. https://doi.org/10.1172/jci.insight.88632
42. Hsieh J-Y, Baraban SC (2017) Medial ganglionic eminence progenitors transplanted into hippocampus integrate in a functional and subtype-appropriate. Manner 4(2): e0359-16.2017 1–17. https://doi.org/10.1523/ENEURO.0359-16.2017
43. Donegan JJ, Boley AM, Lodge DJ (2018) Embryonic stem cell transplants as a therapeutic strategy in a rodent model of autism. Neuropsychopharmacology 43:1789–1798. https://doi.org/10.1038/s41386-018-0021-0
44. Ni P, Noh H, Shao Z et al (2019) Large-scale generation and characterization of homogeneous populations of migratory cortical interneurons from human pluripotent stem cells. Mol Ther Methods Clin Dev 13:414–430. https://doi.org/10.1016/j.omtm.2019.04.002
45. Upadhya D, Hattiangady B, Castro OW et al (2019) Human induced pluripotent stem cell-derived MGE cell grafting after status epilepticus attenuates chronic epilepsy and comorbidities via synaptic integration. Proc Natl Acad Sci 116(1):287–296. https://doi.org/10.1073/pnas.1814185115
46. Ryu J, Vincent PFY, Ziogas NK et al (2019) Optogenetically transduced human ES cell derived neural progenitors and their neuronal progenies: phenotypic characterization and responses to optical stimulation. PLoS ONE 14(11):e0224846. https://doi.org/10.1371/journal.pone.0224846
47. Southwell DG, Seifikar H, Malik R et al (2019) Interneuron transplantation rescues social behavior deficits without restoring wild-type physiology in a mouse model of autism with excessive synaptic inhibition. J Neurosci 40(11):2215–2227. https://doi.org/10.1523/JNEUROSCI.1063-19.2019
48. Xiong M, Tao Y, Gao Q et al (2021) Human stem cell-derived neurons repair circuits and restore neural function. Cell Stem Cell 28: 112–126. https://doi.org/10.1016/j.stem.2020.08.014
49. Santagonisto SF, Ricart Arbona RJ, Nashat MA et al (2017) Pathology of aging in NOD scid gamma female mice. Vet Pathol 55(5): 855–869. https://doi.org/10.1177/2F0300985817698210
50. Kathuria A, Nowosiad P, Jagasia R et al (2017) Stem cell-derived neurons from autistic individuals with SHANK3 mutation show morphogenetic abnormalities during early development. Mol Psychiatry 23:735–746. https://doi.org/10.1038/mp.2017.185
51. Chung S, Shin B-S, Hedlund E et al (2006) Genetic selection of sox1GFP-expressing neural precursors removes residual tumorigenic pluripotent stem cells and attenuates tumor formation after transplantation. J Neurochem 97(5):1467–1480. https://doi.org/10.1111/j.1471-4159.2006.03841.x

52. Nestor MW, Phillips AW, Artimovitch E et al (2016) Human inducible pluripotent stem cells and autism spectrum disorder: emerging technologies. Autism Res 9:513–535. https://doi.org/10.1002/aur.1570
53. Van den Ameele J, Tiberi L, Vanderhaegen P et al (2014) Thinking out of the dish: what to learn about cortical development using pluripotent stem cells. Trends Neurosci 34(6): 334–342. https://doi.org/10.1016/j.tins.2014.03.005
54. Manoli DS, State MW (2021) Autism spectrum disorder genetics and the search for pathological mechanisms. Am J Psychiatry 178(1):30–38. https://doi.org/10.1176/appi.ajp.2020.20111608
55. Villalba A, Götz M, Borrel V (2020) The regulation of cortical neurogenesis. Curr Top Dev Biol 142., ISSN 0070-2153. https://doi.org/10.1016/bs.ctdb.2020.10.003
56. Shabani K, Pigeon J, Zariouh MBT et al (2021) The Amyloid Precursor Protein regulates human cortical neurogenesis. bioRxiv. https://doi.org/10.1101/2021.02.17.431707

DISCUSSION

2. Towards better models of AD

Drug discovery in clinical AD research has proven to be a major challenge, with promising pre-clinical data often failing to translate into successful human trials. This translational gap can be attributed, in part, to inadequate pre-clinical models that fail to accurately mimic the complexity of the human disease.

Cholinergic targeted therapies for AD have shown some success, with AChEI improving cognitive symptoms and quality of life in patients. However, these therapies only offer short-term relief and do not modify the disease progression [296]. More recently, there has been growing interest in the targeted modulation of the α7-nAChR receptor with allosteric modulators due to its interaction with Aβ and its implications in early AD pathophysiology [297]. Unfortunately, clinical trials of these therapies in humans have proved to be unsuccessful. A potential explanation for the translational gap in cholinergic therapies for AD may lie in the absence of the CHRFAM7A gene in classical pre-clinical models. As discussed in this thesis, the gene plays a critical role in modifying both α7-nAChR and neuronal response to Aβ. This highlights the need for models that include this gene and other human-specific contexts to better model AD and reduce the translational gap.

This section briefly presents in-vitro model used to study *CHRFAM7A*, before focusing on the in-vitro method of xenotransplantation, followed by presentation of some preliminary data and discussions of future directions for investigating the role of *CHRFAM7A* in AD in-vivo using this novel approach.

2.1. In-vitro iPSC differentiation and characterization

Since the discovery of iPSCs, numerous protocols have been developed, offering a wide range of options for manipulating gene expression to produce neurons. To achieve neuronal differentiation, gene expression can be manipulated through direct and indirect methods. Direct differentiation involves the use of viral vectors or other techniques to forcefully express transcription factors that are crucial for neural development (reviewed in [298]). On the other hand, indirect methods, such as the one utilized our study, involve the use of pharmacological agents to manipulate iPSCs [231,253,299,300]. These agents mimic the signaling pathways involved in neurodevelopment, thereby inducing a neuronal phenotype, and preventing the cells from adopting non-neuronal fates. Commonly used techniques for neuronal induction include the formation of embryoid bodies and the inhibition of the TGF-β/SMAD signaling pathway (dual SMAD inhibition).

To investigate the role of *CHRFAM7A* in-vitro, a specific protocol was employed to differentiate cells into MGE-interneuron progenitors [253]. Interneurons exhibit elevated levels of nAChR and are known to be significantly affected in AD, making them an appropriate model for studying AD-related phenotypes [301]. In contrast to excitatory cells that follow a default differentiation mechanism, interneurons necessitate ventralizing signals following neuronal induction. This ventralization is accomplished by inhibiting the Wnt signaling pathway while activating the Shh pathway. Once neuronal induction and ventralization have been achieved, further specification toward MGE progenitors is facilitated by the addition of the FGF8 factor [231,253,300]. By precisely modulating these pathways over a period of four weeks, a young interneuron phenotype was achieved (Figure 32). In addition, after 60 days in culture, the cells expressed interneuron mature phenotypes, as shown by the expression of SOM. Notably, within the examined timeframe, no PV cells were detected, which can be attributed to PV being a late marker of interneuron development [225]

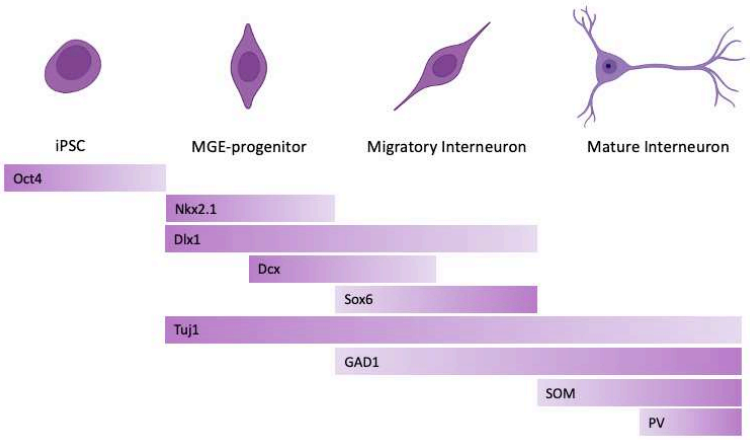

Figure 32. Pattern of gene expression used to characterize interneurons.

After four weeks of differentiation, interneurons showed a progenitor /migratory interneuron phenotype characterized by the expression of progenitor markers like Dlx1 and Nkx2.1, interneuron migratory markers like Dcx and Sox6, and markers associated with young neurons, including Tuj1 and GAD1. During the 4th week, almost no division of cells was detected, meaning that the majority of neurons were post-mitotic. mRNA expression of 60-day-old revealed the downregulation of progenitor and young neuronal markers in 60-year-old cultures, indicating progressive neuronal maturation.

For xenotransplantation experiments, iPSCs were differentiated into NPCs and subsequently into neurons using the established protocol by Boissart and colleagues [299]. This protocol has the advantage of generating a stable and proliferative population of NPCs, which can be expanded and cryopreserved. These NPCs can be further differentiated in-vitro, leading mostly to a majority of glutamatergic excitatory neurons, or they can be transplanted for in-vivo studies. This flexibility allows for the generation of a sufficient number of cells and the effective planning of transplantation surgeries. In our study, GFP-labeled

NPCs were employed, enabling easy tracking of the cells and facilitating morphological analysis following transplantation.

According to the previously published protocol, the neuronal phenotype was observed after 30 days of culture [299]. A comparison between 30-day-old neurons and NPCs revealed a reduction in progenitor markers such as Nestin and Pax6, accompanied by an increase in markers indicative of young to mature neurons, including Tuj1, Cux1, CTIP2, VGAT, and VGLUT. As neurons and glia share a common progenitor, the presence of a certain percentage of astrocytes (GFAP-positive) could be expected in the neuronal cultures. Moreover, it has been observed that extensively passaged NPCs may exhibit a higher proportion of GFAP-positive cells [302]. Given that the NPCs utilized in this study underwent approximately 28 passages prior to transplantation experiments, it was crucial to confirm the absence of high astrocyte proportions in the culture. Encouragingly, no GFAP-positive cells were detected in the cultures, validating the predominance of neuronal populations.

2.2. Xenotransplantation - in-vivo model

The transplantation of hiPSC-derived neurons into the mouse brain offers a valuable opportunity to study these cells under more physiological conditions and for extended periods of time. With the aim of better modeling complex neurological disorders, significant advances in the field have been made in the past years. Two main transplantation techniques are used: transplantation into the brains of adult mice and transplantation into neonatal mice [243–249]. Each technique has distinct advantages and limitations that must be considered. However, both approaches face two significant challenges. The first challenge involves the formation of graft bulks, where the transplanted cells remain isolated rather than integrating into the existing tissue, resulting in limited integration and immature development [244–246]. The second challenge involves graft rejection, which forces the use of immune-suppressed mouse models, which are fragile and not always ideal for modeling the specific disease of interest.

To address and overcome these challenges, we proposed a new option of transplantation of NPCs, at embryonic stages. At this developmental stage, the final laminar positioning of neurons and circuitry is not yet established, potentially providing an advantage for the transplanted neurons to migrate and integrate more effectively within the host brain. Furthermore, the host immune system is not fully developed during embryonic stages, potentially leading to improved tolerance for the human cells and reduced graft rejection.

2.2.1. Migration, maturation and integration of grafted cells

To develop well-integrated grafts, two different injection methods, previously utilized in neonatal xenografting, were investigated. The first method involved injecting cells into the LV of the developing brain [243,244,246,303]. By applying appropriate pressure during injection, cells could penetrate the ventricular wall and integrate into the SVZ, where mouse neuronal precursors originate. While this method offers the potential to better mimic neuronal development and achieve improved graft integration, several technical challenges arise. These include laborious screening of successfully injected brains prior to downstream experiments, dispersed neuronal distribution with harder characterization, and variability within injections.

The second technique tested involved directly transplanting cells into the neocortex. This transplantation approach has shown success in neonatal brains [243–246]. Although this method presents potential solutions to some of the challenges mentioned earlier, it also poses limitations. Specifically, the formation of dense graft cores consisting of non-integrated cells with limited maturation phenotypes has been reported with this technique.

2.2.2. Cell migration and axonal projection pattern

Embryonic neurogenesis in mice takes place between embryonic days (E) 11.5 and E16.5. During this period, neuronal cells originate in the SVZ and undergo tangential migration along the radial glia processes. This migration follows an "inside-out" pattern, where early-born neurons occupy deeper layers of the cortex, while late-born neurons populate the more superficial layers (reviewed in [304]). While it has not been confirmed if transplanted cells naturally exhibit this migration pattern, the transplantation into the LV creates an environment conducive to migration and integration. The hope is that the transplanted cells will migrate in a similar manner to endogenous neurogenesis.

Transplantations described in Results: Article 2 were conducted at E17.5. Although embryonic neurogenesis is almost completed at this time point, previous studies have demonstrated that cells can still migrate along the radial glia present even in neonatal stages [246]. Consistent with other studies involving transplantation into the LV of neonates, cells transplanted in-utero were observed close to the LV and surrounding brain regions one-month post-transplantation (1MPT) [243,244,246]. By 3 MPT, these cells had migrated further to structures such as the septum, cortex, hippocampus, thalamus, basal ganglia, and preoptic areas. Notably, unlike other studies the NPCs transplanted at embryonic stages did not migrate to

the olfactory bulb, suggesting a potentially lower engagement of these cells with the rostral migratory stream (RMS) [243,244].

The RMS serves as a crucial migratory route connecting the SVZ of the LV to the olfactory bulbs. During embryonic development, newly born neuroblasts rely on this pathway to migrate to the olfactory structures. It is noteworthy that the RMS remains active in the adult brain, primarily utilized by interneurons during adult neurogenesis. After birth, specialized astrocytes form a tubular structure around the RMS, serving as a scaffold for migrating progenitors. The formation of the RMS occurs between E15 and E17 before gliogenesis takes place. While neuroblasts can migrate independently of glial support during this period, the astrocytic tube becomes essential for the migration of neuroblasts during adult neurogenesis (reviewed in [305]). Considering that NPCs were transplanted during embryonic days when the RMS is being formed and astrocytes are unavailable to aid migration, it is plausible that there is a reduced inclination of the transplanted cells to utilize this pathway. This potential discrepancy may help explain the observed differences between the experiments presented here and previous data on neonatal transplantations.

In addition to assessing the location of the transplanted cells, it is crucial to evaluate their axonal projections as an indication of their integration into the circuitry and neuronal properties. Consistent with other studies cells transplanted in the LV exhibited dense axonal projections in fibral structures such as the corpus callosum and the septum [243]. Furthermore, human axonal projections were observed exclusively in cortical structures, including the hippocampus, thalamus, and basal ganglia, with no extra-cortical projections detected. Consistent with the mapping of cell somas, no projections were found in the RMS, confirming that the transplanted cells did not participate in the migratory path.

NPCs transplanted into the PFC exhibited minimal migration and remained in proximity to the injection site. Similar to reports from neonatal transplantations, a graft core was observed in the superficial layers of the cortex, with progressively more integrated cells found in deeper layers [244,245]. Although a bulk graft was present in the brain, a much smaller size with no sign of proliferation or change in brain morphology was observed.

2.2.3. Maturation

The speed of maturation and neuronal development differs between species. The human brain develops at a much slower pace than the mouse. Studies in-vitro and in-vivo have shown that neuronal differentiation and maturation are controlled by both intrinsic, cell-autonomous programs and environmental influences.

Interestingly, Vitrac et all showed that hiPSC-derived NPCs differentiated in culture showed more mature phenotypes than neurons transplanted in the cortex of mouse neonates at similar time points [243].

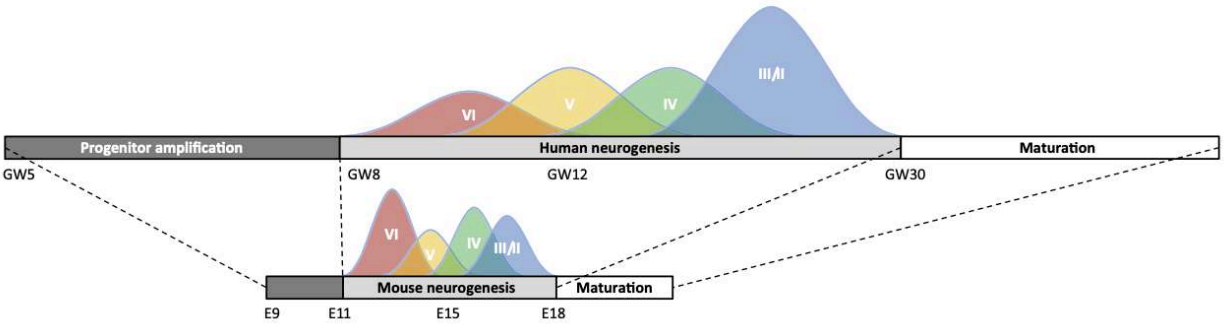

Figure 33. Time scale of human vs mouse neurogenesis.
Both species have inside-out patterns of the cortical layers as deep layers (VII, V) are generated before superficial layers (IV, III/II). Nevertheless, the speed of neurogenesis is much faster in mice when compared to humans, taking 6-7 days in mice while almost 22 weeks in humans [229].

To evaluate hiPSC-derived NPCs maturation and phenotype in the xenografted model described in Results: Article 2, an immunohistochemistry analysis of differentiation markers was performed. Since the NPCs were treated equally in-vitro prior to transplantation, we were able to directly assess whether different physiological cues from the host environment resulting from different injection techniques could impact the cells' maturity status.

Markers indicating proliferative cells (Sox2), young neurons (β-III tubulin), post-mitotic neurons (NeuN), and excitatory pyramidal cells VGLUT were evaluated. Consistent with the presented in-vitro data, both PFC and LV grafted cells showed no expression of the proliferative marker Sox2. Young neurons labeled with β-III tubulin were predominantly detected in the superficial layers of the PFC graft at 1 MPT and to a lesser extent at 3 MPT. This supports the idea that cells in graft cores differentiate more slowly, as observed in neonatal studies [245]. Post-mitotic cells labeled with NeuN were detected in cells after PFC transplantation in the deep part of the graft, but only a very small number in LV transplants after 3 MPT. Interestingly, while the vGLUT1 excitatory cell marker was detected in both conditions, in LV transplants, vGLUT was only present in dendritic shafts, whereas in PFC transplanted cells, it was also present in spines.

Overall, our results suggested a potential higher neuronal maturity phenotype in cells transplanted in the PFC compared to those in the LV. Although human neoteny is conserved and possibly guided by internal

cues, external signaling can alter the cells' speed of development. However, the characterization of these cells was based on observations, and further, more precise quantitative analysis should be done to confirm these findings. To address this need, we have initiated a project aimed at employing 10X single-cell genomics, a cutting-edge technique that enables the sequencing of individual cells at a high resolution. This powerful tool will provide us with a deeper understanding of the molecular profiles and functional properties of the transplanted cells, thereby offering valuable insights into their development, maturation, and integration. It would be interesting to see possible differences in gene expression patterns that could be influenced by the different environments to which the transplanted cells are exposed.

2.2.4. Integration

The integration of cells into a circuitry resides in the ability of cells to establish connections within a network. In embryonic development, once neurons have migrated and positioned themselves within the cortical layers, they begin to establish contact with each other, a process known as synaptogenesis. This primarily occurs during early postnatal life in mice and during childhood in humans. During this period, an excess of synapses is formed, which are subsequently pruned through a process of elimination. In adulthood, although synaptogenesis occurs with less intensity, it remains essential for brain plasticity and learning. Therefore, dysfunction in this mechanism can lead to neurological disorders (reviewed in [306]) (figure 34).

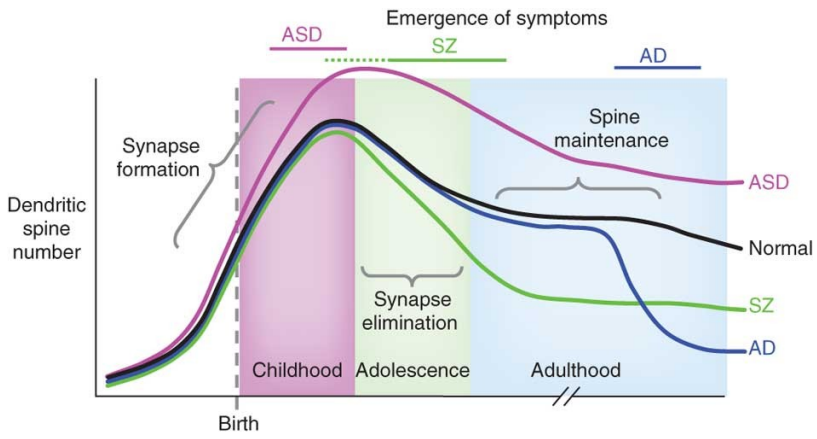

Figure 34. Dynamics of synapse formation and maintenance across lifespan. Defects in spine numbers underlaying synapse dysfunction, occurring at distinct ages throughout an individual's lifespan, are important hallmarks of neurological disorders such as ASD, SZ and AD [306].

In glutamatergic neurons, as well as some interneurons, synapses are formed on small dendrite protrusions called dendritic spines. These specialized structures house all the necessary components for post-synaptic information transmission and play a crucial role in synaptic connectivity. Spines can be classified into different categories based on their morphology [307]. For the study of the in-vivo model

presented here, four categories were included (Figure 35). While filopodia and stubby spines are mostly present in developing neurons and have short lifetimes, thin and mostly mushroom types represent more mature spine structures. Thin spines are plastic and are believed to be important for learning and mushroom spines are more stable and thought to play important roles in long-term memory storage.

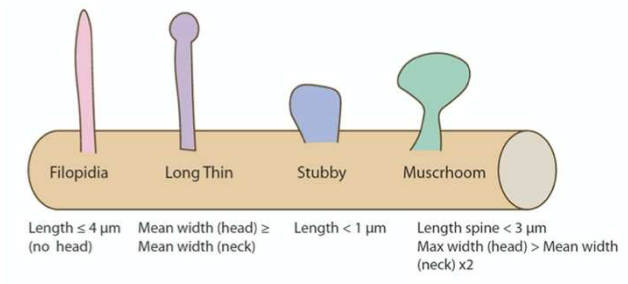

Figure 35. Spine category morphology.
Filopodia and thin spines are characterized by longer necks compared to stubby and mushroom spines. Filopodia and stubby spines do not possess a distinct head region, while thin spines have smaller heads compared to mushroom spines [308].

Using 3D reconstruction, we compared the spines of NPCs transplanted in the LV or the PFC at two different time points. In terms of spine categories, all transplants showed a majority of filopodia, indicating a rather early developmental stage of the transplanted cells. Nevertheless, PFC transplanted cells at 3 MPT showed a significant increase in Stubby spines.

In addition to spine categories, several morphological measurements within the spines can be analyzed to determine the maturity and strength of synaptic connections. Mature and established synapses are characterized by a larger head volume and overall spine volume, indicating a robust connection. On the other hand, less mature spines exhibit smaller volumes, often accompanied by elongated necks. This shrunken morphology represents a less mature phenotype, suggesting an early stage of synaptic development. In our experiments, NPCs transplanted in the LV showed increased maturity of spines defined by bigger head volumes and shorter necks when comparing 1 MPT and 3 MPT. After 3 MPT, NPCs transplanted in the LV showed morphologically more mature spines than PFC-transplanted cells. While in LV transplants, head volumes measured an average of 0.26 μm^3 and 0.36 μm^3 (1 MPT and 3 MPT, respectively), spine head volumes measured 0.16 μm^3 and 0.22 μm^3 in PFC transplants. In adult humans 0.35 μm^3 (40 years-old) and 0.38 μm^3 (85 years-old) have been reported, while in adult mice (8 weeks-old) spine head volumes are about 0.17 μm^3 [309]. Therefore, spines in neurons transplanted in the LV showed comparable spine head volumes to human adult neurons after 3 MPT. Spines of neurons transplanted in the PFC showed more immature morphology similar to the mouse adult cortex.

In addition to morphology and spine category, the density of spines can also give some insight into the integration of the neurons in the circuitry. In this case, cells transplanted in the PFC showed a 4-fold

increase in spine numbers when compared to the other conditions. A comparison between spine density observed in the in-utero xenografting model and other studies is presented in Figure 36.

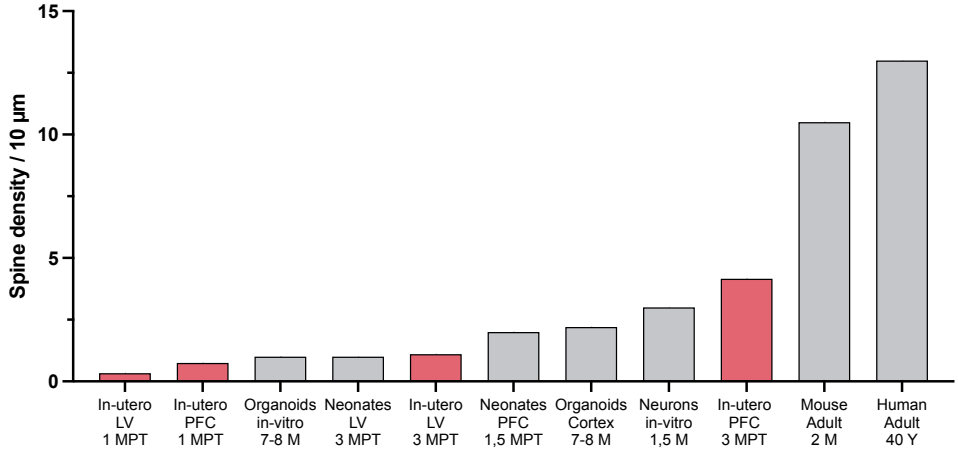

Figure 36. Spine density in various in-vitro and xenografting techniques.
Our method of in-utero transplantation is represented by the red data in the graph. At 1 MPT, our transplants exhibit relatively low spine density. However, at 3 MPT, the spine density of our LV transplants becomes comparable to that observed in organoids cultured in-vitro for 7-8 months [310] and LV transplants in neonates [246]. Our PFC transplants at 3 MPT demonstrate higher spine density compared to other models, such as in-vitro neuronal cultures, cortical transplantation of organoids and neonate transplants at 1.5 MPT [243,310]. Nevertheless, the spine densities observed in our transplants remain significantly lower than those found in the mouse and human adult brain [311,312].

2.2.5. Graft rejection and immune tolerance

The xenografting model presented here challenges the use of immune-deficient mice by transplanting cells at the embryonic stage into immune-competent mice. In the brain, two main types of cells potentially contribute to the rejection of allogenic neurons: T-cells that can infiltrate the brain from the cerebrospinal fluid, and microglia, which are the resident macrophages of the brain. It is important to note that mature T-cells can be detected towards the end of fetal development and undergo a significant proliferation after birth [313]. Microglia, on the other hand, are generated as early as E8 and migrate into the brain in multiple waves from E10.5 to E17.5 [314].

In the presented model, human NPCs were transplanted into immune-competent mice, and at 3 MPT, the presence of human cells was observed without any signs of apoptosis. In contrast, Nato and colleagues reported complete rejection of transplanted NPCs after 1 MPT using a similar transplantation method [303].

These discrepancies could be attributed to several factors, including the type of cells and their differentiation stage, the mouse host at the time of transplantation, the injection site, or the host strain used. An interesting hypothesis proposed by Nato and colleagues suggests that the immunogenicity of human neurons is influenced by their developmental stage. They hypothesize that young human neurons, which develop slowly, may have lower immunogenicity when transplanted during the host's immune system development. However, as human cells continue to develop after transplantation, epitopes that emerge at later stages might be recognized by the fully developed mouse immune system, leading to graft rejection. It is worth noting that in our in-vivo model, we used NPCs at the time of transplantation, while Nato and colleagues used post-mitotic neurons. Thus, it is possible that the "mature immunogenic epitopes" arise earlier in their transplants compared to those observed in our study, resulting in an early rejection at 1 MPT.

Although we did not observe cell death after 3 MPT, we did observe the recruitment of microglia, which exhibited an active phenotype, particularly in the PFC transplants. Microglia have been shown to have a dual role, as they can be both beneficial and detrimental. On one hand, they phagocytose cellular debris and release trophic and anti-inflammatory factors, which can be beneficial. On the other hand, they can produce inflammatory cytokines, leading to detrimental effects (reviewed in [315]). Therefore, the presence of microglia in the PFC area could indicate the initiation of graft rejection or a protective role in clearing non-surviving NPC debris. Additionally, it is possible that the presence of a scar from the injection site in the region could induce microglia recruitment.

It is important to note that when screening some brains at 4 and 6 MPT, we were unable to detect grafted human cells at those time points. This could be due to graft rejection or simply the unlucky selection of non-grafted pups. To reduce potential biases associated with surgeries or litters, pups from a single litter were gradually perfused at different time points. Since we did not dedicate a whole litter to studying a specific time point, we cannot determine whether the absence of grafts was due to graft rejection or the random success rate of the grafting method.

Further exploration at longer time points should be conducted to assess the long-term viability and absence of rejection of the transplanted cells. If rejection is detected, several improvements can be considered. Firstly, one potential improvement is to explore transplantation at early embryonic stages. Although technical and logistical limitations prevented us from using this approach in the current study, earlier transplantation may take advantage of the immunomodulatory environment during early development. Secondly, co-injecting the cells with adult epitopes extracted from older neuronal cultures or protein extracts from adult brains could be investigated. This method, as tested by Nato and colleagues,

demonstrated a 43% increased survival of human neurons when co-transplanted with adult epitopes after neonatal transplantations in the cerebellum [303]. This approach may provide a protective environment for the transplanted cells and enhance their long-term survival. Further studies should explore the feasibility and effectiveness of these strategies in improving the success and longevity of grafts.

3. Future directions

BIBLIOGRAPHY

1. Stelzmann RA, Norman Schnitzlein H, Reed Murtagh F. An english translation of alzheimer's 1907 paper, ?□ber eine eigenartige erkankung der hirnrinde? *Clin Anat*. 1995;8(6):429-431. doi:10.1002/ca.980080612

2. Graeber MB, Mehraein P. Reanalysis of the first case of Alzheimer's disease. *Eur Arch Psychiatry Clin Neurosci*. 1999;249 Suppl 3:10-13. doi:10.1007/pl00014167

3. Wu L, Rosa-Neto P, Hsiung GYR, et al. Early-Onset Familial Alzheimer's Disease (EOFAD). *Can J Neurol Sci J Can Sci Neurol*. 2012;39(4):436-445. doi:10.1017/S0317167100013949

4. The top 10 causes of death. Accessed April 25, 2023. https://www.who.int/news-room/fact-sheets/detail/the-top-10-causes-of-death

5. Global status report on the public health response to dementia. Accessed March 21, 2023. https://www.who.int/publications-detail-redirect/9789240033245

6. 2022 Alzheimer's disease facts and figures. *Alzheimers Dement*. 2022;18(4):700-789. doi:10.1002/alz.12638

7. Jönsson L, Tate A, Frisell O, Wimo A. The Costs of Dementia in Europe: An Updated Review and Meta-analysis. *PharmacoEconomics*. 2023;41(1):59-75. doi:10.1007/s40273-022-01212-z

8. Li X, Feng X, Sun X, Hou N, Han F, Liu Y. Global, regional, and national burden of Alzheimer's disease and other dementias, 1990–2019. *Front Aging Neurosci*. 2022;14:937486. doi:10.3389/fnagi.2022.937486

9. Nandi A, Counts N, Chen S, et al. Global and regional projections of the economic burden of Alzheimer's disease and related dementias from 2019 to 2050: A value of statistical life approach. *eClinicalMedicine*. 2022;51. doi:10.1016/j.eclinm.2022.101580

10. Morris JC. Early-stage and preclinical Alzheimer disease. *Alzheimer Dis Assoc Disord*. 2005;19(3):163-165. doi:10.1097/01.wad.0000184005.22611.cc

11. Jack CR, Bennett DA, Blennow K, et al. A/T/N: An unbiased descriptive classification scheme for Alzheimer disease biomarkers. *Neurology*. 2016;87(5):539-547. doi:10.1212/WNL.0000000000002923

12. Fessel J. Does synaptic hypometabolism or synaptic dysfunction, originate cognitive loss? Analysis of the evidence. *Alzheimers Dement Transl Res Clin Interv*. 2021;7(1):e12177. doi:10.1002/trc2.12177

13. Bottino CMC, Castro CC, Gomes RLE, Buchpiguel CA, Marchetti RL, Neto MRL. Volumetric MRI measurements can differentiate Alzheimer's disease, mild cognitive impairment, and normal aging. *Int Psychogeriatr*. 2002;14(1):59-72. doi:10.1017/s1041610202008281

14. Sørensen L, Igel C, Pai A, et al. Differential diagnosis of mild cognitive impairment and Alzheimer's disease using structural MRI cortical thickness, hippocampal shape, hippocampal texture, and volumetry. *NeuroImage Clin*. 2017;13:470-482. doi:10.1016/j.nicl.2016.11.025

15. Dementia. Accessed April 10, 2023. https://www.who.int/health-topics/dementia

16. Cummings J. The Role of Biomarkers in Alzheimer's Disease Drug Development. *Adv Exp Med Biol*. 2019;1118:29-61. doi:10.1007/978-3-030-05542-4_2

17. McKhann G, Drachman D, Folstein M, Katzman R, Price D, Stadlan EM. Clinical diagnosis of Alzheimer's disease:

18. Knopman DS, DeKosky ST, Cummings JL, et al. Practice parameter: Diagnosis of dementia (an evidence-based review): Report of the Quality Standards Subcommittee of the American Academy of Neurology. *Neurology*. 2001;56(9):1143-1153. doi:10.1212/WNL.56.9.1143

19. Research criteria for the diagnosis of Alzheimer's disease: revising the NINCDS–ADRDA criteria - ScienceDirect. Accessed March 23, 2023. https://www.sciencedirect.com/science/article/pii/S1474442207701783?via%3Dihub

20. Advancing research diagnostic criteria for Alzheimer's disease: the IWG-2 criteria - The Lancet Neurology. Accessed March 7, 2023. https://www.thelancet.com/journals/laneur/article/PIIS1474-4422(14)70090-0/fulltext

21. Sperling RA, Aisen PS, Beckett LA, et al. Toward defining the preclinical stages of Alzheimer's disease: recommendations from the National Institute on Aging-Alzheimer's Association workgroups on diagnostic guidelines for Alzheimer's disease. *Alzheimers Dement J Alzheimers Assoc*. 2011;7(3):280-292. doi:10.1016/j.jalz.2011.03.003

22. Albert MS, DeKosky ST, Dickson D, et al. The diagnosis of mild cognitive impairment due to Alzheimer's disease: Recommendations from the National Institute on Aging-Alzheimer's Association workgroups on diagnostic guidelines for Alzheimer's disease. *Alzheimers Dement*. 2011;7(3):270-279. doi:10.1016/j.jalz.2011.03.008

23. McKhann GM, Knopman DS, Chertkow H, et al. The diagnosis of dementia due to Alzheimer's disease: Recommendations from the National Institute on Aging-Alzheimer's Association workgroups on diagnostic guidelines for Alzheimer's disease. *Alzheimers Dement*. 2011;7(3):263-269. doi:10.1016/j.jalz.2011.03.005

24. Morris GP, Clark IA, Vissel B. Questions concerning the role of amyloid-β in the definition, aetiology and diagnosis of Alzheimer's disease. *Acta Neuropathol (Berl)*. 2018;136(5):663-689. doi:10.1007/s00401-018-1918-8

25. Esparza TJ, Zhao H, Cirrito JR, et al. Amyloid-β oligomerization in Alzheimer dementia versus high-pathology controls. *Ann Neurol*. 2013;73(1):104-119. doi:10.1002/ana.23748

26. Lue LF, Kuo YM, Roher AE, et al. Soluble amyloid beta peptide concentration as a predictor of synaptic change in Alzheimer's disease. *Am J Pathol*. 1999;155(3):853-862. doi:10.1016/s0002-9440(10)65184-x

27. Soluble pool of Abeta amyloid as a determinant of severity of neurodegeneration in Alzheimer's disease - PubMed. Accessed April 3, 2023. https://pubmed.ncbi.nlm.nih.gov/10589538/

28. Wang J, Dickson DW, Trojanowski JQ, Lee VM. The levels of soluble versus insoluble brain Abeta distinguish Alzheimer's disease from normal and pathologic aging. *Exp Neurol*. 1999;158(2):328-337. doi:10.1006/exnr.1999.7085

29. Lee SJC, Nam E, Lee HJ, Savelieff MG, Lim MH. Towards an understanding of amyloid-β oligomers: characterization, toxicity mechanisms, and inhibitors. *Chem Soc Rev*. 2017;46(2):310-323. doi:10.1039/C6CS00731G

30. Müller UC, Deller T, Korte M. Not just amyloid: physiological functions of the amyloid precursor protein family. *Nat Rev Neurosci*. 2017;18(5):281-298. doi:10.1038/nrn.2017.29

31. Jiang S, Li Y, Zhang X, Bu G, Xu H, Zhang Y wu. Trafficking regulation of proteins in Alzheimer's disease. *Mol Neurodegener*. 2014;9(1):6. doi:10.1186/1750-1326-9-6

32. Zhang Y wu, Thompson R, Zhang H, Xu H. APP processing in Alzheimer's disease. *Mol Brain*. 2011;4:3. doi:10.1186/1756-6606-4-3

33. Yang LB, Lindholm K, Yan R, et al. Elevated β-secretase expression and enzymatic activity detected in sporadic Alzheimer disease. *Nat Med*. 2003;9(1):3-4. doi:10.1038/nm0103-3

34. Tyler SJ, Dawbarn D, Wilcock GK, Allen SJ. alpha- and beta-secretase: profound changes in Alzheimer's disease. *Biochem Biophys Res Commun*. 2002;299(3):373-376. doi:10.1016/s0006-291x(02)02635-9

35. β-Secretase Activity Increases with Aging in Human, Monkey, and Mouse Brain - ScienceDirect. Accessed April 3, 2023. https://www.sciencedirect.com/science/article/pii/S0002944010631598

36. Wahlster L, Arimon M, Nasser-Ghodsi N, et al. Presenilin-1 adopts pathogenic conformation in normal aging and in sporadic Alzheimer's disease. *Acta Neuropathol (Berl)*. 2013;125(2):187-199. doi:10.1007/s00401-012-1065-6

37. Xi WH, Wei GH. Amyloid-β peptide aggregation and the influence of carbon nanoparticles*. *Chin Phys B*. 2015;25(1):018704. doi:10.1088/1674-1056/25/1/018704

38. MODELS OF AMYLOID SEEDING IN ALZHEIMER'S DISEASE AND SCRAPIE: Mechanistic Truths and Physiological Consequences of the Time-Dependent Solubility of Amyloid Proteins | Annual Review of Biochemistry. Accessed April 3, 2023. https://www.annualreviews.org/doi/10.1146/annurev.biochem.66.1.385?url_ver=Z39.88-2003&rfr_id=ori%3Arid%3Acrossref.org&rfr_dat=cr_pub++0pubmed

39. Xue C, Lin TY, Chang D, Guo Z. Thioflavin T as an amyloid dye: fibril quantification, optimal concentration and effect on aggregation. *R Soc Open Sci*. 2017;4(1):160696. doi:10.1098/rsos.160696

40. Pagano K, Tomaselli S, Molinari H, Ragona L. Natural Compounds as Inhibitors of Aβ Peptide Aggregation: Chemical Requirements and Molecular Mechanisms. *Front Neurosci*. 2020;14. Accessed April 26, 2023. https://www.frontiersin.org/articles/10.3389/fnins.2020.619667

41. Watts JC, Prusiner SB. β-Amyloid Prions and the Pathobiology of Alzheimer's Disease. *Cold Spring Harb Perspect Med*. 2018;8(5):a023507. doi:10.1101/cshperspect.a023507

42. Walker LC. Aβ Plaques. *Free Neuropathol*. 2020;1:31. doi:10.17879/freeneuropathology-2020-3025

43. Cline EN, Bicca MA, Viola KL, Klein WL. The Amyloid-β Oligomer Hypothesis: Beginning of the Third Decade. *J Alzheimers Dis*. 64(Suppl 1):S567-S610. doi:10.3233/JAD-179941

44. Leon WC, Canneva F, Partridge V, et al. A novel transgenic rat model with a full Alzheimer's-like amyloid pathology displays pre-plaque intracellular amyloid-beta-associated cognitive impairment. *J Alzheimers Dis JAD*. 2010;20(1):113-126. doi:10.3233/JAD-2010-1349

45. Mucke L, Masliah E, Yu GQ, et al. High-level neuronal expression of abeta 1-42 in wild-type human amyloid protein precursor transgenic mice: synaptotoxicity without plaque formation. *J Neurosci Off J Soc Neurosci*. 2000;20(11):4050-4058. doi:10.1523/JNEUROSCI.20-11-04050.2000

46. Shankar GM, Li S, Mehta TH, et al. Amyloid-beta protein dimers isolated directly from Alzheimer's brains impair synaptic plasticity and memory. *Nat Med*. 2008;14(8):837-842. doi:10.1038/nm1782

47. Zhao M, Wang S wei, Wang Y jiong, et al. Pan-amyloid oligomer specific scFv antibody attenuates memory deficits and brain amyloid burden in mice with Alzheimer's disease. *Curr Alzheimer Res*. 2014;11(1):69-78. doi:10.2174/15672050113106660176

48. Fan X, Xia L, Zhou Z, et al. Tau Acts in Concert With Kinase/Phosphatase Underlying Synaptic Dysfunction. *Front Aging Neurosci*. 2022;14. Accessed May 14, 2023. https://www.frontiersin.org/articles/10.3389/fnagi.2022.908881

49. Guo T, Noble W, Hanger DP. Roles of tau protein in health and disease. *Acta Neuropathol (Berl)*. 2017;133(5):665-704. doi:10.1007/s00401-017-1707-9

50. Duan Y, Dong S, Gu F, Hu Y, Zhao Z. Advances in the Pathogenesis of Alzheimer's Disease: Focusing on Tau-Mediated Neurodegeneration. *Transl Neurodegener*. 2012;1(1):24. doi:10.1186/2047-9158-1-24

51. Clavaguera F, Bolmont T, Crowther RA, et al. Transmission and spreading of tauopathy in transgenic mouse brain. *Nat Cell Biol*. 2009;11(7):909-913. doi:10.1038/ncb1901

52. Calafate S, Buist A, Miskiewicz K, et al. Synaptic Contacts Enhance Cell-to-Cell Tau Pathology Propagation. *Cell Rep*. 2015;11(8):1176-1183. doi:10.1016/j.celrep.2015.04.043

53. Braak H, Braak E. Neuropathological stageing of Alzheimer-related changes. *Acta Neuropathol (Berl)*. 1991;82(4):239-259. doi:10.1007/BF00308809

54. Leng F, Edison P. Neuroinflammation and microglial activation in Alzheimer disease: where do we go from here? *Nat Rev Neurol*. 2021;17(3):157-172. doi:10.1038/s41582-020-00435-y

55. Harry GJ. Microglia During Development and Aging. *Pharmacol Ther*. 2013;139(3):313-326. doi:10.1016/j.pharmthera.2013.04.013

56. Salter MW, Stevens B. Microglia emerge as central players in brain disease. *Nat Med*. 2017;23(9):1018-1027. doi:10.1038/nm.4397

57. Y Z, X W, X L, et al. TREM2 Is a Receptor for β-Amyloid that Mediates Microglial Function. *Neuron*. 2018;97(5). doi:10.1016/j.neuron.2018.01.031

58. L Z, Z W, D W, et al. Amyloid-beta modulates microglial responses by binding to the triggering receptor expressed on myeloid cells 2 (TREM2). *Mol Neurodegener*. 2018;13(1). doi:10.1186/s13024-018-0247-7

59. Gratuze M, Leyns CEG, Holtzman DM. New insights into the role of TREM2 in Alzheimer's disease. *Mol Neurodegener*. 2018;13(1):66. doi:10.1186/s13024-018-0298-9

60. Liddelow SA, Guttenplan KA, Clarke LE, et al. Neurotoxic reactive astrocytes are induced by activated microglia. *Nature*. 2017;541(7638):481-487. doi:10.1038/nature21029

61. Thal DR, Schultz C, Dehghani F, Yamaguchi H, Braak H, Braak E. Amyloid beta-protein (Abeta)-containing astrocytes are located preferentially near N-terminal-truncated Abeta deposits in the human entorhinal cortex. *Acta Neuropathol (Berl)*. 2000;100(6):608-617. doi:10.1007/s004010000242

62. Yi C, Mei X, Ezan P, et al. Astroglial connexin43 contributes to neuronal suffering in a mouse model of Alzheimer's disease. *Cell Death Differ*. 2016;23(10):1691-1701. doi:10.1038/cdd.2016.63

63. Jo S, Yarishkin O, Hwang YJ, et al. GABA from reactive astrocytes impairs memory in mouse models of Alzheimer's disease. *Nat Med*. 2014;20(8):886-896. doi:10.1038/nm.3639

64. Andreyev AY, Kushnareva YE, Starkov AA. Mitochondrial metabolism of reactive oxygen species. *Biochem Biokhimiia*. 2005;70(2):200-214. doi:10.1007/s10541-005-0102-7

65. Hulbert AJ, Pamplona R, Buffenstein R, Buttemer WA. Life and death: metabolic rate, membrane composition, and life span of animals. *Physiol Rev*. 2007;87(4):1175-1213. doi:10.1152/physrev.00047.2006

66. Krumova K, Cosa G. Chapter 1 Overview of Reactive Oxygen Species. Published online 2016:1-21. doi:10.1039/9781782622208-00001

67. Rizzuto R, De Stefani D, Raffaello A, Mammucari C. Mitochondria as sensors and regulators of calcium signalling. *Nat Rev Mol Cell Biol*. 2012;13(9):566-578. doi:10.1038/nrm3412

68. Rak M, Bénit P, Chrétien D, et al. Mitochondrial cytochrome c oxidase deficiency. *Clin Sci Lond Engl 1979*. 2016;130(6):393-407. doi:10.1042/CS20150707

69. Swerdlow RH. Brain aging, Alzheimer's disease, and mitochondria. *Biochim Biophys Acta*. 2011;1812(12):1630-1639. doi:10.1016/j.bbadis.2011.08.012

70. BOWEN DM, SMITH CB, WHITE P, DAVISON AN. NEUROTRANSMITTER-RELATED ENZYMES AND INDICES OF HYPOXIA IN SENILE DEMENTIA AND OTHER ABIOTROPHIES. *Brain*. 1976;99(3):459-496. doi:10.1093/brain/99.3.459

71. Davies P, Maloney AJ. Selective loss of central cholinergic neurons in Alzheimer's disease. *Lancet Lond Engl*. 1976;2(8000):1403. doi:10.1016/s0140-6736(76)91936-x

72. Perry EK, Gibson PH, Blessed G, Perry RH, Tomlinson BE. Neurotransmitter enzyme abnormalities in senile dementia: Choline acetyltransferase and glutamic acid decarboxylase activities in necropsy brain tissue. *J Neurol Sci*. 1977;34(2):247-265. doi:10.1016/0022-510X(77)90073-9

73. Mesulam M. A horseradish peroxidase method for the identification of the efferents of acetyl cholinesterase-containing neurons. *J Histochem Cytochem*. 1976;24(12):1281-1285. doi:10.1177/24.12.826585

74. Whitehouse PJ, Price DL, Clark AW, Coyle JT, DeLong MR. Alzheimer disease: Evidence for selective loss of cholinergic neurons in the nucleus basalis. *Ann Neurol*. 1981;10(2):122-126. doi:10.1002/ana.410100203

75. Kim LD, Factora RM. Alzheimer dementia: Starting, stopping drug therapy. *Cleve Clin J Med*. 2018;85(3):209-214. doi:10.3949/ccjm.85a.16080

76. Gotti C, Moretti M, Bohr I, et al. Selective nicotinic acetylcholine receptor subunit deficits identified in Alzheimer's disease, Parkinson's disease and dementia with Lewy bodies by immunoprecipitation. *Neurobiol Dis*. 2006;23(2):481-489. doi:10.1016/j.nbd.2006.04.005

77. Paterson D, Nordberg A. Neuronal nicotinic receptors in the human brain. *Prog Neurobiol*. 2000;61(1):75-111. doi:10.1016/S0301-0082(99)00045-3

78. Perry EK, Perry RH, Smith CJ, et al. Nicotinic receptor abnormalities in Alzheimer's and Parkinson's diseases. *J Neurol Neurosurg Psychiatry*. 1987;50(6):806-809.

79. Whitehouse PJ, Martino AM, Antuono PG, et al. Nicotinic acetylcholine binding sites in Alzheimer's disease. *Brain Res*. 1986;371(1):146-151. doi:10.1016/0006-8993(86)90819-X

80. Lombardo S, Maskos U. Role of the nicotinic acetylcholine receptor in Alzheimer's disease pathology and treatment. *Neuropharmacology*. 2015;96:255-262. doi:10.1016/j.neuropharm.2014.11.018

81. Cecon E, Dam J, Luka M, et al. Quantitative assessment of oligomeric amyloid β peptide binding to α7 nicotinic receptor. *Br J Pharmacol*. 2019;176(18):3475-3488. doi:10.1111/bph.14688

82. Buckingham SD, Jones AK, Brown LA, Sattelle DB. Nicotinic acetylcholine receptor signalling: roles in Alzheimer's disease and amyloid neuroprotection. *Pharmacol Rev*. 2009;61(1):39-61. doi:10.1124/pr.108.000562

83. Liu Q, Huang Y, Xue F, et al. A Novel Nicotinic Acetylcholine Receptor Subtype in Basal Forebrain Cholinergic Neurons with High Sensitivity to Amyloid Peptides. *J Neurosci*. 2009;29(4):918-929. doi:10.1523/JNEUROSCI.3952-08.2009

84. Khiroug SS, Harkness PC, Lamb PW, et al. Rat nicotinic ACh receptor alpha7 and beta2 subunits co-assemble to form functional heteromeric nicotinic receptor channels. *J Physiol*. 2002;540(Pt 2):425-434. doi:10.1113/jphysiol.2001.013847

85. Moretti M, Zoli M, George AA, et al. The Novel α7β2-Nicotinic Acetylcholine Receptor Subtype Is Expressed in Mouse and Human Basal Forebrain: Biochemical and Pharmacological Characterization. *Mol Pharmacol*. 2014;86(3):306-317. doi:10.1124/mol.114.093377

86. Lew AR, Kellermayer TR, Sule BP, Szigeti K. Copy Number Variations in Adult-onset Neuropsychiatric Diseases. *Curr Genomics*. 2018;19(6):420-430. doi:10.2174/1389202919666180330153842

87. Swaminathan S, Huentelman MJ, Corneveaux JJ, et al. Analysis of copy number variation in Alzheimer's disease in a cohort of clinically characterized and neuropathologically verified individuals. *PloS One*. 2012;7(12):e50640. doi:10.1371/journal.pone.0050640

88. The Texas Alzheimer Research and Care Consortium, Szigeti K, Kellermayer B, et al. Ordered Subset Analysis of Copy Number Variation Association with Age at Onset of Alzheimer's Disease. *J Alzheimers Dis*. 2014;41(4):1063-1071. doi:10.3233/JAD-132693

89. Espuny-Camacho I, Arranz AM, Fiers M, et al. Hallmarks of Alzheimer's Disease in Stem-Cell-Derived Human Neurons Transplanted into Mouse Brain. *Neuron*. 2017;93(5):1066-1081.e8. doi:10.1016/j.neuron.2017.02.001

90. St George-Hyslop PH, Tanzi RE, Polinsky RJ, et al. The genetic defect causing familial Alzheimer's disease maps on chromosome 21. *Science*. 1987;235(4791):885-890. doi:10.1126/science.2880399

91. Citron M, Oltersdorf T, Haass C, et al. Mutation of the beta-amyloid precursor protein in familial Alzheimer's disease increases beta-protein production. *Nature*. 1992;360(6405):672-674. doi:10.1038/360672a0

92. N S, Tt C, Xd C, et al. An increased percentage of long amyloid beta protein secreted by familial amyloid beta protein precursor (beta APP717) mutants. *Science*. 1994;264(5163). doi:10.1126/science.8191290

93. Lu T, Aron L, Zullo J, et al. REST and stress resistance in ageing and Alzheimer's disease. *Nature*. 2014;507(7493):448-454. doi:10.1038/nature13163

94. Lleó A, Blesa R, Queralt R, et al. Frequency of mutations in the presenilin and amyloid precursor protein genes in early-onset Alzheimer disease in Spain. *Arch Neurol*. 2002;59(11):1759-1763. doi:10.1001/archneur.59.11.1759

95. Revesz T, Ghiso J, Lashley T, et al. Cerebral Amyloid Angiopathies: A Pathologic, Biochemical, and Genetic View. *J Neuropathol Exp Neurol*. 2003;62(9):885-898. doi:10.1093/jnen/62.9.885

96. Gatz M, Reynolds CA, Fratiglioni L, et al. Role of genes and environments for explaining Alzheimer disease. *Arch Gen Psychiatry*. 2006;63(2):168-174. doi:10.1001/archpsyc.63.2.168

97. Ridge PG, Mukherjee S, Crane PK, Kauwe JSK, Consortium ADG. Alzheimer's Disease: Analyzing the Missing Heritability. *PLOS ONE*. 2013;8(11):e79771. doi:10.1371/journal.pone.0079771

98. Scheltens P, De Strooper B, Kivipelto M, et al. Alzheimer's disease. *The Lancet*. 2021;397(10284):1577-1590. doi:10.1016/S0140-6736(20)32205-4

99. A Armstrong R. Risk factors for Alzheimer's disease. *Folia Neuropathol*. 2019;57(2):87-105. doi:10.5114/fn.2019.85929

100. Haeberlein SB, Chen T, Wu S, et al. EMERGE and ENGAGE Topline Results: Two Phase 3 Studies to Evaluate Aducanumab in Patients With Early Alzheimer's Disease.

101. Research C for DE and. FDA's Decision to Approve New Treatment for Alzheimer's Disease. *FDA*. Published online December 1, 2022. Accessed April 12, 2023. https://www.fda.gov/drugs/news-events-human-drugs/fdas-decision-approve-new-treatment-alzheimers-disease

102. Eisai Inc. *A Placebo-Controlled, Double-Blind, Parallel-Group, 18-Month Study With an Open-Label Extension Phase to Confirm Safety and Efficacy of BAN2401 in Subjects With Early Alzheimer's Disease*. clinicaltrials.gov; 2022. Accessed April 11, 2023. https://clinicaltrials.gov/ct2/show/NCT03887455

103. Newman E, Gupta K, Climer J, Monaghan C, Hasselmo M. Cholinergic modulation of cognitive processing: insights drawn from computational models. *Front Behav Neurosci*. 2012;6. Accessed April 15, 2023. https://www.frontiersin.org/articles/10.3389/fnbeh.2012.00024

104. Picciotto MR, Higley MJ, Mineur YS. Acetylcholine as a Neuromodulator: Cholinergic Signaling Shapes Nervous System Function and Behavior. *Neuron*. 2012;76(1):116-129. doi:10.1016/j.neuron.2012.08.036

105. Everitt BJ, Robbins TW. Central cholinergic systems and cognition. *Annu Rev Psychol*. 1997;48:649-684. doi:10.1146/annurev.psych.48.1.649

106. Mesulam MM, Mufson EJ, Levey AI, Wainer BH. Cholinergic innervation of cortex by the basal forebrain: cytochemistry and cortical connections of the septal area, diagonal band nuclei, nucleus basalis (substantia innominata), and hypothalamus in the rhesus monkey. *J Comp Neurol*. 1983;214(2):170-197. doi:10.1002/cne.902140206

107. Mesulam MM, Mufson EJ, Wainer BH, Levey AI. Central cholinergic pathways in the rat: an overview based on an alternative nomenclature (Ch1-Ch6). *Neuroscience*. 1983;10(4):1185-1201. doi:10.1016/0306-4522(83)90108-2

108. Mike A, Castro NG, Albuquerque EX. Choline and acetylcholine have similar kinetic properties of activation and desensitization on the alpha7 nicotinic receptors in rat hippocampal neurons. *Brain Res*. 2000;882(1-2):155-168. doi:10.1016/s0006-8993(00)02863-8

109. Rye DB, Saper CB, Lee HJ, Wainer BH. Pedunculopontine tegmental nucleus of the rat: cytoarchitecture, cytochemistry, and some extrapyramidal connections of the mesopontine tegmentum. *J Comp Neurol*. 1987;259(4):483-528. doi:10.1002/cne.902590403

110. Mena-Segovia J. Structural and functional considerations of the cholinergic brainstem. *J Neural Transm*. 2016;123(7):731-736. doi:10.1007/s00702-016-1530-9

111. Leanza G, Muir J, Nilsson OG, Wiley RG, Dunnett SB, Bjorklund A. Selective immunolesioning of the basal forebrain cholinergic system disrupts short-term memory in rats. *Eur J Neurosci*. 1996;8(7):1535-1544. doi:10.1111/j.1460-9568.1996.tb01616.x

112. McCormick DA. Chapter 36: Actions of acetylcholine in the cerebral cortex and thalamus and implications for function. In: Cuello AC, ed. *Progress in Brain Research*. Vol 98. Cholinergic Function and Dysfunction. Elsevier; 1993:303-308. doi:10.1016/S0079-6123(08)62412-7

113. Khateb A, Fort P, Williams S, Serafin M, Jones BE, Mühlethaler M. Modulation of cholinergic nucleus basalis neurons by acetylcholine and N-methyl-D-aspartate. *Neuroscience*. 1997;81(1):47-55. doi:10.1016/s0306-4522(97)00167-x

114. Perez-Lloret S, Barrantes FJ. Deficits in cholinergic neurotransmission and their clinical correlates in Parkinson's disease. *Npj Park Dis*. 2016;2(1):1-12. doi:10.1038/npjparkd.2016.1

115. Carlson AB, Kraus GP. Physiology, Cholinergic Receptors. In: *StatPearls*. StatPearls Publishing; 2023. Accessed May 6, 2023. http://www.ncbi.nlm.nih.gov/books/NBK526134/

116. Chen ZR, Huang JB, Yang SL, Hong FF. Role of Cholinergic Signaling in Alzheimer's Disease. *Molecules*. 2022;27(6):1816. doi:10.3390/molecules27061816

117. Wess J. Novel insights into muscarinic acetylcholine receptor function using gene targeting technology. *Trends Pharmacol Sci*. 2003;24(8):414-420. doi:10.1016/S0165-6147(03)00195-0

118. Picciotto MR, Caldarone BJ, King SL, Zachariou V. Nicotinic receptors in the brain. Links between molecular biology and behavior. *Neuropsychopharmacol Off Publ Am Coll Neuropsychopharmacol*. 2000;22(5):451-465. doi:10.1016/S0893-133X(99)00146-3

119. Kudlak M, Tadi P. Physiology, Muscarinic Receptor. In: *StatPearls*. StatPearls Publishing; 2023. Accessed May 6, 2023. http://www.ncbi.nlm.nih.gov/books/NBK555909/

120. Zoli M, Pucci S, Vilella A, Gotti C. Neuronal and Extraneuronal Nicotinic Acetylcholine Receptors. *Curr Neuropharmacol*. 2018;16(4):338-349. doi:10.2174/1570159X15666170912110450

121. Changeux JP, Bertrand D, Corringer PJ, et al. Brain nicotinic receptors: structure and regulation, role in learning and reinforcement. *Brain Res Brain Res Rev*. 1998;26(2-3):198-216. doi:10.1016/s0165-0173(97)00040-4

122. Cetin H, Beeson D, Vincent A, Webster R. The Structure, Function, and Physiology of the Fetal and Adult Acetylcholine Receptor in Muscle. *Front Mol Neurosci*. 2020;13. Accessed April 17, 2023. https://www.frontiersin.org/articles/10.3389/fnmol.2020.581097

123. Skok VI. Nicotinic acetylcholine receptors in autonomic ganglia. *Auton Neurosci Basic Clin*. 2002;97(1):1-11. doi:10.1016/s1566-0702(01)00386-1

124. Taly A, Corringer PJ, Guedin D, Lestage P, Changeux JP. Nicotinic receptors: allosteric transitions and therapeutic targets in the nervous system. *Nat Rev Drug Discov*. 2009;8(9):733-750. doi:10.1038/nrd2927

125. Gotti C, Clementi F, Fornari A, et al. Structural and functional diversity of native brain neuronal nicotinic receptors. *Biochem Pharmacol*. 2009;78(7):703-711. doi:10.1016/j.bcp.2009.05.024

126. Brisson A, Unwin PNT. Quaternary structure of the acetylcholine receptor. *Nature*. 1985;315(6019):474-477. doi:10.1038/315474a0

127. Cartaud J, Benedetti EL, Cohen JB, Meunier JC, Changeux JP. Presence of a lattice structure in membrane fragments rich in nicotinic receptor protein from the electric organ of Torpedo marmorata. *FEBS Lett*. 1973;33(1):109-113. doi:10.1016/0014-5793(73)80171-1

128. Bocquet N, Nury H, Baaden M, et al. X-ray structure of a pentameric ligand-gated ion channel in an apparently open conformation. *Nature*. 2009;457(7225):111-114. doi:10.1038/nature07462

129. Gulsevin A, Papke RL, Horenstein N. In Silico Modeling of the α7 Nicotinic Acetylcholine Receptor: New Pharmacological Challenges Associated with Multiple Modes of Signaling. *Mini Rev Med Chem*. 2020;20(10):841-864. doi:10.2174/1389557520666200130105256

130. Noviello CM, Gharpure A, Mukhtasimova N, et al. Structure and gating mechanism of the α7 nicotinic acetylcholine receptor. *Cell*. 2021;184(8):2121-2134.e13. doi:10.1016/j.cell.2021.02.049

131. Wonnacott S. Nicotinic Receptors. In: Offermanns S, Rosenthal W, eds. *Encyclopedia of Molecular Pharmacology*. Springer International Publishing; 2020:1-7. doi:10.1007/978-3-030-21573-6_102-1

132. Heidmann T, Bernhardt J, Neumann E, Changeux JP. Rapid kinetics of agonist binding and permeability response analyzed in parallel on acetylcholine receptor rich membranes from Torpedo marmorata. *Biochemistry*. 1983;22(23):5452-5459. doi:10.1021/bi00292a029

133. Heidmann T, Changeux JP. Fast Kinetic Studies on the Interaction of a Fluorescent Agonist with the Membrane-Bound Acetylcholine Receptor from Torpedo marmorata. *Eur J Biochem*. 1979;94(1):255-279. doi:10.1111/j.1432-1033.1979.tb12893.x

134. Heidmann T, Changeux JP. Interaction of a fluorescent agonist with the membrane-bound acetylcholine receptor from Torpedomarmorata in the millisecond time range: Resolution of an "intermediate" conformational transition and evidence for positive cooperative effects. *Biochem Biophys Res Commun*. 1980;97(3):889-896. doi:10.1016/0006-291X(80)91460-6

135. Neubig RR, Boyd ND, Cohen JB. Conformations of Torpedo acetylcholine receptor associated with ion transport and desensitization. *Biochemistry*. 1982;21(14):3460-3467. doi:10.1021/bi00257a032

136. Corradi J, Bouzat C. Understanding the Bases of Function and Modulation of α7 Nicotinic Receptors: Implications for Drug Discovery. *Mol Pharmacol*. 2016;90(3):288-299. doi:10.1124/mol.116.104240

137. Cecchini M, Changeux JP. The nicotinic acetylcholine receptor and its prokaryotic homologues: Structure, conformational transitions & allosteric modulation. *Neuropharmacology*. 2015;96:137-149. doi:10.1016/j.neuropharm.2014.12.006

138. Gill-Thind JK, Dhankher P, D'Oyley JM, Sheppard TD, Millar NS. Structurally similar allosteric modulators of α7 nicotinic acetylcholine receptors exhibit five distinct pharmacological effects. *J Biol Chem*. 2015;290(6):3552-3562. doi:10.1074/jbc.M114.619221

139. Cheng Q, Yakel JL. The effect of α7 nicotinic receptor activation on glutamatergic transmission in the hippocampus. *Biochem Pharmacol*. 2015;97(4):439-444. doi:10.1016/j.bcp.2015.07.015

140. Winek K, Soreq H, Meisel A. Regulators of cholinergic signaling in disorders of the central nervous system. *J Neurochem*. 2021;158(6):1425-1438. doi:10.1111/jnc.15332

141. Piovesana R, Salazar Intriago MS, Dini L, Tata AM. Cholinergic Modulation of Neuroinflammation: Focus on α7 Nicotinic Receptor. *Int J Mol Sci*. 2021;22(9):4912. doi:10.3390/ijms22094912

142. Miller DT, Shen Y, Weiss LA, et al. Microdeletion/duplication at 15q13.2q13.3 among individuals with features of autism and other neuropsychiatric disorders. *J Med Genet*. 2009;46(4):242-248. doi:10.1136/jmg.2008.059907

143. Swaminathan S, Huentelman MJ, Corneveaux JJ, et al. Analysis of Copy Number Variation in Alzheimer's Disease in a Cohort of Clinically Characterized and Neuropathologically Verified Individuals. *PLoS ONE*. 2012;7(12):e50640. doi:10.1371/journal.pone.0050640

144. van Bon BWM, Mefford HC, Menten B, et al. Further delineation of the 15q13 microdeletion and duplication syndromes: a clinical spectrum varying from non-pathogenic to a severe outcome. *J Med Genet*. 2009;46(8):511-523. doi:10.1136/jmg.2008.063412

145. Gault J, Robinson M, Berger R, et al. Genomic Organization and Partial Duplication of the Human α7 Neuronal Nicotinic Acetylcholine Receptor Gene (CHRNA7). *Genomics*. 1998;52(2):173-185. doi:10.1006/geno.1998.5363

146. Wanamaker CP, Christianson JC, Green WN. Regulation of nicotinic acetylcholine receptor assembly. *Ann N Y Acad Sci*. 2003;998:66-80. doi:10.1196/annals.1254.009

147. Colombo SF, Mazzo F, Pistillo F, Gotti C. Biogenesis, trafficking and up-regulation of nicotinic ACh receptors. *Biochem Pharmacol*. 2013;86(8):1063-1073. doi:10.1016/j.bcp.2013.06.023

148. Keller SH, Lindstrom J, Ellisman M, Taylor P. Adjacent basic amino acid residues recognized by the COP I complex and ubiquitination govern endoplasmic reticulum to cell surface trafficking of the nicotinic acetylcholine receptor alpha-Subunit. *J Biol Chem*. 2001;276(21):18384-18391. doi:10.1074/jbc.M100691200

149. Smith MM, Lindstrom J, Merlie JP. Formation of the alpha-bungarotoxin binding site and assembly of the nicotinic acetylcholine receptor subunits occur in the endoplasmic reticulum. *J Biol Chem*. 1987;262(9):4367-4376. doi:10.1016/S0021-9258(18)61357-2

150. Halevi S, McKay J, Palfreyman M, et al. The C.elegans ric-3 gene is required for maturation of nicotinic acetylcholine receptors. *EMBO J*. 2002;21(5):1012-1020. doi:10.1093/emboj/21.5.1012

151. Wang Y, Yao Y, Tang XQ, Wang ZZ. Mouse RIC-3, an Endoplasmic Reticulum Chaperone, Promotes Assembly of the α7 Acetylcholine Receptor through a Cytoplasmic Coiled-Coil Domain. *J Neurosci*. 2009;29(40):12625-12635. doi:10.1523/JNEUROSCI.1776-09.2009

152. Deshpande A, Vinayakamoorthy RM, Garg BK, et al. Why Does Knocking Out NACHO, But Not RIC3, Completely Block Expression of α7 Nicotinic Receptors in Mouse Brain? *Biomolecules*. 2020;10(3):470. doi:10.3390/biom10030470

153. Koperniak TM, Garg BK, Boltax J, Loring RH. Cell-specific effects on surface α7 nicotinic receptor expression revealed by over-expression and knockdown of rat RIC3 protein. *J Neurochem*. 2013;124(3):300-309. doi:10.1111/jnc.12095

154. Kuryatov A, Mukherjee J, Lindstrom J. Chemical chaperones exceed the chaperone effects of RIC-3 in promoting assembly of functional α7 AChRs. *PloS One*. 2013;8(4):e62246. doi:10.1371/journal.pone.0062246

155. Gu S, Matta JA, Lord B, et al. Brain α7 Nicotinic Acetylcholine Receptor Assembly Requires NACHO. *Neuron*. 2016;89(5):948-955. doi:10.1016/j.neuron.2016.01.018

156. Castillo M, Mulet J, Gutiérrez LM, et al. Dual Role of the RIC-3 Protein in Trafficking of Serotonin and Nicotinic Acetylcholine Receptors *. *J Biol Chem*. 2005;280(29):27062-27068. doi:10.1074/jbc.M503746200

157. Kweon HJ, Gu S, Witham E, et al. NACHO Engages N-Glycosylation ER Chaperone Pathways for α7 Nicotinic Receptor Assembly. *Cell Rep*. 2020;32(6). doi:10.1016/j.celrep.2020.108025

158. Ke L, Eisenhour CM, Bencherif M, Lukas RJ. Effects of chronic nicotine treatment on expression of diverse nicotinic acetylcholine receptor subtypes. I. Dose- and time-dependent effects of nicotine treatment. *J Pharmacol Exp Ther*. 1998;286(2):825-840.

159. Schwartz RD, Kellar KJ. In vivo regulation of [3H]acetylcholine recognition sites in brain by nicotinic cholinergic drugs. *J Neurochem*. 1985;45(2):427-433. doi:10.1111/j.1471-4159.1985.tb04005.x

160. Corringer PJ, Sallette J, Changeux JP. Nicotine enhances intracellular nicotinic receptor maturation: A novel mechanism of neural plasticity? *J Physiol-Paris*. 2006;99(2):162-171. doi:10.1016/j.jphysparis.2005.12.012

161. Sinkus ML, Graw S, Freedman R, Ross RG, Lester HA, Leonard S. The human CHRNA7 and CHRFAM7A genes: A review of the genetics, regulation, and function. *Neuropharmacology*. 2015;96:274-288. doi:10.1016/j.neuropharm.2015.02.006

162. Lasala M, Corradi J, Bruzzone A, Esandi M del C, Bouzat C. A human-specific, truncated α7 nicotinic receptor subunit assembles with full-length α7 and forms functional receptors with different stoichiometries. *J Biol Chem*. 2018;293(27):10707-10717. doi:10.1074/jbc.RA117.001698

163. Araud T, Graw S, Berger R, et al. The chimeric gene CHRFAM7A, a partial duplication of the CHRNA7 gene, is a dominant negative regulator of α7*nAChR function. *Biochem Pharmacol*. 2011;82(8):904-914. doi:10.1016/j.bcp.2011.06.018

164. Lucas-Cerrillo AM de, Maldifassi MC, Arnalich F, et al. Function of Partially Duplicated Human α7 Nicotinic Receptor Subunit CHRFAM7A Gene: POTENTIAL IMPLICATIONS FOR THE CHOLINERGIC ANTI-INFLAMMATORY RESPONSE *. *J Biol Chem*. 2011;286(1):594-606. doi:10.1074/jbc.M110.180067

165. Flomen RH, Davies AF, Di Forti M, et al. The copy number variant involving part of the alpha7 nicotinic receptor gene contains a polymorphic inversion. *Eur J Hum Genet EJHG*. 2008;16(11):1364-1371. doi:10.1038/ejhg.2008.112

166. Flomen RH, Collier DA, Osborne S, et al. Association study of CHRFAM7A copy number and 2 bp deletion polymorphisms with schizophrenia and bipolar affective disorder. *Am J Med Genet Part B Neuropsychiatr Genet Off Publ Int Soc Psychiatr Genet*. 2006;141B(6):571-575. doi:10.1002/ajmg.b.30306

167. Petrovsky N, Schmechtig A, Flomen RH, et al. CHRFAM7A copy number and 2-bp deletion polymorphisms and antisaccade performance. *Int J Neuropsychopharmacol*. 2009;12(2):267-273. doi:10.1017/S1461145708009784

168. Raux G, Bonnet-Brilhault F, Louchart S, et al. The −2 bp deletion in exon 6 of the 'alpha 7-like' nicotinic receptor subunit gene is a risk factor for the P50 sensory gating deficit. *Mol Psychiatry*. 2002;7(9):1006-1011. doi:10.1038/sj.mp.4001140

169. Sinkus ML, Lee MJ, Gault J, et al. A 2-base pair deletion polymorphism in the partial duplication of the alpha7 nicotinic acetylcholine gene (CHRFAM7A) on chromosome 15q14 is associated with schizophrenia. *Brain Res*. 2009;1291:1-11. doi:10.1016/j.brainres.2009.07.041

170. Cameli C, Bacchelli E, De Paola M, et al. Genetic variation in CHRNA7 and CHRFAM7A is associated with nicotine dependence and response to varenicline treatment. *Eur J Hum Genet*. 2018;26(12):1824-1831. doi:10.1038/s41431-018-0223-2

171. Szigeti K, Kellermayer B, Lentini JM, et al. Ordered subset analysis of copy number variation association with age at onset of Alzheimer's disease. *J Alzheimers Dis JAD*. 2014;41(4):1063-1071. doi:10.3233/JAD-132693

172. Szigeti K, Ihnatovych I, Birkaya B, et al. CHRFAM7A: A human specific fusion gene, accounts for the translational gap for cholinergic strategies in Alzheimer's disease. *EBioMedicine*. 2020;59:102892. doi:10.1016/j.ebiom.2020.102892

173. Chen D, Dang H, Patrick JW. Contributions of N-Linked Glycosylation to the Expression of a Functional α7-Nicotinic Receptor in Xenopus Oocytes. *J Neurochem*. 1998;70(1):349-357. doi:10.1046/j.1471-4159.1998.70010349.x

174. Liu D, de Souza JV, Ahmad A, Bronowska AK. Structure, Dynamics, and Ligand Recognition of Human-Specific CHRFAM7A (Dupα7) Nicotinic Receptor Linked to Neuropsychiatric Disorders. *Int J Mol Sci*. 2021;22(11):5466. doi:10.3390/ijms22115466

175. Wang Y, Xiao C, Indersmitten T, Freedman R, Leonard S, Lester HA. The Duplicated α7 Subunits Assemble and Form Functional Nicotinic Receptors with the Full-length α7. *J Biol Chem*. 2014;289(38):26451-26463. doi:10.1074/jbc.M114.582858

176. Martín-Sánchez C, Alés E, Balseiro-Gómez S, et al. The human-specific duplicated α7 gene inhibits the ancestral α7, negatively regulating nicotinic acetylcholine receptor-mediated transmitter release. *J Biol Chem*. 2021;296. doi:10.1016/j.jbc.2021.100341

177. Ihnatovych I, Nayak TK, Ouf A, et al. iPSC model of CHRFAM7A effect on α7 nicotinic acetylcholine receptor function in the human context. *Transl Psychiatry*. 2019;9(1):59. doi:10.1038/s41398-019-0375-z

178. Maldifassi MC, Martín-Sánchez C, Atienza G, et al. Interaction of the α7-nicotinic subunit with its human-specific duplicated dupα7 isoform in mammalian cells: Relevance in human inflammatory responses. *J Biol Chem*. 2018;293(36):13874-13888. doi:10.1074/jbc.RA118.003443

179. Maroli A, Lascio SD, Drufuca L, et al. Effect of donepezil on the expression and responsiveness to LPS of CHRNA7 and CHRFAM7A in macrophages: A possible link to the cholinergic anti-inflammatory pathway. *J Neuroimmunol*. 2019;332:155-166. doi:10.1016/j.jneuroim.2019.04.012

180. Costantini TW, Dang X, Yurchyshyna MV, Coimbra R, Eliceiri BP, Baird A. A Human-Specific α7-Nicotinic Acetylcholine Receptor Gene in Human Leukocytes: Identification, Regulation and the

Consequences of CHRFAM7A Expression. *Mol Med*. 2015;21(1):323-336. doi:10.2119/molmed.2015.00018

181. Benfante R, Antonini RA, De Pizzol M, et al. Expression of the α7 nAChR subunit duplicate form (CHRFAM7A) is down-regulated in the monocytic cell line THP-1 on treatment with LPS. *J Neuroimmunol*. 2011;230(1-2):74-84. doi:10.1016/j.jneuroim.2010.09.008

182. Cedillo JL, Arnalich F, Martín-Sánchez C, et al. Usefulness of α7 Nicotinic Receptor Messenger RNA Levels in Peripheral Blood Mononuclear Cells as a Marker for Cholinergic Antiinflammatory Pathway Activity in Septic Patients: Results of a Pilot Study. *J Infect Dis*. 2015;211(1):146-155. doi:10.1093/infdis/jiu425

183. Baird A, Coimbra R, Dang X, Eliceiri BP, Costantini TW. Up-regulation of the human-specific CHRFAM7A gene in inflammatory bowel disease. *BBA Clin*. 2016;5:66-71. doi:10.1016/j.bbacli.2015.12.003

184. Wang HY, Lee DHS, Davis CB, Shank RP. Amyloid Peptide Aβ1-42 Binds Selectively and with Picomolar Affinity to α7 Nicotinic Acetylcholine Receptors. *J Neurochem*. 2000;75(3):1155-1161. doi:10.1046/j.1471-4159.2000.0751155.x

185. Wang HY, Lee DH, D'Andrea MR, Peterson PA, Shank RP, Reitz AB. beta-Amyloid(1-42) binds to alpha7 nicotinic acetylcholine receptor with high affinity. Implications for Alzheimer's disease pathology. *J Biol Chem*. 2000;275(8):5626-5632. doi:10.1074/jbc.275.8.5626

186. Dineley KT, Bell KA, Bui D, Sweatt JD. beta -Amyloid peptide activates alpha 7 nicotinic acetylcholine receptors expressed in Xenopus oocytes. *J Biol Chem*. 2002;277(28):25056-25061. doi:10.1074/jbc.M200066200

187. Dougherty JJ, Wu J, Nichols RA. Beta-amyloid regulation of presynaptic nicotinic receptors in rat hippocampus and neocortex. *J Neurosci Off J Soc Neurosci*. 2003;23(17):6740-6747. doi:10.1523/JNEUROSCI.23-17-06740.2003

188. Lasala M, Fabiani C, Corradi J, Antollini S, Bouzat C. Molecular Modulation of Human α7 Nicotinic Receptor by Amyloid-β Peptides. *Front Cell Neurosci*. 2019;13. doi:10.3389/fncel.2019.00037

189. Puzzo D, Privitera L, Leznik E, et al. Picomolar amyloid-beta positively modulates synaptic plasticity and memory in hippocampus. *J Neurosci Off J Soc Neurosci*. 2008;28(53):14537-14545. doi:10.1523/JNEUROSCI.2692-08.2008

190. Parri HR, Hernandez CM, Dineley KT. Research update: Alpha7 nicotinic acetylcholine receptor mechanisms in Alzheimer's disease. *Biochem Pharmacol*. 2011;82(8):931-942. doi:10.1016/j.bcp.2011.06.039

191. Pettit DL, Shao Z, Yakel JL. β-Amyloid $_{1–42}$ Peptide Directly Modulates Nicotinic Receptors in the Rat Hippocampal Slice. *J Neurosci*. 2001;21(1):RC120-RC120. doi:10.1523/JNEUROSCI.21-01-j0003.2001

192. Hernandez CM, Kayed R, Zheng H, Sweatt JD, Dineley KT. Loss of α7 nicotinic receptors enhances β-amyloid oligomer accumulation, exacerbating early-stage cognitive decline and

septohippocampal pathology in a mouse model of Alzheimer's disease. *J Neurosci*. 2010;30(7):2442-2453. doi:10.1523/JNEUROSCI.5038-09.2010

193. Dziewczapolski G, Glogowski CM, Masliah E, Heinemann SF. Deletion of the α7 nicotinic acetylcholine receptor gene improves cognitive deficits and synaptic pathology in a mouse model of Alzheimer's disease. *J Neurosci*. 2009;29(27):8805-8815. doi:10.1523/JNEUROSCI.6159-08.2009

194. Fehér A, Juhász A, Rimanóczy A, Csibri E, Kálmán J, Janka Z. Association between a genetic variant of the alpha-7 nicotinic acetylcholine receptor subunit and four types of dementia. *Dement Geriatr Cogn Disord*. 2009;28(1):56-62. doi:10.1159/000230036

195. Heinzen EL, Need AC, Hayden KM, et al. Genome-wide scan of copy number variation in late-onset Alzheimer's disease. *J Alzheimers Dis JAD*. 2010;19(1):69-77. doi:10.3233/JAD-2010-1212

196. Chapman J, Rees E, Harold D, et al. A genome-wide study shows a limited contribution of rare copy number variants to Alzheimer's disease risk. *Hum Mol Genet*. 2013;22(4):816-824. doi:10.1093/hmg/dds476

197. Ihnatovych I, Birkaya B, Notari E, Szigeti K. iPSC-Derived Microglia for Modeling Human-Specific DAMP and PAMP Responses in the Context of Alzheimer's Disease. *Int J Mol Sci*. 2020;21(24):9668. doi:10.3390/ijms21249668

198. Zakrzewski W, Dobrzyński M, Szymonowicz M, Rybak Z. Stem cells: past, present, and future. *Stem Cell Res Ther*. 2019;10(1):68. doi:10.1186/s13287-019-1165-5

199. Waddington CH. The strategy of the genes. A discussion of some aspects of theoretical biology. With an appendix by H. Kacser. *Strategy Genes Discuss Some Asp Theor Biol Append H Kacser*. Published online 1957. Accessed April 27, 2023. https://www.cabdirect.org/cabdirect/abstract/19580101706

200. Takahashi K, Yamanaka S. Induction of Pluripotent Stem Cells from Mouse Embryonic and Adult Fibroblast Cultures by Defined Factors. *Cell*. 2006;126(4):663-676. doi:10.1016/j.cell.2006.07.024

201. Takahashi K, Yamanaka S. A decade of transcription factor-mediated reprogramming to pluripotency. *Nat Rev Mol Cell Biol*. 2016;17(3):183-193. doi:10.1038/nrm.2016.8

202. Evans MJ, Kaufman MH. Establishment in culture of pluripotential cells from mouse embryos. *Nature*. 1981;292(5819):154-156. doi:10.1038/292154a0

203. Thomson JA, Itskovitz-Eldor J, Shapiro SS, et al. Embryonic stem cell lines derived from human blastocysts. *Science*. 1998;282(5391):1145-1147. doi:10.1126/science.282.5391.1145

204. Chung Y, Klimanskaya I, Becker S, et al. Human embryonic stem cell lines generated without embryo destruction. *Cell Stem Cell*. 2008;2(2):113-117. doi:10.1016/j.stem.2007.12.013

205. Gilley JA, Yang CP, Kernie SG. Developmental profiling of postnatal dentate gyrus progenitors provides evidence for dynamic cell-autonomous regulation. *Hippocampus*. 2011;21(1):33-47. doi:10.1002/hipo.20719

206. Doetsch F, Caillé I, Lim DA, García-Verdugo JM, Alvarez-Buylla A. Subventricular zone astrocytes are neural stem cells in the adult mammalian brain. *Cell*. 1999;97(6):703-716. doi:10.1016/s0092-8674(00)80783-7

207. Fuentealba LC, Rompani SB, Parraguez JI, et al. Embryonic Origin of Postnatal Neural Stem Cells. *Cell*. 2015;161(7):1644-1655. doi:10.1016/j.cell.2015.05.041

208. Lucassen PJ, Fitzsimons CP, Salta E, Maletic-Savatic M. Adult neurogenesis, human after all (again): Classic, optimized, and future approaches. *Behav Brain Res*. 2020;381:112458. doi:10.1016/j.bbr.2019.112458

209. Chan RK, Zamora DO, Wrice NL, et al. Development of a Vascularized Skin Construct Using Adipose-Derived Stem Cells from Debrided Burned Skin. *Stem Cells Int*. 2012;2012:e841203. doi:10.1155/2012/841203

210. Clarke MF, Fuller M. Stem Cells and Cancer: Two Faces of Eve. *Cell*. 2006;124(6):1111-1115. doi:10.1016/j.cell.2006.03.011

211. Gurdon JB. The developmental capacity of nuclei taken from intestinal epithelium cells of feeding tadpoles. *J Embryol Exp Morphol*. 1962;10:622-640.

212. Gurdon JB, Elsdale TR, Fischberg M. Sexually Mature Individuals of Xenopus laevis from the Transplantation of Single Somatic Nuclei. *Nature*. 1958;182(4627):64-65. doi:10.1038/182064a0

213. Wilmut I, Schnieke AE, McWhir J, Kind AJ, Campbell KHS. Viable offspring derived from fetal and adult mammalian cells. *Nature*. 1997;385(6619):810-813. doi:10.1038/385810a0

214. Chun YS, Byun K, Lee B. Induced pluripotent stem cells and personalized medicine: current progress and future perspectives. *Anat Cell Biol*. 2011;44(4):245-255. doi:10.5115/acb.2011.44.4.245

215. Pereira IM, Marote A, Salgado AJ, Silva NA. Filling the Gap: Neural Stem Cells as A Promising Therapy for Spinal Cord Injury. *Pharmaceuticals*. 2019;12(2):65. doi:10.3390/ph12020065

216. Shahbazi MN. Mechanisms of human embryo development: from cell fate to tissue shape and back. *Dev Camb Engl*. 2020;147(14):dev190629. doi:10.1242/dev.190629

217. Levine AJ, Brivanlou AH. Proposal of a model of mammalian neural induction. *Dev Biol*. 2007;308(2):247-256. doi:10.1016/j.ydbio.2007.05.036

218. 28.2 Embryonic Development - Anatomy and Physiology | OpenStax. Accessed May 15, 2023. https://openstax.org/books/anatomy-and-physiology/pages/28-2-embryonic-development

219. Brady MV, Vaccarino FM. Role of SHH in Patterning Human Pluripotent Cells towards Ventral Forebrain Fates. *Cells*. 2021;10(4):914. doi:10.3390/cells10040914

220. Takahashi T, Nowakowski RS, Caviness VS. The leaving or Q fraction of the murine cerebral proliferative epithelium: a general model of neocortical neuronogenesis. *J Neurosci Off J Soc Neurosci*. 1996;16(19):6183-6196. doi:10.1523/JNEUROSCI.16-19-06183.1996

221. Huttner WB, Kosodo Y. Symmetric versus asymmetric cell division during neurogenesis in the developing vertebrate central nervous system. *Curr Opin Cell Biol*. 2005;17(6):648-657. doi:10.1016/j.ceb.2005.10.005

222. Ortega JA, Memi F, Radonjic N, et al. The Subventricular Zone: A Key Player in Human Neocortical Development. *The Neuroscientist*. 2018;24(2):156-170. doi:10.1177/1073858417691009

223. Hernández-Miranda LR, Parnavelas JG, Chiara F. Molecules and Mechanisms Involved in the Generation and Migration of Cortical Interneurons. *ASN Neuro*. 2010;2(2):AN20090053. doi:10.1042/AN20090053

224. Villalba A, Götz M, Borrell V. Chapter One - The regulation of cortical neurogenesis. In: Bashaw GJ, ed. *Current Topics in Developmental Biology*. Vol 142. Molecular Mechanisms of Neural Development and Insights into Disease. Academic Press; 2021:1-66. doi:10.1016/bs.ctdb.2020.10.003

225. Lim L, Mi D, Llorca A, Marín O. Development and Functional Diversification of Cortical Interneurons. *Neuron*. 2018;100(2):294-313. doi:10.1016/j.neuron.2018.10.009

226. Muñoz-Sanjuán I, Brivanlou AH. Neural induction, the default model and embryonic stem cells. *Nat Rev Neurosci*. 2002;3(4):271-280. doi:10.1038/nrn786

227. Chambers SM, Fasano CA, Papapetrou EP, Tomishima M, Sadelain M, Studer L. Highly efficient neural conversion of human ES and iPS cells by dual inhibition of SMAD signaling. *Nat Biotechnol*. 2009;27(3):275-280. doi:10.1038/nbt.1529

228. Zhu Y, Wan S, Zhan R ya. Inducible pluripotent stem cells for the treatment of ischemic stroke: current status and problems. *Rev Neurosci*. 2012;23(4):393-402. doi:10.1515/revneuro-2012-0042

229. Ameele J van den, Tiberi L, Vanderhaeghen P, Espuny-Camacho I. Thinking out of the dish: what to learn about cortical development using pluripotent stem cells. *Trends Neurosci*. 2014;37(6):334-342. doi:10.1016/j.tins.2014.03.005

230. Li XJ, Zhang X, Johnson MA, Wang ZB, Lavaute T, Zhang SC. Coordination of sonic hedgehog and Wnt signaling determines ventral and dorsal telencephalic neuron types from human embryonic stem cells. *Dev Camb Engl*. 2009;136(23):4055-4063. doi:10.1242/dev.036624

231. Kim TG, Yao R, Monnell T, et al. Efficient specification of interneurons from human Pluripotent stem cells by dorsoventral and rostrocaudal modulation. *Stem Cells Dayt Ohio*. 2014;32(7):1789-1804. doi:10.1002/stem.1704

232. Ortiz-Virumbrales M, Moreno CL, Kruglikov I, et al. CRISPR/Cas9-Correctable mutation-related molecular and physiological phenotypes in iPSC-derived Alzheimer's PSEN2N141Ineurons. *Acta Neuropathol Commun*. 2017;5(1):77. doi:10.1186/s40478-017-0475-z

233. Ochalek A, Mihalik B, Avci HX, et al. Neurons derived from sporadic Alzheimer's disease iPSCs reveal elevated TAU hyperphosphorylation, increased amyloid levels, and GSK3B activation. *Alzheimers Res Ther*. 2017;9(1):90. doi:10.1186/s13195-017-0317-z

234. Wezyk M, Szybinska A, Wojsiat J, et al. Overactive BRCA1 Affects Presenilin 1 in Induced Pluripotent Stem Cell-Derived Neurons in Alzheimer's Disease. *J Alzheimers Dis JAD*. 2018;62(1):175-202. doi:10.3233/JAD-170830

235. Tcw J. Human iPSC application in Alzheimer's disease and Tau-related neurodegenerative diseases. *Neurosci Lett*. 2019;699:31-40. doi:10.1016/j.neulet.2019.01.043

236. Israel MA, Yuan SH, Bardy C, et al. Probing sporadic and familial Alzheimer's disease using induced pluripotent stem cells. *Nature*. 2012;482(7384):216-220. doi:10.1038/nature10821

237. Kondo T, Asai M, Tsukita K, et al. Modeling Alzheimer's disease with iPSCs reveals stress phenotypes associated with intracellular Aβ and differential drug responsiveness. *Cell Stem Cell*. 2013;12(4):487-496. doi:10.1016/j.stem.2013.01.009

238. Lin YT, Seo J, Gao F, et al. APOE4 Causes Widespread Molecular and Cellular Alterations Associated with Alzheimer's Disease Phenotypes in Human iPSC-Derived Brain Cell Types. *Neuron*. 2018;98(6):1141-1154.e7. doi:10.1016/j.neuron.2018.05.008

239. Wang C, Najm R, Xu Q, et al. Gain of toxic apolipoprotein E4 effects in human iPSC-derived neurons is ameliorated by a small-molecule structure corrector. *Nat Med*. 2018;24(5):647-657. doi:10.1038/s41591-018-0004-z

240. Wadhwani AR, Affaneh A, Van Gulden S, Kessler JA. Neuronal apolipoprotein E4 increases cell death and phosphorylated tau release in alzheimer disease. *Ann Neurol*. 2019;85(5):726-739. doi:10.1002/ana.25455

241. Raja WK, Mungenast AE, Lin YT, et al. Self-Organizing 3D Human Neural Tissue Derived from Induced Pluripotent Stem Cells Recapitulate Alzheimer's Disease Phenotypes. *PLOS ONE*. 2016;11(9):e0161969. doi:10.1371/journal.pone.0161969

242. Thiberge C, Pou ML, Vitrac A, Maskos U, Cloëz-Tayarani I. Humanized Chimeric Mouse Models to Study Human Neural Development and Pathogenesis of Brain Diseases. In: Martin S, Laumonnier F, eds. *Translational Research Methods in Neurodevelopmental Disorders*. Vol 185. Neuromethods. Springer US; 2022:135-158. doi:10.1007/978-1-0716-2569-9_8

243. Vitrac A, Pons S, Balkota M, et al. A chimeric mouse model to study human iPSC-derived neurons: the case of a truncating SHANK3 mutation. *Sci Rep*. 2020;10(1):13315. doi:10.1038/s41598-020-70056-4

244. D'Alessio R, Koukouli F, Blanchard S, et al. Long-term development of human iPSC-derived pyramidal neurons quantified after transplantation into the neonatal mouse cortex. *Dev Biol*. 2020;461(1):86-95. doi:10.1016/j.ydbio.2020.01.009

245. Espuny-Camacho I, Michelsen KA, Gall D, et al. Pyramidal Neurons Derived from Human Pluripotent Stem Cells Integrate Efficiently into Mouse Brain Circuits In Vivo. *Neuron*. 2013;77(3):440-456. doi:10.1016/j.neuron.2012.12.011

246. Linaro D, Vermaercke B, Iwata R, et al. Xenotransplanted Human Cortical Neurons Reveal Species-Specific Development and Functional Integration into Mouse Visual Circuits. *Neuron*. 2019;104(5):972-986.e6. doi:10.1016/j.neuron.2019.10.002

247. Espuny-Camacho I, Michelsen KA, Linaro D, et al. Human Pluripotent Stem-Cell-Derived Cortical Neurons Integrate Functionally into the Lesioned Adult Murine Visual Cortex in an Area-Specific Way. *Cell Rep*. 2018;23(9):2732-2743. doi:10.1016/j.celrep.2018.04.094

248. Upadhya D, Hattiangady B, Castro OW, et al. Human induced pluripotent stem cell-derived MGE cell grafting after status epilepticus attenuates chronic epilepsy and comorbidities via synaptic integration. *Proc Natl Acad Sci U S A*. 2019;116(1):287-296. doi:10.1073/pnas.1814185115

249. Real R, Peter M, Trabalza A, et al. In vivo modeling of human neuron dynamics and Down syndrome. *Science*. 2018;362(6416):eaau1810. doi:10.1126/science.aau1810

250. Hargus G, Cooper O, Deleidi M, et al. Differentiated Parkinson patient-derived induced pluripotent stem cells grow in the adult rodent brain and reduce motor asymmetry in Parkinsonian rats. *Proc Natl Acad Sci U S A*. 2010;107(36):15921-15926. doi:10.1073/pnas.1010209107

251. Donegan JJ, Boley AM, Lodge DJ. Embryonic stem cell transplants as a therapeutic strategy in a rodent model of autism. *Neuropsychopharmacol Off Publ Am Coll Neuropsychopharmacol*. 2018;43(8):1789-1798. doi:10.1038/s41386-018-0021-0

252. Cunningham CL, Martinez-Cerdeno V, Noctor SC. Microglia Regulate the Number of Neural Precursor Cells in the Developing Cerebral Cortex. *J Neurosci*. 2013;33(10):4216-4233. doi:10.1523/JNEUROSCI.3441-12.2013

253. Ni P, Noh H, Shao Z, et al. Large-Scale Generation and Characterization of Homogeneous Populations of Migratory Cortical Interneurons from Human Pluripotent Stem Cells. *Mol Ther Methods Clin Dev*. 2019;13:414-430. doi:10.1016/j.omtm.2019.04.002

254. Itakura G, Kobayashi Y, Nishimura S, et al. Controlling immune rejection is a fail-safe system against potential tumorigenicity after human iPSC-derived neural stem cell transplantation. *PloS One*. 2015;10(2):e0116413. doi:10.1371/journal.pone.0116413

255. Brundin P, Nilsson OG, Gage FH, Björklund A. Cyclosporin A increases survival of cross-species intrastriatal grafts of embryonic dopamine-containing neurons. *Exp Brain Res*. 1985;60(1):204-208. doi:10.1007/BF00237035

256. Mattis VB, Wakeman DR, Tom C, et al. Neonatal immune-tolerance in mice does not prevent xenograft rejection. *Exp Neurol*. 2014;254:90-98. doi:10.1016/j.expneurol.2014.01.007

257. Preman P, TCW J, Calafate S, et al. Human iPSC-derived astrocytes transplanted into the mouse brain undergo morphological changes in response to amyloid-β plaques. *Mol Neurodegener*. 2021;16(1):68. doi:10.1186/s13024-021-00487-8

258. Lu MH, Ji WL, Chen H, et al. Intranasal Transplantation of Human Neural Stem Cells Ameliorates Alzheimer's Disease-Like Pathology in a Mouse Model. *Front Aging Neurosci*. 2021;13:650103. doi:10.3389/fnagi.2021.650103

259. Ben-David Y, Mizrachi T, Kagan S, et al. RIC-3 expression and splicing regulate nAChR functional expression. *Mol Brain*. 2016;9(1):47. doi:10.1186/s13041-016-0231-5

260. Wichern F, Jensen MM, Christensen DZ, Mikkelsen JD, Gondré-Lewis MC, Thomsen MS. Perinatal nicotine treatment induces transient increases in NACHO protein levels in the rat frontal cortex. *Neuroscience*. 2017;346:278-283. doi:10.1016/j.neuroscience.2017.01.026

261. Alexander JK, Sagher D, Krivoshein AV, Criado M, Jefford G, Green WN. Ric-3 Promotes α7 Nicotinic Receptor Assembly and Trafficking through the ER Subcompartment of Dendrites. *J Neurosci*. 2010;30(30):10112-10126. doi:10.1523/JNEUROSCI.6344-09.2010

262. Benwell MEM, Balfour DJK, Anderson JM. Evidence that Tobacco Smoking Increases the Density of (−)-[3H]Nicotine Binding Sites in Human Brain. *J Neurochem*. 1988;50(4):1243-1247. doi:10.1111/j.1471-4159.1988.tb10600.x

263. Breese CR, Marks MJ, Logel J, et al. Effect of Smoking History on [3H]Nicotine Binding in Human Postmortem Brain. *J Pharmacol Exp Ther*. 1997;282(1):7-13.

264. Breese CR, Lee MJ, Adams CE, et al. Abnormal regulation of high affinity nicotinic receptors in subjects with schizophrenia. *Neuropsychopharmacol Off Publ Am Coll Neuropsychopharmacol*. 2000;23(4):351-364. doi:10.1016/S0893-133X(00)00121-4

265. Marks MJ, Stitzel JA, Romm E, Wehner JM, Collins AC. Nicotinic binding sites in rat and mouse brain: comparison of acetylcholine, nicotine, and alpha-bungarotoxin. *Mol Pharmacol*. 1986;30(5):427-436.

266. Rezvani K, Teng Y, Shim D, De Biasi M. Nicotine Regulates Multiple Synaptic Proteins by Inhibiting Proteasomal Activity. *J Neurosci*. 2007;27(39):10508-10519. doi:10.1523/JNEUROSCI.3353-07.2007

267. Peng X, Gerzanich V, Anand R, Wang F, Lindstrom J. Chronic Nicotine Treatment Up-Regulates α3 and α7 Acetylcholine Receptor Subtypes Expressed by the Human Neuroblastoma Cell Line SH-SY5Y. *Mol Pharmacol*. 1997;51(5):776-784. doi:10.1124/mol.51.5.776

268. Barrantes GE, Rogers AT, Lindstrom J, Wonnacott S. alpha-Bungarotoxin binding sites in rat hippocampal and cortical cultures: initial characterisation, colocalisation with alpha 7 subunits and up-regulation by chronic nicotine treatment. *Brain Res*. 1995;672(1-2):228-236. doi:10.1016/0006-8993(94)01386-v

269. Henderson BJ, Lester HA. Inside-out neuropharmacology of nicotinic drugs. *Neuropharmacology*. 2015;96(Pt B):178-193. doi:10.1016/j.neuropharm.2015.01.022

270. Pauly JR, Marks MJ, Gross SD, Collins AC. An autoradiographic analysis of cholinergic receptors in mouse brain after chronic nicotine treatment. *J Pharmacol Exp Ther*. 1991;258(3):1127-1136.

271. Mexal S, Berger R, Logel J, Ross RG, Freedman R, Leonard S. Differential Regulation of α7 Nicotinic Receptor Gene (CHRNA7) Expression in Schizophrenic Smokers. *J Mol Neurosci MN*. 2010;40(1-2):185-195. doi:10.1007/s12031-009-9233-4

272. Peng X, Gerzanich V, Anand R, Whiting PJ, Lindstrom J. Nicotine-induced increase in neuronal nicotinic receptors results from a decrease in the rate of receptor turnover. *Mol Pharmacol*. 1994;46(3):523-530.

273. Darsow T, Booker TK, Piña-Crespo JC, Heinemann SF. Exocytic trafficking is required for nicotine-induced up-regulation of α4β2 nicotinic acetylcholine receptors. *J Biol Chem*. 2005;280(18):18311-18320. doi:10.1074/jbc.M501157200

274. Wang F, Nelson ME, Kuryatov A, et al. Chronic nicotine treatment up-regulates human but not α3β4 acetylcholine receptors stably transfected in human embryonic kidney cells. *J Biol Chem*. 1998;273(44):28721-28732. doi:10.1074/jbc.273.44.28721

275. Kuryatov A, Luo J, Cooper J, Lindstrom J. Nicotine acts as a pharmacological chaperone to up-regulate human alpha4beta2 acetylcholine receptors. *Mol Pharmacol*. 2005;68(6):1839-1851. doi:10.1124/mol.105.012419

276. Sallette J, Pons S, Devillers-Thiery A, et al. Nicotine upregulates its own receptors through enhanced intracellular maturation. *Neuron*. 2005;46(4):595-607. doi:10.1016/j.neuron.2005.03.029

277. Nashmi R, Xiao C, Deshpande P, et al. Chronic nicotine cell specifically upregulates functional alpha 4* nicotinic receptors: basis for both tolerance in midbrain and enhanced long-term potentiation in perforant path. *J Neurosci Off J Soc Neurosci*. 2007;27(31):8202-8218. doi:10.1523/JNEUROSCI.2199-07.2007

278. Huang LZ, Abbott LC, Winzer-Serhan UH. Effects of chronic neonatal nicotine exposure on nicotinic acetylcholine receptor binding, cell death and morphology in hippocampus and cerebellum. *Neuroscience*. 2007;146(4):1854-1868. doi:10.1016/j.neuroscience.2007.03.008

279. Al-Wadei MH, Al-Wadei HAN, Schuller HM. Effects of chronic nicotine on the autocrine regulation of pancreatic cancer cells and pancreatic duct epithelial cells by stimulatory and inhibitory neurotransmitters. *Carcinogenesis*. 2012;33(9):1745-1753. doi:10.1093/carcin/bgs229

280. Vallejo YF, Buisson B, Bertrand D, Green WN. Chronic Nicotine Exposure Upregulates Nicotinic Receptors by a Novel Mechanism. *J Neurosci*. 2005;25(23):5563-5572. doi:10.1523/JNEUROSCI.5240-04.2005

281. Moroni M, Zwart R, Sher E, Cassels BK, Bermudez I. α4β2 Nicotinic Receptors with High and Low Acetylcholine Sensitivity: Pharmacology, Stoichiometry, and Sensitivity to Long-Term Exposure to Nicotine. *Mol Pharmacol*. 2006;70(2):755-768. doi:10.1124/mol.106.023044

282. Nelson ME, Kuryatov A, Choi CH, Zhou Y, Lindstrom J. Alternate stoichiometries of α4β2 nicotinic acetylcholine receptors. *Mol Pharmacol*. 2003;63(2):332-341. doi:10.1124/mol.63.2.332

283. Andersen N, Corradi J, Sine SM, Bouzat C. Stoichiometry for activation of neuronal α7 nicotinic receptors. *Proc Natl Acad Sci*. 2013;110(51):20819-20824. doi:10.1073/pnas.1315775110

284. Costantini TW, Dang X, Coimbra R, Eliceiri BP, Baird A. CHRFAM7A, a human-specific and partially duplicated α7-nicotinic acetylcholine receptor gene with the potential to specify a human-specific inflammatory response to injury. *J Leukoc Biol*. 2015;97(2):247-257. doi:10.1189/jlb.4RU0814-381R

285. Govind AP, Walsh H, Green WN. Nicotine-Induced Upregulation of Native Neuronal Nicotinic Receptors Is Caused by Multiple Mechanisms. *J Neurosci*. 2012;32(6):2227-2238. doi:10.1523/JNEUROSCI.5438-11.2012

286. Rose JE, Mukhin AG, Lokitz SJ, et al. Kinetics of brain nicotine accumulation in dependent and nondependent smokers assessed with PET and cigarettes containing 11C-nicotine. *Proc Natl Acad Sci*. 2010;107(11):5190-5195. doi:10.1073/pnas.0909184107

287. Smith RC, Lindenmayer JP, Davis JM, et al. Cognitive and antismoking effects of varenicline in patients with schizophrenia or schizoaffective disorder. *Schizophr Res*. 2009;110(1):149-155. doi:10.1016/j.schres.2009.02.001

288. Hong LE, Thaker GK, McMahon RP, et al. Effects of Moderate-Dose Treatment With Varenicline on Neurobiological and Cognitive Biomarkers in Smokers and Nonsmokers With Schizophrenia or Schizoaffective Disorder. *Arch Gen Psychiatry*. 2011;68(12):1195-1206. doi:10.1001/archgenpsychiatry.2011.83

289. Gage SH, Munafò MR. Smoking as a causal risk factor for schizophrenia. *Lancet Psychiatry*. 2015;2(9):778-779. doi:10.1016/S2215-0366(15)00333-8

290. Guan ZZ, Zhang X, Blennow K, Nordberg A. Decreased protein level of nicotinic receptor α7 subunit in the frontal cortex from schizophrenic brain. *NeuroReport*. 1999;10(8):1779.

291. Tozaki H, Matsumoto A, Kanno T, et al. The inhibitory and facilitatory actions of amyloid-beta peptides on nicotinic ACh receptors and AMPA receptors. *Biochem Biophys Res Commun*. 2002;294(1):42-45. doi:10.1016/S0006-291X(02)00429-1

292. Lee KH, Cha M, Lee BH. Neuroprotective Effect of Antioxidants in the Brain. *Int J Mol Sci*. 2020;21(19):7152. doi:10.3390/ijms21197152

293. Huang S, Li SX, Bren N, et al. Complex between α-bungarotoxin and an α7 nicotinic receptor ligand-binding domain chimaera. *Biochem J*. 2013;454(2):303-310. doi:10.1042/BJ20130636

294. Liu Q, Xie X, Lukas RJ, John PAS, Wu J. A Novel Nicotinic Mechanism Underlies β-Amyloid-Induced Neuronal Hyperexcitation. *J Neurosci*. 2013;33(17):7253-7263. doi:10.1523/JNEUROSCI.3235-12.2013

295. Stine WB, Dahlgren KN, Krafft GA, LaDu MJ. In Vitro Characterization of Conditions for Amyloid-β Peptide Oligomerization and Fibrillogenesis *. *J Biol Chem*. 2003;278(13):11612-11622. doi:10.1074/jbc.M210207200

296. Marucci G, Buccioni M, Ben DD, Lambertucci C, Volpini R, Amenta F. Efficacy of acetylcholinesterase inhibitors in Alzheimer's disease. *Neuropharmacology*. 2021;190:108352. doi:10.1016/j.neuropharm.2020.108352

297. Yang T, Xiao T, Sun Q, Wang K. The current agonists and positive allosteric modulators of α7 nAChR for CNS indications in clinical trials. *Acta Pharm Sin B*. 2017;7(6):611-622. doi:10.1016/j.apsb.2017.09.001

298. Oh Y, Jang J. Directed Differentiation of Pluripotent Stem Cells by Transcription Factors. *Mol Cells*. 2019;42(3):200-209. doi:10.14348/molcells.2019.2439

299. Boissart C, Poulet A, Georges P, et al. Differentiation from human pluripotent stem cells of cortical neurons of the superficial layers amenable to psychiatric disease modeling and high-throughput drug screening. *Transl Psychiatry*. 2013;3(8):e294-e294. doi:10.1038/tp.2013.71

300. Ahn S, Kim TG, Kim KS, Chung S. Differentiation of human pluripotent stem cells into Medial Ganglionic Eminence vs. Caudal Ganglionic Eminence cells. *Methods San Diego Calif*. 2016;101:103-112. doi:10.1016/j.ymeth.2015.09.009

301. Chen GJ, Xiong Z, Yan Z. Aβ impairs nicotinic regulation of inhibitory synaptic transmission and interneuron excitability in prefrontal cortex. *Mol Neurodegener*. 2013;8(1):3. doi:10.1186/1750-1326-8-3

302. Bowles KR, T. C. W. J, Qian L, Jadow BM, Goate AM. Reduced variability of neural progenitor cells and improved purity of neuronal cultures using magnetic activated cell sorting. *PLoS ONE*. 2019;14(3):e0213374. doi:10.1371/journal.pone.0213374

303. Nato G, Corti A, Parmigiani E, et al. Immune-tolerance to human iPS-derived neural progenitors xenografted into the immature cerebellum is overridden by species-specific differences in differentiation timing. *Sci Rep*. 2021;11(1):651. doi:10.1038/s41598-020-79502-9

304. Greig LC, Woodworth MB, Galazo MJ, Padmanabhan H, Macklis JD. Molecular logic of neocortical projection neuron specification, development and diversity. *Nat Rev Neurosci*. 2013;14(11):755-769. doi:10.1038/nrn3586

305. Sun W, Kim H, Moon Y. Control of neuronal migration through rostral migratory stream in mice. *Anat Cell Biol*. 2010;43(4):269-279. doi:10.5115/acb.2010.43.4.269

306. Penzes P, Cahill ME, Jones KA, VanLeeuwen JE, Woolfrey KM. Dendritic spine pathology in neuropsychiatric disorders. *Nat Neurosci*. 2011;14(3):285-293. doi:10.1038/nn.2741

307. Gouder L, Tinevez JY, Goubran-Botros H, Benchoua A, Bourgeron T, Cloëz-Tayarani I. Three-dimensional Quantification of Dendritic Spines from Pyramidal Neurons Derived from Human Induced Pluripotent Stem Cells. *J Vis Exp*. 2015;(104):53197. doi:10.3791/53197

308. Vitrac A. *Analyses Phénotypiques in Vitro et in Vivo de Mutations de Novo Tronquantes Dans Le Gène SHANK3*. These de doctorat. Université Paris Cité; 2020. Accessed May 16, 2023. https://www.theses.fr/2020UNIP7173

309. Ofer N, Benavides-Piccione R, DeFelipe J, Yuste R. Structural Analysis of Human and Mouse Dendritic Spines Reveals a Morphological Continuum and Differences across Ages and Species. *eNeuro*. 2022;9(3). doi:10.1523/ENEURO.0039-22.2022

310. Revah O, Gore F, Kelley KW, et al. Maturation and circuit integration of transplanted human cortical organoids. *Nature*. 2022;610(7931):319-326. doi:10.1038/s41586-022-05277-w

311. Boros BD, Greathouse KM, Gearing M, Herskowitz JH. Dendritic spine remodeling accompanies Alzheimer's disease pathology and genetic susceptibility in cognitively normal aging. *Neurobiol Aging*. 2019;73:92-103. doi:10.1016/j.neurobiolaging.2018.09.003

312. Benavides-Piccione R, Ballesteros-Yáñez I, DeFelipe J, Yuste R. Cortical area and species differences in dendritic spine morphology. *J Neurocytol*. 2002;31(3):337-346. doi:10.1023/A:1024134312173

313. Mold JE, McCune JM. Immunological tolerance during fetal development: from mouse to man. *Adv Immunol*. 2012;115:73-111. doi:10.1016/B978-0-12-394299-9.00003-5

314. Tay TL, Savage JC, Hui CW, Bisht K, Tremblay M. Microglia across the lifespan: from origin to function in brain development, plasticity and cognition. *J Physiol*. 2017;595(6):1929-1945. doi:10.1113/JP272134

315. Gomes-Leal W. Microglial physiopathology: how to explain the dual role of microglia after acute neural disorders? *Brain Behav*. 2012;2(3):345-356. doi:10.1002/brb3.51